Androgen receptor dysregulation in Amyotrophic Lateral Sclerosis

Victoria M. McLeod

ORCID 0000-0002-3973-6029

Submitted in total fulfilment for the degree of Doctor of Philosophy

March 2021

Florey Institute of Neuroscience & Mental Health

Faculty of Medicine, Dentistry & Health Science

University of Melbourne

Abstract

Amyotrophic lateral sclerosis (ALS) is a fatal adult-onset neurodegenerative disorder, resulting in the death of motor neurons. Sexual dimorphism is clear in ALS patients and mouse models. Capable of modifying disease onset and progression, sex differences can also manifest in the responsiveness and outcomes to drug therapies and interventions. Understanding the biological components contributing to the clinical heterogeneity in ALS is of great interest. The androgen receptor (AR), a nuclear steroid hormone receptor which mediates the biological actions of androgens, has strong links to motor neuron function and survival. Androgens are neuroprotective to cultured motor neurons and in response to nerve injury in vivo. An expansion mutation in the AR gene gives rise to lower motor neuron degeneration in the disorder known as spinal and bulbar muscular atrophy (SBMA). This thesis explores a potential role for AR in mediating the sex-differences in ALS using the transgenic SOD1G93A mouse model of ALS.

Firstly, changes to the level and cellular localisation of AR, estrogen receptor alpha (ERα) and beta (ERβ), and progesterone receptor (PR), were analysed within the lumbar spinal cord of male and female SOD1G93A mice relative to wildtype control mice, over the disease course. A robust decrease in spinal cord AR level occurred in symptomatic male SOD1G93A mice. This occurred in parallel with decreases in transcript levels of androgen metabolising enzyme, 5α-reductase type II. AR level in females was half that of males, whereas levels and localisation of ER and PR were comparable between sexes. ERα showed a robust localisation to astrocytic processes in symptomatic SOD1G93A mice; ERβ was upregulated, possibly contributing to multiple glial cell responses.

Secondly, a closer inspection of AR expression within the various motor neurons (MN) throughout the central nervous system (CNS) neuraxis was conducted. It was strikingly apparent that by endstage disease, the majority of MNs remaining in SOD1G93A male mice had reduced nuclear AR. A clear correlation between AR expression and vulnerability in ALS was not immediately evident, although unique MN clusters with high AR content were all preserved in endstage disease. In the vulnerable lumbar spinal cord MNs, AR levels were reduced in presymptomatic stages of disease. This was paralleled by a downregulation in AR within target skeletal muscle. The consequences of these perturbations to AR level remains unclear, although their early disruption could suggest their contribution to disease pathogenesis.

Finally, this thesis explored the impact of disrupted AR signalling and expression levels, to SOD1G93A disease course. Firstly, chronic administration of AR antagonist, flutamide, worsened muscle pathology and exacerbated onset without affecting neurodegeneration and survival. Secondly, the Cre/LoxP system was used to conditionally delete AR from neuronal and glial cells of SOD1G93A male mice using the Nestin-Cre transgenic.

Central AR deletion was not observed to have an impact on disease course, however, the metabolic phenotype of the Nestin-Cre mouse had a noticeable, and confounding, effect the on SOD1G93A lifespan. Thirdly, global overexpression of AR in SOD1G93A mice, showed subtle effects on disease onset, although did not have an appreciable impact on ALS disease course.

In summary, the work of this thesis provides a robust characterisation of sex steroid hormone receptors in the SOD1G93A mouse model of ALS. Evidence of reduced AR level in MNs through disrupted local androgen metabolism may present a target for future intervention studies. Peripheral AR was identified as a modulator of disease onset, through chronic AR antagonism. Genetic manipulation studies did not identify AR as a modifier of disease outcome in the SOD1G93A.

Declaration

I hereby certify that:

i) This thesis comprises only my original work towards the degree of Doctor of Philosophy, except where indicated in the preface.

ii) due acknowledgement has been made in the thesis to all other material used,

iii) the thesis comprises less than 100,000 words in length, exclusive of tables, figures, bibliographies, and appendices.

Victoria McLeod 01/03/2021

Preface

The work presented in this thesis was the authors own with the exception of the contributions hereby acknowledged.

Chapter 2:

This work was published in July 2020: *Endocrinology* 161: 1–20. Technical assistance was provided by Dr. Mathew Chiam in the sample preparation for steroid analysis. Technical expertise was provided by Dr. Thusitha Rupasinghe in method development and instrument operation for liquid chromatography/mass spectrometry analysis of steroids. All other co-authors provided editing of manuscript.

Chapter 3:

This chapter has been prepared as a manuscript but not yet submitted to *Neurobiology of Disease*. Technical assistance was provided by Dr. Mathew Chiam in performing some of the blinded image analysis.

Chapter 4:

This chapter has been prepared as a '*basic science short report'* but not yet submitted to *Muscle and Nerve*. The work is the author's own.

Chapter 5:

This work was published in June 2019: *British Journal of Pharmacology* 176:2111–2130. Technical assistance was provided by Dr. Mathew Chiam in establishing Western blot protocols. Dr. Linda Lau performed differentiation of human embryonic stem cell derived motor neurons. Technical expertise were provided by Dr. Thusitha Rupasinghe in method development and instrument operation for liquid chromatography/mass spectrometry analysis of testosterone and flutamide. All other co-authors provided editing of manuscript.

Chapter 6:

This work was published in April 2021: *Scientific Reports* 11(1):9255. Doris Tomas performed $SOD1^{G93A}$ mouse studies presented in Figures 3 & 4 and shares co-primary authorship of the manuscript. Nayomi Wanniarachchillage assisted with genotyping. All other co-authors provided editing of manuscript.

These studies were supported by funding from Motor Neuron Disease Research Institute of Australia (Grant/Award Number1557), Stafford Fox Medical Research Foundion, National Health and Medical Research Council of Australia Project (Grant ID 1104295 and 1104299) awarded to Associate Professor Bradley Turner; and the Australian Postgraduate Award and the Motor Neuron Disease Research Institute of Australia PhD Scholarship Top up Grant awarded to myself.

Acknowledgements

There are many people I wish to thank for their involvement and contributions during this long, seemingly never-ending, journey.

My primary supervisor, Brad Turner, thank you for accepting me into your lab, having the patience to allow me independence, and showing a tenacity to secure funding and grow the lab which has been inspiring. I wish to thank my co-supervisor, Wah Chin Boon, for your helpful insights into the wonderful and confusing world of steroid neurobiology. Thank you to Tony Hannan, my PhD committee chair, for bringing enthusiasm and thought-provoking suggestions to my candidature meetings.

To Linda, your encouragement and fierce belief in me during your time as my supervisor provided much reassurance to my early candidature, thank you for your unwavering support and friendship throughout the years that followed.

I cannot imagine this enduring adventure would have been quite the same without this group of people. Mathew – what a journey it has been, thank you for putting up with me all day/every day – we laughed a lot. I have found a kindred spirit. Thank you also for your ideas and troubleshooting, willingness to help no matter what the hour, and editing commas into my work. Nirma – your friendship and support have become invaluable. We have endured together the highs and lows of our own science journey's – I can now only remember our highs. Doris - my top collaborator - in science and in office shenanigans. I truly appreciate the contributions you make to all of our successes and I hope this has been aptly recognised. Nayomi – always diligent and hardworking yet always front and centre to any unfolding theatrics. Thank you for always being positive, kind and loyal. I will cherish the memories of this time we were all together.

Thank you to all of the Florey MND lab for helpful advice and entertainment over the years. Kat and Eli, thank you for always making our coffee catch ups a priority amidst your busy schedules. Fatemeh, I will have fond memories of our many office escapades. Bec, you were always a beacon of encouragement in the early days.

Finally, to my family, friends, and mentors in the outside world. Your patience, support and belief in me, always, has undoubtedly contributed to me reaching the end of this journey. Thank you.

Table of Contents

List of Figures

List of Tables

Abbreviations

3β-HSD	3β-Hydroxysteroid dehydrogenase
5α-R	5α-reductase
17β-HSD	17β-Hydroxysteroid dehydrogenase
AIS	Androgen insensitivity syndrome
ALS	Amyotrophic lateral sclerosis
AR	Androgen receptor
ARKO	Androgen receptor knockout
BDNF	Brain derived neurotrophic factor
C9orf72	Chromosome 9 open reading frame 72
CN	Cranial nerve
CNS	Central nervous system
CNTF	Ciliary neurotrophic factor
CSF	Cerebrospinal fluid
CSMN	Corticospinal motor neuron
DHP	5α-dihydroprogesterone
DHEA	Dehydroepiandrosterone
DHT	5α-dihydrotestosterone
DLN	Dorsolateral nucleus
E2	17β-estradiol
EDL	Extensor digitorum longus
ER	Estrogen receptor
ERα	Estrogen receptor alpha
ERβ	Estrogen receptor beta
fALS	Familial amyotrophic lateral sclerosis
FTD	Frontotemporal dementia
FUS	Fused in sarcoma
GDNF	Glial cell-derived neurotrophic factor
GnRH	Gonadotropin-releasing hormone
HF	2-hydroxyflutamine
HPA	Hypothalamic-pituitary-adrenal
HPG	Hypothalamic-pituitary-gonadal
HSP	Heat shock protein
IGF-1	Insulin-like growth factor 1
KO	Knockout
LH	Luteinizing hormone

LMN	Lower motor neuron
LVPN	Layer V pyramidal neuron
MN	Motor neurons
MND	Motor neuron disease
NGF	Nerve growth factor
NMJ	Neuromuscular junction
PBS	Phosphate buffered saline
PCR	polymerase chain reaction
PLS	Primary lateral sclerosis
PMA	Progressive muscular atrophy
PR	Progesterone receptor
PROG	Progesterone
RDLN	Retrodorsolateral nucleus
sALS	Sporadic amyotrophic lateral sclerosis
SBMA	Spinal and bulbar muscular atrophy
SHBG	Sex hormone binding globulin
SNB	Spinal nucleus of the bulbocavernosus
SOD1	Superoxide dismutase 1
SREBP	Sterol regulatory element-binding protein
SV	Seminal vesicles
T	Testosterone
TDP-43	TAR DNA-binding protein 43
TGFβ1	Transforming growth factor beta 1
TrkA	Tropomyosin receptor kinase A
TrkB	Tropomyosin receptor kinase B
UMN	Upper motor neurons
VEGF	Vascular endothelial growth factor
WT	Wild type

Publications & Presentations

Conferences

McLeod, V., Lau, C., Boon, W., Turner, B. (2018, March). Androgen receptor activity is dysregulated in the spinal cord of SOD1G93A mice. *Poster presentation at Fight MND Australasian Motor Neuron Disease Symposium, Melbourne, Australia.*

McLeod, V., Lau, C., Boon, W., Turner, B. (2016, December). Androgen receptor transcriptional targets in muscle and motor neurons. *Poster presentation at the 37th Annual Scientific Meeting of the Australasian Neuroscience Society 2017*, *Sydney, Australia.*

McLeod, V., Lau, C., Rupasinghe, T., Boon, W., Turner, B. (2017, December). Effect of androgen receptor antagonism on disease progression in the SOD1G93A mouse model of amyotrophic lateral sclerosis. *Poster presentation at the 37th Annual Scientific Meeting of the Australasian Neuroscience Society 2017, Sydney, Australia.*

McLeod, V., Lau, C., Rupasinghe, T., Boon, W., Turner, B. (2017, October). Effect of androgen receptor antagonism on disease progression in the SOD1G93A mouse model of amyotrophic lateral sclerosis. *Poster presentation at the MND Australia Research Meeting 2017, Sydney, Australia.*

McLeod, V., Lau, C., Sheean, R., Boon, W., Turner, B. (2016, December). A role for androgen receptor in modulating disease progression in ALS. *Poster presentation at the 27th International Symposium on ALS/MND, Dublin, Ireland.*

McLeod, V., Lau, C., Rupasinghe, T., Roessner, U., Boon, W., Turner, B. (2016, November). Characterising androgen and androgen receptor dysregulation in the SOD1G93A mouse. *Poster presentation at the MND Australia Research Meeting 2016, Brisbane, Australia.*

Publications

Tomas D*, **McLeod VM***, Chiam MDF, Wanniarachchillage N, Boon WC, Turner BJ. (2021). Dissociation of disease onset, progression and sex differences from androgen receptor levels in a mouse model of amyotrophic lateral sclerosis. *Sci Rep*. 11(1):9255. DOI: 10.1038/s41598-021-88415-0. (*equal first author)

McLeod VM, Cuic B, Chiam MDF, Lau CL, Turner BJ. (2020). Exploring germline recombination in Nestin-Cre transgenic mice using floxed androgen receptor. *Genesis*. 58(10-11):e23390. doi: 10.1002/dvg.23390.

McLeod VM, Chiam MDF, Lau CL, Rupasinghe TW, Boon WC, Turner BJ. (2020). Dysregulation of steroid hormone receptors in motor neurons and glia associates with disease progression in ALS mice. *Endocrinology*. 161(9):bqaa113. doi: 10.1210/endocr/bqaa113.

McLeod VM, Lau CL, Chiam MDF, Rupasinghe TW, Roessner U, Djouma E, Boon WC, Turner BJ. (2019). Androgen receptor antagonism accelerates disease onset in the SOD1G93A mouse model of amyotrophic lateral sclerosis. *Br J Pharmacol.* 176(13):2111-2130. DOI: 10.1111/bph.14657.

Chapter 1. Introduction

1.1. Introduction

Amyotrophic lateral sclerosis (ALS) is a motor neuron disease (MND) with clinical onset typically in mid to later life and an average life expectancy of 3 years from diagnosis [1]. Pathology involves the progressive loss of upper and lower motor neurons and gradual muscle wasting, weakness, and paralysis. Multiple causes and risk factors have been suggested with epidemiological studies of ALS patients consistently indicating a higher incidence in males with additional gender differences in age of onset and anatomical site of onset, suggestive of hormonal involvement [2]. The androgen receptor (AR) primarily plays a role in the development of male secondary sexual characteristics and prostate development; however, its presence is widespread outside of the reproductive system. A potential role of the AR in ALS was first proposed in 1980 [3] which suggested that motor neuron degeneration may be related to a loss of AR function, based largely on evidence indicating a bias toward male incidence and the high androgen concentrations found in rodent spinal cord and bulbar motor neurons [4] which was absent in neurons largely spared in ALS. The discovery more than a decade later that a mutation in the AR was responsible for the motor neuron disorder, spinal and bulbar muscular atrophy (SBMA), or more commonly known as Kennedy's disease [5], provided a direct pathogenic link between AR and motor neuron degeneration. However, after several decades of research which suggests a correlational relationship between androgens and ALS [6-8], a clear mechanism for AR involvement in neuromuscular disorders other than SBMA has not been well explored. Conflicting evidence exists for the impact of androgens on ALS disease progression with suggestions that androgens may also be detrimental, despite the evidence for neuroprotective effects of AR signalling in motor neurons [9, 10]. This may be due to: 1) the widespread systemic role of androgens and AR within peripheral tissues and throughout the central nervous system (CNS); 2) difficulty in achieving generation of animal and cellular models to accurately explore the role of AR in specific tissues or neuronal populations; 3) the ability of androgens to act independently of the classical androgen receptor signalling pathway, as well as AR activity, to be modulated by alternative signalling pathways; and 4) poor consideration of physiologically relevant exogenous hormone doses and downstream disruptions in steroid biogenesis pathways. This chapter seeks to explore the current evidence for sexual dimorphism in ALS and animal models and examine how androgens and AR may play a role in neuroprotection and ALS pathogenesis.

1.2. Sex Steroid Hormones Overview

Sex steroid hormones are part of a biosynthetic pathway incorporating other major steroid hormones, including mineralocorticoids and glucocorticoids, originating from cholesterol and sharing a common 4 ring backbone (Figure 1.1). Sex hormones, like other steroids, bind to their respective receptors belonging to the nuclear receptor superfamily. Collectively these receptors incorporate a large family of diverse transcriptional regulators. Nuclear receptors are classified into three subfamilies according to their dimerisation and DNA-binding properties [11]. Sharing a similar canonical structure, the N-terminal domain (NTD) of these receptors shows variable sequence homology, whereas the DNA-binding domain (DBD) is highly conserved and ligand

binding domain (LBD) is moderately conserved across the superfamily [12]. AR belongs to subfamily III along with the other steroid hormone receptors, sharing most similarity with the 99 kDa progesterone receptor (PR).

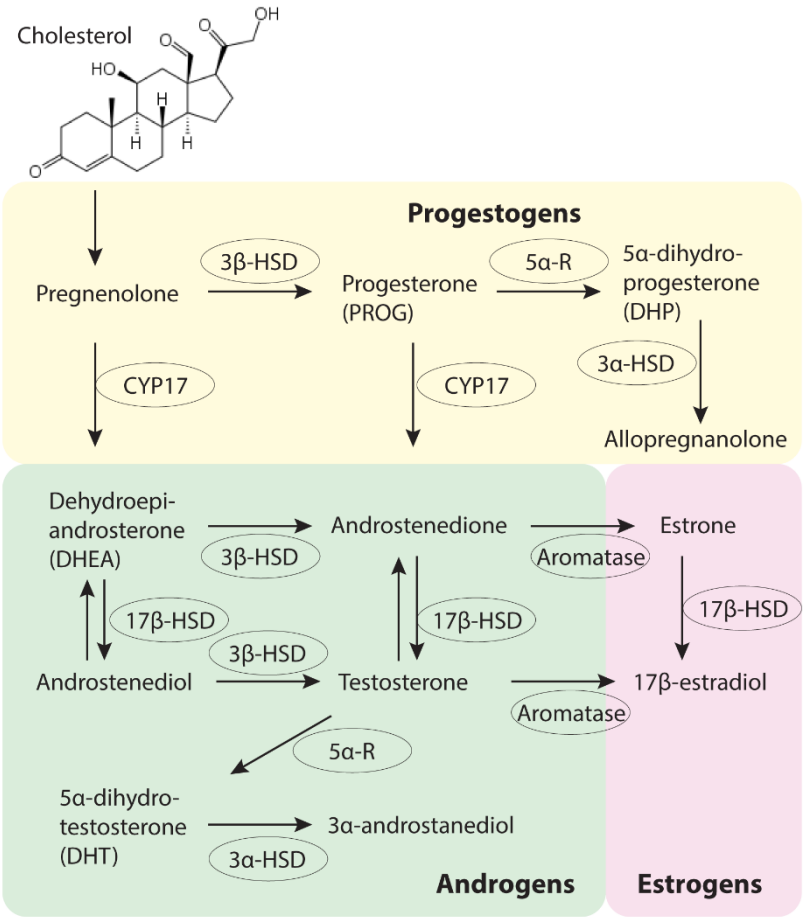

Figure 1.1. Sex hormone biosynthesis pathways. Sex steroid hormones are derived from cholesterol via various conversions by cytochrome P450 enzymes (CYP), hydroxysteroid dehydrogenases (HSD) and reductases (R). Testosterone is produced by the conversion from two precursors, androstenedione and androstenediol. 5α-reductase converts testosterone to the more potent 5α-dihydrotestosterone. Estrogens are formed by the conversion of androgens by aromatase also known as CYP19A1.

1.3. Amyotrophic Lateral Sclerosis

1.3.1. Basic overview of aetiology and pathology

ALS is classified as a neurodegenerative disease in which upper motor neurons (UMNs) in the motor cortex and lower motor neurons (LMNs) in the brainstem and spinal cord are susceptible to degeneration and death. This leads to progressive skeletal muscle atrophy upon denervation, presenting with worsening of paralysis until ultimately the respiratory muscles are compromised and death ensues. Up to 90% of ALS cases are sporadic (sALS) while ~10% are familial (fALS) with an extensive number of causative genes having now been identified and characterised over the past decade [13, 14]. These include genes encoding RNA-binding proteins, cytoskeletal proteins and proteins with important homeostatic functions, such as autophagy pathway

involvement [15]. Hexanucleotide repeat expansions in chromosome 9 opening reading frame 72 (C9orf72), an intron encoding sequence, are the most common genetic cause of ALS attributed to ~40% of familial cases, as well as being present in ~10% of sporadic cases [16]. The C9orf72 expansion is also a genetic cause of frontotemporal dementia (FTD) which exists on a clinical spectrum with ALS. Among the most common mutations causing fALS is the earliest discovered superoxide dismutase 1 (SOD1) gene which now harbours over 120 mutations [14] and accounts for ~20% of cases, and genes encoding RNA-binding proteins, TAR DNA binding protein 43 (TARDBP/TDP-43) and fused in sarcoma (FUS), both contributing to ~5% of fALS cases, respectively.

Motor neurons are the susceptible neurons at the core of ALS pathophysiology and undergo a range of pathogenic processes leading to functional impairments, such as oxidative stress, mitochondrial dysfunction and protein aggregation [17, 18]. These are collectively referred to as cell autonomous mechanisms. An increasing understanding of the important contribution from surrounding neuronal and glial cells to disease pathogenesis is being recognised, referred to as non-cell autonomous mechanisms [14, 19]. Glial cells, including astrocytes, microglia and oligodendrocytes, can provide both trophic support to MNs, as well as contributing to toxic insults, often participating in neuroinflammatory and excitotoxicity cascades with advancing disease [20, 21]. The contribution of skeletal muscle to ALS pathogenesis remains unclear due to conflicting evidence. Studies have shown early changes in muscle prior to MN loss and the loss of synaptic connection between MN and muscle fibres is an initial event in the "dying back" phenomenon in ALS [22]. The current role of muscle and targeted therapies has been reviewed by Loeffler and colleagues [23]. As extensive reviews on the both genetics and pathophysiological mechanisms in ALS have been recently published [15, 18, 24], this thesis will largely focus on the incidence and prevalence surrounding sex-based differences.

The emergence of geographical and occupational clusters in ALS incidence has led to suggestions of risk factors which may predispose an individual to the development of ALS in later life and have been reviewed recently [25, 26]. Differential exposures and responses to the environment have been suggested as a possible reason for gender differences in ALS [2]. Briefly, these include evidence of the following: smoking history; exposure to environmental toxins including heavy metals, pesticides and solvents; athleticism, fitness level and professional sports; dietary factors and body mass index; military service and traumatic brain injury; and possible history of viral exposure.

1.3.2. Evidence of sexual dimorphism

Multiple population studies conducted on gender bias in ALS incidence and prevalence have led to wide acceptance that ALS more commonly affects males, with age and site of onset variables [2, 27-30]. In the majority of population registers assessed, incidence is greater in males across most age-groups, although the ratio tightens with increasing age [2, 27], hence in younger age groups, the bias toward males is more prominent. ALS, and more broadly MNDs, are classified by their site of onset and also the type of motor neuron involvement (Figure 1.2) [31], which can give an indication of disease course and severity [13, 28, 29]. Primary lateral sclerosis (PLS) represents approximately 5% of MND cases. Patients present with only signs of UMN involvement; therefore, the disease is not classified as ALS. PLS has a slow disease progression and shows no gender bias [13,

29, 31]. Likewise, in the predominantly UMN variant of ALS, no age and sex interaction effect was found, and again this phenotype shows low incidence and longer survival than other forms of ALS [30]. Progressive muscular atrophy (PMA) represents 4-5% of MND cases and is defined as having only LMN involvement. Although some debate exists as to whether PMA exists as part of the ALS spectrum, rather than a distinct MND [31, 32]. It carries a slightly better prognosis than patients with typical ALS [13] and occurs more frequently in males [32].

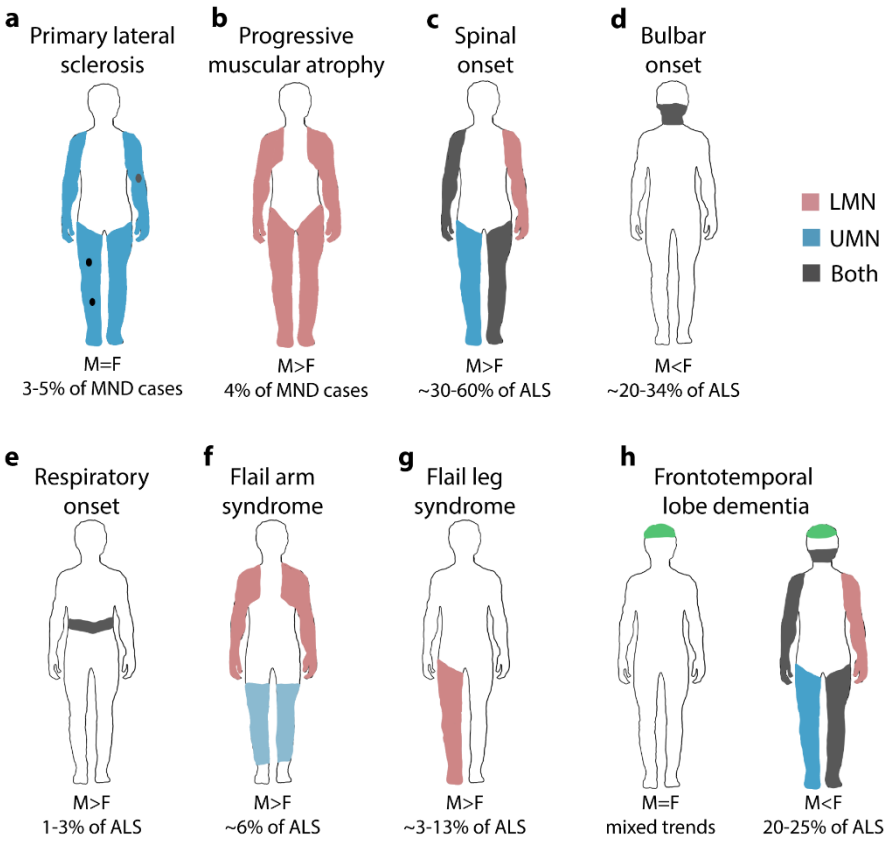

Figure 1.2. Classification of different motor neuron disease phenotypes and motor involvement. Upper motor neuron (UMN) involvement indicated in blue shading and lower motor neuron (LMN) involvement in red shading, mixed involvement and more severe symptom presentation is indicated by grey shading. (a) Primary lateral sclerosis consists of UMN involvement, with discrete involvement of LMN observed in late-stage disease, (b) progressive muscular atrophy consists only of LMN involvement, these two phenotypes represent both ends of the motor neuron disease (MND) spectrum. (c) "classical" spinal ALS presents with UMN and LMN involvement in all limbs, more commonly in males, and (d) bulbar ALS presents with UMN and LMN involvement confined to the bulbar region, more commonly in females. (e) Respiratory onset ALS, an aggressive male predominant form, presents with UMN and LMN involvement compromising the diaphragm muscle and respiratory function. (f) Flail arm syndrome consists of LMN involvement in the upper limbs with mild UMN signs presenting in the lower limbs. (g) Fail arm syndrome presents with asymmetric LMN involvement in lower limbs. (h) ALS exists on a phenotypic spectrum with frontotemporal dementia (FTD) represented by green shading, which can occur in up to 25% of all ALS. Adapted from **[31]**.

Predominantly LMN variant of ALS is also reported to have a 2:1 increased incidence in males [28]. When age of onset is considered, all spinal onset and related ALS phenotypes more frequently occur in males, especially at younger ages. In older patients, bulbar onset in females is much more frequent [2, 30]. Of particular note is the

robust gender bias evident towards males in flail arm and respiratory onset variants [28, 29]. Flail arm is characterised by initial weakness and paralysis isolated initially in the upper limbs before progressing to include lower limbs, showing signs of UMN involvement (Figure 1.3). Male to female incidence is reported to range from 2:1 [30] up to 4:1 [29, 33]. Respiratory onset ALS carries a very poor prognosis and striking male predominance reportedly 3:1 [34] to as high as 6:1 [28, 30]. These studies indicate a clear male bias associated with onset patterns involving the cervical LMNs, reflected in data from an Australian cohort showing the largest gender ratio in cervical onset compared to lumbar and bulbar onset [29].

ALS often includes an impairment in cognitive functions with pure ALS and pure FTD at opposite ends of a continuum, encompassing motor-cognitive impairment [31]. FTD occurs in up to 25% of ALS patients with a higher incidence of ALS-FTD in women with increasing age, however, this was found to correlate with bulbar onset which also occurs more frequently in older women [30, 35]. The length of the C9orf72 hexanucleotide repeat expansion is the strongest genetic determinant of ALS-FTD. Carriers of the C9orf72 mutation tend to have more severe cognitive dysfunction with a 16% higher prevalence of the expansion mutation found in females with ALS, but not observed in carriers presenting with FTD [36, 37]. Again, the C9orf72 mutation correlates with bulbar onset phenotype ALS [30]; it remains unclear if there is a sex-specific modulation on genetics and phenotype. However, several findings support the potential of sex-specific influences in cognitive components of ALS; a 33% increased prevalence of females carrying a mutation in progranulin, another common FTD causing mutation, was reported in an FTD population [36]; and ALS patients presenting with cognitive impairment with executive dysfunction, females were observed to have a 2-fold higher incidence to males [38]. Prior to the discovery of C9orf72 mutations accounting for a large proportion of inherited ALS, there was little evidence for sex affecting penetrance of familial ALS [2]. Similar to sporadic ALS, male patients carrying C9orf72 repeat expansion display an earlier disease onset [39] and a shorter survival [40] with evidence this male bias is driven by spinal onset phenotype [41].

The presence of clear sex-based differences in sALS and fALS points toward gonadal hormone influences. With the gender bias in incidence closing with increasing age, it is hypothesised that this coincides with menopause and that life-long estrogen and progesterone exposure in females minimised risk [42]. This is evident in some population analyses where oral contraceptive use and longer reproductive time-span both negatively associated with risk of ALS development in females [43, 44], while others did not find any association [45]. Interestingly, several studies have indicated that hormone replacement therapy in postmenopausal women may conversely increase the risk of ALS [45, 46]. Testosterone, similar to estrogen, is associated with neuroprotective actions [47, 48], encouraging a hypothesis that reduction in testosterone may be associated with ALS [3]. Testosterone levels naturally decrease with age in males [49] and several studies in male ALS patients suggest decreased circulating plasma testosterone [50] and decreased DHT in cerebrospinal fluid [51], however, in both cases very small sample sizes were used and no stratification for age was performed. A positive association was found between increased intrauterine testosterone exposure and development of ALS [52]. Intrauterine exposure is determined by index-finger to ring-finger ratio (2D:4D) ratio, and while it does not correlate with adult circulating

testosterone, it may serve as a predilection toward certain physical occupations, such as professional sports and manual professions associated with increased ALS risk [53].

1.4. Evidence of sexual dimorphism in ALS rodent models

The SOD1^{G93A} mouse is the most commonly used and well characterised model of ALS, recapitulating many of the pathologies observed in human ALS [54]. This mutation occurs in the *SOD1* gene whereby glycine is replaced with alanine at the 93rd amino acid position. SOD1 mutations represent approximately 20% of fALS, the second most common ALS disease causing mutation after *C9orf72*, and typically autosomal dominantly inherited [55]. The high copy number SOD1^{G93A} mouse (~25 copies of the human mutant transgene) follows an aggressive disease course [56]. Disease onset may vary depending on how it is defined, in the case of some studies this will be ~90-100 days when a tremor becomes evident in hindlimbs when the mouse is suspended, cessation of weight gain, or gross motor function deficit may be first detected [56]. Survival is typically between ~120-160 days [57], with the dominant phenotype being progressive hindlimb paralysis and ultimately loss of righting-reflexing if allowed to advance [56, 58].

This model also shows sexual dimorphism with disease onset occurring earlier in males, and survival influenced by background strain. When the SOD1^{G93A} transgene was bred onto different backgrounds including SJL, C57BL/6 (B6) and B6/SJL, disease course was significantly altered with mean survivals of 119, 144 and 130 days, respectively [59]. There was also a significantly longer female survival in the SJL and B6/SJL strains with an extension of 8 and 5 days, compared to respective male mice [59]. A recent meta-analysis performed across 97 studies using the SOD1^{G93A} transgenic mouse, examined the effects of background and sex on major disease parameters including onset, duration and survival [60]. On the B6 background, male mice show significantly earlier disease onset compared to females, although they have comparable survival, reflecting the typical clinical scenario. The SOD1^{G93A} low copy number transgenic mouse (~8-10 copies) has a slower disease course with hindlimb paralysis manifesting around ~24-34 weeks age [61]. Similar to high copy transgenic, the onset of disease, defined by moderate tremor, occurs earlier in males at ~27 weeks compared to ~31 weeks in females [61]. Two other mouse models containing human SOD1 mutations are also frequently used: the G37R and G85R SOD1 transgenics. The SOD1^{G37R} mouse has a less aggressive disease course than the SOD1^{G93A} mouse, surviving several months longer, although it displays similar sex-differences with females exhibiting a delayed disease onset with overall survival comparable to male mice [62]. The SOD1^{G85R} mouse differs from both models with a much later disease onset and very short disease course surviving ~12-13 months [63], whilst showing little difference between males and females [64].

The search for an alternative mouse model of ALS which replicates the defective RNA processing and metabolism frequent in clinical ALS, as well as cognitive dysfunction, has led to the creation of various *TDP-43* and *C9orf72* mutant transgenics, however, these are not as widely used and are accompanied by several caveats which will be discussed. The multitude of TDP-43 mouse lines developed has been reviewed recently by Philips and Rothstein [65]. Of note, one of the earliest models, quick to gain initial popular use in the field, was the TDP-

43^{A315T} mutant transgenic driven by the ubiquitously expressed mouse prion protein promoter (PrP) [66]. This mouse develops an intestinal dysmotility phenotype due to mutant TDP-43 causing neurodegeneration of the myenteric plexus of the colon, occurring prior to the development of motor neuron degeneration [67]. This phenotype was later shown to be alleviated by the use of jellified diet [68]. These mice show clear sexual dimorphism in disease onset, although highly variable in both sexes, males had a median onset of 118 days compared to 278 days in females when fed a gel diet. More recently developed TDP-43 models, including TDP-43^{Q331K} and TDP-43^{M337V}, tend to show variable disease course dependent on the level of TDP-43 overexpression, where at levels comparable to those found endogenously, mice can develop motor neuron pathology which rarely progresses to lethality [69]. The development of a robust C9orf72 mouse model is still in early stages, with one commercially available line exhibiting ~500 hexanucleotide repeat expansions. These mice develop a slowly progressive disease appearing initially in female mice characterised by motor neuron loss and focal cortical neurodegeneration [70]. However, this model has come under scrutiny for a lack of a reproducible phenotype, low penetrance of a motor phenotype and questions regarding the stability of the repeat length [71, 72]. In summary, it is evident that a strong sex-bias toward males having a much earlier disease course compared to female mice, consistent with clinical ALS and SOD1 models [73].

Table 1.1 Sex steroid hormone therapeutic intervention in ALS animal models

Model	Background	Intervention	Onset	Survival	Reference
High $SOD1^{G93A}$ ms female	B6SJL x BALB/c	Ovariectomy with 17β-estradiol (E2) in drinking water from P40	No effect	Ovariectomy decreased by 10 days, E2 reversed the effect	[74]
High $SOD1^{G93A}$ ms male	B6SJL	E2 supplement at P42-63 or P77-98	ND	ND	[75]
High $SOD1^{G93A}$ ms female	B6SJL	Ovariectomy at 5 weeks age	Earlier by 14 days	ND	[76]
High $SOD1^{G93A}$ ms male and female	B6	Genistein, a phytoestrogen, twice daily oral from 8 weeks	Males: delay of 17 days, Females: delay of 10 days	Increased in both males and females ~10 days	[77]
$SOD1^{G93A}$ rat male and female	SD	Gonadectomy at P60 with DHEA at P85	No effect	No effect	[78]
High $SOD1^{G93A}$ ms male	B6	Castration at 5 weeks age	ND	No effect	[79]
High $SOD1^{G93A}$ ms male	B6SJL	Castration at 5 weeks with nandrolone decanoate from 7 weeks	Earlier in cast/ND group by 6 days	No effect	[80]
High $SOD1^{G93A}$ ms male	B6SJL	Nandrolone +/- exercise from P50	No effect	ND	[81]
High $SOD1^{G93A}$ ms male	B6	Castration and DHT implant at P75	ND	Extended lifespan by 8 days	[82]
High $SOD1^{G93A}$ ms male	B6SJL	Progesterone (2,4 or 6 mg/kg) daily i.p. from P70	Delayed	Only dose of 4 mg/kg extended survival	[83]

Dehydroepiandrosterone (DHEA); 17β-estradiol (E2); high = high copy number transgene; low = low copy number transgene; ms = mouse; ND= not determined

Animal models of ALS show sex-based diversity in their responsiveness to genetic background, environmental changes such as diet, steroid hormone manipulations (Table 1.1) and also drug therapies [84]. In $SOD1^{G93A}$ mice ovariectomy decreased survival in females [74], conversely, in $SOD1^{G93A}$ rats ovariectomy had no effect on survival even though in gonadally intact rats, females had a significantly longer survival compared to males [78]. Castration repeatedly had no impact on survival in $SOD1^{G93A}$ rodents [78-80]. DHT, progesterone and genistein which are agonists for AR, PR and ERβ, respectively, were all neuroprotective, extending survival in $SOD1^{G93A}$ mice [77, 82, 83].

1.5. Androgen Receptor Biology

1.5.1. Androgens

Testosterone (T) is the primary circulating androgen in both humans and rodents. Two T surges have been described during development in rodents; one occurring at E17-19 in rats [85] and another at P0 in mice [86] which are believed to be important in the activation and expression of the AR gene and protein. T levels in human development has only been described in the context of maternal exposure [87]. Development and maintenance of the male sexual phenotype through AR signalling is under the continuous control of T. Primarily synthesised by the Leydig cells within the testes (95%), T and androgen production is under regulatory control by the hypothalamic-pituitary-gonadal (HPG) feedback loop. Gonadotrophin-releasing hormone (GnRH) production by hypothalamic neurons acts upon gonadotrophs in the anterior pituitary to stimulate circulatory release of luteinising hormone (LH) and follicle stimulating hormone (FSH) [88]. These in turn stimulate the production and release of T from the gonads which then provides feedback to the HPG neurons to maintain homeostatic control over steroidogenesis. Dehydroepiandrosterone (DHEA) and androstenedione, are primarily secreted by the adrenal glands, and both are precursors in the synthesis of T (Figure 1.1), while also exhibiting weak agonist activity on AR (Table 1.1) [89, 90]. Only 1-3% of circulating T is in its free form, available for cellular uptake, while 55% is bound with high affinity to sex hormone binding globulin (SHBG) and the remaining bound to albumin [91]. Several key differences between rodent and human androgen hormone systems have been identified. Firstly, a lack of hepatic SHBG expression in rodents leads to an absence in circulating levels of the secreted protein [92]. Adult mice have half the circulating T level (total and free) compared to eugonadal adult humans, and wide fluctuations in levels which may be due to the lack of T binding proteins to buffer against rapid changes [93]. Secondly, silencing of CYP17A in the rodent adrenal gland during development reportedly leads to lack of production of local androgens, including T precursors [94]. This historically led to adrenal androgen contributions being overlooked in rodents. However, more recent evidence and refinements in methodology to detect and quantify steroid hormones, has shown functional adrenal CYP17A is present in mice and detectable levels of DHEA, androstenedione and T are also present and undisrupted following castration [95]. Extrapolating findings from androgen intervention studies in mice to humans should be interpreted with some caution.

The contribution of local biosynthesis and metabolism of sex-steroids within target tissues is increasing being recognised, in addition to secreted circulating androgens. Within tissues, T undergoes conversion to its more

potent metabolite, 5α-dihydrotestosterone (DHT), or to 17β-estradiol (E2), catalysed by the enzymes 5α-reductase (5α-R) or aromatase, respectively (Figure 1.1) [96]. 5α-R exists as two isoforms and is located intracellularly. The type 2 isoform has a high affinity for androgens and expression is more localised than type 1, showing predominance in the prostate and spinal motor neurons [97], indicating androgen dependency of these tissues. An alternative mechanism of DHT synthesis in the absence of T and androstenedione, referred to as the "backdoor" pathway, has also been described [98]. Different androgens, including both endogenous and synthetic anabolic steroids, for example nandrolone, differ in transcriptional regulation across AR responsive tissues, resulting in differential systemic physiological actions (Table 1.2) [99, 100].

Table 1.2 Biological & synthetic androgen receptor ligands

Androgen	Biosynthesis	~K_D (M)	Androgenic	Anabolic	Anabolic: androgenic ratio
Testosterone	Testis, adrenals	10^{-10}	High	High	1
Dihydrotestosterone	*In situ*	10^{-11}	Very High	Moderate	
Androstenedione	Adrenals	10^{-8}	Weak	Weak	
DHEA	Adrenals	10^{-6}	Weak	Weak	
Androstenediol	Adrenals	10^{-9}	Weak	Weak	
3α-androstanediol	*In situ*	10^{-6}	Very weak		
Methylandrostenediol	Synthetic				2
Nandrolone	Synthetic				10
Stanozol	Synthetic				30

1.5.2. Androgen Receptor

The *AR* gene is located on the X chromosome at position q11-12, consisting of 8 exons giving rise to a 919 amino acid, 110 kDa protein. The amino-terminal transactivation domain (NTD) is considered to be critical in the transcriptional activation function of AR comprised of the primarily important transcriptional activation function-1 (AF1) [101]. The NTD is also subject to several highly variable trinucleotide repeat sites [102], including the CAG repeat, and is the site for many key protein-protein interactions including SRC/P160 family coactivators [103]. Androgens can act via the AR in the "classical" or genomic signalling pathway, resulting in the regulation of androgen-responsive genes (Figure 1.3; pathway 1). In the absence of ligands (T or DHT), AR resides in the cytoplasm tethered to heat shock protein (HSP) chaperones, namely HSP70 and HSP90, which hold the receptor in a conformation facilitating ligand access and binding. Androgen binding to AR causes conformational change through N/C terminal interaction, releasing AR from cytoplasmic protein chaperones [104]. AR dimerises [105] and translocates to the nucleus, binding to androgen response elements (AREs) on target genes [106, 107]. ARE binding also involves recruitment of transcriptional machinery, as well as a host of coregulatory molecules which modulate gene transcription [108]. This signalling pathway occurs over a period of several hours, resulting in expression changes in AR regulated genes. Receptor phosphorylation is required for genomic activity mainly at serine residues 213, 506 and 650 [109, 110] and is enhanced by the action of several protein kinases including; ERK, p38, Akt and JNK [111].

Several alternative signalling pathways have emerged for AR, as occurs with other steroid hormone receptors, collectively known as non-genomic signalling. This signalling is rapid and occurs within seconds to minutes. A key step in this signalling pathway is increases in intracellular calcium [112] through androgens interacting with the plasma membrane or AR binding to cytoplasmic kinases to initiate second messenger pathways (Figure 1.3; pathway 2 & 3) [113-116]. Phosphorylation of AR at serine, threonine and tyrosine residues can occur in the presence or absence of androgen binding, with the latter believed to enhance receptor stability by preventing proteolytic cleavage [109, 110]. A thorough review of the major AR phosphorylation sites has been provided by Koryakina and colleagues [117] which outlines over 13 of the phosphorylation sites, along with the corresponding kinases and functional significance on AR action. Two major cytoplasmic targets of ligand bound AR are protein kinases Src and P13K. These in turn activate, through phosphorylation, multiple downstream effector pathways, including ras-raf-MAPK and Akt, which can in turn phosphorylate AR (Figure 1.3) [113, 118]. The identity of the membrane AR/sensor remains poorly characterised, however 4 candidate receptors have been recently reviewed by Thomas, 2019 [119]. Two of which are ion channels; calcium channel transient receptor potential melastatin 8 (TRPM8) and zinc transporter Zrt- and Irt-like protein 9 (ZIP9). Two are G-protein coupled receptors (GPCR); oxoeicosanoid receptor 1 (OXER1) and G protein-coupled receptor family C group 6 member A (GPRC6A). Finally, a recently described AR signalling pathway, thought to be involved in neurite growth of neurons, involves AR binding to filamin A at the plasma membrane in an interaction with nerve growth factor (NGF) and its receptor, tropomyosin receptor kinase A (TrkA) (Figure 1.3; pathway 4) [116, 120].

1.5.3. Functional role of AR – animal models

The tissue-specific functions of AR have been largely studied in mouse models using genetic knock out (KO) approaches. This section will focus mainly on neuronal specific KO models of AR and their utility in studying the role of AR within the CNS. In humans, mutations in the *AR* gene typically result in androgen insensitivity syndrome (AIS). The extent of loss to AR function is dependent on the site of the mutation and the resulting phenotypic spectrum ranges from complete, in which genetically male patients appear as female, to partial and mild forms. The testicular feminisation mutant (Tfm) mouse model of AIS contains a spontaneous single nucleotide deletion in exon 1 which leads to a frameshift mutation [121], resulting in a stop codon at residue 412 [122, 123]. This model equates to the ubiquitous AR knockout KO (ARKO) models generated using the Cre-Lox system, in which male mice also display a female-like appearance and infertility [124]. Tissue-specific conditional models have been generated to study the specific effects of AR in a wide variety of different tissues and these models have been extensively reviewed [125-129]. Most global KO models use cytomegalovirus (CMV) or β-actin promotor driven Cre recombinase to ubiquitously KO a floxed AR (AR^{loxP}) gene through exon 1 or 2 deletion, typically resulting in a frameshift mutation [127, 128]. An in-frame mutation resulting from a floxed exon 3 (encoding the DBD) has been shown to retain non-genomic receptor function [130]. From these techniques, it has been possible to delineate the functional roles of AR outside of the male reproductive tissues which include involvement in development of neuronal and immune cells, development and maintenance of bone and skeletal muscle mass, insulin sensitivity, metabolic and cardiovascular function (as reviewed by Chang

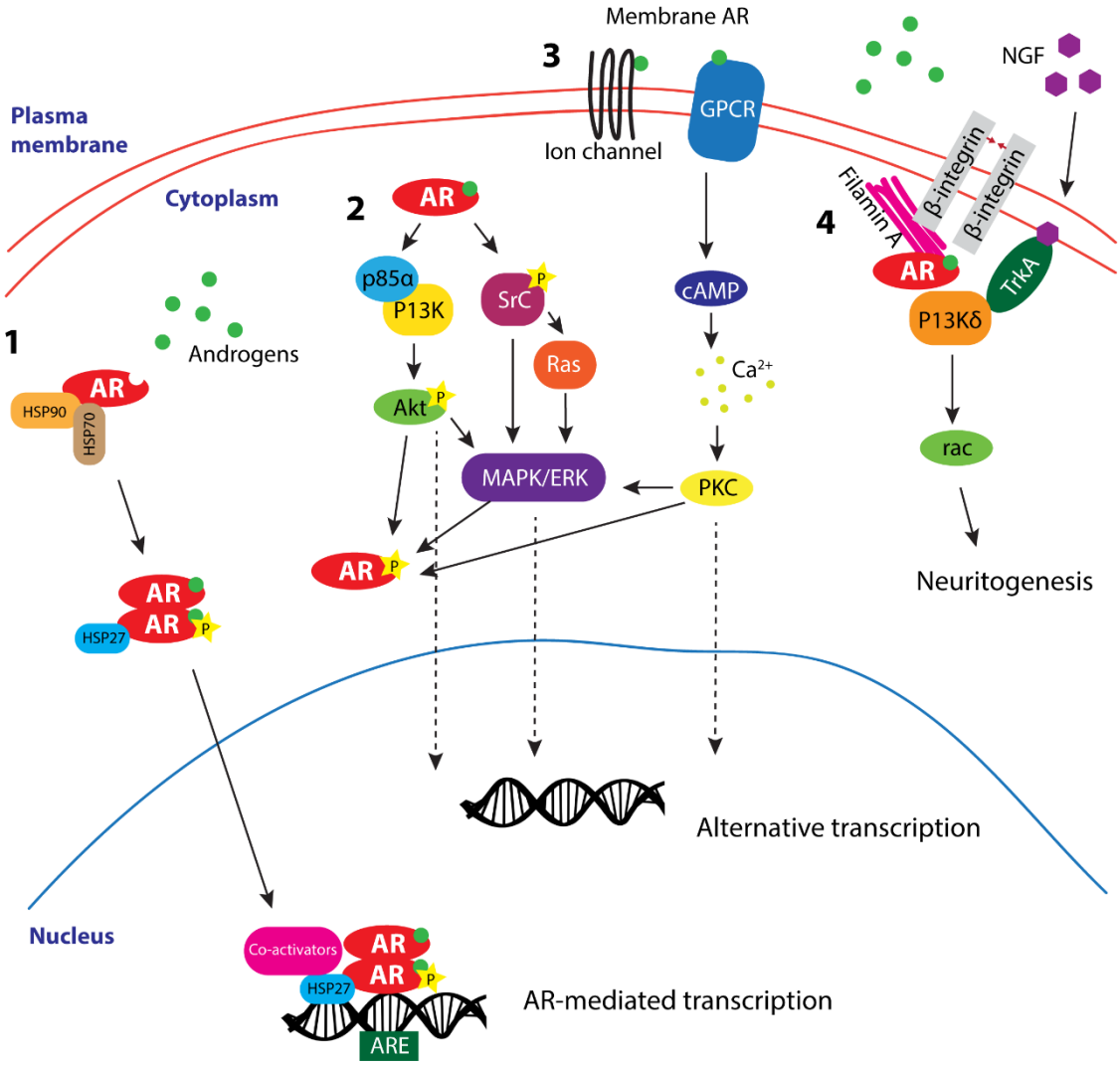

Figure 1.3. Genomic and non-genomic signalling pathways of androgen receptor. (1) Classical genomic signalling pathway of AR signalling. Androgen binding induces a conformational change in AR, leading to dissociation from chaperone heat shock proteins (HSP), dimerisation, phosphorylation and translocation to the nucleus. The AR complex binds to androgen response elements (ARE) on DNA, along with transcriptional co-activators and regulates transcription of AR-responsive genes. (2) AR interacts with multiple signalling pathways in the cytoplasm and plasma membrane constituting the nongenomic signalling pathway. Ligand-bound AR interacts with p85α regulatory subunit of phosphoinositide 3-kinase (P13K) and tyrosine-protein kinase Src. These lead to the activation of Akt, mitogen activated protein kinases and extracellular signal-regulated protein kinases (MAPK/ERK) signalling pathways which can phosphorylate unliganded AR. (3) Androgens are known to signal via a plasma membrane receptor, both ion channels and G-protein coupled receptors (GPCRs) have been identified as candidates. This activates second messenger signalling cascades, such as cyclic adenosine monophosphate (cAMP), resulting in calcium release. (4) Ligand-bound AR also signals with nerve growth factor via its tyrosine kinase receptor, TrkA. This interaction involves AR forming a complex with filamin A at the plasma membrane along with β1-integrin. The subsequent activation of protein kinases is believed to be the signalling mechanism involved in neuritogenesis.

and colleagues [128]). Within the CNS, studies on neuronal specific ARKO mice have focused on establishing a role for AR in the central control of brain masculinisation and male behaviours, neuroendocrine function, as well as centrally driven insulin sensitivity [131]. Currently described models and their major biological outcome are reported in Table 1.2. Most of these have used Nestin promotor driven Cre to conditionally delete AR from neuronal and glial cells within the central and peripheral nervous systems [132] (see Table 1.3).

Common to most brain AR deletion models, disinhibition of the HPG feedback system results from absent or reduced hypothalamic AR, giving rise to increased LH release from the pituitary and elevated T production within the testis. Elevated levels of circulating testosterone, DHT, LH, in addition to reduced testicular weight, were reported by one group using the Nestin-cre driver [133], alongside decreased fertility resulting from impaired sexual behaviour [134]. AR is required by glial cells for oligodendrocyte-mediated remyelination in a lysolecithin-induced demyelination model [135]. More recently, central AR has been shown to modulate skeletal muscle mass. Using calcium/calmodulin-dependent protein kinase IIα (CaMKIIα) promoter to drive Cre expression predominantly in forebrain and hippocampal neurons [136], excised AR led to decreased muscle mass in fast-twitch hindlimb muscles - gastrocnemius and extensor digitorum longus [137]. In a subsequent study, selective deletion of AR from hypothalamic neurons using AAV-eSynapsin-iCre driver, produced the same reductions in muscle mass [138]. However, it is worth noting in both instances, a marked reduction in voluntary physical activity occurred in neuronal KO mice. In all models of neuronal AR deletion, no indication of gross motor deficits have been observed, where muscle strength and force generation remained normal, as did motor co-ordination and function.

Table 1.3 Conditional AR knockout models utilised to explore central nervous system function.

Flox region	Cre-driver	HPG dysregulation	Used Cre control	Biological effects	Reference
Exon 2	Nestin	↑ serum T, LH, ↑ SV weight	No	Impaired sexual motivation and performance, reduced aggression	[133]
Exon 2	Nestin	↑ serum T	Yes	AR regulates the execution & extent of male typical sexual behaviours	[134]
Exon 2	Synapsin 1	No change in T	No	Impaired insulin sensitivity and lipid metabolism	[131]
Exon 2	Nestin		Yes	No change in corticosterone level, no effect of medial prefrontal cortex AR on anxiety	[139]
Exon 2	Nestin		Mixed groups	AR regulates social recognition	[140]
Exon 2	Nestin	castration + T supplementation	No	Impaired temporal memory and processing of visual objects, reduction in NMDA receptor activation in CA1 of hippocampus	[141]
Exon 2	Nestin	Castration + T supplementation	No	AR required for astrocyte recruitment & oligodendrocyte progenitor differentiation for remyelination	[135]
Exon 3	CaMKIIα-iCre	↑ serum T, LH, ↑ SV weight	Yes	Decrease in limb muscle mass	[137]
Exon 3	AAV-eSynapsin-iCre	↑ serum LH, ↑ SV weight	Yes	AR deletion in hypothalamic neurons mediates a decrease in limb muscle mass	[138]

Adeno-associated virus (AAV), calcium /calmodulin-dependent protein kinase IIα (CaMKIIα), hypothalamic-pituitary-gonadal (HPG), luteinising hormone (LH), seminal vesicle (SV)

In addition to KO strategies, transgenic and knock-in mouse models of AR have also been used to model expansion mutations in AR giving rise to SBMA or Kennedy's disease. These mutations and SBMA will be discussed in more detail in the subsequent sections exploring AR in human disease. Briefly, these models either contain insertion of the polyglutamine expanded human AR gene, for example the AR97Q transgenic [142]; or the murine AR gene is humanised to contain a longer polyglutamine tract, or example the AQ113Q knock-in model [143]. These models have been reviewed elsewhere and are outside the scope of the studies in this thesis [125].

1.5.4. Functional role of AR –human disease

Mouse models manipulating AR expression have been useful in studying the functions of AR in different tissues. However, the complexity of polymorphisms in human AR is difficult to model using mice. The majority of known mutations in the *AR* gene have been characterised in the context of AIS or prostate cancer. The gene-encoding region of exon 1 also contains several variable trinucleotide repeat sites, namely the polyglutamine (polyQ) and polyglycine tracts [102]. Repeats of the CAG trinucleotide (encoding the amino acid glutamine), typically between 9-36, occur naturally in exon 1 of the *AR* gene. The CAG repeat length inversely correlates with AR mRNA expression, most likely due to transcriptional interference occurring with longer expansions [102]. Epidemiological studies have revealed that the length of the polyQ tract associates with various human diseases [144]. Not surprisingly, these are typically related to fertility, reproductive function and hormonally driven cancers. Longer polyQ tract is associated with infertility [145] and breast cancer [146], while shorter polyQ tracts have been associated with more aggressive prostate cancer, benign prostate hyperplasia [147] and male pattern baldness [148]. Interestingly, shorter repeat lengths are also linked to cognitive and behavioural impairments (reviewed by [144]). Expanded repeats >37 in the *AR* polyQ tract are responsible for causing the monogenic disorder, spinal and bulbar muscular atrophy (SBMA) [5], with these patients usually having between 40-62 repeats. This disorder is discussed further in section 1.4.6 below.

Repeat expansions are increasingly being recognised as contributors in polygenic diseases, especially with the rapid increase in genome wide association studies (GWAS). Short polyglutamine repeat length in *AR* was associated with Alzheimer's Disease in male patients, although only in a small cohort ~200 [149]. More recently, an association was reported between longer polyQ tract length in both *AR* and Ataxin-1 (ATXN1) alleles and increased brain atrophy and memory impairment in Alzheimer's Disease [150]. The ataxin-2 (ATXN2) gene contains a polyQ tract normally 22-23 repeats long with >34 repeats responsible for causing spinocerebellar ataxia type 2. An intermediate length polyQ tract (23-33 CAG repeats) is associated with ALS and ATXN2 is a modifier of TDP-43 pathology [151]. More recently, an expanded polyQ tract in ATXN1 showed association with ALS in a large-scale GWAS study [152] and ataxin-1 cytoplasmic inclusions also prompted TAR DNA-binding protein 43 (TDP-43) mislocalisation. Interestingly, spinocerebellar ataxia type 1, resulting from an expanded polyQ tract (>39 repeats) also has a phenotypic overlap with ALS showing upper motor neuron (UMN) signs and loss of Betz cells [153]. A third polyQ expansion-containing gene candidate has also recently emerged as a risk

variant for ALS. Expansions in the huntingtin (HTT) polyQ tract are increased in ALS patients with frontotemporal dementia (FTD) [154]. To date, a relationship between the *AR* polyQ tract and ALS has not been indicated in low powered analyses conducted on ~100-200 male ALS patient cohorts [8, 155].

1.5.5. Spinal and bulbar muscular atrophy

SBMA, also known as Kennedy's disease, is an inherited X-linked disorder characterised by degeneration of spinal and brainstem lower motor neurons [156]. SBMA predominantly affects males due to higher circulating T levels which trigger the hormone-dependent dysregulation of AR and also due to females typically possessing heterozygous expression of X-linked mutant AR, thus making them carriers of the disease [157]. SBMA molecular pathology has been described primarily as a toxic gain of function through misfolded mutant AR protein aggregates and formation of polyQ AR oligomers [158]. A loss of function in *AR* also contributes to the disease with altered transcriptional activity and post-translational modification of the protein [159, 160]. Nuclear inclusions of misfolded AR are considered to be the pathological hallmark of SBMA [161]. It has been suggested that perhaps more diffuse nuclear aggregates initiate the toxicity, showing correlation with CAG repeat length [161], and that inclusions better reflect a cellular mechanism to eliminate toxic protein build up by facilitating degradation [162]. While it is undisputed that androgen exposure and ligand binding to AR is a key precipitating factor in the disease process [142], controversy over whether it is localisation to the nucleus that is primarily responsible for inducing neurotoxicity, or rather that androgens initiate and stabilise aggregation of the protein [163, 164].

1.6. Androgens and Neuroprotection

1.6.1. Cortical and motor neurons in culture

Early evidence suggesting neuroprotective actions of androgens toward motor neurons comes from testosterone-treated organotypic cultures of mouse fetal lumbosacral spinal cord which showed improved survival [165]. T has since shown neuroprotective actions in multiple neuronal culture systems: primary cultured human neurons against apoptosis induced through serum starvation [166]; mouse hippocampal neurons against β-amyloid induced toxicity [167]; and rat cerebellar granule neurons against oxidative stress [168]. Likewise, similar effects were observed in mouse neuroblastoma-embryonic motor neuron hybrid cell lines expressing human AR [169]. DHT, and the synthetic AR agonist, metribolone, increased soma size and neurite branching in these MN hybrid lines, increasing transcript level of neuritin [169, 170]. Neuritin is an important regulator of neuritogenesis, promoting axonal elongation and dendritic arborisation [171]. Other cytoskeletal proteins, including α- and β-tubulin are upregulated in neuroblastoma cells via AR-mediated mechanisms [172]. However, androgens have been shown to elicit differential responses in neuronal cultures, dependent on the cellular environment, becoming neurotoxic in cells under oxidative stress conditions [173].

1.6.2. Axotomy recovery

One mechanism of MN death proposed in ALS is degeneration initiating in the distal aspects of MNs, in what has become known as the 'dying back' phenomenon [174]. This pattern of death involving destabilisation of the NMJ [22], retraction of the axon and subsequent cell death [175], is evident in both the $SOD1^{G93A}$ mouse and ALS patients and has been likened to a distal axonopathy [176, 177]. Hence, evidence that androgens can protect against axonal damage could be beneficial in ALS neurodegeneration. Early studies conducted on rodent nerve resection or nerve crush injury models robustly showed that androgens, namely T, provided improved recovery and regeneration if administered within an appropriate window following injury. Yu and colleagues showed T and DHT promoted recovery and axonal outgrowth in rat hypoglossal nerve injury models [178-180]. T hastens recovery from facial nerve crush injury in male hamsters [181], an effect blocked by the AR antagonist, flutamide [182], and not observed in females [183]. Time-course studies of optimal treatment response revealed that T must be given within 6 hours of injury to provide axonal and functional recovery [184]. Studies in the rat sciatic nerve crush injury model show similar T stimulated recovery could be achieved in the spinal MNs [185, 186]. Axonal injury also leads to retraction of the dendrites in the weeks and months following injury [187, 188]. Testosterone is also protective against dendritic retraction and secondary atrophy in surrounding neurons. This is discussed further in the following sections as dendritic retraction is a typical response of injured neurons following a broad range of insults.

1.6.3. Studies on spinal nucleus of the bulbocavernosus

Much of the evidence supporting neuroprotective effects of androgens in MNs may be overrepresented by the MNs of the spinal nucleus of the bulbocavernosus (SNB) and their target perineal muscles: bulbocavernosus (BC) and levator ani (LA) muscles [189]. These MNs are dependent on androgens for survival during development and are highly receptive to androgens during adulthood [190, 191]. Androgens maintain the mass of BC/LA musculature [192]. The endogenous expression of AR in muscle tissue appears to precede MNs, as evidenced in the SNB in male mice [190] where AR appears to be expressed postnatally between P4-7 in MNs, compared to E15 in perineal muscles. This is consistent with the previously described ontogeny of AR expression observed in rats where lumbar MNs in the SNB, dorsolateral nucleus (DLN) and also the sexually monomorphic retrodorsolateral (RDLN) nucleus all show expression developing over a postnatal period [191]. In adult SNB MNs, T is the main driver of AR expression and is enhanced by brain-derived neurotrophic factor (BDNF) and contact with muscle targets [193]. This idea that target innervation with muscle is key for driving AR expression in motor neurons has also been suggested based on evidence from rodent axotomy models of SNB MNs [194]. Many of the very early studies investigating the androgenic regulation of SNB MNs have found an increased soma size [195], length of dendrites [196], increased synaptic input [197] and inter-motor neuronal gap junction connections [198] in response to T. The molecular mechanism behind these structural changes was thought to involve, in part, AR signalling upregulation of mRNA for structural cytoskeletal proteins β-actin and β-tubulin in response to androgens [199, 200]. T is neuroprotective preventing dendritic atrophy and secondary death of neighbouring MNs following insult [201, 202].

1.6.4. Studies on somatic limb motor neurons

The typical MNs found in the LMC of spinal cord innervating limb muscles express a more moderate level of AR compared to SNB MNs [203]. Their muscle targets, e.g. quadriceps and gastrocnemius, also express AR at a lower level and their mass is not directly regulated in response to androgens as compared to BC/LA muscle [192]. Intramuscular delivery of retrogradely transported cholera toxin-conjugated saporin into the quadriceps was used to induce partial depletion of MNs, with T attenuating dendritic atrophy in surviving MNs [203]. This effect was reproducible in both gonadally intact male and female rats [204]. In this model, both E2 and DHT were shown to similarly mediate this neuroprotective effect on dendrites via their respective receptors [205]. Similarly, both E2 and DHT are protective against dendritic atrophy in a model of spinal cord contusion injury, with only DHT showing trophic effects in skeletal muscle [206]. In normal male rats, castration has no effect on MN dendritic arbour in non-disease models [207]. Overexpression of AR in the quadriceps muscle confers sensitivity of MNs to the effects of androgens, with increased dendritic arbour observed in innervating MNs compared to non-transgenic counterparts, which could be abolished by castration [207]. This effect is similar to that observed in BC/LA muscles which naturally express high levels of AR and can regulate the dendritic arbour of innervating SNB MNs [208].

1.6.5. Neurotrophic factor support to motor neurons

AR signalling has been linked to the transcriptional regulation of many neurotrophic factors believed to be important in the survival of MNs. The greatest trophic support to MNs comes from glial cell-derived neurotrophic factor (GDNF) [209, 210], BDNF [211, 212], ciliary neurotrophic factor (CNTF) [213, 214] and insulin-like growth factor 1 (IGF-1) [215, 216]. Most of these neurotrophins are produced by surrounding support cells, such as glial cells, and also muscle tissue where they are taken up and retrogradely transported by innervating motor neurons [217]. This transport mechanism has been shown to occur for several neurotrophins, including BDNF delivery to MNs [218, 219]. Blockade of CNTF inhibits the androgen induced rescue action on SNB MNs [220]. Decreases in several trophic factors has been found in SBMA mouse models including; GDNF, IGF-1 [143] and vascular endothelial growth factor (VEGF) [221].

1.7. Motor neuron classification

AR is present throughout the CNS and peripheral muscle tissue with regional variation in expression reported in different MN populations. To understand its potential sites and mechanisms of action in ALS, it is important to understand in detail the mouse motor system. Motor neurons are diversely classified according to their origin, location, morphological and molecular properties, and innervation targets. The broadest classification is the distinction between upper and lower MNs. UMNs, which are also referred to as corticospinal motor neurons (CSMNs), as well as Betz cells in humans, have cell bodies located in the layer V motor cortex. UMNs use the

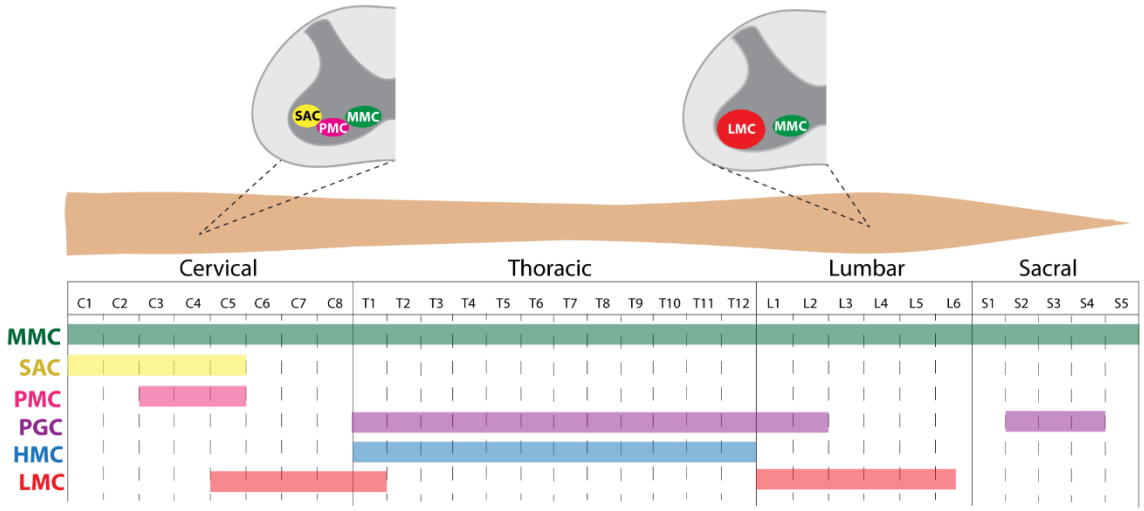

Figure 1.4. Organisation of spinal motor neurons into motor columns. The medial motor column (MMC) is depicted in green, spans the entire spinal cord located medially within the ventral horn connecting with the axial musculature. The spinally accessory column (SAC) in yellow, spans C1-C5 innervating neck muscles. The phrenic motor column (PMC) depicted in pink, spans C3-C5. Positioned inter-mediolaterally in the ventral horn innervating the diaphragm. The preganglionic column (PGC) spanning the thoracic and sacral regions of the spinal cord. Located in the dorsolateral aspect of the ventral horn innervating the sympathetic chain ganglia. The hypaxial motor column (HMC) is restricted to the thoracic region innervating the body wall and intercostal muscles. The lateral motor column (LMC) spans C5-C8, innervating upper limbs, and L1-L6, innervating the lower limbs. Adapted from [222]

neurotransmitter glutamate to signal to distal LMN targets via the corticospinal tract [223]. In humans, UMNs are much larger neurons with a prominent apical dendrite, predominantly forming monosynaptic connections directly on LMNs in the brainstem and spinal cord, whereas in mice, this connection is indirect via interneurons [224]. LMNs are located throughout the brainstem, with many forming the main cranial nerves and often referred to as bulbar MNs in humans, and throughout the length of the spinal cord ventral horn as spinal MNs.All LMNs can be identified by their choline acetyltransferase (ChAT) expression [225], using the neurotransmitter acetylcholine to signal with target muscle via the neuromuscular junction (NMJ) [223].

LMNs can be classified based on their efferent targets; i) somatic MNs innervate skeletal muscle derived from the somites, including the extraocular, tongue and limb muscles; ii) branchial MNs innervate skeletal muscle derived from the branchial arches which include the muscles of mastication and facial expression and are mainly located within the brainstem; and iii) visceral MNs that innervate involuntary smooth muscle of the autonomic nervous systems [222]. Spinal MNs are predominantly somatic and visceral and anatomically organised into columns running rostro-caudally along the ventral horn spinal cord as detailed in Figure 1.4. These consists of: i) spinal accessory column situated laterally in the ventral horn traversing C1-C5, innervating the mastoid and neck muscles; ii) phrenic motor column situated intermedio-laterally in the ventral horn C3-C5, innervating the diaphragm muscle; iii) median motor column situated in the medial region of the ventral horn spanning C1-S4, innervating the axial muscles controlling posture; iv) lateral motor column which dominates the largest cross-sectional region in the ventral horn situated laterally traversing two regions, C5-T1 and L1-L5, innervating the upper and lower limb muscles; v) hypaxial motor column in the thoracic region innervating the muscles of the

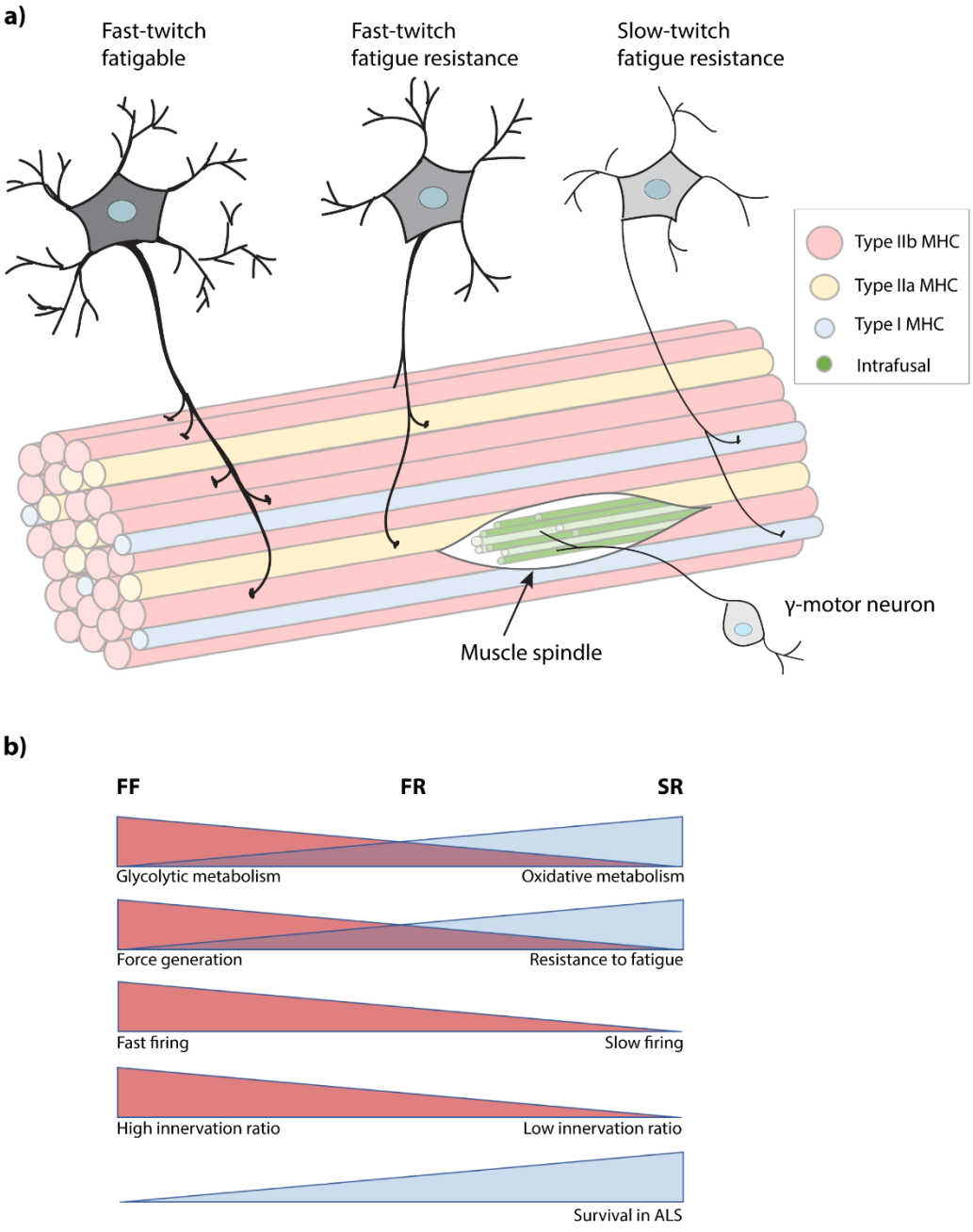

Figure 1.5. Comparison of alpha motor neuron subtypes innervating extrafusal muscle fibres. (a) Alpha motor neurons (α-MNs) are subclassified into motor units based on their morphology, function and characteristics. Fast-twitch fatigable (FF) MNs are characterised by abundant dendritic arbours, greater axon thickness and greater innervation ratio with a single MN innervating between 300-2000 myosin heavy chain (MHC) type IIb fibres. Fast-twitch resistant (FR) MNs show moderately smaller dendritic arbour, axon thicken and innervation ratio, innervating type IIa MHC fibres. Slow-twitch resistant (SR) MNs are characterised by small dendritic arbours, thinner axons and the smallest innervation ratio out of the three subtypes, innervating <200 type I fibres in a single motor unit. The γ-MNs innervate the intrafusal muscle fibres of the muscle spindle regulating proprioception and muscle contraction. (b) Properties of the extrafusal motor units from muscle metabolism, force generation, firing capacity and susceptibility to fatigue upon sustained activation. FF motor units more sensitive to degeneration in ALS with SR motor units often degenerating later in the disease course.

body wall and intercostal; and vi) preganglionic motor column contains the visceral MNs and traverses T1-L2 and S2-S4, innervating the sympathetic ganglia [222]. Different subclassifications of somatic MNs exist with i) alpha, ii) beta and iii) gamma MNs defined by the type of muscle fibre innervated [226]. Due to their divergent anatomical and functional properties, they exhibit differential vulnerability to degeneration in ALS [227, 228]. This review will only focus on motor units related to skeletal muscle innervation. The larger α-MNs innervate the extrafusal muscle fibres which are primarily responsible for generating force and contraction; with three further subdivisions based on extrafusal muscle fibre type, classified according to their excitability and fatiguability summarised in (Figure 1.5). The fast-twitch fatigable α-MNs are vulnerable in ALS [229, 230] and typically found to innervate the hindlimb muscles in mice, such as the tibialis anterior and gastrocnemius, which undergoes early and severe atrophy [177, 231]. Conversely, the soleus muscle which is predominately innervated by slow-twitch fatigue resistant α-MN undergoes degeneration later in the disease [232]. The γ-MNs are smaller, less branched neurons innervating the intrafusal muscle fibres which are responsible for proprioception [233] and are relatively resistant to ALS degeneration and age-related loss [227] (Figure 1.5).

1.8. Proposed Research & Aims

Sexual dimorphism is well documented in both clinical ALS and animal models of the disease. In patients, distinct differences in the incidence and site of onset between the sexes is widely accepted. In mouse models, disease progression is modified by hormonal manipulations, and responses to drug interventions often show sex-based differences. Yet, our understanding of the mechanisms underpinning how hormones modify disease pathogenesis remains limited. ALS is a heterogenous disorder, with an emerging model of a multistep process requiring acquisition of multiple biological "hits" converging over time, ultimately resulting in the initiation of an irreversible disease cascade [234]. Influences of a patient's sex, whether it be hormonal changes and exposures, or genetic differences conferred by X or Y chromosomes, likely contributes a biological "hit". Currently, only two treatment options have been approved for use in ALS, riluzole and edaravone [235]. These treatments offer a modest slowing of disease progression usually in a limited subset of patients. Hence, better understanding of the basic biological components of ALS and disease heterogeneity is critical in translating future therapies.

Through epidemiological and clinical evidence, a possible dysregulation in androgen production and AR function in ALS has been suggested. I hypothesised that these perturbances may be evident in the $SOD1^{G93A}$ mouse model of ALS and could influence disease progression and outcome. This was investigated under two major aims:

Aim 1: To characterise the temporospatial changes in AR expression and cellular localisation throughout the CNS of the $SOD1^{G93A}$ mouse over disease course, compared to wildtype (WT).

Aim 2: To evaluate the role of AR in mediating disease onset and progression using pharmacological inhibition and genetic disruption or overexpression of AR levels in the $SOD1^{G93A}$ mouse model of ALS.

Chapter 2. Dysregulation of steroid hormone receptors in motor neurons and glia associates with disease progression in ALS mice

Dysregulation of Steroid Hormone Receptors in Motor Neurons and Glia Associates with Disease Progression in ALS Mice

Victoria M. McLeod,[1] Mathew D. F. Chiam,[1] Chew L. Lau,[1] Thusitha W. Rupasinghe,[2] Wah C. Boon,[1] and Bradley J. Turner[1,3]

[1]Florey Institute of Neuroscience and Mental Health, University of Melbourne, Parkville, VIC 3052, Australia; [2]Metabolomics Australia, School of BioSciences, University of Melbourne, VIC 3010, Australia; and [3]Perron Institute for Neurological and Translational Science, Queen Elizabeth Medical Centre, Nedlands, WA 6150, Australia

ORCiD number: 0000-0001-6580-7655 (B. J. Turner).

Amyotrophic lateral sclerosis (ALS) is a neurodegenerative disease targeting motor neurons which shows sexual dimorphism in its incidence, age of onset, and progression rate. All steroid hormones, including androgens, estrogens, and progestogens, have been implicated in modulating ALS. Increasing evidence suggests that steroid hormones provide neuroprotective and neurotrophic support to motor neurons, either directly or via surrounding glial cell interactions, by activating their respective nuclear hormone receptors and initiating transcriptional regulatory responses. The SOD1^{G93A} transgenic mouse also shows sex-specific differences in age of onset and progression, and remains the most widely used model in ALS research. To provide a more comprehensive understanding of the influences of steroid hormone signaling in ALS, we systemically characterized sex hormone receptor expression at transcript and protein levels, cellular localization, and the impact of disease course in lumbar spinal cords of male and female SOD1^{G93A} mice. We found that spinal motor neurons highly express nuclear androgen receptor (AR), estrogen receptor (ER)α, ERβ, and progesterone receptor with variations in glial cell expression. AR showed the most robust sex-specific difference in expression and was downregulated in male SOD1^{G93A} mouse spinal cord, in association with depletion in 5α-reductase type 2 isoform, which primarily metabolizes testosterone to 5α-dihydrotestosterone. ERα was highly enriched in reactive astrocytes of SOD1^{G93A} mice and ERβ was strongly upregulated. The 5α-reductase type 1 isoform was upregulated with disease progression and may influence local spinal cord hormone levels. In conclusion, steroid hormone receptor expression is dynamic and cell-type specific in SOD1^{G93A} mice which may provide targets to modulate progression in ALS. **(*Endocrinology* 161: 1–20, 2020)**

Key Words: Androgen, estrogen, progesterone, ALS, SOD1^{G93A} mouse, spinal cord

Amyotrophic lateral sclerosis (ALS) is a progressive neurodegenerative disorder defined by upper and lower motor neuron loss. Like most neurodegenerative diseases, ALS also shows sex-specific differences, indicating that steroid hormones may be actively involved in disease mechanisms or that underlying differences in the biology of male and female nervous systems underpin neuronal vulnerability (1-4). ALS has a greater frequency and a younger age of onset in males, spinal and limb onset occurs more in males, whereas bulbar onset is more common in females, and females exhibit higher susceptibility to cognitive impairments

ISSN Online 1945-7170

Received 4 May 2020. Accepted 30 June 2020.
First Published Online 5 July 2020.
Corrected and Typeset 8 August 2020.

Abbreviations: AR, androgen receptor; ALS, amyotrophic lateral sclerosis; PBS, phosphate-buffered saline; CNS, central nervous system; DHT, 5α-dihydrotestosterone; DHP, 5α-dihydroprogesterone; E2, 17β-estradiol; ER, estrogen receptor; HPA, hypothalamic–pituitary–adrenal; PCR, polymerase chain reaction; PR, progesterone receptor; PROG, progesterone; RNA, ribonucleic acid; SOD1, superoxide dismutase 1; T, testosterone.

(5). Sex bias is also prevalent in familial ALS (fALS) cohorts with males having spinal onset showing reduced survival among C9orf72 repeat expansion patients (6, 7).

Progesterone (PROG) is primarily produced by the gonads and adrenals, and also de novo in the central nervous system (CNS), where its metabolism gives rise to active neurosteroids: 5α-dihydroprogesterone (DHP) and allopregnanolone (8). PROG is also a precursor in the production pathway of circulating androgens and estrogens. The predominant circulating androgen in males, testosterone (T), is produced by the testis and converted within tissues to the more potent 5α-dihydrotestosterone (DHT) by the enzyme 5α-reductase. Androgens can also be converted to estrogens in tissues expressing aromatase, including regions of the CNS. The predominant circulating estrogens and progestogens in females are produced by the ovaries. Estrogens, androgens, and progestogens act via the classical ligand-activated nuclear receptors, estrogen receptors (ERα and ERβ), androgen receptor (AR), and progesterone receptor (PR), respectively, resulting in transcriptional regulation of target genes and biological pathways.

Multiple lines of evidence support steroid hormones as important determinants of ALS onset and progression. Plasma cortisol levels were elevated in sporadic ALS (sALS) patients (9, 10) which was linked to dysfunction in the hypothalamic–pituitary–adrenal (HPA) axis with potential to impact sex steroid hormone regulation and production. Serum PROG is also elevated in ALS patients and levels correlated with favorable prognostic factors (9, 11). The sex bias in ALS incidence dissipates in patients at >55 years and is no longer present >65 years (12), suggesting the higher circulating estrogen levels in premenopausal women may be protective (13). These studies were supported by findings from the Euro-MOTOR Study, which associated a lifetime exposure to exogenous estrogen and PROG with a reduced risk of developing ALS (13). The case for androgen involvement is more complex higher prenatal circulating T was associated with increased ALS risk (14) and supports the notion that early-life influences may underpin future neuronal vulnerability, rather than circulating T in adulthood. Like other sex steroid hormones, circulating T levels also decline with age in males (15) and is accelerated in men with sALS (16). Interestingly in sALS females, T levels were elevated compared with control counterparts (17). Finally, there has been an ongoing theory that increased frequency of ALS occurring among several male clusters is linked to the possible use of anabolic steroids, including athletes (18), professional footballers (19), and military personnel (20).

Mutations in superoxide dismutase 1 (SOD1) account for 20% of fALS cases with over 100 different mutations described (21). The SOD1^{G93A} transgenic mouse model remains one of the most robust and well characterized models used in ALS preclinical research today. Sexually dimorphic differences have been shown in this model with males exhibiting consistently earlier disease onset with survival differences observed only on specific genetic background (22) and differential responses to drugs and therapeutic interventions often observed between sexes (23). Castration of male SOD1^{G93A} mice does not alter disease onset or survival; the subsequent treatment of castrated mice with DHT preserves motor neurons and improves survival (24), but the opposite occurs when anabolic steroid nandrolone is given (25). Ovariectomy in female SOD1^{G93A} mice accelerates disease progression (26, 27) and 17β-estradiol (E2) given to male SOD1^{G93A} mice decreased inflammasome components typically produced by astrocytes (28). PROG administration to male SOD1^{G93A} was similarly found to be neuroprotective delaying progression of motor dysfunction, reducing mutant SOD1 levels and motor neuron loss (29). With clear evidence that circulating steroid hormones are modulating the disease in both ALS patients and mouse models, little focus has been given to the mechanisms underlying these observations and how these impact upon motor neurons. Previously our group showed less AR expression in the spinal cord of SOD1^{G93A} symptomatic male mice which was further reduced by castration (30). Conversely, both ERα and ERβ are elevated in the spinal cords of male SOD1^{G93A} mice (28).

Here, we comprehensively determined the expression of the major sex steroid hormone receptors in motor neuron and glial cell populations within lumbar spinal cords of male and female mice. More importantly, we explored potential dysregulation of all key sex hormone receptors over disease progression in male and female SOD1^{G93A} mice for the first time.

Materials and Methods

Materials

Culture media and reagents were Gibco™ brand purchased from Life Technologies (Australia). Dextran-coated charcoal was purchased from Sigma (Australia) and serum was treated overnight (2 g/100 mL) according to the manufacturer's protocol to remove hormones. Cycloheximide solution, dansyl chloride, 5α-androstan-17β-ol-3-one (5α-DHT), 5α-pregnane-3, 20-dione (DHP), E2, 17α-hydroxyprogesterone-d_8, PROG, and T were purchased from Sigma-Aldrich.

C2C12 cell line

C2C12 myoblasts (RRID:CVCL_0188) were kindly gifted by Professor Gordon Lynch, University of Melbourne. AR expression in the C2C12 cell line has been well characterized and was selected to confirm AR protein stability in response to agonist DHT (31). We confirmed the validity of these cells in the absence of available Short Tandem Repeat (STR) DNA profiling for murine cell lines through morphological features and specific myocyte markers following differentiation (all supplementary material and figures are located in a digital research materials repository (32)). Briefly, C2C12 myoblasts were maintained in a 37°C, 5% CO_2, humidified incubator in pyruvate-free Dulbecco's modified Eagle's medium containing L-glutamine and supplemented with 100 U/mL penicillin, 100 µg/mL streptomycin, and 10% fetal bovine serum. Myoblasts were seeded into 6-well plates or onto collagen-coated glass coverslips in 48-well plates. Once myoblasts reached confluency, cells were switched to media containing 2% horse serum and differentiated for 5 days with daily media replacement.

Androgen receptor protein stability in C2C12 cell line

For treatment, after 5 days of differentiation, all media were replaced with phenol red free containing 2% charcoal-stripped horse serum for 12 hours prior to sample lysis to ensure no exposure to endogenous steroid hormones present in the media. Cells were treated with vehicle (0.1% ethanol:dimethyl sulfoxide), 10 nM DHT, 50 µg/mL cycloheximide, or combined cycloheximide with DHT. Cycloheximide was added 30 minutes prior to DHT to ensure cessation of protein translation. Following 1, 3, 6, and 12 hours of treatment, cells were processed for protein or ribonucleic acid (RNA) extraction as detailed below. Cells grown on coverslips were fixed in 4% paraformaldehyde for 10 minutes before being twice washed in phosphate-buffered saline (PBS) and processed for immunocytochemistry as detailed in (32).

Animals and tissue collection

Animal experiments were approved by the Florey Institute of Neuroscience and Mental Health Animal Ethics Committee (approval number 15-060-FINMH) and conducted in accordance with the Australian National Health and Medical Research Council published Code of Practice. Transgenic $SOD1^{G93A}$ mice (B6.Cg-Tg($SOD1*^{G93A}$)1Gur/J line, stock number 004435) purchased from the Jackson Laboratory (Bar Harbor, ME, USA) were maintained on a C57BL/6J background. Animals were group housed under standard 12 hours light–dark conditions with access to standard rodent chow and water ad libitum. At P60, P90, P120, and P150 days of age, animals were killed by administering a lethal dose of sodium pentobarbitone (100 mg/kg, intraperitoneally) and blood was collected via cardiac puncture into ethylenediamine tetraacetate (2.5 µmol/tube) tubes; organs were collected, weighed, and snap frozen in dry ice for further processing. Serial blood sampling was obtained by monthly submandibular bleed. An additional cohort of P120-140 mice were collected for spinal cord steroid hormone analysis. Females were assessed for estrous cycle staging by vaginal cytology (33) and killed during diestrus. These mice were cardiac perfused with 0.1 M PBS to remove circulating steroid hormones and whole spinal cords were snap frozen and stored at –80°C prior to analysis. For immunohistochemistry mice were cardiac perfused with 0.1 M PBS followed by 4% paraformaldehyde and cryoprotected in a sucrose gradient for up to 5 days prior to snap freezing in isopentane.

RT-qPCR analysis

Cells were treated with DHT as above for 1, 6, and 12 hours alongside vehicle control before RNA was extracted using the RNeasy Mini Kit (Qiagen, Cat# 74104) according to manufacturer's protocol. RNA was extracted from lumbar spinal cord using the RNeasy Mini Kit following manufacturer's protocol with the following modifications: tissue was homogenized in QIAzol Lysis Reagent (Qiagen, Cat# 79306) using the TissueLyserLT (Qiagen) for 5 minutes at 50 Hz and RNA containing phase isolated using chloroform prior to further extraction. cDNA was reverse transcribed using iScript™ Reverse Transcription Supermix (Bio-Rad, Cat# 1708841) under the following polymerase chain reaction (PCR) conditions: 5 minutes at 25°C, 30 minutes at 42°C, and 5 minutes at 85°C. qPCR was performed as previously described (34) using SsoAdvanced™ Universal SYBR® Green Supermix (Bio-Rad, Cat# 1725270) and run in 96-well format using CFX Manager™ 3.1 software (RRID:SCR_003375) on a CFX96™ Touch Real-Time PCR Detection System (Bio-Rad). Primers were designed using Primer3 v0.4.0 design tool (http://bioinfo.ut.ee/primer3-0.4.0/, RRID:SCR_003139) and detailed in Table 1. Triplicate samples were analyzed and Ct values normalized to a housekeeping gene. Fold change between groups was determined using the $2^{-\Delta\Delta Ct}$ method. P60 to P120 data were normalized to housekeeping gene *Hprt1*, and P150 data were normalized to *PPIA* (35), which is not affected by endstage $SOD1^{G93A}$ phenotype.

Immunoblotting. Cells were lysed on ice in Triton-X lysis buffer containing protease and phosphatase inhibitor cocktail tablets (Roche). Supernatants were quantified for protein using the Direct Detect® Infrared Spectrometer (Millipore). Spinal cord was homogenized by sonication in ice-cold RIPA buffer (50 mM Tris-Cl, pH 7.4, 150 mM NaCl, 0.1% sodium dodecyl sulfate, 1% sodium deoxycholate, and 1% Triton-X 100) containing protease and phosphatase inhibitor cocktail tablets. Sonication was performed at 50% amplitude (Q55 Sonicator, Sonica, Newtown, CT, USA) with pulses applied over 10 to 15 seconds and samples incubated on ice prior to centrifugation at 4°C to isolate soluble protein fraction. Total protein of supernatants was quantified using the BCA assay according to the manufacturer's protocol (Pierce® BCA assay kit, Thermo Fisher, Cat# 23225). Protein lysates were denatured and electrophoresed through 4% to 20% Mini-PROTEAN® TGX Stain-Free™ gels (for cell, SPD5A1 and PR

Table 1. Mouse primers

Gene name	Target protein	Forward Primer 5′-3′	Reverse Primer 5′-3′
Ar	AR	GTG AAA TGG GAC CTT GGA TG	GCC AGA AGC TTC ATC TCC AC
Esr1	ERα	TGC AAT GAC TAT GCC TCT GG	CTC CGG TTC TTG TCA ATG GT
Esr2	ERβ	ACT GCC AAT CAT CGC TTC TC	AGT AAC AGG GCT GGC ACA AC
Pgr	PR	GGT GGA GGT CGT ACA AGC AT	GGA TTT GCC ACA TGG TAA GG
Srd5a1	5α-reductase 1	TTG CGG TGT ATG CTG AAG AC	CAG GAT GTG GTC TGA GTG GA
Srd5a2	5α-reductase 2	AAT GTG CTG CTG GGT CTC TT	AGA AGG CAG TGG CTT TCA GA
Hprt1	HPRT1	GAT CAG TCA ACG GGG GAC AT	CAT TTT GGG GCT GTA CTG CTT
PPIA	Cyclophilin A	CTT GGG CCG CGT CTC CTT C	TGC CGC CAG TGC CAT TAT

Table 2. Primary antibodies

Target	Host/Clonality (target)	Manufacturer	Application dilution	RRID
AR	Rabbit monoclonal (EPR1535(2))	Abcam	WB 1:1000, IHC 1:200, IF 1:100	AB_11156085 (85)
PR	Mouse monoclonal (PR-AT 4.14)	Invitrogen	WB 1:1000	AB_2164327 (86)
PR	Rabbit monoclonal (SP2)	Invitrogen	IHC 1:20	AB_10980030 (87)
ERα	Rabbit polyclonal (MC-20)	Santa Cruz	WB 1:500	AB_631470 (88)
ERα	Rabbit polyclonal (C1355)	Millipore	IHC 1:200	AB_310305 (89)
ERβ	Rabbit Monoclonal (clone 68-4)	Millipore	WB 1:2000, IHC 1:400	AB_11212759 (90)
SRD5A1	Goat polyclonal	Abcam	WB 1:500	AB_10859343 (91)
NFH/SMI-32	Mouse monoclonal	Biolegend	IHC 1:1000	AB_2715852 (92)
Iba1	Mouse monoclonal (Iba1/AIF1)	Millipore	IHC 1:200	AB_10917271 (93)
CD11b	Rat monoclonal (clone 5C6)	Bio-Rad	IHC 1:100	AB_321292 (94)
GFAP	Rat monoclonal (2.2B10)	Invitrogen	IHC 1:500	AB_2532994 (95)
APC	Mouse monoclonal (clone CC-1)	Millipore	IHC 1:13	AB_213434 (96)
Olig2	Mouse monoclonal (clone 211F1.1)	Millipore	IHC 1:200	AB_10807410 (97)

blots lysate) or 4% to 15% Criterion™ TGX Stain-Free™ gels (Bio-Rad Laboratories, NSW, Australia) and transferred onto a PVDF membrane using a Trans-Blot® Turbo™ Transfer System (Bio-Rad). For PR blots transfer was conducted using wet-transfer cassette overnight at 20 V, 4°C. Total protein on the membrane was imaged on a ChemiDoc™ MP Imaging System (Bio-Rad Laboratories, NSW, Australia) prior to blocking with 5% low-fat milk powder in Tris-Buffered Saline, 0.1% Tween® 20 Detergent (TBST). 5α-reductase 1 (SRD5A1) blots were alternatively blocked in animal-free blocking solution (Cell Signalling Technology). Blots were probed with primary antibodies overnight at 4°C as detailed in Table 2. Membranes were probed with respective secondary antibodies; StarBright™ Blue 700 goat antirabbit secondary antibody (1:5000, Bio-Rad, Cat# 12004161, RRID:AB_2721073 (36)), DyLight 800 goat antimouse secondary antibody (1:5000, Bio-Rad, Cat. #STAR117D800GA, RRID:AB_10845157 (37)) or Alexa Fluor®-488 donkey antigoat (1:3000, Jackson ImmunoResearch, Cat. #705-545-147, RRID:AB_2336933 (38)) for 1 hour at room temperature and imaged on a ChemiDoc™ MP. For analysis, background adjusted total band intensity was normalized against background adjusted total lane protein intensity using Image Lab 6.0 software (Bio-Rad, www.bio-rad.com/en-au/product/image-lab-software, RRID:SCR_014210). Average group values were then expressed fold relative to averaged control group values (expressed as 1.0).

Immunohistochemistry. Lumbar spinal cord tissue was cryosectioned at 20 µm and mounted 1:10 series onto poly-L-lysine coated slides. Antigen retrieval was performed prior to AR staining by baking slides for 2 hours at 95°C in 10 mM citrate buffer (pH 6.0). Sections were blocked in 10% (v/v) normal donkey serum with 0.3% (v/v) Triton-X 100 in 0.1 M PBS for 1 hour room temperature. Prior to AR and PR staining, endogenous avidin–biotin blocking was performed according to the manufacturer's kit (Endogenous Avidin/Biotin Blocking Kit, Abcam, Cat# ab64212). Primary antibodies, detailed in Table 2, were prepared in 2% (v/v) normal donkey serum in 0.3% (v/v) Triton-X 100 in 0.1 M PBS for 48 hours of incubation at 4°C. An additional 2 hours of incubation at room temperature with donkey biotinylated antirabbit (1:100, Jackson ImmunoResearch Cat# 711-065-152, RRID:AB_2340593 (39)) was included to amplify the AR and PR detection. Secondary antibodies were incubated for 2 hours at room temperature in the same antibody diluent, including streptavidin Alexa Fluor®-488 (1:200, Jackson ImmunoResearch Cat. #016-540-084, RRID:AB_2337249 (40)), antirabbit Alexa Fluor®-488 (1:200, Jackson ImmunoResearch Cat. #711-545-152, RRID:AB_2313584 (41)), antimouse DyLight®-550 (1:200, Invitrogen, Cat. #SA5-10167, RRID:AB_2556747 (42)), antimouse F(ab′)$_2$ Fragment Alexa Fluor®-647 (1:200, Jackson ImmunoResearch, Cat. #715-606-151, RRID:AB_2340866 (43)), antirat DyLight®-550 (1:200, Invitrogen, Cat. #SA5-10027, RRID:AB_2556607 (44)), and antirat Alexa Fluor®-647 (1:200, Jackson ImmunoResearch, Cat. #712-605-153, RRID:AB_2340694 (45)). For APC and Olig2 dual staining, tissue was blocked with additional M.O.M® blocking reagent (Vector Laboratories, Cat #MKB-2213) and APC

Table 3. Quantification of steroid hormone receptor expression in male spinal cord

Receptor	Cell population	% cells expressing receptor		*P* value[b]	Figure reference
		WT	SOD1^{G93A}		
AR	Motor neurons	81 ± 3.4	67 ± 3.5	**.025**	1A
	Motor neurons (female)[a]	50 ± 6.2	42 ± 8.9	.525	1A
ERα	Astrocytes	79 ± 2.2	76 ± 4.0	.500	3B
	Astrocytes (processes)	13 ± 1.5	82 ± 7.9	**.0002**	3B
	Microglia	0	15 ± 4.6	**.032**	3C
	Oligodendrocytes	37 ± 7.5	36 ± 2.2	.910	3D
ERβ	Astrocytes (processes)	78 ± 7.2	73 ± 3.9	.568	5B
	Microglia	0	31 ± 2.6	**.0003**	5C
	Oligodendrocytes	61 ± 5.5	67 ± 14	.731	5D

Bold represents significant *P* values (<.05).
[a]*P* = .0004 comparing male and female by 2-way ANOVA.
[b]Student's t-test to compare WT and SOD1^{G93A}.

staining detected using secondary antibody—antimouse IgG2b Alexa Fluor®-647 (1:250, Invitrogen, Cat. #A-21242, RRID:AB_2535811 (46)). Sections were re-blocked with antimouse Fab fragment (1:30, Jackson ImmunoResearch, Cat. #115-007-003, RRID:AB_ 2338476 (47)) for 1 hour at room temperature before Olig2 primary antibody incubation for 24 hours at 4°C followed by antimouse DyLight®-550 secondary antibody as above. Hoechst 33342 (Invitrogen) was used as a nuclear stain. Images were acquired at 40× magnification on a Leica SP8 confocal microscope with Z-stacked fields taken at 0.5 µm per step through a 10 µm stack. For quantification of images, steroid hormone receptor presence was counted in relevant cell types and expressed as a percentage of total cell type (Table 3). A minimum of 2 fields of view were counted per ventral horn and averages of n = 3 mice were quantified.

LC/MS-MS analysis of steroid hormones in the spinal cord

Extraction procedure for steroid from plasma was performed as previously described (34). Frozen spinal cord ~50 mg was homogenized in 0.5 mL of ice cold methanol containing 100 pg/mL of internal standard using TissueLyserLT (Qiagen) for 2 × 5 minutes at 50 Hz. Another 0.5 mL of methanol was added and samples sonicated using probe sonicator at 30% until no course tissue remained. Homogenates were incubated at 4°C overnight with gentle agitation. Samples were centrifuged at maximum speed for 10 minutes and supernatant collected. Pellets were washed twice in additional volumes of methanol. Combined supernatants were dried down using a rotary evaporator under 200 mbar, and pellets reconstituted in 200 µL of 50/50 (v/v) methanol and water. For E2 detection, samples were derivatized with dansyl chloride for detection; samples were resuspended in 50 µL of a 1 g/L dansyl chloride (prepared in acetone) and 50 µL 100 mM sodium bicarbonate at pH 10.5 and vortexed. Tubes were heated at 70°C for 10 minutes, and cooled before and additional 100 µL of a 50:50 (v/v) acetonitrile and water was added. After an additional centrifuge at maximum speed for 10 min samples.

T, DHT, E2, PROG, DHP, and 17α-hydroxyprogesterone-d8 as an internal standard, were analyzed by ultrahigh pressure liquid chromatography (UHPLC) tandem mass spectrometry (MS/MS). UHPLC-MS/MS coupled with an Agilent 6490 triple quadrupole (QQQ) mass spectrometer. Liquid chromatography was performed on an Agilent UHPLC system equipped with a 1290 Infinity II pump, degasser, an autosampler, and a temperature-controlled column compartment. Chromatographic separation for steroids was achieved on an Agilent Poroshell 120 C18 (2.1 µm, 1.8 internal diameter × 100 mm) column connected with a guard column. The column oven temperature was maintained at 35°C and the injection volume was set to 10 µL. A gradient mobile phase consisting of 1 mM ammonium fluoride in water (A) and methanol (B), at a flow rate of 0.25 mL/min was used. Quantitation of the target analytes was performed in multiple reaction monitoring mode on an Agilent Jet Stream/ESI source in dual (positive and negative) mode. The specific multiple reaction monitoring transitions for DHT, PROG, DHP, and E2 (derivatized) were monitored (20 ms dwell time/transition) at *m/z* 291.2 > 255.2, 315.3 > 109.2, 317.3 > 109.2, and 506.7 > 156.1, respectively, and have been previously reported for T and internal standard (34). All analyses were quantified using retention times and the ratios of selected precursor and product ions with those of standards. Data analysis was performed using Agilent Mass Hunter software (version B. 07.1, RRID:SCR_015040). Steroids in spinal cord tissue were calculated based on solvent standards adjusted for extraction and processing recovery from tissue spiked standards, with a limit of quantitation and method validation details provided in McLeod et al. (32).

Data analysis and statistics

Steroid receptor transcript data, western blot data, plasma T, and PROG data were analyzed using 2-way analysis of variance (ANOVA) with Sidak's multiple comparison test for planned comparisons between wildtype (WT) and SOD1^{G93A} counterparts where F-value indicated a statistically significant difference ($P < .05$). AR levels in C2C12 cells were analyzed by 2-way ANOVA with Tukey's multiple comparisons test to compare treatments within each time point. Receptor expressing cell counts, PROG, SRD5A1 western blot data, and

steroid level in spinal cord data were compared by Student's t-test between WT and SOD1^{G93A} or where equal variance assumption was violated the nonparametric Mann–Whitney test was used. All analyses were performed using GraphPad Prism 8.0 software (San Diego, CA, USA) and data presented as mean ± standard error of the mean (SEM).

Results

AR is enriched in spinal motor neurons and is downregulated in symptomatic SOD1^{G93A} mice

AR immunostaining was present in nuclei of neurons in the spinal cord with robust staining in the spinal motor neurons of P150 WT male mice identified by SMI-32 neurofilament marker (Fig. 1A). AR staining was markedly less intense in SOD1^{G93A} males. The frequency of AR^{+} motor neuron nuclear staining in female spinal cords was ~38% lower than male counterparts (Table 3), with representative motor neurons positive for AR shown Fig. 1A and quantified in Table 3. In male spinal cord, no AR signal was detected in GFAP^{+} astrocytes (Fig. 1B) or Iba1^{+} microglia (Fig. 1C).

Levels of AR transcript in lumbar spinal cord were comparable between males and females at all time points P60-150 (Fig. 2A-2D). At P150, male and female SOD1^{G93A} mice showed 20% to 30% reduced AR transcript levels, compared to WT counterparts (Fig. 2D). AR protein was detected as a single 110 kDa band in lumbar spinal cord (Fig. 2E-2H) as validated using several anti-AR antibodies against testis lysate and AR knockout tissue as positive and negative controls, respectively, and reported in McLeod et al. (32). Consistent with our previous findings, AR protein expression in females was <50% of male levels (34). In males, AR protein was depleted in SOD1^{G93A} mice, compared with WT, over the disease course with 43% and 22% reduction in AR observed at P120 and P150, respectively (Fig. 2I-2L). This AR protein loss was reflected in the ventral horn immunohistochemistry at P150, AR^{+} nuclei were detected in 81% of motor neurons and significantly decreased in SOD1^{G93A} mice with only 67% of remaining motor neurons positive for AR (Fig. 1A and Table 3).

ERα is expressed in motor neurons and glial cells of the spinal cord and becomes abundant in the reactive astrocytes of symptomatic SOD1^{G93A} mice

ERα immunostaining showed most intensity in the nuclei of SMI-32^{+} motor neurons in male and female ventral horns (Fig. 3A). In WT male spinal cord, ERα was similarly present in nuclei of GFAP^{+} astrocytes and in symptomatic SOD1^{G93A} mice, with immunoreactivity

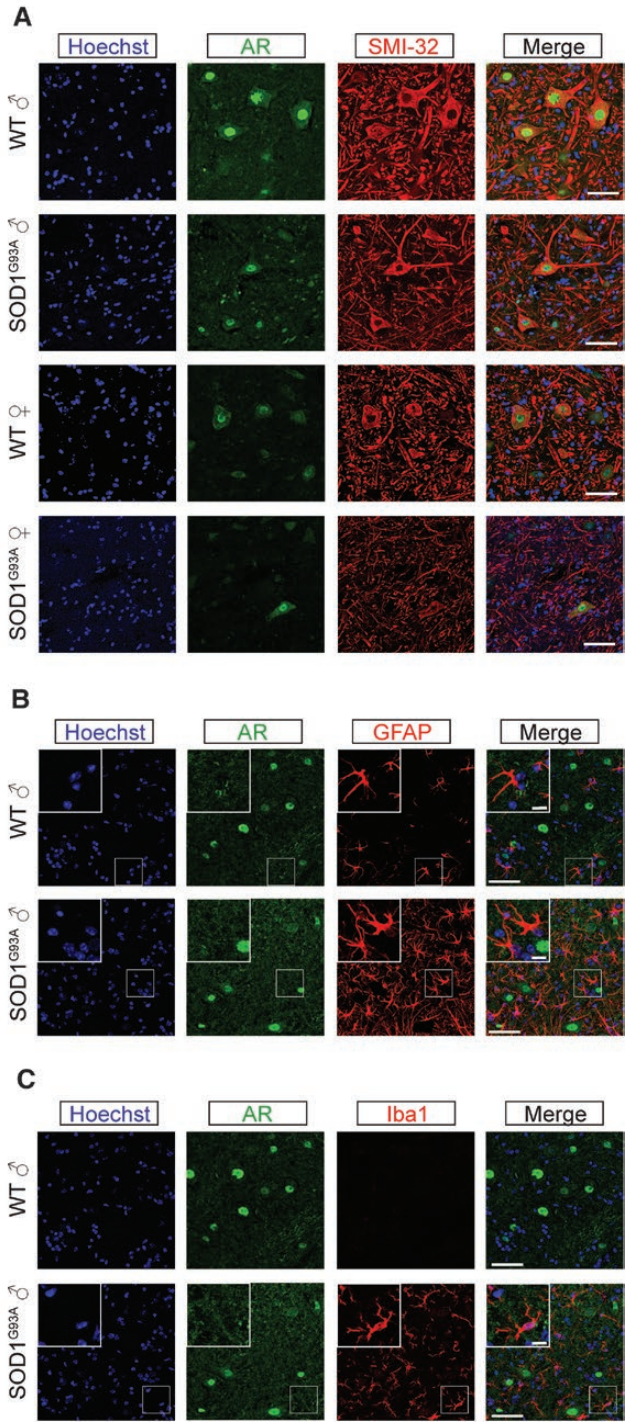

Figure 1. AR immunostaining in motor neurons and glial cells within the lumbar spinal cord of WT and SOD1^{G93A} mice at 150 days. (A) AR localization to the nucleus of SMI-32 positive motor neurons in the ventral horn of male and female mice. (B) AR does not show localization in GFAP-positive astrocytes or (C) Iba1-positive microglia in WT or SOD1^{G93A} male spinal cords. Scale bar = 50 μm; inset = 10 μm.

in the cytoplasm and processes of reactive astrocytes increasing ~6-fold in SOD1^{G93A} mice (Fig. 3B and Table 3). Similar staining patterns were observed in female mice (32). While ERα was rarely detectable in CD11b^{+} microglia of male mice (Fig. 3C), it was present

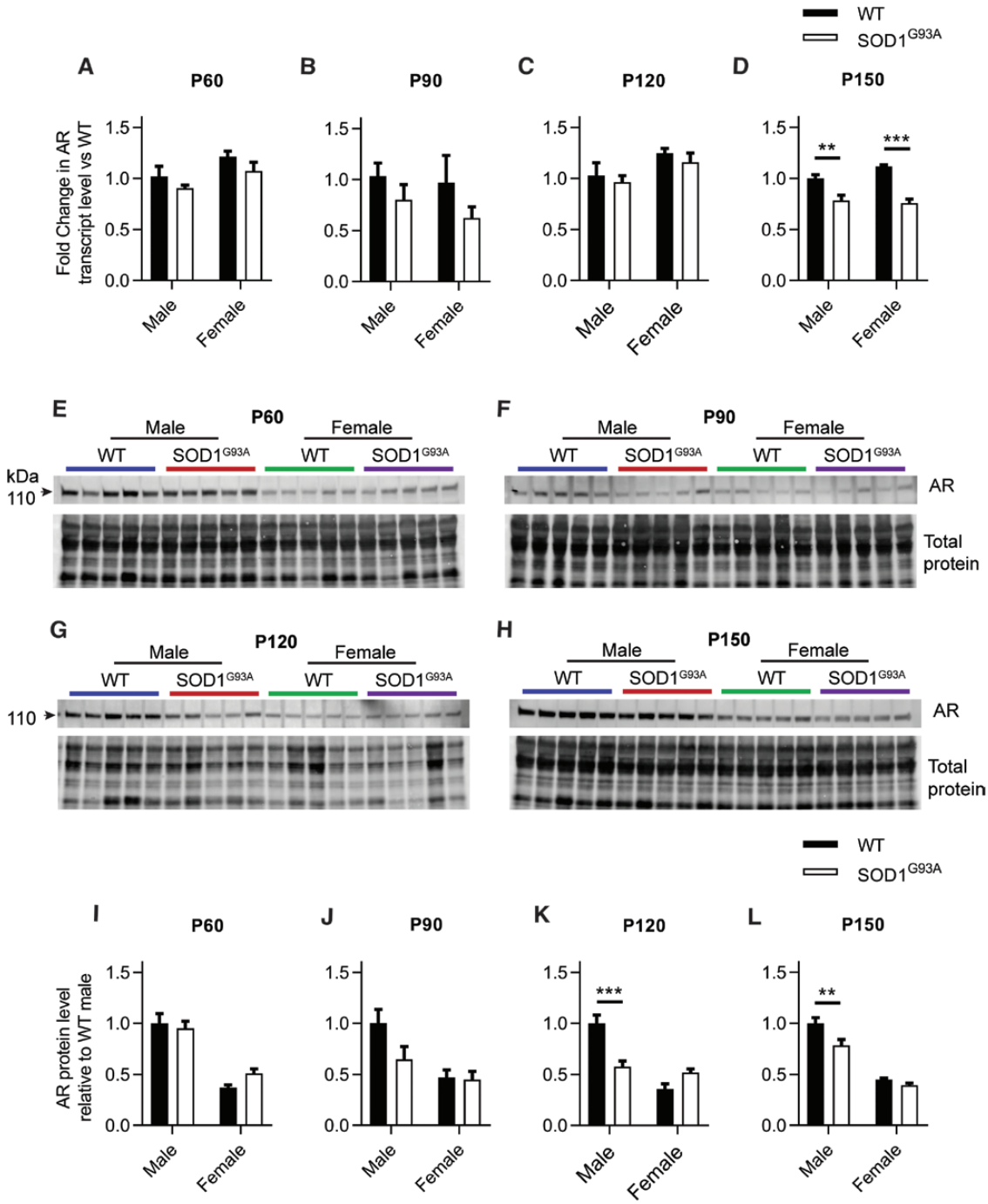

Figure 2. AR expression changes in the lumbar spinal cords of male and female WT and SOD1^{G93A} mice. (A-D) AR transcript changes at P60, 90, 120, and 150. (e-h) AR immunoblots and (I-L) quantification of AR levels relative to male control group is shown for P60, 90, 120 and 150. Mean ± SEM, n = 5; $^{**}P < .01$, $^{***}P < .001$ by 2-way ANOVA with Sidak's multiple comparisons test comparing genotype effect.

in microglia in females (32), and at a lower abundance than astrocytes (Table 3).

To identify oligodendrocytes, we used dual markers against Olig2 and APC (CC-1). Due to previously reported overlap of these markers with developing astrocytes, we determined staining overlap between GFAP, Olig2, and APC in WT and SOD1^{G93A} spinal cord ventral horns (32). Olig2 localized in the nuclei of GFAP^{+} astrocytes predominantly in WT spinal cords (32) and these Olig2^{+}/GFAP^{+} astrocytes did not show APC staining (32). This matches the expression profile found by Guo and colleagues (48) where in the ventral horn spinal cord gray matter of healthy adult mice, 91% of GFAP^{+} cells were also Olig2^{+}, but not in white matter astrocytes. Olig2 is also present in oligodendrocyte progenitor cells and mature oligodendrocytes, the latter expressing cytoplasmic APC (48). APC^{+} oligodendrocytes in both WT and SOD1^{G93A} mice showed Olig2^{+}

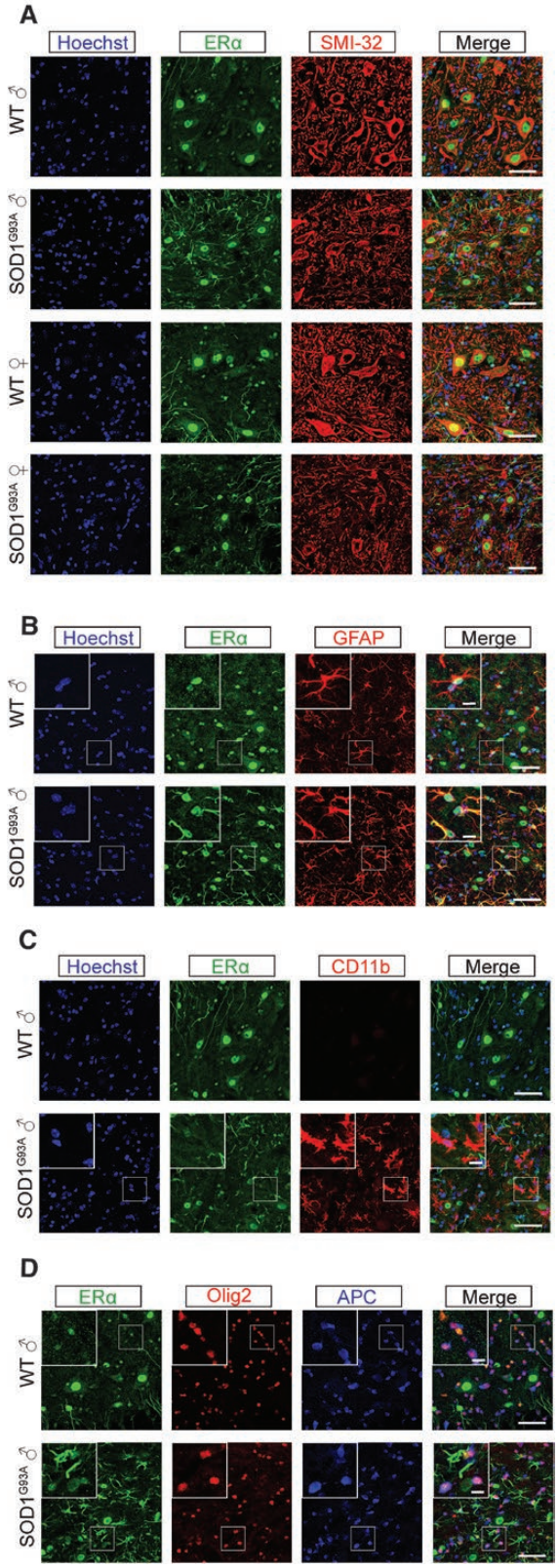

Figure 3. ERα immunostaining in motor neurons and glial cells within the lumbar spinal cord of WT and SOD1^{G93A} mice at 150 days. (A) ERα localization to the nucleus of SMI-32 positive motor neurons in the ventral horn of male and female mice. (B) ERα localization in the nuclei of GFAP-positive astrocytes and prominent in astrocytic processes of reactive SOD1^{G93A} spinal cord, (C) Iba1-positive microglia show minimal ERα expression, and (D) olig2 and APC-positive oligodendrocytes in WT or SOD1^{G93A} male spinal cords. Scale bar = 50 μm; inset = 10 μm.

nuclear staining (32). Conversely, SOD1^{G93A} mouse reactive astrocytes (identified by their hypertrophic cell body and abundant ramifications) lacked Olig2 nuclear expression, unlike WT astrocytes (32). This is possibly due to reactive astrocytes arising from proliferation and transformation of local quiescent protoplasmic astrocytes (48), rather than from oligodendrocyte progenitor cells as previously thought. ERα showed weak expression in nuclei of Olig2$^+$/APC$^+$ oligodendrocytes of WT males (Fig. 3D and Table 3) with noticeably higher expression in Olig2$^+$/APC$^-$ nuclei, most likely representing astrocytes (32). Similarly, in SOD1^{G93A} male mice, most Olig2$^+$/APC$^+$ oligodendrocytes showed weak positive ERα staining with noticeably less ERα$^+$/Olig2$^+$/APC$^-$ astrocytes present. Similar staining profiles were observed in female mice (32).

Levels of ERα transcript (*ESR1*) in the lumbar spinal cord were comparable between males and females at time points P90-150 (Fig. 4B-D), with P60 showing significantly higher transcription in females than in males in WT mice only (Fig. 4A). At P150, male and female SOD1^{G93A} mice revealed 36% and 21% elevated ERα transcription, respectively, compared with WT counterparts (Fig. 4D). ERα protein was detected as a ~65 kDa band in the lumbar spinal cord (Fig. 4E-H) as validated using 2 anti-ERα antibodies against mouse uterus lysate and human ER-overexpressing cell lines as positive controls as reported in McLeod et al. (32). ERα protein expression was comparable between WT and SOD1^{G93A} across disease progression for both male and female mice (Fig. 4I-4L) and largely similar between male and female spinal cords. Conversely to transcript levels, ERα protein levels were significantly lower in female WT than in WT males (Fig. 4I). The impact of this transient sex difference in WT mice at P60 appears unlikely to be meaningful to the disease course.

ERβ protein expression is upregulated in symptomatic SOD1^{G93A} spinal cord where it is expressed by most glial cells

ERβ was abundant in the nuclei of SMI-32$^+$ motor neurons in the ventral horn spinal cord of male and female SOD1^{G93A} mice, similar to WT mice (Fig. 5A). ERβ was detectable in nuclei only of GFAP$^+$ astrocytes of both WT and SOD1^{G93A} males (Fig. 5B) and females (32). In symptomatic male SOD1^{G93A} mice, ERβ was also present in CD11b$^+$ microglia (Fig. 5C) and in most Olig2$^+$/APC$^+$ oligodendrocyte nuclei in both WT and SOD1^{G93A} male ventral horn gray matter (Fig. 5D), showing approximately twice the number of glia expressing nuclear ERβ compared with ERα in these 2 cell populations (Table 3). Levels of ERβ transcript (*ESR2*) in the lumbar spinal cord were

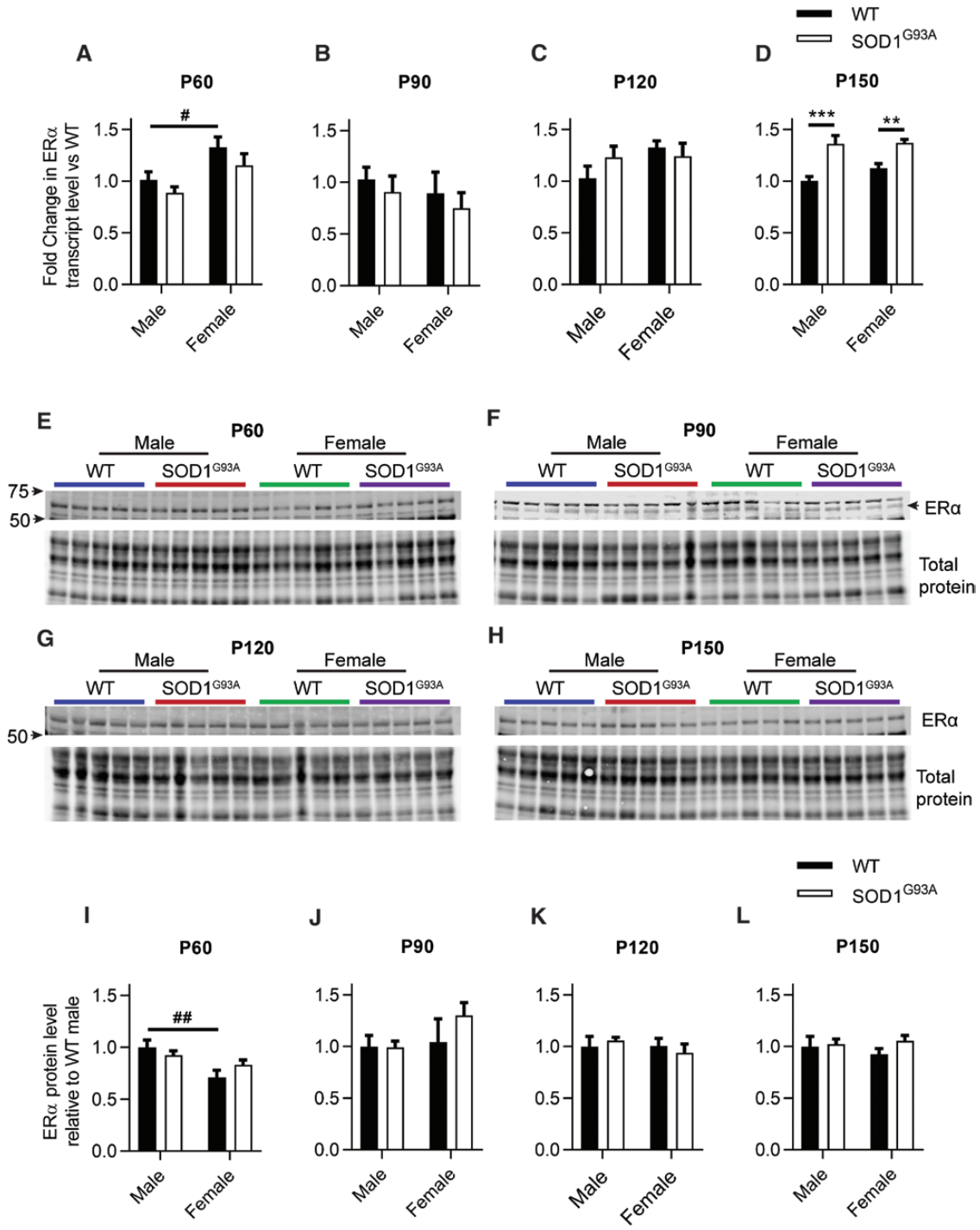

Figure 4. ERα expression changes in the lumbar spinal cords of male and female WT and SOD1^{G93A} mice. (A-D) ERα transcript changes at P60, 90, 120, and 150. (E-H) ERα immunoblots and (I-L) quantification of ERα levels relative to male control group is shown for P60, 90, 120, and 150. Mean ± SEM, n = 5; $^{**}P < .01$, $^{***}P < .001$ by 2-way ANOVA with Sidak's multiple comparisons test comparing genotype effect. $^{\#}P < .05$, $^{\#\#}P < .01$, by 2-way ANOVA with Sidak's multiple comparisons test comparing sex effect.

comparable between males and females at time points P90-150 (Fig. 6B-6D), with the exception of P60 females showing significantly higher transcription than male counterparts in both WT and SOD1^{G93A} mice (Fig. 6A). At P150, male SOD1^{G93A} mice revealed 18% reduction in ERβ transcript levels ($P = .067$ approaching significance) and female SOD1^{G93A} mice showed significant 15% reduction in ERβ transcript compared with WT counterparts (Fig. 6D). ERβ protein was detected as a ~69 kDa band in the lumbar spinal cord (Fig. 6E-H) appearing as a single clean band presentation on immunoblot (32). ERβ was identified by sodium dodecyl sulfate polyacrylamide gel electrophoresis as a band migrating between ~55

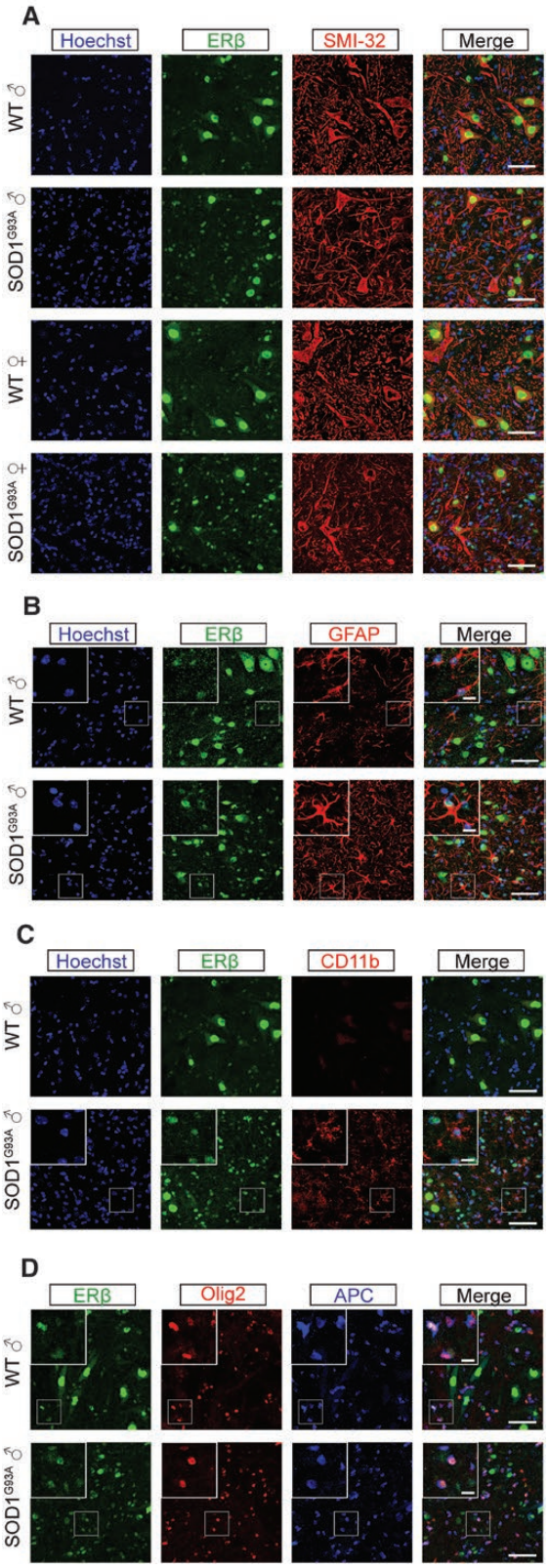

Figure 5. ERβ immunostaining in motor neurons and glial cells within the lumbar spinal cord of WT and SOD1^{G93A} mice at 150 days. (A) ERβ localization to the nucleus of SMI-32 positive motor neurons in the ventral horn of male and female mice. (B) ERβ localization in the nuclei of GFAP-positive astrocytes in WT and SOD1^{G93A} spinal cord, (C) Iba1-positive microglia, and (D) olig2 and APC-positive oligodendrocytes in WT and SOD1^{G93A} male spinal cords. Scale bar = 50 μm; inset = 10 μm.

and 70 kDa depending on the tissue, and our detection matches results previously described for both mouse and rat brain ERβ (49). ERβ protein expression was comparable between WT and SOD1^{G93A} in presymptomatic disease stages for both male and female mice (Fig. 6I and 6J) and increased in symptomatic SOD1^{G93A} spinal cord (Fig. 6K and 6L). At P120, male SOD1^{G93A} mice showed 36% increase in ERβ protein levels (P = .077 trending significance) and female SOD1^{G93A} mice demonstrated a significant 67% increase in ERβ protein levels compared with WT counterparts (Fig. 6K). At P150, male SOD1^{G93A} mice showed a significant 114% increase in ERβ protein levels, while female SOD1^{G93A} mice revealed a 44% increase in ERβ protein levels compared with WT counterparts (Fig. 6L). Interestingly, ERβ transcript and protein expression changes were opposing. There was a marked increase in ERβ immunoreactive nuclei abundance in both SOD1^{G93A} male and female spinal cord and the elevation in ERβ protein expression detected by western blot is likely a reflection of infiltration and or proliferation of ERβ^{+} glial cells, namely microglia and oligodendrocytes.

PR is primarily expressed in motor neurons and glial cells of the spinal cord

Like other sex steroid hormone receptors, PR predominated in the nucleus of motor neurons in the spinal cord (Fig. 7A). PR was difficult to detect outside motor neurons in the ventral horn which may reflect its low abundance and limitations of antibody-mediated detection. WT spinal cords did not show PR staining in GFAP^{+} astrocytes, although it was detected in a few reactive astrocytes within SOD1^{G93A} mouse cord (Fig. 7B). No PR immunoreactivity was evident in WT or SOD1^{G93A} mouse CD11b^{+} microglia in ventral horns of either male (Fig. 7C) and female mice (32). In SOD1^{G93A} male ventral horn gray matter, PR was found at low frequency and abundance in some Olig2^{+}/APC^{+} oligodendrocytes (Fig. 7D). In the white matter border of the ventral horn, colocalization of PR within the cytoplasm of APC^{+} oligodendrocytes was more apparent (Fig. 7D). These oligodendrocytes were mixed positive or negative for Olig2 expression (Fig. 7D inset). Similar immunoreactivity was observed in the white and gray matter within female spinal cord (32).

Levels of PR transcript in the lumbar spinal cord were comparable between males and females at all time points P60-150 (Fig. 8A-8D). At P150, male and female SOD1^{G93A} mice revealed ~20% reduced PR transcription compared with WT counterparts (Fig. 8D). PR protein in the lumbar spinal cord was detected as

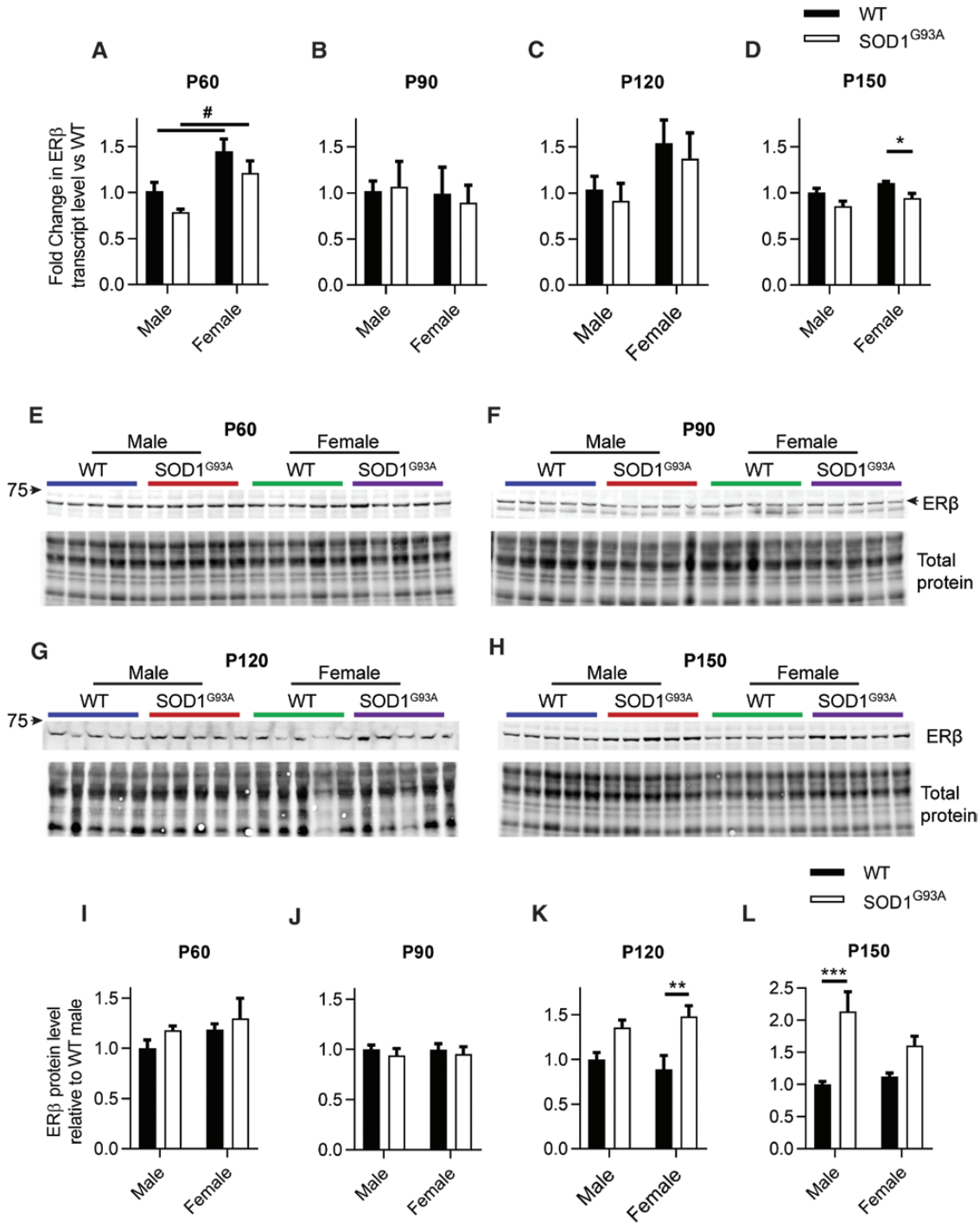

Figure 6. ERβ expression changes in the lumbar spinal cords of male and female WT and SOD1^{G93A} mice. (A-D) ERβ transcript changes at P60, 90, 120, and 150. (E-H) ERβ immunoblots and (I-L) quantification of ERβ levels relative to male control group is shown for P60, 90, 120, and 150. Mean ± SEM, n = 5; $^{*}P < .05$, $^{**}P < .01$, $^{***}P < .001$ by 2-way ANOVA with Sidak's multiple comparisons test comparing genotype effect. $^{\#}P < .05$ by 2-way ANOVA with Sidak's multiple comparisons test comparing sex effect.

a 94 kDa band (Fig. 8E-8H) representing the PR-A isoform as validated against mouse reproductive tissues and PR-expressing human cell lysates as positive controls (32). Male and female spinal cords were analyzed on separate immunoblots; therefore, we cannot report this comparison, although based on unpublished findings we believe levels are similar. PR protein expression was comparable between WT and SOD1^{G93A} male and female mice (Fig. 8I-L).

AR protein stability is increased by androgen presence

To confirm the regulation of AR transcript and protein expression by androgens, we used the C2C12 muscle

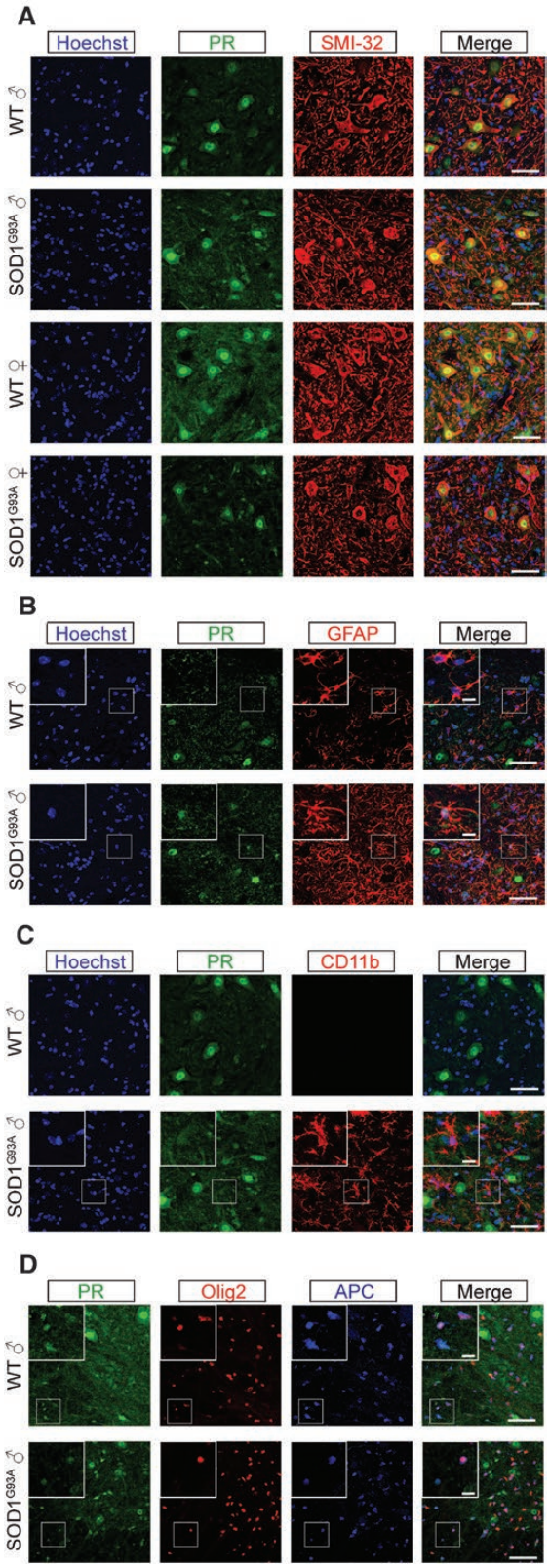

Figure 7. PR immunostaining in motor neurons and glial cells within the lumbar spinal cord of WT and SOD1^{G93A} mice at 150 days. (A) PR localization to the nucleus of SMI-32 positive motor neurons in the ventral horn of male and female mice. (B) PR does not show localization in GFAP-positive astrocytes or (C) Iba1-positive microglia in WT or SOD1^{G93A} male spinal cords, (D) with olig2 and APC-positive oligodendrocytes showing PR immunostaining. Scale bar = 50 μm; inset = 10 μm.

cell line as it abundantly expresses endogenous AR (31). Cycloheximide is a known protein synthesis inhibitor in eukaryotes (50). As C2C12 myoblasts are highly proliferative and likely sensitive to translation blockade, we differentiated cultures into terminal myotubules and quiescent reserve cells which were confirmed by immunocytochemistry (32). The impact of cycloheximide on cell viability was determined by MTT assay (32) and the optimal dose of 50 μg/mL effectively decreased polyubiquitinated proteins (32). AR protein levels show a time-dependent increases in response to DHT treatment and time-dependent reduction in response to cycloheximide treatment (Fig. 9A and 9B and (32)) with AR transcript levels unaltered by DHT (Fig. 9C). With protein synthesis blocked by cycloheximide, AR protein turnover ceases and declining AR levels reflect rate of AR degradation. When cells are treated with DHT in the presence of cycloheximide, this degradation rate is reduced through the stabilization of AR, most evident after 12 hours. In the absence of cycloheximide, the rate of AR synthesis most likely exceeds the degradation of DHT-bound AR, thereby receptor levels accumulate over time. Similarly, we observed AR protein stabilization in human embryonic stem cell-derived motor neurons in response to DHT treatment, without an increase in AR transcriptional activity (32). Together these data support the idea that androgens increase AR through protein stabilization, rather than increased translation. Hence, AR protein depletion in the spinal cord of male SOD1^{G93A} mice may be the result of local androgen deficiency.

5α-Reductase enzyme isoforms (SRD5A1 and 2) are differentially altered in symptomatic SOD1^{G93A} spinal cord

5α-Reductase or SRD5A is a group of 3 isoenzymes that are involved in sex steroid metabolism, namely the conversion of T to DHT and PROG to DHP. Levels of SRD5A1 transcript in the lumbar spinal cord were comparable between males and females at all time points P60-150 (Fig. 10A-D). At P150, male and female SOD1^{G93A} mice showed 36% and 80% increase in SRD5A1 transcript levels compared with WT counterparts, respectively (Fig 10D). As the SRD5A1 isoform is highly expressed in the liver, we compared P150 liver transcripts of SOD1^{G93A} mice with WT and found a 28% reduction in males compared to WT with females unchanged (32). Hence, SRD5A1 transcript appears to be differentially altered in central and peripheral tissues of male SOD1^{G93A} mice. SRD5A1 protein in WT lumbar spinal cord was detectable at very low levels as a 29 kDa band (Fig. 10E) which was more prominent in symptomatic SOD1^{G93A} tissue. To confirm the specificity

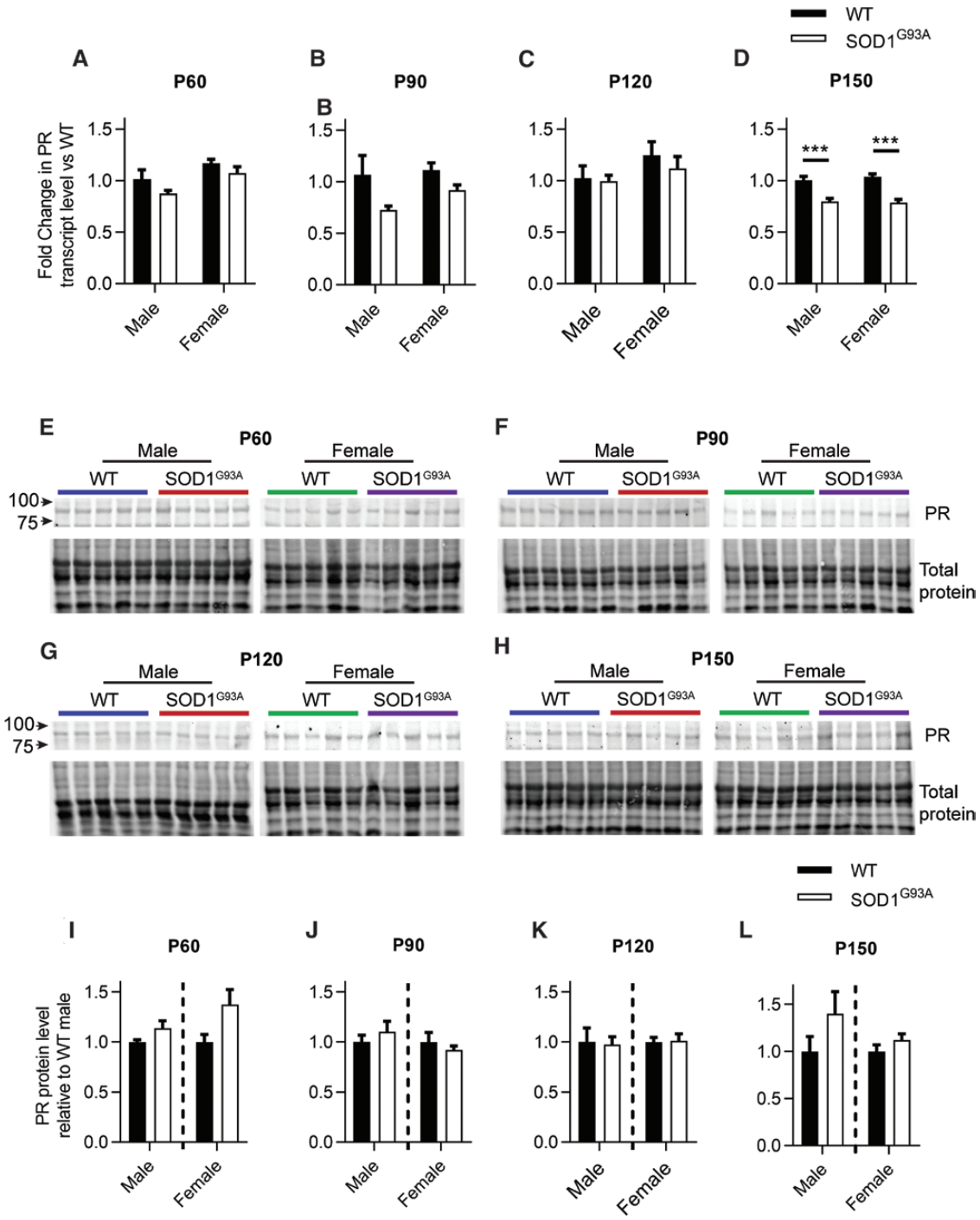

Figure 8. PR expression changes in the lumbar spinal cords of male and female WT and SOD1^{G93A} mice. (A-D) PR transcript changes at P60, 90, 120, and 150. (E-H) PR immunoblots and (I-L) quantification of PR levels relative to WT counterpart is shown for P60, 90, 120, and 150. Mean ± SEM, n = 5; ***P < .001 by 2-way ANOVA with Sidak's multiple comparisons test comparing genotype effect.

of this band, we compared immunoblot against the isotype control antibody (32). Male and female spinal cords were analyzed on separate immunoblots; therefore, we cannot report this protein level comparison. SRD5A1 protein expression reflected P150 transcriptional changes, with a 9-fold and 3-fold increase in SOD1^{G93A} male and female spinal cord, respectively, when compared with WT counterparts (Fig. 10F). The 5α-reductase 2 (SRD5A2) isoform showed sex-specific differences in expression with transcript levels on average 70% lower in WT females compared with males (Fig. 10G-J). In males, there was a progressive decline in SRD5A2 transcript level of SOD1^{G93A} mice spinal cord over disease course with a 40% reduction at P120 (P = .055 approaching significance) and significant 60% reduction at P150 compared with WT level.

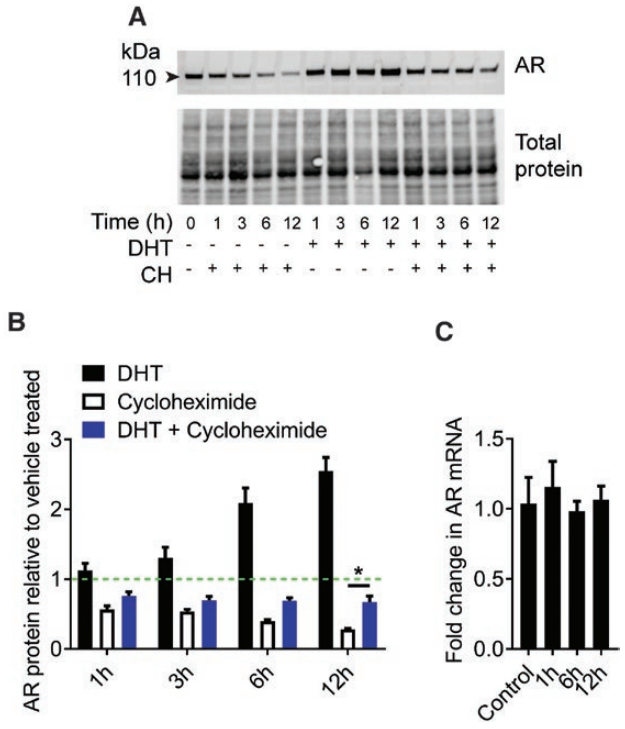

Figure 9. Effect of DHT on AR transcript and protein level in C2C12 muscle cell line. (A) Immunoblot of AR in C2C12 cell lysates following 0-12 hours of treatment with AR agonist dihydrotestosterone (DHT) and/or protein translation inhibitor, cycloheximide (CH). (B) Quantification of AR levels relative to untreated control cell lysate. Mean ± SEM, n = 4; *P < .05 by 2-way ANOVA with Tukey's multiple comparisons test to compare treatments within each time point. (C) AR transcript changes in C2C12 cell lysates following 1, 6, and 12 hours of DHT treatment compared with baseline. Mean ± SEM, n = 3.

SRD5A2 is highly expressed in the male prostate; therefore, we determined if this altered transcript was present in male SOD1^{G93A} prostate and found levels to be comparable to WT (32). Hence the reduction in SRD5A2 transcript level appears to be specific to the spinal cord. We were unable to confirm protein expression levels due to lack of effective antibodies against mouse SRD5A2.

Steroid hormone profiles in symptomatic SOD1^{G93A} mouse spinal cord

Steroid hormones were profiled in the spinal cord and plasma of SOD1^{G93A} and WT counterparts to investigate changes which may reflect the alterations in steroid receptors and metabolic enzymes observed in symptomatic SOD1^{G93A} mice. Male circulating total T levels showed a high degree of variation (Fig. 11A) even when serially sampled from the same mice over time, a phenomenon which has been previously described (51). Plasma T levels increased from P60 onwards with a mean of 1 to 2.5 ng/mL typical of adult male mice with minimal evidence of a change in SOD1^{G93A} compared with WT. This was mirrored in unchanged seminal vesicle weights (32) which reflect circulating T levels. Similarly, prostate weights were comparable between WT and SOD1^{G93A} males (32), while testes were significantly smaller in SOD1^{G93A} mice across all time points (32). With testis weight largely not impacted by circulating androgen levels (34), this may reflect the direct action of altered SOD1 activity within the testis (52). Male circulating PROG levels declined over time from ~1 to 0.2 ng/mL from P60-150 (Fig. 11B) with a clear drop in the SOD1^{G93A} PROG levels at P120 compared with WT (656 vs 377 ng/mL in WT and SOD1^{G93A}, respectively, but not significant by 2-way ANOVA analysis). With circulating levels not necessarily reflecting tissue levels due to local steroid synthesis and metabolism, we measured tissue levels of the major steroid hormones in symptomatic male and female SOD1^{G93A} mice. T levels reflected circulating levels trending towards decrease in SOD1^{G93A} mice (3.7 ± 1.3 pg/mg vs 2.2 ± 0.7 pg/mg WT and SOD1^{G93A} males, respectively) and again highly variable levels observed between individual mice (Fig. 11C). Females showed no genotype influence with T levels only ~2% of males (0.07 ± 0.02 pg/mg vs 0.08 ± 0.02 pg/mg WT and SOD1^{G93A} females, respectively). DHT, the product of 5α-reductase metabolism of T and a more potent ligand of AR, reflected trends in T at ~10-fold lower concentrations in males (0.29 ± 0.08 pg/mg vs 0.22 ± 0.4 pg/mg WT and SOD1^{G93A} males, respectively) and was not quantifiable in female spinal cord (Fig. 11D). In the spinal cord, E2 levels may reflect circulating concentrations and local production from the conversion of T by aromatase. Previous analysis of circulating E2 levels in symptomatic SOD1^{G93A} mice showed no changes in male or female mice when compared with respective WT counterparts, with levels being 3- to 4-fold higher in female mice, although possible estrous cycle variability was not mentioned (28). In spinal cord we observed ~3-fold higher E2 levels in females than in males during diestrus when circulating E2 levels would be expected to be at their lowest in females (Fig. 11E). Interestingly, female SOD1^{G93A} mice exhibited a significant 35% reduction in spinal cord E2 levels, compared to WT females (0.40 ± 0.03 pg/mg vs 0.26 ± 0.02 pg/mg WT and SOD1^{G93A} females, respectively). PROG levels in male spinal cord also showed no change in SOD1^{G93A} mice (Fig. 11F) with general levels of PROG being twice as high in females spinal cord during diestrus when circulating PROG levels peak. Female SOD1^{G93A} mice exhibited a striking 49% reduction in spinal cord PROG levels, compared to WT females (1.76 ± 0.20 pg/mg vs 0.91 ± 0.14 pg/mg WT and SOD1^{G93A} females, respectively). DHP, the product of 5α-reductase metabolism of PROG, showed

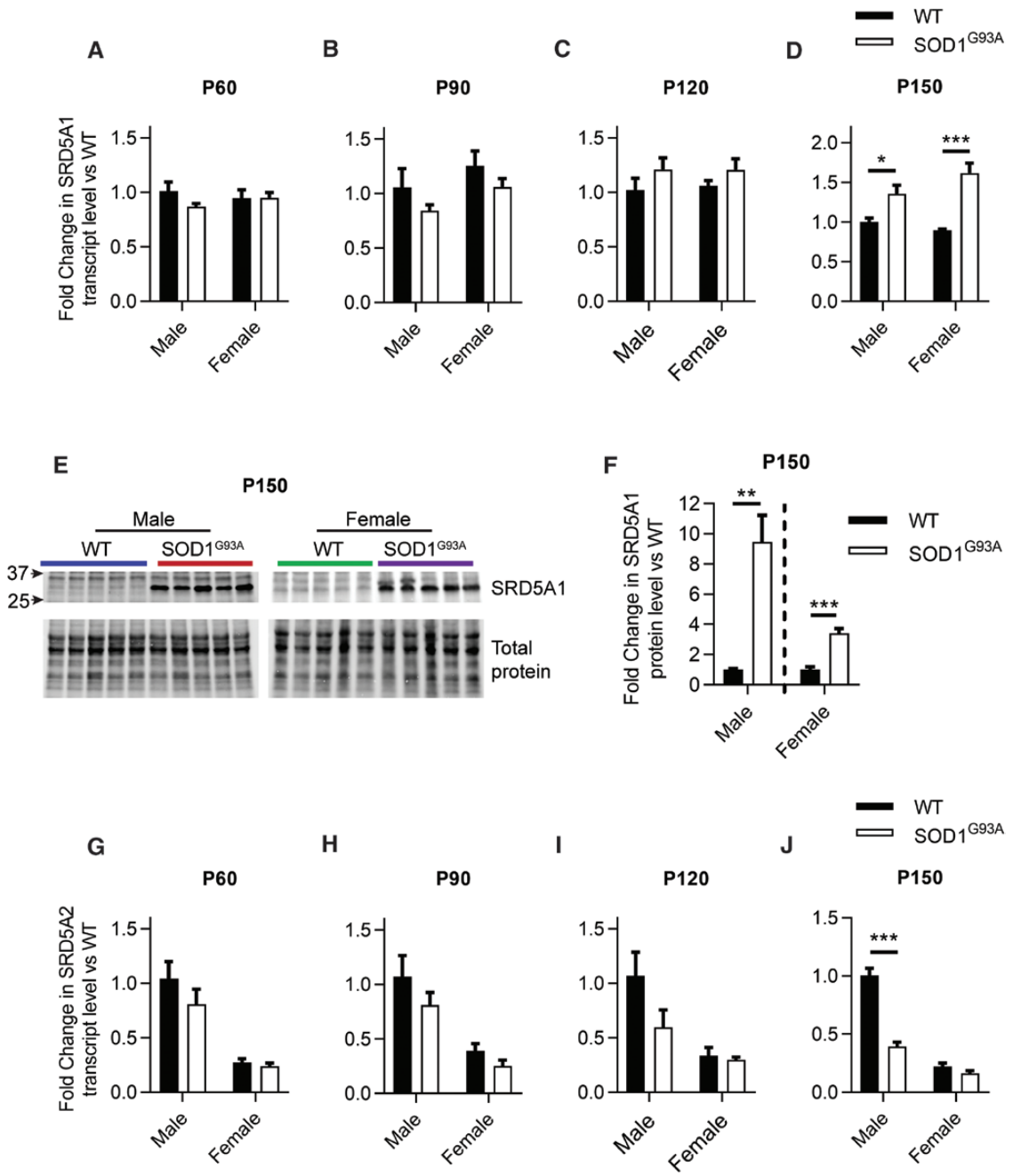

Figure 10. 5α-Reductase isoform (SRD5A1 and SRD5A2) expression changes in the lumbar spinal cords of male and female WT and SOD1^{G93A} mice. (A-D) SRD5A1 transcript changes at P60, 90, 120 and 150. (E) SRD5A1 immunoblots and (F) quantification relative to WT counterparts in P150 male and female spinal cord. Mean ± SEM, n = 5; $^{**}P < .01$, $^{***}P < .001$ by Mann–Whitney test and Student's t-test for male and female analysis, respectively. (G-J) SRD5A2 transcript changes at P60, 90, 120, and 150. Mean ± SEM, n = 5; $^{*}P < .05$, $^{***}P < .001$ by 2-way ANOVA with Sidak's multiple comparisons test comparing genotype effect.

~10-fold lower concentrations in males (5.9 ± 1.6 pg/mg vs 4.9 ± 0.8 pg/mg WT and SOD1^{G93A} males, respectively) than in females (42 ± 5.7 pg/mg vs 56.8 ± 21 pg/mg WT and SOD1^{G93A} female, respectively), with no difference seen between WT and SOD1^{G93A} levels (Fig. 11G). Uterine and ovary weights (32) were comparable between symptomatic SOD1^{G93A} and WT mice, and did not indicate any physiological changes in reproductive organs or estrous status between genotypes. We observed no difference in the duration of estrous cycling between WT and SOD1^{G93A} which was approximately 4 days for both genotypes.

Discussion

Sex-specific differences in epidemiology and clinical phenotypes are well known in sporadic and familial

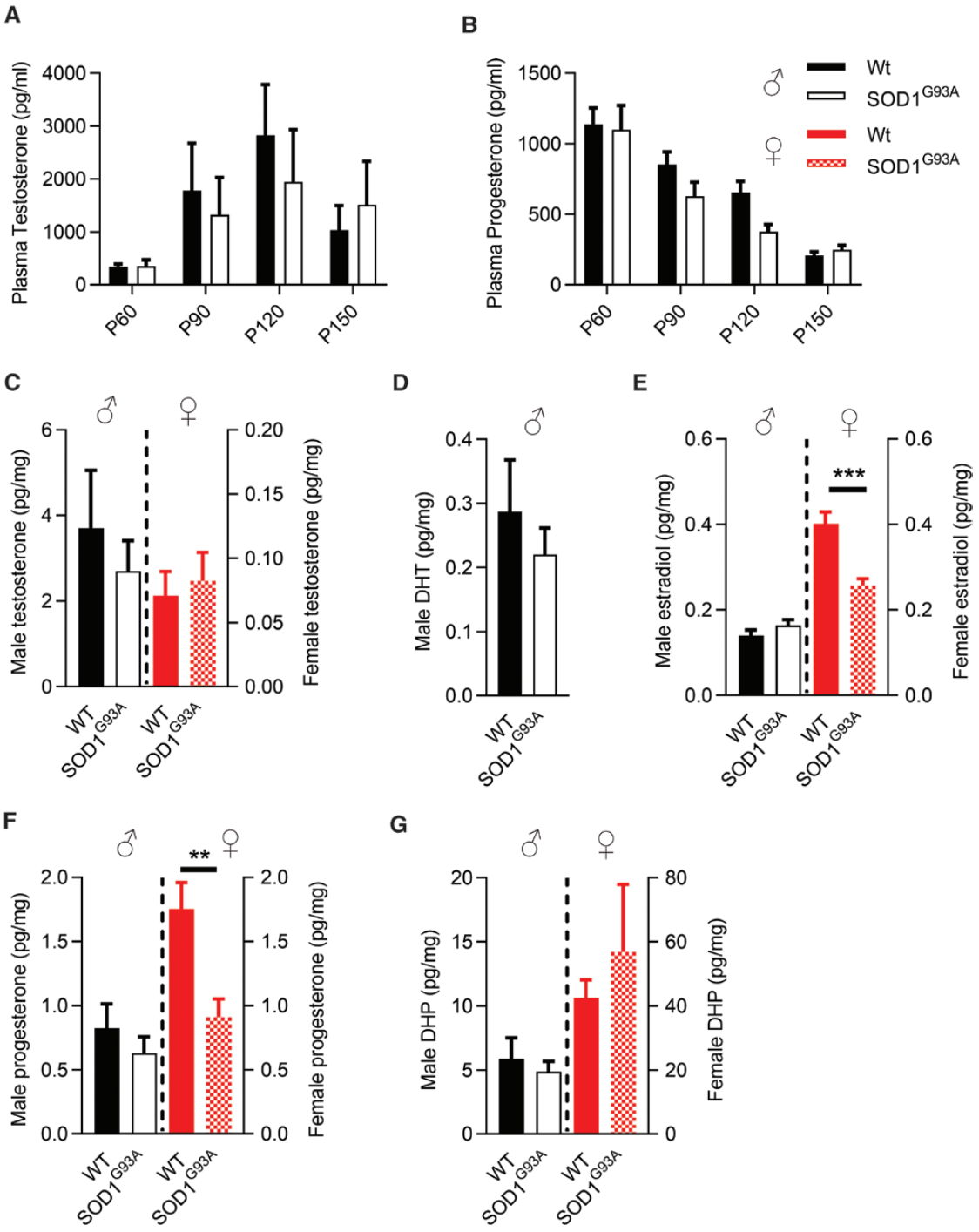

Figure 11. Plasma and spinal cord steroid hormone profiles in WT and SOD1^{G93A} mice. (A) Plasma testosterone and (B) progesterone concentrations in male mice at P60, 90, 120, and 150. Mean ± SEM, n = 5-15. Steroid analysis in whole spinal cords of male (left axis, black bars) and female (right axis, red bars) symptomatic SOD1^{G93A} mice compared with WT for (C) testosterone, (D) DHT, (E) 17β-estradiol, (F) progesterone, and (G) DHP. Mean ± SEM, n = 7-12; $^{**}P < .01$, $^{***}P < .001$ by Student's t-test.

ALS with links to circulating steroids (1, 2, 6). Likewise, the SOD1^{G93A} and TDP43^{A315T} transgenic mouse models of ALS reflect this sexual dimorphism (22, 53). Our study examined the fundamental mediators of androgen, estrogen and progestogen signaling pathways, namely nuclear receptors, their cellular expression in the ventral horn spinal cord and expression changes over disease course in the SOD1^{G93A} mice. We observed that AR was decreased in symptomatic SOD1^{G93A} mice without major disruptions to spinal cord T and DHT levels. ERα strongly associated with astrocytes and ERβ was upregulated in symptomatic SOD1^{G93A} spinal cord where it is present in glial cells.

AR, ERα, ERβ, and PR were observed in the nucleus of motor neurons where they are required to actively bind to response elements of target genes. AR uniquely

was the only steroid hormone receptor showing sex-specific differences in expression level within the spinal cord and disease-dependent dysregulation in SOD1^{G93A} male mice. We confirmed that androgen presence is influencing AR levels in both cultured myocytes and motor neurons through stabilization of the AR protein, as previously described (54, 55). This is reflected in the comparable transcript level in the spinal cords of male and female mice, whereas females have spinal cord T levels that are 2% of those found in male cord and about half the protein expression detectable by immunoblot. The primary AR ligands present in the spinal cord are T and its more potent metabolite DHT. The 2 ligands differ in their binding kinetics with AR, with DHT dissociating from AR ~3 to 5 times slower than T (56) giving rise to 10-fold higher potency of DHT in motor neurons (34). Analysis of steroid hormone levels in whole cord revealed no significant net changes in T or DHT between WT and SOD1^{G93A} male mice although subregional spinal cord changes cannot be ruled out. The ratio of T to DHT in the lumbar region of WT male mice was ~1.3 compared with ~6 in the cervical spinal cord (57), highlighting the abundance of DHT in lumbar and potentially SRD5A2 activity.

SRD5A2 primarily converts T to DHT (58) and its expression tends to follow the trajectory of androgens and AR localization (59). In rat brain and spinal cord, SRD5A2 is expressed in large pyramidal neurons and ventral horn motor neurons and is absent from glial cells (60, 61). In male rat lumbar spinal cord, this isoform predominates over SRD5A1 transcript (61). Therefore, the loss in SRD5A2 transcription in SOD1^{G93A} male mice localizes the androgen deficit to vulnerable motor neurons, as evidenced by the reduced AR detectable in the nuclei of motor neurons of male P150 male SOD1^{G93A} mice. Systemic DHT administration to SOD1^{G93A} male mice was neuroprotective (24), selectively improving survival of motor neurons in the lumbar region relative to cervical spinal cord and increased survival time in mice by approximately 8 days. DHT is more effective than T at upregulating AR protein level in the CNS (62). DHT stimulates dendritic arborization and synaptic plasticity in hypothalamic neurons (63), promotes neurite outgrowth in cultured motor neurons (64) and stabilizes dendritic outgrowth of the spinal nucleus bulbocavernosus motor neurons (65). Taken together, our data support evidence of an inherent loss in DHT production within lumbar motor neurons of SOD1^{G93A} male mice via a downregulation of SRD5A2 enzyme, and likely renders them vulnerable through the loss of androgen trophic support.

A robust increase in SRD5A1 mRNA and protein levels occurred in the lumbar spinal cord of both female and male SOD1^{G93A} mice. This isoform is generally more widely expressed at higher levels than SRD5A2 and is found in both neurons and glial cells (66) catalyzing the conversion of T to DHT and PROG to DHP. In females, we determined a reduction in PROG levels in the spinal cord which may indicate increased metabolism, however in males appears to be unchanged. Interestingly, we also detected lower levels of E2, alongside PROG, in the female SOD1^{G93A} spinal cord which could indicate altered steroid production within the ovaries. Females exhibited much higher DHP levels than males, which reflects findings in the spinal cords of rats (67) although levels were unchanged in SOD1^{G93A} mouse counterparts. DHP is further metabolized to the neurosteroid allopregnanolone, which was highly upregulated in lumbar of Wobbler mouse model of motor neuron degeneration (68). An anticipated increase in DHP level through upregulation in SRD5A1 in SOD1^{G93A} mice could be balanced by increased DHP metabolism, therefore, further characterization of these steroidogenesis pathways in the SOD1^{G93A} mouse spinal cord is warranted to understand these changes.

Interestingly we found that ERα and ERβ mRNA, protein expression, and localization were comparable between male and female lumbar spinal cord, despite E2 being lower in male mice. In males, E2 is formed in situ from the aromatase conversion of T in the spinal cord. While others have shown aromatase presence in motor neurons and glial cells of mouse spinal cord (69, 70) we were unable to accurately detect quantifiable mRNA or protein levels of aromatase further supporting the notion that DHT is the steroid hormone central to male lumbar spinal cord functions. Unlike AR, ERα resides in the nucleus with and without ligand bound (71, 72) and E2 can induce ERα degradation via the proteasome pathway (72). Hence, receptor localization to the nucleus is not necessarily indicative of activation of classical signaling pathways. We found ERα was strongly present in motor neurons and astrocytes and to a lesser extent microglia and oligodendrocytes in line with other studies (28, 73). In symptomatic SOD1^{G93A} mice, ERα presence was striking in the cytoplasmic processes, as well as nuclei of GFAP-positive astrocytes, similarly to ALS patients, where ERα strongly localizes within reactive astrocytes but not microglia or macrophage lineage cells (74). ERα is considered to be primarily responsible for E2 signaling in astrocytes and acts via extranuclear located receptors (75, 76) modulating the neuroprotective and anti-inflammatory actions of E2 in the CNS (77). We previously reported a lower

astrocyte presence in SOD1^{G93A} female mice than in males at symptomatic age (34) and exogenous E2 administration in SOD1^{G93A} males reduced astrocytic mediated neuroinflammation molecules NLRP3, activated caspase 1, and IL-1β (28). Our data show that reactive astrocytes express high levels of extranuclear ERα regardless of local E2 level and present a therapeutic target to modulate neuroinflammation in ALS.

We showed a robust increase in ERβ protein in male and female SOD1^{G93A} lumbar spinal cords in line with others (28). Nuclear ERβ staining was seen in all glial cell types, including microglia of SOD1^{G93A} mice, and this increased protein level may reflect an infiltration of glial cells into the spinal cord. Our data show ERβ is present in a greater proportion of microglia and oligodendrocytes than ERα and these may be preferential sites of action for E2 signaling via ERβ. ERβ in neurons and astrocytes was not shown to mediate the neuroprotective or anti-inflammatory effects of E2 within the CNS (78). The ERβ agonist, genistein, protected motor neurons against interferon γ-activated microglial cytokines by reducing apoptosis and upregulating ERβ protein (79), suggesting a protective mechanism of increased ERβ. In a model of autoimmune encephalomyelitis, ERβ was found to be expressed by microglia and ERβ signaling modulated microglial activation and T-cell reactivity in spinal cord, improving symptoms (80). In ALS activated microglia, phenotypes can switch from the neuroprotective M2 to neurotoxic M1 phenotypes with disease progression (81). E2 treatment in male SOD1^{G93A} mice reduced microglia presence only when administered presymptomatically (28), which could indicate that the role of ERβ in microglial function may also be dependent on disease stage. The role of ERβ in microglial activation in ALS and potential targeting by selective ERβ agonists therefore warrants further investigation.

PR was expressed mainly in spinal cord motor neurons and oligodendrocytes within the white matter and is weakly detectable in reactive astrocytes in SOD1^{G93A} mice. PR is activated by both PROG and DHP, having neuroprotective and myelin-promoting actions in the central and peripheral nervous systems (82). SRD5A1, the isoform upregulated in symptomatic SOD1^{G93A} mice, is present in both neuronal and glial cells (66) and has been shown to be highly localized in myelin membranes (83). Given the locality of PR within motor neurons and white matter oligodendrocytes in mouse lumbar spinal cord, our data support previous findings these are likely targets of PROG's neuroprotective actions. White matter damage, axonal demyelination, and oligodendrocyte loss occur in ALS patients (84) and in SOD1^{G93A} mice (29) and may precede motor neuron loss. Hence, PR targeted therapies may present an early disease-modifying treatment for oligodendrocytes.

In conclusion, we have fully characterized the expression of AR, ERα, ERβ, and PR in the lumbar spinal cord of SOD1^{G93A} male and female mice. AR is downregulated with disease progression in male mice and may be associated with disruption to local steroidogenesis pathways via dysregulation of 5α-reductase expression. ERα, ERβ, and PR could present as potential targets in modulating the neuroprotective and anti-inflammatory actions of glial cells in the SOD1^{G93A} spinal cord.

Acknowledgments

Financial Support: Funding for this project was provided by the Australian NHMRC (Project Grants 1104295, 1104299), Stafford Fox Medical Research Foundation, MND Research Institute of Australia (Ted Dimmick Memorial MND Research Grant), Pratt Foundation and Mr. Tony Gray. V.M. was supported by an MND Research Institute of Australia PhD Scholarship Top-Up Grant; B.T. was supported by an NHMRC-ARC Dementia Research Leadership Fellowship 1137024.

Additional information

Correspondence: Bradley J. Turner, Florey Institute of Neuroscience and Mental Health, University of Melbourne, 30 Royal Parade, Parkville, VIC, Australia, 3052 (bradley.turner@florey.edu.au).

Disclosure Summary: The authors have nothing to disclose.

Data Availability: All data generated or analyzed during this study are included in this published article or in the data repositories listed in the References.

References

1. Blasco H, Guennoc AM, Veyrat-Durebex C, et al. Amyotrophic lateral sclerosis: a hormonal condition? *Amyotroph Lateral Scler.* 2012;**13**(6):585-588.
2. McCombe PA, Henderson RD. Effects of gender in amyotrophic lateral sclerosis. *Gend Med.* 2010;**7**(6):557-570.
3. Zubeldia-Brenner L, Roselli CE, Recabarren SE, Gonzalez Deniselle MC, Lara HE. Developmental and functional effects of steroid hormones on the neuroendocrine axis and spinal cord. *J Neuroendocrinol.* 2016;**28**(7). Doi: 10.1111/jne.12401.
4. Vegeto E, Villa A, Della Torre S, et al. The role of sex and sex hormones in neurodegenerative diseases. *Endocr Rev.* 2019;**41**(2):273-319. Doi: 10.1210/endrev/bnz005.
5. Palmieri A, Mento G, Calvo V, et al. Female gender doubles executive dysfunction risk in ALS: a case-control study in 165 patients. *J Neurol Neurosurg Psychiatry.* 2015;**86**(5):574-579.
6. Rooney J, Fogh I, Westeneng HJ, et al. C9orf72 expansion differentially affects males with spinal onset amyotrophic lateral sclerosis. *J Neurol Neurosurg Psychiatry.* 2017;**88**(4):281.

7. Trojsi F, Siciliano M, Femiano C, et al. Comparative analysis of C9orf72 and sporadic disease in a large multicenter ALS population: the effect of male sex on survival of C9orf72 positive patients. *Front Neurosci*. 2019;**13**:485.
8. Mendell AL, MacLusky NJ. Neurosteroid metabolites of gonadal steroid hormones in neuroprotection: implications for sex differences in neurodegenerative disease. *Front Mol Neurosci*. 2018;**11**:359.
9. Monachelli GG, Meyer M, Rodríguez G, et al. Progesterone and cortisol levels in sporadic amyotrophic lateral sclerosis (sALS): correlation with prognostic factors. *Horm Mol Biol Clin Investig*. 2011;**6**(1):167-173.
10. Spataro R, Volanti P, Vitale F, et al. Plasma cortisol level in amyotrophic lateral sclerosis. *J Neurol Sci*. 2015;**358**(1-2):282-286.
11. Gargiulo Monachelli G, Meyer M, Rodríguez GE, et al. Endogenous progesterone is associated to amyotrophic lateral sclerosis prognostic factors. *Acta Neurol Scand*. 2011;**123**(1):60-67.
12. de Jong S, Huisman M, Sutedja N, et al. Endogenous female reproductive hormones and the risk of amyotrophic lateral sclerosis. *J Neurol*. 2013;**260**(2):507-512.
13. Rooney JPK, Visser AE, D'Ovidio F, et al.; Euro-MOTOR Consortium. A case-control study of hormonal exposures as etiologic factors for ALS in women: Euro-MOTOR. *Neurology*. 2017;**89**(12):1283-1290.
14. Vivekananda U, Manjalay ZR, Ganesalingam J, et al. Low index-to-ring finger length ratio in sporadic ALS supports prenatally defined motor neuronal vulnerability. *J Neurol Neurosurg Psychiatry*. 2011;**82**(6):635-637.
15. Feldman HA, Longcope C, Derby CA, et al. Age trends in the level of serum testosterone and other hormones in middle-aged men: longitudinal results from the Massachusetts male aging study. *J Clin Endocrinol Metab*. 2002;**87**(2):589-598.
16. Militello A, Vitello G, Lunetta C, et al. The serum level of free testosterone is reduced in amyotrophic lateral sclerosis. *J Neurol Sci*. 2002;**195**(1):67-70.
17. Gargiulo-Monachelli GM, Sivori M, Meyer M, Sica RE, De Nicola AF, Gonzalez-Deniselle MC. Circulating gonadal and adrenal steroids in amyotrophic lateral sclerosis: possible markers of susceptibility and outcome. *Horm Metab Res*. 2014;**46**(6):433-439.
18. Harwood CA, McDermott CJ, Shaw PJ. Physical activity as an exogenous risk factor in motor neuron disease (MND): a review of the evidence. *Amyotroph Lateral Scler*. 2009;**10**(4):191-204.
19. Chiò A, Benzi G, Dossena M, Mutani R, Mora G. Severely increased risk of amyotrophic lateral sclerosis among Italian professional football players. *Brain*. 2005;**128**(Pt 3):472-476.
20. Horner RD, Kamins KG, Feussner JR, et al. Occurrence of amyotrophic lateral sclerosis among Gulf War veterans. *Neurology*. 2003;**61**(6):742-749.
21. Turner BJ, Talbot K. Transgenics, toxicity and therapeutics in rodent models of mutant SOD1-mediated familial ALS. *Prog Neurobiol*. 2008;**85**(1):94-134.
22. Pfohl SR, Halicek MT, Mitchell CS. Characterization of the contribution of genetic background and gender to disease progression in the SOD1 G93A mouse model of amyotrophic lateral sclerosis: a meta-analysis. *J Neuromuscul Dis*. 2015;**2**(2):137-150.
23. Bame M, Pentiak PA, Needleman R, Brusilow WS. Effect of sex on lifespan, disease progression, and the response to methionine sulfoximine in the SOD1 G93A mouse model for ALS. *Gend Med*. 2012;**9**(6):524-535.
24. Yoo YE, Ko CP. Dihydrotestosterone ameliorates degeneration in muscle, axons and motoneurons and improves motor function in amyotrophic lateral sclerosis model mice. *PLoS One*. 2012;**7**(5):e37258.
25. Aggarwal T, Polanco MJ, Scaramuzzino C, et al. Androgens affect muscle, motor neuron, and survival in a mouse model of SOD1-related amyotrophic lateral sclerosis. *Neurobiol Aging*. 2014;**35**(8):1929-1938.
26. Groeneveld GJ, Van Muiswinkel FL, Sturkenboom JM, Wokke JH, Bär PR, Van den Berg LH. Ovariectomy and 17beta-estradiol modulate disease progression of a mouse model of ALS. *Brain Res*. 2004;**1021**(1):128-131.
27. Yan L, Liu Y, Sun C, et al. Effects of ovariectomy in an hSOD1-G93A transgenic mouse model of Amyotrophic Lateral Sclerosis (ALS). *Med Sci Monit*. 2018;**24**:678-686.
28. Heitzer M, Kaiser S, Kanagaratnam M, et al. Administration of 17β-estradiol improves motoneuron survival and down-regulates inflammasome activation in male SOD1(G93A) ALS mice. *Mol Neurobiol*. 2017;**54**(10):8429-8443.
29. Kim J, Kim TY, Cho KS, Kim HN, Koh JY. Autophagy activation and neuroprotection by progesterone in the G93A-SOD1 transgenic mouse model of amyotrophic lateral sclerosis. *Neurobiol Dis*. 2013;**59**:80-85.
30. Sheean RK, Weston RH, Perera ND, D'Amico A, Nutt SL, Turner BJ. Effect of thymic stimulation of CD4+ T cell expansion on disease onset and progression in mutant SOD1 mice. *J Neuroinflammation*. 2015;**12**:40.
31. Wannenes F, Caprio M, Gatta L, Fabbri A, Bonini S, Moretti C. Androgen receptor expression during C2C12 skeletal muscle cell line differentiation. *Mol Cell Endocrinol*. 2008;**292**(1-2):11-19.
32. McLeod VM, Chiam MDF, Lau CL, Rupasinghe TW, Boon WC, Turner BJ. Dysregulation of steroid hormone receptors in motor neurons and glia associates with disease progression in ALS mice. Deposited 15 June 2020. Figshare. https://doi.org/10.6084/m9.figshare.12480179.v2.
33. McLean AC, Valenzuela N, Fai S, Bennett SA. Performing vaginal lavage, crystal violet staining, and vaginal cytological evaluation for mouse estrous cycle staging identification. *J Vis Exp*. 2012;(67):e4389.
34. McLeod VM, Lau CL, Chiam MDF, et al. Androgen receptor antagonism accelerates disease onset in the SOD1G93A mouse model of amyotrophic lateral sclerosis. *Br J Pharmacol*. 2019;**176**(13):2111-2130.
35. Boon WC, Diepstraten J, van der Burg J, Jones ME, Simpson ER, van den Buuse M. Hippocampal NMDA receptor subunit expression and watermaze learning in estrogen deficient female mice. *Brain Res Mol Brain Res*. 2005;**140**(1-2):127-132.
36. RRID:AB_2721073. https://scicrunch.org/resolver/RRID:AB_2721073.
37. RRID:AB_10845157. https://scicrunch.org/resolver/RRID:AB_10845157.
38. RRID:AB_2336933. https://scicrunch.org/resolver/RRID:AB_2336933.
39. RRID:AB_2340593. https://scicrunch.org/resolver/RRID:AB_2340593.
40. RRID:AB_2337249. https://scicrunch.org/resolver/RRID:AB_2337249.
41. RRID:AB_2313584. https://scicrunch.org/resolver/RRID:AB_2313584.
42. RRID:AB_2556747. https://scicrunch.org/resolver/RRID:AB_2556747.
43. RRID:AB_2340866. https://scicrunch.org/resolver/RRID:AB_2340866.
44. RRID:AB_2556607. https://scicrunch.org/resolver/RRID:AB_2556607.
45. RRID:AB_2340694. https://scicrunch.org/resolver/RRID:AB_2340694.
46. RRID:AB_2535811. https://scicrunch.org/resolver/RRID:AB_2535811.
47. RRID:AB_2338476. https://scicrunch.org/resolver/RRID:AB_2338476.
48. Guo F, Maeda Y, Ma J, et al. Macroglial plasticity and the origins of reactive astroglia in experimental autoimmune encephalomyelitis. *J Neurosci*. 2011;**31**(33):11914-11928.

49. Mitra SW, Hoskin E, Yudkovitz J, et al. Immunolocalization of estrogen receptor beta in the mouse brain: comparison with estrogen receptor alpha. *Endocrinology*. 2003;**144**(5):2055-2067.
50. Schneider-Poetsch T, Ju J, Eyler DE, et al. Inhibition of eukaryotic translation elongation by cycloheximide and lactimidomycin. *Nat Chem Biol*. 2010;**6**(3):209-217.
51. Michiel Sedelaar JP, Dalrymple SS, Isaacs JT. Of mice and men–warning: intact versus castrated adult male mice as xenograft hosts are equivalent to hypogonadal versus abiraterone treated aging human males, respectively. *Prostate*. 2013;**73**(12):1316-1325.
52. Selvaratnam JS, Robaire B. Effects of aging and oxidative stress on spermatozoa of superoxide-dismutase 1- and catalase-null mice. *Biol Reprod*. 2016;**95**(3):60.
53. Hatzipetros T, Bogdanik LP, Tassinari VR, et al. C57BL/6J congenic Prp-TDP43A315T mice develop progressive neurodegeneration in the myenteric plexus of the colon without exhibiting key features of ALS. *Brain Res*. 2014;**1584**:59-72.
54. Lee DK, Chang C. Endocrine mechanisms of disease: Expression and degradation of androgen receptor: mechanism and clinical implication. *J Clin Endocrinol Metab*. 2003;**88**(9):4043-4054.
55. Kemppainen JA, Lane MV, Sar M, Wilson EM. Androgen receptor phosphorylation, turnover, nuclear transport, and transcriptional activation. Specificity for steroids and antihormones. *J Biol Chem*. 1992;**267**(2):968-974.
56. Grino PB, Griffin JE, Wilson JD. Testosterone at high concentrations interacts with the human androgen receptor similarly to dihydrotestosterone. *Endocrinology*. 1990;**126**(2):1165-1172.
57. Gonzalez Deniselle MC, Liere P, Pianos A, et al. Steroid profiling in male wobbler mouse, a model of amyotrophic lateral sclerosis. *Endocrinology*. 2016;**157**(11):4446-4460.
58. Jin Y, Penning TM. Steroid 5alpha-reductases and 3alpha-hydroxysteroid dehydrogenases: key enzymes in androgen metabolism. *Best Pract Res Clin Endocrinol Metab*. 2001;**15**(1):79-94.
59. Eicheler W, Tuohimaa P, Vilja P, Adermann K, Forssmann WG, Aumüller G. Immunocytochemical localization of human 5 alpha-reductase 2 with polyclonal antibodies in androgen target and non-target human tissues. *J Histochem Cytochem*. 1994;**42**(5):667-675.
60. Castelli MP, Casti A, Casu A, et al. Regional distribution of 5α-reductase type 2 in the adult rat brain: an immunohistochemical analysis. *Psychoneuroendocrinology*. 2013;**38**(2):281-293.
61. Pozzi P, Bendotti C, Simeoni S, et al. Androgen 5-alpha-reductase type 2 is highly expressed and active in rat spinal cord motor neurones. *J Neuroendocrinol*. 2003;**15**(9):882-887.
62. Lu S, Simon NG, Wang Y, Hu S. Neural androgen receptor regulation: effects of androgen and antiandrogen. *J Neurobiol*. 1999;**41**(4):505-512.
63. Beyer C, Hutchison JB. Androgens stimulate the morphological maturation of embryonic hypothalamic aromatase-immunoreactive neurons in the mouse. *Brain Res Dev Brain Res*. 1997;**98**(1):74-81.
64. Marron TU, Guerini V, Rusmini P, et al. Androgen-induced neurite outgrowth is mediated by neuritin in motor neurones. *J Neurochem*. 2005;**92**(1):10-20.
65. Goldstein LA, Sengelaub DR. Differential effects of dihydrotestosterone and estrogen on the development of motoneuron morphology in a sexually dimorphic rat spinal nucleus. *J Neurobiol*. 1994;**25**(7):878-892.
66. Aumüller G, Eicheler W, Renneberg H, Adermann K, Vilja P, Forssmann WG. Immunocytochemical evidence for differential subcellular localization of 5 alpha-reductase isoenzymes in human tissues. *Acta Anat (Basel)*. 1996;**156**(4):241-252.
67. Caruso D, Pesaresi M, Abbiati F, et al. Comparison of plasma and cerebrospinal fluid levels of neuroactive steroids with their brain, spinal cord and peripheral nerve levels in male and female rats. *Psychoneuroendocrinology*. 2013;**38**(10):2278-2290.
68. Meyer M, Garay LI, Kruse MS, et al. Protective effects of the neurosteroid allopregnanolone in a mouse model of spontaneous motoneuron degeneration. *J Steroid Biochem Mol Biol*. 2017;**174**:201-216.
69. O'Brien EE, Smeester BA, Michlitsch KS, Lee JH, Beitz AJ. Colocalization of aromatase in spinal cord astrocytes: differences in expression and relationship to mechanical and thermal hyperalgesia in murine models of a painful and a non-painful bone tumor. *Neuroscience*. 2015;**301**:235-245.
70. Ji YX, Zhao M, Liu YL, Chen LS, Hao PL, Sun C. Expression of aromatase and estrogen receptors in lumbar motoneurons of mice. *Neurosci Lett*. 2017;**653**:7-11.
71. Maruvada P, Baumann CT, Hager GL, Yen PM. Dynamic shuttling and intranuclear mobility of nuclear hormone receptors. *J Biol Chem*. 2003;**278**(14):12425-12432.
72. Kocanova S, Mazaheri M, Caze-Subra S, Bystricky K. Ligands specify estrogen receptor alpha nuclear localization and degradation. *BMC Cell Biol*. 2010;**11**:98.
73. Platania P, Laureanti F, Bellomo M, et al. Differential expression of estrogen receptors alpha and beta in the spinal cord during postnatal development: localization in glial cells. *Neuroendocrinology*. 2003;**77**(5):334-340.
74. Platania P, Seminara G, Aronica E, et al. 17beta-estradiol rescues spinal motoneurons from AMPA-induced toxicity: a role for glial cells. *Neurobiol Dis*. 2005;**20**(2):461-470.
75. Kuo J, Hamid N, Bondar G, Prossnitz ER, Micevych P. Membrane estrogen receptors stimulate intracellular calcium release and progesterone synthesis in hypothalamic astrocytes. *J Neurosci*. 2010;**30**(39):12950-12957.
76. Fuente-Martin E, Garcia-Caceres C, Morselli E, et al. Estrogen, astrocytes and the neuroendocrine control of metabolism. *Rev Endocr Metab Disord*. 2013;**14**(4):331-338.
77. Spence RD, Hamby ME, Umeda E, et al. Neuroprotection mediated through estrogen receptor-alpha in astrocytes. *Proc Natl Acad Sci U S A*. 2011;**108**(21):8867-8872.
78. Spence RD, Wisdom AJ, Cao Y, et al. Estrogen mediates neuroprotection and anti-inflammatory effects during EAE through ERα signaling on astrocytes but not through ERβ signaling on astrocytes or neurons. *J Neurosci*. 2013;**33**(26):10924-10933.
79. McDowell ML, Das A, Smith JA, Varma AK, Ray SK, Banik NL. Neuroprotective effects of genistein in VSC4.1 motoneurons exposed to activated microglial cytokines. *Neurochem Int*. 2011;**59**(2):175-184.
80. Wu WF, Tan XJ, Dai YB, Krishnan V, Warner M, Gustafsson JA. Targeting estrogen receptor beta in microglia and T cells to treat experimental autoimmune encephalomyelitis. *Proc Natl Acad Sci U S A*. 2013;**110**(9):3543-3548.
81. Lall D, Baloh RH. Microglia and C9orf72 in neuroinflammation and ALS and frontotemporal dementia. *J Clin Invest*. 2017;**127**(9):3250-3258.
82. González-Orozco JC, Camacho-Arroyo I. Progesterone actions during central nervous system development. *Front Neurosci*. 2019;**13**:503.
83. Poletti A, Celotti F, Rumio C, Rabuffetti M, Martini L. Identification of type 1 5alpha-reductase in myelin membranes of male and female rat brain. *Mol Cell Endocrinol*. 1997;**129**(2):181-190.
84. Philips T, Bento-Abreu A, Nonneman A, et al. Oligodendrocyte dysfunction in the pathogenesis of amyotrophic lateral sclerosis. *Brain*. 2013;**136**(Pt 2):471-482.
85. RRID:AB_11156085. https://scicrunch.org/resolver/AB_11156085.
86. RRID:AB_2164327. https://scicrunch.org/resolver/AB_2164327.
87. RRID:AB_10980030. https://scicrunch.org/resolver/AB_10980030.
88. RRID:AB_631470. https://scicrunch.org/resolver/AB_631470.
89. RRID:AB_310305. https://scicrunch.org/resolver/AB_310305.
90. RRID:AB_11212759. https://scicrunch.org/resolver/AB_11212759.
91. RRID:AB_10859343. https://scicrunch.org/resolver/AB_10859343.
92. RRID:AB_2715852. https://scicrunch.org/resolver/AB_2715852.
93. RRID:AB_10917271. https://scicrunch.org/resolver/AB_10917271.
94. RRID:AB_321292. https://scicrunch.org/resolver/AB_321292.
95. RRID:AB_2532994. https://scicrunch.org/resolver/AB_2532994.
96. RRID:AB_2057371. https://scicrunch.org/resolver/AB_2057371.
97. RRID:AB_10807410. https://scicrunch.org/resolver/AB_10807410.

Supplementary Material

Dysregulation of steroid hormone receptors in motor neurons and glia associates with disease progression in ALS mice

Victoria M. McLeod[1], Mathew D.F. Chiam[1], Chew L. Lau[1], Thusitha W. Rupasinghe[2], Wah C. Boon[1], Bradley J. Turner[1,*]

[1]*Florey Institute of Neuroscience and Mental Health, University of Melbourne, Parkville, VIC 3052, Australia*

[2]*Metabolomics Australia, School of BioSciences, University of Melbourne, VIC 3010 Australia*

* Corresponding author
Bradley J. Turner
Florey Institute of Neuroscience and Mental Health
University of Melbourne
30 Royal Parade
Parkville, VIC, Australia, 3052
Tel: +61 3 9035 6521, Fax: +61 3 9035 3107
Email: bradley.turner@florey.edu.au

Validation of Steroid Hormones in Spinal cord LC-MS-MS

Standards were prepared over 0.001-5000 ng/ml range in 50/50 MeOH/water. For quantification (Table S1) linear standard curves prepared in solvent were analysed in triplicate. For estradiol standards were prepared in sodium bicarbonate and derivatised in dansyl chloride according to Method sample preparation. Tissue standards were prepared from pooled spinal cord tissue (containing basal level steroids) and spiking known concentrations of steroids to adjust for processing and extraction loses.

Table S1. LC-MS-MS Method Validation

Steroid	Solvent LOQ (ng/ml)	[Low] % CV	[Low] % accuracy	[High] % CV	[High] % accuracy	Tissue LOQ (pg/mg)	Tissue Recovery %
Testosterone	0.004	8.8	90.7	0.45	100.1	0.016	61 ± 5
Progesterone	0.038	7.4	101.2	0.16	100.4	0.15	65 ± 15
DHT	0.021	17.6	102.3	0.76	100.0	0.083	60 ± 1.9
DHP	0.36	2.75	92.9	2.26	101.5	1.43	70 ± 1.8
17β-estradiol	0.025	7.76	91.4	2.89	103.3	1.00	100

MTT Assay of C2C12 cells

Cells were seeded in a 96 well plate and differentiated as previously described. Cells were treated with 0.1-1000 µg/ml cycloheximide in 0.1% DMSO final concentration and cells were treated for 24h. MTT assay was performed by adding 10% volume of 5 mg/ml 3-[4,5-dimethylthiazol-2-yl]-2,5-diphenyltetrazolium bromide (MTT) for 2h at 37°C. Media was then removed and purple formazan crystals solubilised in DMSO before absorbance was measured at 570 nm. The percent viability was calculated by normalising against vehicle control: $([Abs]_0 / [Abs]_x) \times 100$.

Immunocytochemistry

Cells were blocked in 10% normal donkey serum with 0.1% (v/v) Triton-X 100 in 0.1 M PBS and incubated overnight at 4°C in the following primary antibodies; rabbit anti-AR (1:100), mouse anti-PAX-7 (1:50, R & D Systems Cat #MAB1675, RRID:AB_2159833), and mouse anti-MF-20 (2 µg/ml, Developmental Studies Hybridoma Bank, RRID:AB_2147781) in antibody diluent 5% (v/v) normal donkey serum with 0.1% (v/v) Triton-X 100 in 0.1 M PBS. Cells were incubated in the following secondary antibodies in the same diluent for 2h at room temperature; anti-rabbit Alexa Fluor®-488, Goat anti-Mouse IgG2b Cross-Adsorbed Alexa Fluor 647, Goat anti-Mouse IgG1 Cross-Adsorbed Alexa Fluor 555; followed by 10 min incubation in 0.5 µg/ml Hoechst 33342 nuclear stain (LifeTech, Cat# H1399). Cells were imaged at 40x magnification on a Zeiss AxioObserver Z1 (Carl Zeiss Pty Ltd, North Ryde, Australia).

Human embryonic stem cell-derived motor neurons

Cells were acquired, differentiated and validated using methods previously published [1]. Briefly, at stage 4, cells were seeded into 6-well plates for 24 h prior to the addition of 10 nM DHT with or without flutamide (10-100 µM) for 12h. Cells were harvested, RNA was extracted or protein quantified according to the methods in the main paper. Western blot was performed by electrophoresing 50 µg protein on 4–15% Criterion™ TGX Stain-Free™ gels (Bio-Rad) and probed with primary antibody against human AR; rabbit anti-AR (1:1000, Cell Signalling Technology Cat# 5153, RRID:AB_10691711). For transcript analysis the following primer sequences were used *Ar* forward 5'- CTCACCAAGCTCCTGGACTC -3', *Ar* reverse 5'- GAAAGGATCTTGGGCACTTG -3'; and housekeeping gene *Hprt1* forward 5'- GCTGAGGATTTGGAAAGGGTG -3', *Hprt1* reverse 5'- GCTACAATGTGATGGCCTCC -3'. Immunocytochemistry was performed as described above and previously [1]. Primary antibodies rabbit anti-ChAT (1:500, Millipore Cat# AB143, RRID:AB_2079760) and chicken anti-beta III tubulin (1:500, Abcam Cat# ab107216, RRID:AB_10899689) were incubated overnight at 4 °C and secondary antibodies anti-rabbit Alexa Fluor®-488 (1:400, Jackson ImmunoResearch Labs Cat# 711-545-152, RRID:AB_2313584), and anti-chicken Cy™3 (1:200, Jackson ImmunoResearch Labs Cat# 703-165-155, RRID:AB_2340363) were incubated for 2 h at room temperature. hESC-derived motor neurons show high expression of neuronal marker, Tuj1, and motor neuron specific marker, ChAT.

1. McLeod, V.M., et al., *Androgen receptor antagonism accelerates disease onset in the SOD1(G93A) mouse model of amyotrophic lateral sclerosis.* Br J Pharmacol, 2019. **176**(13): p. 2111-2130.

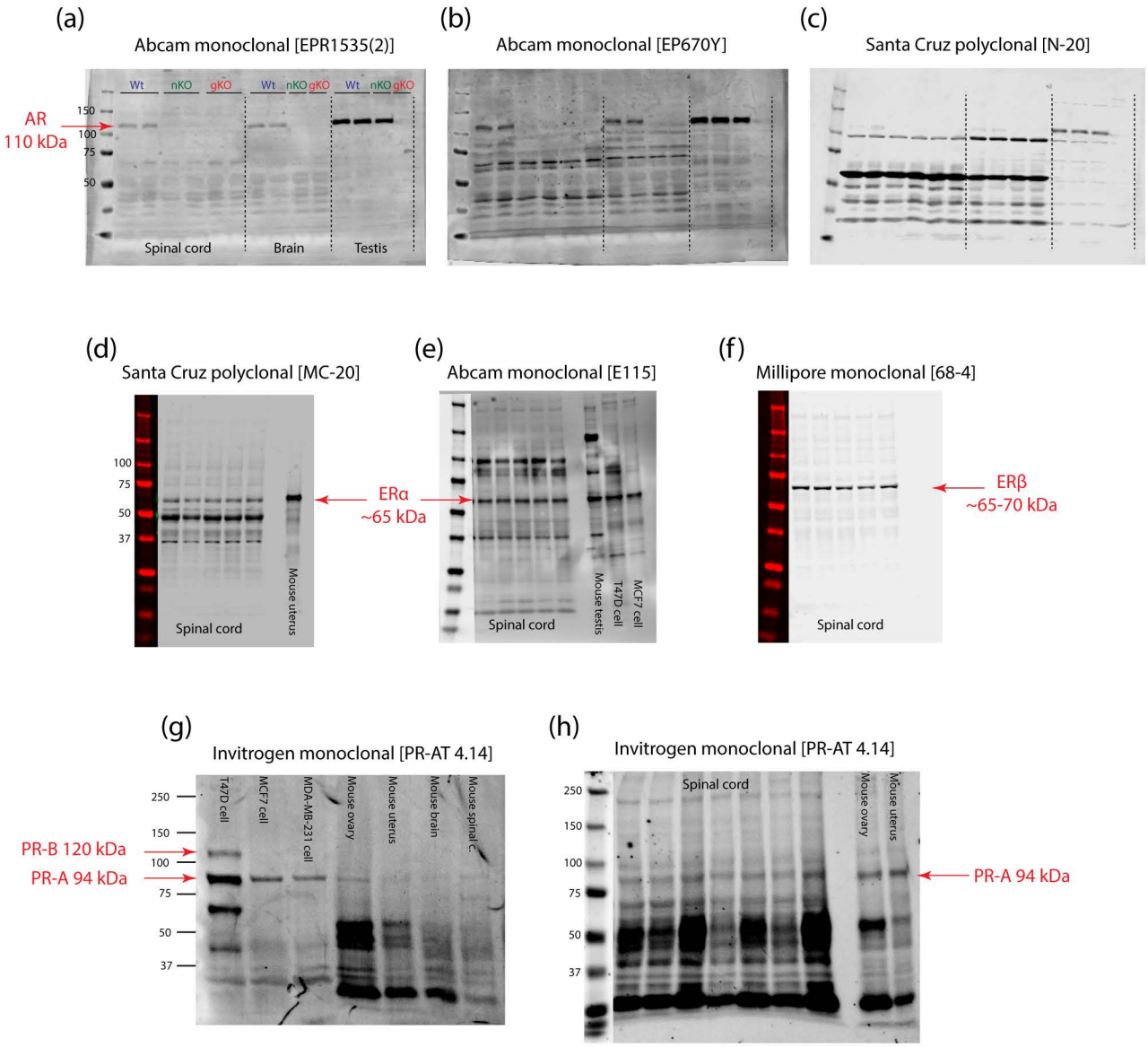

Figure S1. Validation of steroid hormone receptor protein detection by immunoblot. (a) AR monoclonal antibody detects AR in spinal cord, brain and testis tissue with null staining in knockout tissue. (b) similar staining pattern in other monoclonal antibodies and (c) non-specific bands appearing in polyclonal anti-AR antibody. (d) ERα band identified using mouse uterus as positive control and (e) staining confirmed using anti-ERα monoclonal antibody. (f) A single band identified for ERβ in spinal cord tissue. (g) PR-A identified in all human cell line and mouse control tissues with PR-B present in T47D cell lysate only, (h) staining of PR-A indentified in mouse spinal cord tissue.

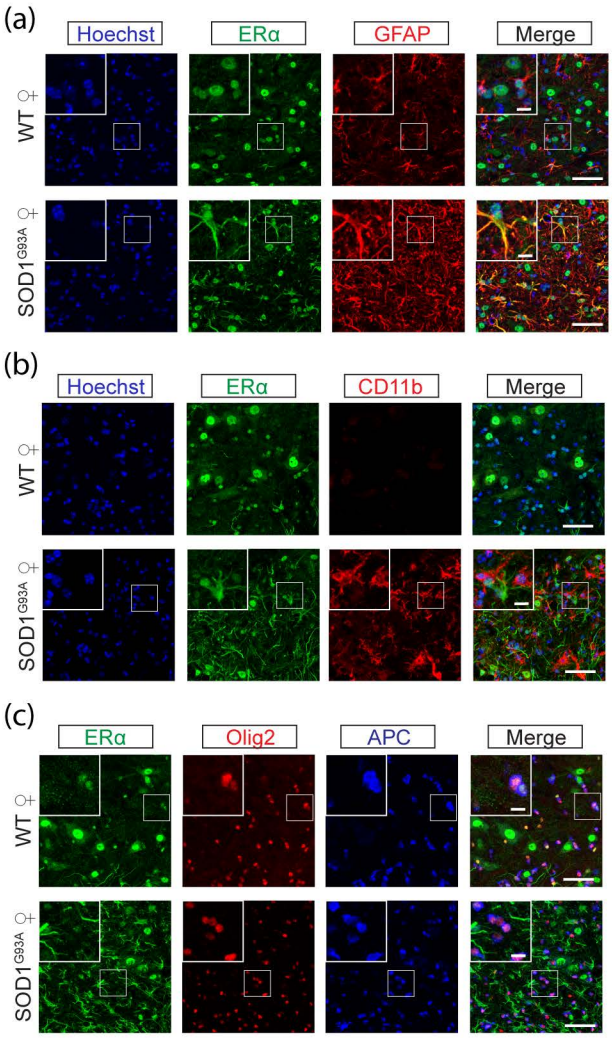

Figure S2. Estrogen receptor alpha (ERα) immunostaining in motor neurons and glial cells within the lumbar spinal cord of female wildtype and SOD1^{G93A} mice at 150 days. (a) ERα localisation in the nuclei of GFAP-positive astrocytes and prominent in astrocytic processes of reactive SOD1^{G93A} spinal cord. (b) Iba1-positive microglia show minimal ERα expression and (d) olig2 and APC-positive oligodendrocytes in wildtype or SOD1^{G93A} female spinal cords.
Scale bar = 50 µm; inset = 10 µm.

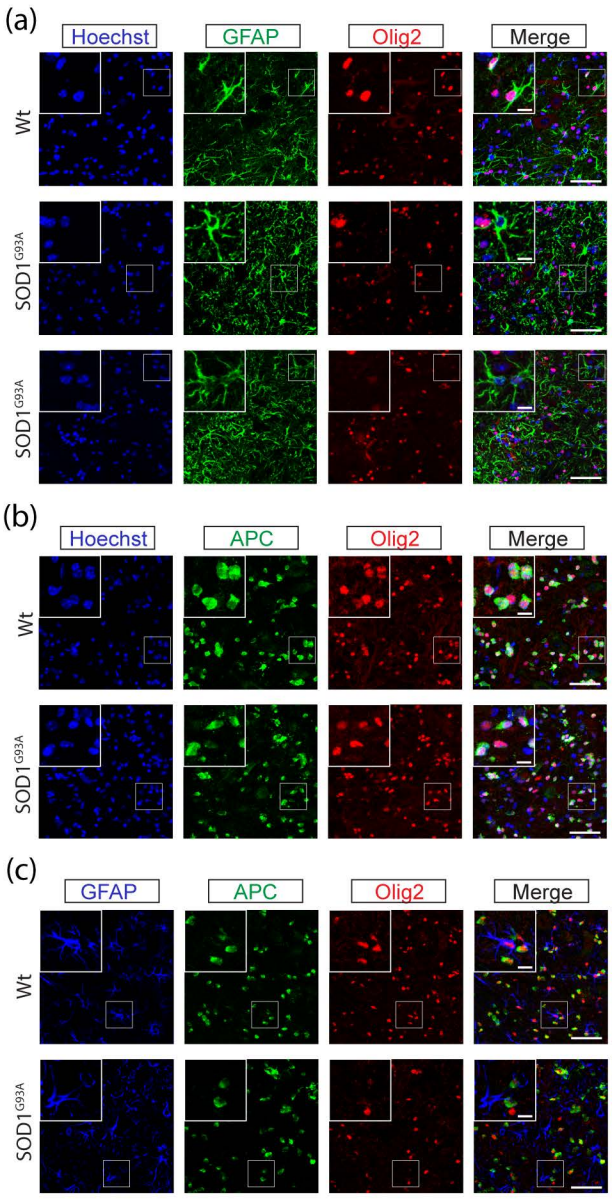

Figure S3. Identification of glial cell populations through their staining with GFAP, Olig2 and APC in mouse spinal cord. (a) GFAP^{+} astrocytes show positive nuclear Olig2 staining in wildtype mice which are largely void of Olig2 in symptomatic SOD1^{G93A}. (b) APC^{+} glia stain positive for olig2 in both wildtype and SOD1^{G93A}. (c) Comparison of GFAP, APC and Olig2 staining.

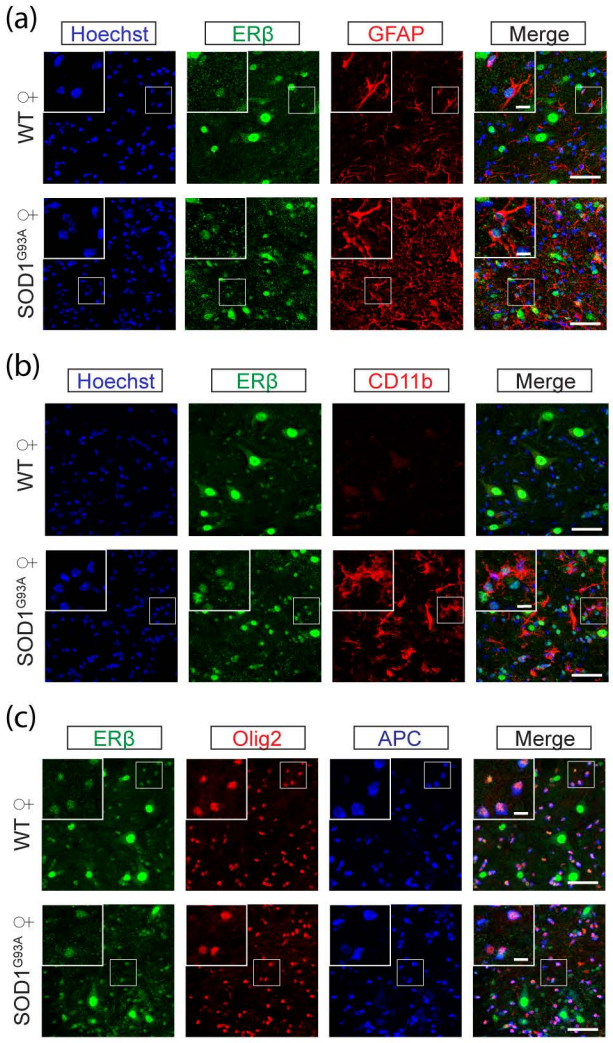

Figure S4. Estrogen receptor beta (ERβ) immunostaining in motor neurons and glial cells within the lumbar spinal cord of female wildtype and SOD1^{G93A} mice at 150 days. (a) ERβ localisation in the nuclei of GFAP-positive astrocytes in wildtype and SOD1^{G93A} spinal cord. (b) Iba1-positive microglia show minimal ERβ expression and (d) olig2 and APC-positive oligodendrocytes in wildtype or SOD1^{G93A} female spinal cords. Scale bar = 50 µm; inset = 10 µm.

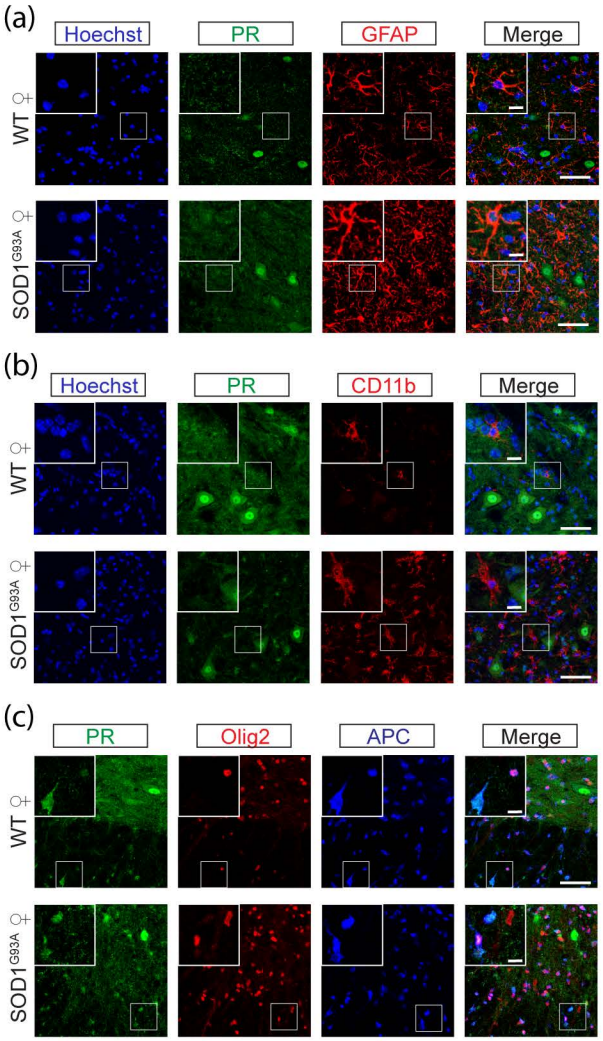

Figure S5. Progesterone receptor (PR) immunostaining in motor neurons and glial cells within the lumbar spinal cord of female wildtype and SOD1^{G93A} mice at 150 days. (a) PR does not show localisation in GFAP-positive astrocytes or (b) Iba1-positive microglia (d) with olig2 and APC-positive oligodendrocytes showing PR immunostain. Scale bar = 50 µm; inset = 10 µm.

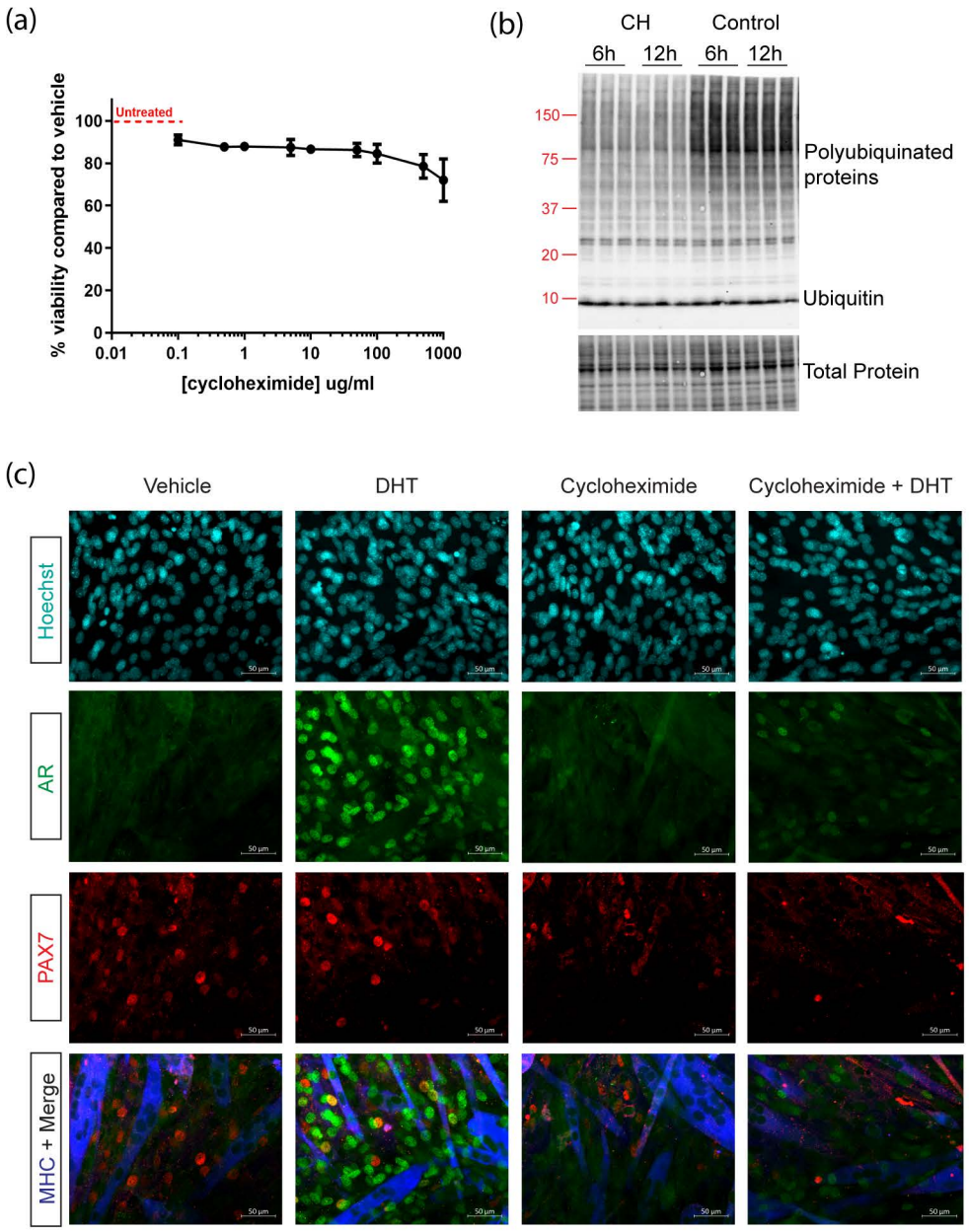

Figure S6. Validation of cycloheximide (CH) as a protein syntheis inhibitor in muscle C2C12 cells. (a) Cell viability assay to determine optimal dose of CH. (b) Immunoblot of cell lysates from 6 and 12h CH treatments compared with controls probed with anti-ubiquitin (1:1000, Cell Signaling Technology Cat # 3933). (c) Immunocytochemistry of differentiated C2C12 cells in response to various treatments. PAX7 positive reserve cells express AR and multi-nucleated myofibres stain positive for myosin heavy chain (MHC).

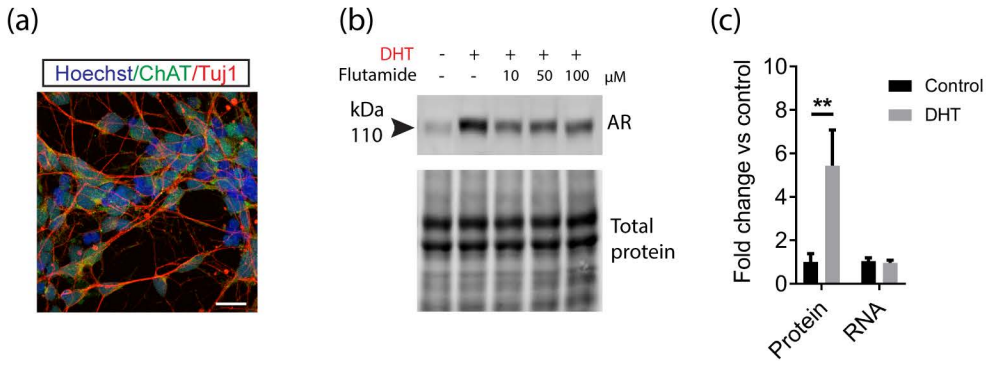

Figure S7. Effect of DHT on AR transcript and protein levels in human embyonic stem cell-derived motor neurons. (a) Motor neurons express markers, ChAT and Tuj1. Scale bar = 20 μm. (b) Immunoblot of AR protein in motor neuron lysates following 12h treatment with DHT. (c) Quantification of AR and transcript level relative to control level. Mean ± SEM, n=3. ** P<0.01 by two-way ANOVA with Sidak's multiple comparisons test.

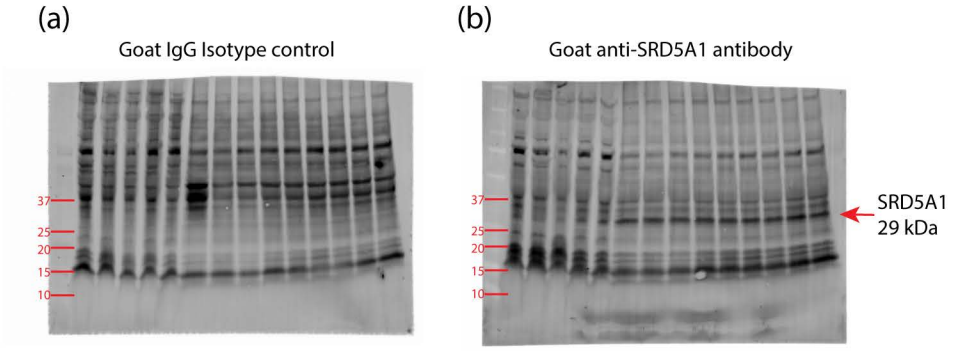

Figure S8. Validation of SRD5A1 in spinal cord against non-specific staining in IgG isotype control (a). A positive band is clearly identifiable at 29 kDa in lanes 4-14 (b).

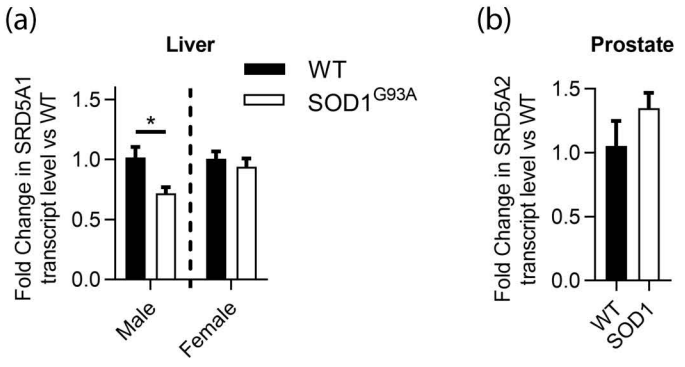

Figure S9. 5α-reductase isoform transcripts in non-CNS tissue of P150 wildype and SOD1^{G93A} mice. (a) SRD5A1 in male and female liver and (b) SRD5A2 in male prostate. Mean ± SEM, n=5; * P<0.05 analysed by Student's t-test.

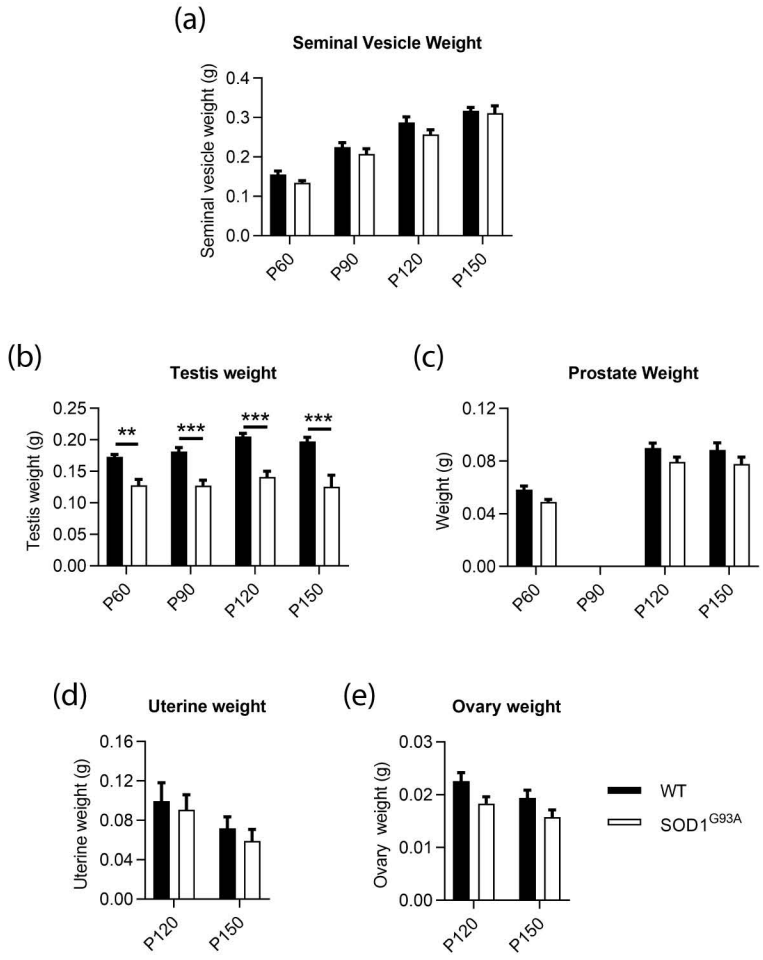

Figure S10. Tissue weights in WT and SOD1^{G93A} mice during disease progression; (a) seminal vesicles (b) testis, (c) prostate, (e) uterus, (f) ovary. Mean ± SEM, n=4-6. **P<0.01, ***P<0.001 by two-way ANOVA with Sidak's multiple comparisons test comparing genotype effect.

2.3. Results not included in publication

1.3.1. AR expression is not changed in SOD1^{G93A} testis or prostate

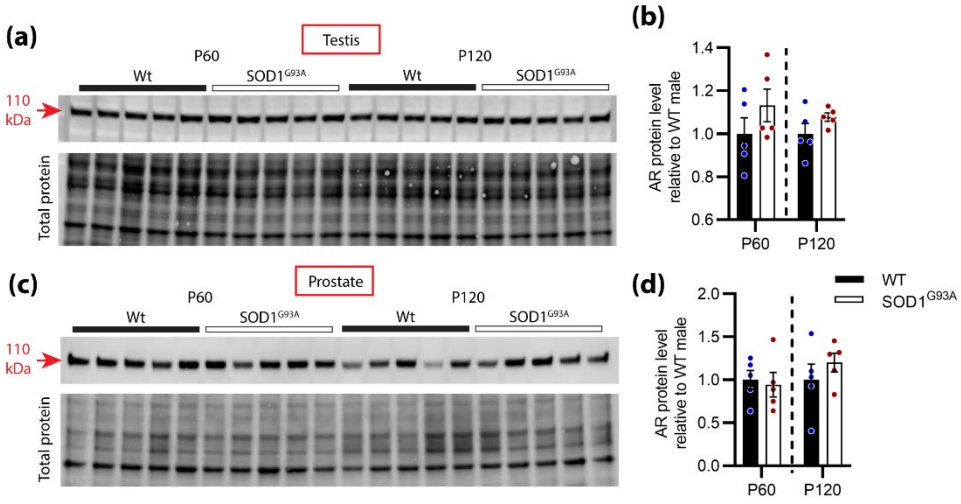

Figure 2.1 AR protein expression levels in testis and prostate from presymptomatic (P60) and symptomatic (P120) WT and SOD1G93A transgenic male mice. (a) AR immunoblot of testis with (b) quantification of AR protein levels relative to corresponding WT group. (c) AR immunoblot of prostate with (d) quantification of AR protein levels relative to corresponding WT group. Data represents mean ± SEM, n=5 mice per group.

Chapter 3. Mapping motor neuron vulnerability in the neuraxis of male SOD1^{G93A} mice reveals widespread loss of androgen receptor occurring early in spinal cord motor neurons

3.1. Manuscript in preparation

This manuscript has been prepared for submission to Neurobiology of Disease

Mapping motor neuron vulnerability in the neuraxis of male SOD1^{G93A} mice reveals widespread loss of androgen receptor occurring early in spinal cord motor neurons

Victoria M. McLeod[1], Mathew D.F. Chiam[1], Nirma D. Perera[1], Chew L. Lau[1], Wah C. Boon[1], Bradley J. Turner[1,2,*]

[1]*Florey Institute of Neuroscience and Mental Health, University of Melbourne, Parkville, VIC 3052, Australia.*

[2]*Perron Institute for Neurological and Translational Science, Queen Elizabeth Medical Centre, Nedlands, WA 6150, Australia*

* Corresponding author
Bradley J. Turner
Florey Institute of Neuroscience and Mental Health
University of Melbourne
30 Royal Parade
Parkville, VIC, Australia, 3052
Tel: +61 3 9035 6521, Fax: +61 3 9035 3107
Email: bradley.turner@florey.edu.au

Keywords: androgen receptor, ALS, SOD1^{G93A} mouse, motor neurons, sexual dimorphism, neurodegeneration

Abbreviations: amyotrophic lateral sclerosis (ALS), androgen receptor (AR), cranial nerve (CN), central nervous system (CNS), cerebrospinal fluid (CSF), corticospinal motor neuron (CSMN), dihydrotestosterone (DHT), dorsolateral nucleus (DLN), estrogen receptor (ER), lower motor neurons (LMN), layer V pyramidal neuron (LVPN), motor neuron (MN), neuromuscular junction (NMJ), retrodorsolateral nucleus (RDLN), spinal bulbar and muscular atrophy (SBMA), spinal nucleus of the bulbocavernosus (SNB), superoxide dismutase 1 (SOD1), upper motor neuron (UMN), ventral medial nucleus (VMN), wildtype (WT).

Highlights

- Widespread androgen receptor (AR) loss occurs in motor neurons of endstage SOD1^{G93A} male mice
- Reduced AR is evident in spinal motor neurons at pre-symptomatic age
- Sexually dimorphic high AR expressing motor neurons are preserved in male SOD1^{G93A} mice
- Mapping reveals differential vulnerability along the neuraxis

Abstract

Sex steroid hormones have been implicated as disease modifiers in the neurodegenerative disorder, amyotrophic lateral sclerosis (ALS). Androgens, signalling via the androgen receptor (AR), predominate in males, and have widespread actions in the periphery and the central nervous system (CNS). AR translocates to the cell nucleus when activated upon binding androgen, whereby it regulates transcription of target genes via the classical genomic signalling pathway. We previously reported that AR protein is decreased in the lumbar spinal cord tissue of symptomatic male SOD1^{G93A} mice. Here, we further explored the changes in AR within motor neurons (MN) of the CNS, assessing their nuclear AR content and propensity to degenerate by endstage disease in male SOD1^{G93A}. We observed that almost all motor neuron populations had undergone significant loss in nuclear AR in the SOD1^{G93A} mouse. Interestingly, it was observed that the loss in nuclear AR was evident as early as pre-symptomatic, P60, in the lumbar spinal MNs. Several MN populations with high AR content were identified which did not degenerate in SOD1^{G93A} mice. These included the brainstem ambiguus and vagus nuclei, and the sexually dimorphic spinal motor neurons: cremaster, dorsolateral nucleus (DLN) and spinal nucleus of bulbocavernosus (SNB). In conclusion, we provided evidence directly associating AR loss with MN vulnerability and disease progression in the SOD1^{G93A} mouse model of ALS.

1. Introduction

Amyotrophic lateral sclerosis is a progressive and fatal neurodegenerative disorder characterised by the loss of motor neurons [1]. Clinical ALS is defined by the loss of both upper and lower motor neurons. Motor neurons are found throughout the length of the central nervous system (CNS) neuraxis with axonal processes spanning the peripheral nervous system to distant effector muscles. Glutamatergic upper motor neurons (UMN), are referred to as corticospinal motor neurons (CSMNs), have cell bodies located in the layer V brain motor cortex. In humans, these large projection neurons are known as Betz cells, forming monosynaptic connections directly on lower motor neurons (LMN) in the brainstem and spinal cord. In mice, cortical to brainstem/spinal connectivity is indirect via interneurons [2]. Cholinergic LMNs have cell bodies located in discrete brainstem clusters, also known as cranial nerve (CN) nuclei, and throughout the spinal cord ventral horn, known as spinal MNs.

Populations of somatic motor neurons show resistance to degeneration in clinical ALS and mouse models. Two well established examples of this include, brainstem MNs innervating the extraocular muscles, and Onuf's nucleus, innervating the pelvic-perineal muscles controlling urinary and faecal continence and sexual function [3-6]. MNs are also differentially susceptible to degeneration based on their target fibre type innervation. The alpha (α)-MNs forming fast-twitch, fast-fatigable motor units are more vulnerable, compared to slow-twitch, fatigue-resistant motor units [7]. The gamma (γ)-MNs which innervate the intrafusal muscle fibres, are resistant in ALS [8]. Understanding the differences in molecular signatures of these MNs and the mechanisms of vulnerability are of great therapeutic interest in ALS.

To date, there has been little exploration into how sex steroid hormones may influence MN vulnerability. It is known that clinical heterogeneity in ALS stems from the site of onset and subsequent patterns of spread [9, 10]. Sex-based differences in site of onset are now well established in clinical ALS [11]. Bulbar onset occurs in one third of classical ALS patients and is characterised by loss of brainstem LMNs supplying oropharyngeal muscles. It is associated with a faster disease progression compared to limb/spinal onset [12] and is more common in females [11]. Conversely, limb onset, which accounts for approximately two thirds of classical ALS cases, is more common in males where the male:female ratio can approach 2:1 in sporadic ALS [12]. Respiratory onset, resulting from loss of phrenic MNs within the cervical spinal cord, occurs in 3-5% of cases and carries a poor survival prognosis with male bias [9, 13]. The ALS variant, flail arm syndrome, resulting from degeneration in cervical LMNs innervating the upper limbs, also has a high male:female ratio of 4:1 [13]. Insights into a potential relationship between sex hormone action and MN vulnerability could be beneficial in understanding the mechanisms of sex dimorphism inherent in ALS.

AR is a nuclear steroid hormone receptor, activated by androgen binding, to initiate the classical AR signalling pathway resulting in transcriptional regulation of target genes. Upon binding testosterone or dihydrotestosterone (DHT), AR protein conformation is stabilised [14], and the complex dimerises [15] and translocates to the nucleus where it binds to androgen response elements on DNA of target genes. A hypothesis that loss or dysfunction in AR may play a role in ALS was first proposed in 1980 [16], however, findings supporting an association are not well established. An original exploration into AR distribution, assessing tritium-labelled DHT binding, reported high AR binding in the α-MNs of the lower thoracic and lumbar spinal cord, and in some CN brainstem MN populations, excluding those resistant in ALS [17]. Later, Ogata *et al*, reported that AR immunoreactivity was evident in the resistant MNs of CNs III, IV and VI, as well as Onuf's nucleus, challenging the theory that AR absence conferred resistance in ALS [18]. The discovery that an expansion mutation in the AR gene was responsible for LMN degeneration in spinal bulbar muscular atrophy (SBMA) [19], highlighted AR abundance in MNs and their selective vulnerability to aggregating disease proteins. The primary mechanism in SBMA is induction of nuclear aggregation of AR upon binding of androgens, however, evidence also suggests a loss in AR function may contribute to disease pathogenesis [20, 21]. Although, this gain of function mutation shares similar pathogenic mechanisms with ALS, a potential overlap in AR dysfunction in MNs remains unclear.

Here we provide a comprehensive analysis of AR presence in MN populations vulnerable in the endstage SOD1^{G93A} mouse. Importantly, we mapped AR expression throughout the motor neuraxis of male mice observing a profound loss in MN AR staining intensity within SOD1^{G93A} mice, with spinal and bulbar populations highly expressing AR, being preserved. Our assessment of MN populations in the SOD1^{G93A} mouse revealed that spinal MN in the lumbar cord showed greatest vulnerability, followed by cervical MNs. CSMNs and the majority of brainstem MN populations were spared, other than the trigeminal and facial nuclei which showed mild losses. Further analysis revealed that lumbar MNs in SOD1^{G93A} mice showed loss in nuclear localised AR, which was apparent at pre-symptomatic age, prior to any overt MN loss. To our knowledge, this is the first evidence directly associating AR loss with MN vulnerability and disease progression in the SOD1^{G93A} mouse model of ALS.

2. Materials and Methods

2.1 Animals and Tissue collection

All animal experiments were conducted in accordance with the Australian National Health and Medical Research Council published Code of Practice and the ARRIVE Guidelines [22]. Approval was granted

by Florey Institute of Neuroscience and Mental Health Animal Ethics Committee (approval number 15-060-FINMH) to conduct this project. Transgenic SOD1^{G93A} mice (B6.Cg-Tg(SOD1*^{G93A})1Gur/J line, stock number 004435, Jackson Laboratory) were bred on a C57BL/6 background and group housed at the Florey Institute of Neuroscience and Mental Health Core Animal Services under standard 12 h light-dark conditions with access to standard rodent chow and water *ad libitum*. For motor neuron counts and AR mapping SOD1^{G93A} males were aged to clinical endstage. This was defined as advanced but incomplete paralysis of the hindlimbs or complete hemiparalysis in either hindlimb, and/or a decline in body condition resulting in a cumulative loss of 20% peak body weight. In the current study, the average age of endstage was 160 ± 12 days for SOD1^{G93A} males. Tissue from non-transgenic (wildtype) littermates was collected at P150. Additional cohorts of mice age P60 (presymptomatic) and P120 (symptomatic) were used for lumbar tissue collection. Mice were killed by administration of sodium pentobarbitone (100 mg/kg, i.p.) followed by cardiac perfusion with 0.1 M PBS then 4% paraformaldehyde. Dissected brains and spinal cords were post-fixed for 2-4h, rinsed and cryoprotected in a sucrose gradient of 10, 20 and 30% sucrose in 0.1 M PB over 5 days. Tissue was frozen in isopentane cooled over dry ice and stored at -80°C prior to analysis.

2.2 Immunohistochemistry – DAB staining for ChAT

Brains and spinal cords were embedded in Tissue-Tek O.C.T embedding media (Sakura Finetek, CA) and cryosectioned at 20 µm in a 1 in 10 series onto poly-L-lysine coated glass slides. Antigen retrieval was performed by baking slides for 2 h at 98 °C in 10 mM citric acid, pH 6.0. Sections were blocked for 15 minutes in 0.5% hydrogen peroxide in PBS and 1 h at room temperature in 10% normal donkey serum in 0.3% Triton X-100 containing PBS. Slides were incubated in goat anti-ChAT primary antibody (1:200, Millipore, Cat# AB144P, RRID:AB_2079751) in 6% donkey serum:0.3% Triton X-100 containing PBS, at 4 °C for 48 h. Donkey anti-Goat IgG HRP-conjugate secondary antibody (1:500, Thermo Fisher Scientific, Cat# A16005, RRID:AB_2534679) was added to slides and incubated for 2 h at room temperature. DAB colorimetric reaction was performed using SignalStain® DAB Substrate Kit (CST, Cat# 8059) according to manufacturer's instructions.

2.3 Immunohistochemistry – fluorescent staining for AR

Brains and spinal cords were cryosectioned using a Leica CM1860 cryostat at 20 µm in a 1 in 10 series onto poly-L-lysine coated glass slides. A subset of forebrains were cut as 50 µm free-floating and stored at -20 °C in cryoprotectant. Antigen retrieval was performed as outlined above. Sections were

blocked in 10% normal donkey serum 0.3% Triton-X containing PBS for 1 h at room temperature (1% Triton-X was used for free floating sections). Endogenous avidin-biotin blocking was performed according to the manufacturer's protocol (Endogenous Avidin/Biotin Blocking Kit, Abcam, Cat# ab64212). Slides were incubated in the following primary antibodies prepared in SignalStain® Antibody Diluent (CST, Cat# 8112) for 48 h at 4 °C: rabbit anti-AR (1:200, Abcam, cat# ab133273, RRID:AB_11156085), rat anti-Ctip2 (1:500, Abcam Cat# ab18465, RRID:AB_2064130), chicken anti-MAP2 (1:400, Abcam Cat# ab5392, RRID:AB_2138153), goat anti-ChAT (1:200), mouse anti-NeuN (1:1000, Millipore Cat# MAB377, RRID:AB_2298772) and mouse anti-SMI-32 (1:1000, Biolegend, cat# 801701, RRID:AB_ 2564642). A biotin amplification step was performed to increase AR detection where slides were incubated for 2 h at room temperature in donkey biotinylated-anti-rabbit antibody (1:200, Jackson ImmunoResearch Cat# 711-065-152, RRID:AB_2340593). Slides were incubated in the following secondary antibodies for 2 h at room temperature: streptavidin Alexa Fluor®-488 (1:200, Jackson ImmunoResearch Cat# 016-540-084, RRID:AB_2337249), anti-chicken F(ab')$_2$ fragment Cy™3 (1:200, Jackson ImmunoResearch, Cat# 703-166-155, RRID:AB_2340364), anti-rat Alexa Fluor®-647 (1:200, Jackson ImmunoResearch, Cat# 712-605-153, RRID:AB_2340694), anti-goat DyLight®-550 (1:200, Thermo Fisher Scientific Cat# SA5-10087, RRID:AB_2556667) and anti-mouse F(ab')$_2$ fragment Alexa Fluor®-647 (1:200, Jackson ImmunoResearch Labs, Cat# 715-606-151, RRID:AB_2340866). Hoechst 33342 was used as a nuclear stain (ThermoFisher, Australia).

2.4 Image acquisition and analysis

Chromogenic-stained sections were imaged on a Leica DM LB2 microscope (Leica Microsystems, Germany). For brainstem cranial nerve counts, nuclei regions were captured using 20x objective tiled scan, and where possible 3 sections were counted and averaged to give single hemisphere counts for each mouse. Counts for CNs X and XII represent both hemispheres due to their medial location and the merging of hemispheres. A count from n=6 mice was averaged for each genotype. For spinal cord cervical (C1-8) and lumbar (L1-5) regions, ChAT-stained motor neurons were counted in both hemispheres of the ventral horn under 20x objective, and averaged across 28-33 sections to give a count per mouse. A ventral horn count from n=5 mice was averaged for each genotype. In cranial nerves V and VII and spinal cord sections the smaller γ-MNs, were distinguished from larger α-MNs predominantly by their size, their more rounded cell morphology and more intense ChAT-staining. For phrenic MN counts, sections containing the phrenic motor column were identified by anatomical location, appearing as a MN cluster within an inter-medio-lateral position of the ventral horn of C3-5. All identifiable MNs sections were counted to provide an average count across 6 sections. The spinal

nucleus of the bulbocavernosus (SNB), ventral medial nucleus(VMN), dorsolateral nuclus (DLN) and retrodorsolateral nucleus (RDLN) were located anatomically within L6 region of the lumbar spinal cord. All sections were counted and sum reported per mouse, before being averaged across n=5 mice per genotype. All counting was performed with investigator blinded to genotype.

For endstage mapping studies, fluorescent images were acquired on a Zeiss Axio 780 confocal microscope (Carl Zeiss AG, Germany). The location of the M1 motor cortex was guided by several anatomical landmarks including the corpus callosum, alignment of the lateral ventricles and anterior commissure and appearance of the third ventricle. The area containing M1 layer V was traced and CSMN were identified as large, pyramidal shaped neurons, staining positive for MAP2 and nuclear Ctip2. For quantification, 1 µm Z-stack images of the M1 cortex from 20 µm slide-mounted sections were acquired at 20x magnification at Bregma 1.10, 0.86 and 0.62. CSMNs were counted manually by two independent counters blinded to genotype and reported as number per unit of area. Counts were then averaged across n=5 mice per genotype. For AR quantification in CSMN, 50 µm free floating sections were used, and for cranial nerve nuclei, 20 µm slide-mounted sections were used. Z-stack images were acquired at 1 µm intervals and from an average of n=3 mice and manually counted on Zen 2.5 lite software programme (Carl Zeiss). For quantitative analysis of AR nuclear staining intensity in P60 and P120 tissue, images of α-MNs in L2-5 spinal cord were acquired on a Leica SP8 confocal microscope at 40x magnification with experimenter blinded to genotype. Mean grey values were determined for the nuclear area and cytoplasmic area of individual motor neurons using Leica Application Suite X (RRID:SCR_013673) and an average of ~35 neurons were analysed per mouse lumbar.

2.5 Data and statistical analysis

CSMNs, ChAT positive and AR positive CN MNs, and spinal MNs were analysed by unpaired Student's t-test comparing WT and $SOD1^{G93A}$ mice. For layer V AR nuclei; α and γ MN subpopulations; P60 and P120 comparisons of AR staining intensity and AR positive nuclei, data were analysed by two-way ANOVA (with repeated measures where quantification came from within the same mouse). Sidak's multiple comparison test was performed to compare WT and $SOD1^{G93A}$ counterparts, where F-value indicated a significant difference ($P<0.05$). All analyses were performed using GraphPad Prism 8.0 software (San Diego, CA, USA) and data is presented as mean ± SEM.

3. Results

3.1 SOD1^{G93A} mice showed regional losses in AR within the motor cortex with no loss in layer V projection neuron number at endstage.

We identified CSMNs within M1 cortex of male mice using Ctip2 and MAP2 markers (Figure 1a-c). Ctip2 is a nuclear marker most prominent in layer V neurons including CSMNs in the motor cortex [23]. MAP2 was used to determine the overall neuronal architecture to select for CSMNs based on their large cell body and apical dendrite. SOD1^{G93A} mice showed no detectable loss in large Ctip2^{+}/MAP2^{+} LVPNs, presumed to represent the CSMN population (Figure 1d). Likewise, no evidence of somal atrophy or dendrite retraction, indicative of cellular degeneration, was observed in SOD1^{G93A} mice at disease endstage (Figure 1e). Within the motor cortex of P150 WT mice, AR appeared in all cortical layers (Figure 1b, f) with the highest intensity nuclei observed in layer V and layer II/III. In contrast, AR nuclei appeared markedly reduced in all layers except II/III in the SOD1^{G93A} mice motor cortex (Figure 1f, g). A 67% reduction in the abundance of AR occurred in SOD1^{G93A} layer V neurons compared to WT mice (Figure 1g). AR was highly expressed in the nuclei of almost all LVPNs of WT mice (Figure 1h; Table 1), with SOD1^{G93A} males displaying a reduction in LVPNs with detectable nuclear AR staining (94% vs. 73% for WT and SOD1^{G93A} mice, respectively; figure 1i). This was paralleled by a similar reduction in the nuclei staining intensity of AR in SOD1^{G93A} LVPNs (Figure 1j). In summary, CSMNs in male mice expressed high levels of AR and were resistant to degeneration in SOD1^{G93A} mice. These neurons displayed a moderate loss in AR by endstage disease.

3.2 Somatic motor neurons of the brainstem cranial nerves III (Oculomotor), IV (Trochlear) and VI (Abducent) displayed low level AR and did not degenerate in SOD1^{G93A} mice.

MNs innervating the extraocular eye muscles are known to be preserved in SOD1^{G93A} mice [3]. The oculomotor nerve or cranial nerve III (CN III) is the most rostrally located of the MN nuclei in the brainstem, located within the midbrain in the position of the superior colliculus (Figure 2a). These MNs innervate most of the muscles controlling eye and eyelid movement. No change in ChAT^{+} MN numbers within CN III nuclei were observed in SOD1^{G93A} mice (Figure 2b, c). A significant reduction in AR^{+} nuclear expression was evident in MNs from SOD1^{G93A} mice (Figure 2b,2d) with AR detectable in 21 ± 4% of MNs compared to 49 ± 5% of in WT mice (Table 1). To explore AR expression among MN subpopulations, we used NeuN staining to identify α-MNs, distinguishable from γ-MN which have low abundance or non-detectable NeuN. The loss in AR detected in SOD1^{G93A} mice occurred similarly across both MN populations within CN III (Figure 2d). The α-MNs predominate in CN III nuclei (73% of

ChAT$^+$ MNs) and AR was slightly more abundant in this subpopulation with 55% staining positive, compared to 31% of the total γ-MN in WT mice. The trochlear nerve or cranial nerve IV (CN IV) MNs are located caudolaterally to the CN III nuclei with the two cranial nuclei are often grouped together (Figure 2e). The CN IV innervates a single extraocular muscle of the eye controlling internal rotation. Likewise, no loss in CN IV MNs was observed in SOD1^{G93A} mice (Figure 2f,g) although a significant reduction is nuclear AR was evident, with only 16 ± 4% of MNs having detectable AR compared to 48 ± 7% of MNs in WT mice (Figure 2f,h; Table 1). The representation of AR staining by MN subpopulation in CN IV was similar to that of CN III MNs in both genotypes. Finally, the abducens nerve or cranial nerve VI (CN VI) is the third CN to innervate the extraocular eye muscles, controlling lateral eye movement, with MNs located medially within the brainstem between the pons and medulla junction (Figure 2i). Again, no loss in CN VI MNs occurred in SOD1^{G93A} mice (Figure 2j,k) with very low detection of nuclear AR in both genotypes (Figure 2l, Table 1). Taken together, the cluster of CNs innervating the eye muscles show weak AR expression detectable in less than 50% of MNs. No degeneration was evident in these MNs, despite SOD1^{G93A} mice having reduced AR compared to WT.

3.3 Branchial motor neurons of the brainstem cranial nerves V (Trigeminal) and VII (Facial) displayed a moderate level AR and were lost in endstage SOD1^{G93A} mice.

The trigeminal nerve or cranial nerve V (CN V) is the first of the larger multi-branched CNs with MN nuclei located in the brainstem pons, laterally to CN VI (Figure 3a). CN V innervates eight muscles involved in chewing, biting and swallowing functions [24]. In ChAT-stained sections, γ-MNs were delineated from α-MNs based on their small, rounded morphology and higher ChAT signal intensity. SOD1^{G93A} mice lost ~41% of CN V α-MNs (Figure 3b,c) while γ-MNs (making up ~23 of CN V MNs in WT mice) were preserved (Figure 3c). In fluorescent stained tissue, the γ-MNs were also identified by a lack of NeuN [25]; based on this delineation 82% of ChAT MNs in WT mice were positive for NeuN and 18% were negative for NeuN. In the SOD1^{G93A} mouse CN V, a reduction in nuclear AR was evident, with only 18 ± 2% of MNs having AR$^+$ nuclear staining compared to 68 ± 3% of MNs in WT mice (Figure 3d). This loss was preferentially in NeuN$^+$ α-MNs, with only 16% of the remaining population staining positive for AR compared to 75% of α-MNs in WT mice. In SOD1^{G93A}mice, 20% of NeuN$^-$ γ-MNs were AR$^+$, which is a slight reduction compared to WT γ-MNs where 37% were AR$^+$.

The facial nerve or cranial nerve VII (CN VII) is the largest CN with motor neuron nuclei located in the ventral aspect of the pons (Figure 2g) innervating the muscles of the face controlling facial expression [26]. In SOD1^{G93A} mice ~22% of CN VII α-MNs were lost by endstage disease with no loss in γ-MN (which represented 15% of total CV VII MNs in WT mice; Figure 3e,f). In fluorescent stained tissue,

there was regional variation in ChAT and NeuN staining intensity across MN populations (Figure 3e) and NeuN was also present in the nuclei of most small MNs. In the CNs, γ-MNs can appear similar in size to smaller α-MN [27] making subtype delineation difficult. In WT mice, $NeuN^+$ staining was detected in 93% of ChAT MNs with variable cytoplasmic and/or nuclear intensity. Therefore, we quantified AR staining in the total MN population. Again, a significant reduction in AR was evident in the $SOD1^{G93A}$ CN VII, with only 26 ± 8% of MNs observed to have AR^+ nuclear staining compared to 69 ± 9% of $ChAT^+$ neurons in WT mice (Figure 3e,3g; Table 1).

Within the CN VII, clusters of lower expressing AR^+ were evident in the ventral-lateral zone (Figure 3e, inset a), while subnuclei in the dorsal-medial zones exhibited some more intensely stained AR^+ $ChAT^+$ neurons (Figure 3e, inset b). To explore further the regional specific variation in MN vulnerability and AR expression, the CN VII was divided into 6 subnuclei, which are named relative to their anatomical location within CN VII nucleus (Figure 2h), also reflecting topographical innervation of the facial muscles [28]. We selected two MN abundant subnuclei for further investigation; the lateral subnucleus (7VL) innervating the nasolabialis muscles, and the dorsal intermediate (7DI) subnucleus innervating the facial eye area (Figure 3h, i). In $SOD1^{G93A}$ mice, there was a 30% loss in MN within the 7VL subnucleus (Figure 3j), whereas MNs in the 7DI subnucleus were preserved (Figure 3l). A reduction in AR^+ MNs was evident in both subnuclei of $SOD1^{G93A}$ mice, although this was more pronounced in the 7VL region, which was reduced from 72% to 14% AR^+ MNs in WT vs. $SOD1^{G93A}$, respectively (Figure 3k), compared to 88% vs. 41% in the 7DI region (Figure 3m). In summary, the CNs V and VII were vulnerable to MN degeneration in $SOD1^{G93A}$ mice and showed a prominent loss in AR expression.

3.4 Visceral motor neurons of the brainstem vagus nerve complex; X (Vagus) and Amb (Nucleus ambiguus) displayed high AR expression, retained in $SOD1^{G93A}$ mice, and did not undergo neurodegeneration.

A CN nucleus rich in AR expression is the dorsal nucleus of the vagus nerve, also known as cranial nerve X (CN X), with MNs located in the medulla oblongata of the brainstem below the fourth ventricle (Figure 4a). These MNs differ from the other CNs in that their projections form visceral efferents innervating the parasympathetic autonomic ganglia of the thorax and abdomen. The CN X MNs showed a tightly packed and rounded cell morphology with consistent low level NeuN expression (Figure 4b). No decrease in ChAT cell count was observed in $SOD1^{G93A}$ mice (Figure 4c). AR was highly expressed in the nuclei of CN X MNs of irrespective of genotype, detectable in 86 ± 2% of MNs in WT and 90 ± 10% of MNs $SOD1^{G93A}$ (Figure 4f,g). The nucleus ambiguus (Amb) is a group of motor neurons

situated in the medullary reticular formation of the brainstem (Figure 4j) and has a branchial MN component innervating the muscles of the palate, pharynx and larynx, as well as a visceral MN component innervating the heart [29]. Amb MNs were preserved in SOD1^{G93A} mice at endstage disease (Figure 4k,l). SOD1^{G93A} mice showed high nuclear AR expression, detectable in 95 ± 2% of ChAT^{+} neurons within the Amb nucleus, similar to WT mice exhibiting detectable nuclear AR in 91 ± 3% (Figure 4k,m, Table 1) of MNs. Together, the CN X and Amb MNs represented a unique class of MNs having some visceral innervation. They also displayed the highest AR expression among the CN MN populations and showed no evidence of AR loss or degeneration in SOD1^{G93A} mice.

3.5 Somatic motor neurons of the brainstem cranial nerve XII (Hypoglossal) displayed low to moderate AR level and showed early signs of degeneration in SOD1^{G93A} mice.

Situated immediately ventral to the CN X is the hypoglossal nerve or cranial nerve XII (CN XII), which innervates the muscles of the tongue. No loss in ChAT^{+} CN XII MNs was observed in SOD1^{G93A} mice (Figure 4b,d). Further analysis performed on the morphology of the CN XII MNs revealed a 17% loss in soma volume in SOD1^{G93A} mice (Figure 4e). A clear delineation between α- and γ-MNs was not evident in the CN XII MNs and NeuN^{+} was detectable in 97% of ChAT^{+} MNs. CN XII MNs expressed a low to moderate level of AR^{+} which was decreased in SOD1^{G93A} mice, where 21 ± 5% of MNs had AR^{+} nuclear staining (Figure 4i) compared to 74 ± 5% of MNs in WT mice (Figure 4h,i; Table 1). In conclusion, somatic CN MNs, similar to those described earlier innervating the eye muscles, the CN XII also did not show any cell loss in SOD1^{G93A} mice. These CN XII MNs displayed a low AR level and showed early morphological evidence of degeneration.

3.6 Motor neurons in the cervical spinal cord showed consistent AR level and increased susceptibility to degeneration.

The cervical spinal cord contains several motor columns innervating the neck and mastoid musculature (C1-5) and the upper limbs (C5-8). It also contains the phrenic motor column, extending from C3-C5, innervating the diaphragm which we have located and shown in Figure 5a. In SOD1^{G93A} mice, 53% of phrenic MN were lost by endstage disease (Figure 5b, c) and AR staining was notably reduced in the remaining MN pool. The ChAT^{+} cervical spinal MNs showed a clear delineation between α- AND γ-MN populations, where γ-MNs had small, rounded morphology (Figure 5d) and an absence in cytoplasmic and nuclear NeuN (Figure 5e). In SOD1^{G93A} mice, 54% of α-MNs were lost through C1-C8 while there was no change in γ-MNs comparable to WT mice (Figure 5f) A significant reduction in

AR detection was observed in SOD1^{G93A} cervical MNs, with 46 ± 6% of remaining MNs having AR^{+} nuclear staining (compared to 69 ± 3% in WT mice), although with markedly reduced intensity (Figure 5e,g). In remaining NeuN^{+} α-MNs, 55% had low level AR nuclear staining (compared to 69% of α-MNs in WT mice) and AR was mostly absent in the NeuN^{-} γ-MN population with only 6% having detectable AR signal (compared to 58% of NeuN^{-} γ-MNs in WT mice). In summary, the spinal MNs in the cervical region showed pronounced cell loss in SOD1^{G93A} mice, much greater than the cell loss described in the brainstem MNs.

3.7 Motor neurons in the lumbar spinal cord were most vulnerable to degeneration in SOD1^{G93A} mice with clusters of highly AR expressing neurons being preserved.

The lumbar spinal cord predominantly contains MNs innervating the lower limb and pelvis musculature. Most of the ChAT^{+} MNs are found in two motor columns within the ventral horn, the medial motor column (MMC) innervating axial muscles of posture and the larger lateral motor column (LMC) innervating the limbs. We observed a high AR containing cluster of MNs present in the early sections of the lumbar spinal cord located intermediate to the MMC and lateral to LMC motor nuclei (Figure 6a). These likely represented the cremaster (Cr9) MNs which innervate the cremaster reflex [30], a superficial reflex which serves a protective physiological function within of the testes of males. The Cr9 MNs did not undergo degeneration in SOD1^{G93A} mice (Figure 6c) and AR staining was highly conserved in these neurons (Figure 6b, 7c). Conversely, the MNs present in the MMC and LMC throughout L1-5 were the most vulnerable MN population in SOD1^{G93A} mice (Figure 6d-f) with 67% of the α-MNs lost through L1-L5 (Figure 6f) and no loss in γ-MNs (which made up 26% of the total ChAT^{+} ventral horn MN population in WT mice). A significant reduction in AR detection was evident in SOD1^{G93A} mice, with 55 ± 9% of remaining MNs retaining AR nuclear staining, albeit at markedly reduced intensity, compared to 81 ± 2% of MNs in WT mice (Figure 6e,g). Consistent with that observed in cervical MNs, in SOD1^{G93A} mice the remaining NeuN^{+} lumbar α-MNs, had very low level AR nuclear staining, detectable in 55% of α-MNs (compared to 85% of α-MNs in WT mice; Figure 6g). In the NeuN^{-} γ-MN population from SOD1^{G93A} mice, 53% maintained detectable but weaker nuclear AR (compared to 75% of γ-MN in WT mice).

The caudal section of the lumbar spinal cord running into the early sacral regions contains several sexually dimorphic MN populations which innervate the pelvic/perineal musculature in male mice. This includes the highly AR expressing spinal nucleus of the bulbocavernosus (SNB), located in the central area of L5-S1, and the dorsolateral nucleus (DLN) located, as the name suggests, in the dorsal lateral aspect of the ventral horn of L6-S1 (Figure 6h). In SOD1^{G93A} mice, neither of these nuclei

exhibited significant MN loss compared to WT mice (Figure 6m,o) and maintained high AR expression (Figure 6i,k) in endstage disease. The sparse neurons contained in the ventromedial nucleus (VMN; Figure 6j,n) and the monomorphic retrodorsolateral nucleus (RDLN; Figure 6l,p) were typical of the general lumbar MN population and showed significant reductions in $ChAT^{+}$ counts in $SOD1^{G93A}$ mice, with 60% loss in the VMN (Figure 6n) and 42% loss in the RDLN (Figure 6p). In $SOD1^{G93A}$ mice, the intensity of AR staining in MNs was observed to be decreased in both VMN and RDLN, although we did not quantify the detectable expression. The results from the lumbar spinal cord when taken together, showed that the lumbar MNs were the most vulnerable population in $SOD1^{G93A}$ mice and displayed the greatest cell loss in the neuraxis. AR staining intensity was also profoundly decreased in the surviving MNs although a low level was still detectable in half of these MNs. The lumbar cord also contained several MN populations with high AR expression which did not undergo degeneration in $SOD1^{G93A}$ mice.

3.8 AR expression was decreased in lumbar motor neurons of $SOD1^{G93A}$ male mice from pre-symptomatic age

With AR expression noticeably diminished throughout MNs of the CNS we further explored this loss within the vulnerable MNs of the lumbar spinal cord over the disease course in male $SOD1^{G93A}$ mice. α-MNs were identified by ChAT and SMI-32 positive cytoplasmic staining and were selected from ventral horn regions through L2-L5 (Figure 7a). L6 was excluded as this region contains high AR-expressing sexually dimorphic MN populations [31]. At pre-symptomatic age (P60), $SOD1^{G93A}$ mice did not show any MN loss (Figure 7b). AR nuclear staining intensity was significantly reduced by approximately 30% in $SOD1^{G93A}$ MNs compared to WT MNs (Figure 7a,c) with AR being detected in 60% of α-MNs (compared to 84% of α-MNs in WT mice; Figure 7d). At P120, $aSOD1^{G93A}$ mice showed a 32% loss in $ChAT^{+}$ MNs (Figure 7b). In the remaining α-MNs, AR nuclear staining intensity was reduced by 28% the level in WT mice (Figure 7a,c) with AR being detected in 50% of α-MNs (Figure 7d). By contrast, the highly expressing AR MN population, Cr9 (described in section 3.4), showed ~3.8-fold higher AR staining intensity compared to α-MNs, and was comparable between $SOD1^{G93A}$ and WT MNs at P120 (Figure 7e).

4. Discussion

Determining what influences MN vulnerability in ALS is critical for developing therapeutic interventions. MNs in the motor cortex, brainstem and spinal cord diverge across multiple

physiological and biochemical properties. These include synaptic connectivity, composition of effector targets, gene expression profiles and protein homeostasis [32-34]. AR is known to be differentially expressed throughout the neuraxis and the role of androgen signalling within various MN populations remains poorly understood. We previously reported that AR protein expression and androgen metabolising enzyme, 5α-reductase type 2, were reduced in the lumbar spinal cords of symptomatic SOD1^{G93A} male mice [35]. Building on this preliminary evidence, we hypothesised that AR may influence MN vulnerability in this ALS model. In the present study, we mapped AR expression in the MNs of the male mouse motor system, and in parallel assessed MN loss in the SOD1^{G93A} model of ALS. All ALS vulnerable MN populations consistently showed moderate AR nuclear expression in WT counterparts, which was robustly downregulated in endstage SOD1^{G93A} male mice. In the lumbar spinal cord, this downregulation in nuclear AR appeared to be present from pre-symptomatic age, prior to MN loss.

4.1 CSMN in SOD1^{G93A} and cortical AR

In sporadic and familial ALS patients, the large pyramidal Betz cells in layer V motor cortex show extensive vacuolisation of the apical dendrites [36]. Betz cells are synonymous with CSMNs in the mouse M1 cortex, however in mice, CSMNs are much smaller and difficult to identify [37]. The clinical endstage in SOD1^{G93A} mice was determined by complete or hemiparalysis in the hindlimbs. At this stage we did not identify a loss or change in the CSMNs. This contrasted with two studies in SOD1^{G93A} mice which reported significant losses in CSMNs. Ozdinler and colleagues reported up to 67% reduction in CSMNs in P120 SOD1^{G93A}, compared to WT, with CSMNs identified by retrograde fluorogold tracer [38]. CSMNs were reportedly decreased by 58% in P120 SOD1^{G93A} mice, when identified using GFP-expression under the UCHL-1 promotor [39]. Interestingly, in both cases there were parallel losses in subcerebral projection neurons in other cortical areas including the somatosensory cortex. While using axonally transported, retrograde labelling with either virus or tracer remains the gold standard for identifying CSMN populations, these may only capture a specific vulnerable pool of the MN population. Factors such as 1) the integrity of the corticospinal tract, spinal grey matter or muscle at injection location; 2) accuracy and timing of administration; 3) confinement of retrograde label to the target area, may impact the effectiveness of these labelling techniques. Additionally, the UCHL-1 gene is known to be downregulated in sporadic ALS motor cortex [40], hence, it may be lost in a disease-progressive manner, as is the case in several other neurodegenerative disorders [41, 42]. It is also possible that other cortical projection neurons were included in our count. In the mouse M1, corticospinal, corticothalamic, corticostriatal and corticocortical projections all

emerge from layer V, with corticothalamic projection neurons showing similar size and locality to the corticospinal neurons [43]. Taken together, concerns over the legitimacy of accurate detection and quantification of CSMN loss in SOD1^{G93A} mice remain, and no change was found in LVPNs projection neurons resembling CSMN in ~P160 endstage SOD1^{G93A} male mice in the current study.

AR signalling has been shown to regulate spine density in hippocampal pyramidal neurons [44] and attenuates dendritic atrophy in spinal MNs [45], in addition, providing neuroprotection to a range of neurons [46]. Therefore, AR signalling may also play a role in supporting the health of CSMN. In the present study we observed decreased AR staining in layer V of the motor cortex of SOD1^{G93A} mice, with moderately decreased nuclear AR in the larger LVPNs, representing CSMNs. With no evidence of CSMN degeneration in SOD1^{G93A} mice in the present study, this mouse model may not best reflect clinical ALS in which UMNs are also involved. It is possible that AR does not influence CSMNs, at least to the same extent as LMNs. In support of this, there is no sex bias in clinical ALS presenting with predominantly UMN involvement [47], nor are UMNs involved in SBMA, a LMN disorder caused by an expansion mutation in AR [48].

We observed that AR staining was most abundant in the layer II/III neurons, with nuclear expression maintained in these neurons of SOD1^{G93A} mice. In rat cortex, AR was found to be present predominantly in the pyramidal neurons of layers II/III and V/VI in sensory and motor cortices [49], consistent with our findings in the mouse motor cortex. Retrograde tracer studies revealed that a large proportion of the layer V AR positive nuclei are associated with corticocortical projection neurons [49]. Layer II/III neurons provide the major excitatory input to CSMN dendrites, including the thalamocortical inputs relaying cognitive and sensory information from other cortical areas [50]. Cognitive impairment occurs in ~50% of ALS patients with 15-20% classified as having frontotemporal dementia (FTD) [51]. ALS-FTD occurs more frequently in women with increasing age [47] and cognitive impairment with executive dysfunction is also more frequent in women [52]. Androgens regulate executive function [53] and are protective against cognitive decline with multiple reports of androgen-deprivation therapy being associated with increased dementia in prostate cancer patients [54]. Taken together, this evidence supports androgens and AR influencing cognitive impairments in ALS more strongly than providing neurotrophic support to UMNs.

4.2 Vulnerability of Brainstem Motor Neurons

We showed that CSMNs in SOD1^{G93A} do not degenerate by endstage disease. In the brainstem, we observed MN loss in several CN populations. MN loss was clearly evident in both trigeminal (CN V)

and facial (CN VII) nuclei, in line with other SOD1 transgenic mouse models observed [3, 55]. We observed no loss in hypoglossal CN XII MNs, however, these MN displayed soma volume loss, an early indicator of degeneration. This data is in line with clinical ALS, where the CNs V, VII and CN XII are all affected in early stages of disease [33]. We showed that the high AR expressing MNs, innervating viscera, exhibited no degeneration and maintained their nuclear AR in endstage $SOD1^{G93A}$ mice. Conversely, the MNs of the oculomotor (CN III), trochlear (CN IV) and abducens (CN VI) all expressed AR at lower levels which was detectable in less than half of the MN population. Our data gives further insight into the conflicting theories on the role of AR in MNs which may have over generalised a relationship between AR level and MN vulnerability across LMN populations. Early hypothesis suggested that AR presence coincided with MN vulnerability and resistant CN MNs showed absence or low-level AR [16, 17]. Our findings are in support of this, whereby the LMNs which contained moderate intensity staining of AR, were more likely to degenerate in $SOD1^{G93A}$ mice, possibly being more susceptible to the loss in AR evident throughout MNs of the neuraxis in disease. We saw this throughout the brainstem and spinal cord MNs, with the low-level AR populations in CNs III, IV, VI and XII showing no cell loss by endstage disease in $SOD1^{G93A}$ mice. An alternative hypothesis proposed evidence that AR expression in MNs conferred resistance in ALS and this included CNs III, IV, VI and Onuf's nucleus [18]. We dispute high AR presence in the oculomotor nuclei, although our findings support a theory that subpopulations of MNs expressing a high level of nuclear AR do show resistance to degeneration as well as retaining their AR in endstage disease.

Androgens are protective to injured brainstem MNs. Facial nerve MNs show evidence of AR mediated neuroprotection in axotomy models; testosterone permanently rescued ~20% of MN in the postnatal hamster facial nerve axotomy model [56] and DHT transiently enhanced facial MN survival in the adult mouse facial nerve crush model [57]. Testosterone improved regeneration of hypoglossal MNs following nerve crush injury in rats [58] with the tongue muscle being the primary target for testosterone-mediated neuroprotection following axotomy of the hypoglossal nerve [59]. While these studies infer that androgens have neuroprotective actions against direct axonal damage in the CN nuclei, it is unknown if androgens confer the same protection against neurodegenerative MN death.

4.3 Vulnerability of spinal motor neurons

Similar to cranial nerve injury models, androgens promote spinal MN recovery following sciatic nerve crush injury in rats [60], with evidence supporting androgen-mediated neurite growth and axonal recovery well documented [61]. The $SOD1^{G93A}$ mouse model best replicates spinal MN pathology and

the dying back phenomenon, which has been likened to an axonopathy, whereby loss in synaptic connectivity at the NMJ the initiating site of the disease [62]. AR is enriched in cells at the NMJ [63] and presents as a potential target site for androgen neuroprotection. In endstage SOD1^{G93A} rodents, there is an amplification in activity of remaining phrenic MNs to maintain stimulation to the diaphragm [64]. Testosterone improves diaphragm neurotransmission, reducing fatigue during repetitive firing [65]. The loss of AR within MNs may further impair their ability to mount effective compensatory mechanisms to maintain NMJ integrity in ALS.

Alongside protecting the NMJ and axonal health, the dendritic arbour of MNs is critical in regulating synaptic input, excitation and supporting MN health [36, 66]. The fast-fatigable motor units are most vulnerable in ALS compared to slow and fatigue-resistant motor units and most cranial MNs such as oculomotor. These vulnerable MNs tend to show greater soma volume and increased dendritic complexity compared to the resistant subtypes [32, 67, 68]. Androgens provide neuroprotection against secondary dendritic atrophy induced by injury to surrounding somatic MNs [45, 69]. In the SOD1^{G93A} mouse lumbar MNs, maladaptive dendrite morphology occurs as early as postnatally with degeneration in dendrites evident by pre-symptomatic P60 age [67], when we observed a reduced nuclear AR. While most MNs exhibit a decrease in AR in endstage SOD1^{G93A}, larger spinal MNs with more extensive dendritic arborisations may be more susceptible to the impact of local androgen changes and AR downregulation.

Androgens such as testosterone and DHT bind to AR, prompting translocation of the complex into the nucleus, which also stabilises AR protein from degradation [14]. In lumbar α-MNs, we report here a reduction in nuclear AR from as early as P60 prior to any cell death, remaining diminished over disease course. The enzyme that primarily converts testosterone to the more potent DHT within androgen-responsive tissues, 5α-reductase type 2, is expressed in large pyramidal neurons in the brain and ventral horn MN in male spinal cord [70, 71]. We previously reported that transcript levels of this enzyme were selectively reduced in the spinal cord of symptomatic SOD1^{G93A} male mice, while being conserved in prostate tissue [35], and may be responsible for localising the loss in AR to MNs of the ventral horn and LVPNs in the brain. Further evidence is provided from ALS patients who have markedly reduced DHT concentration detectable in CSF, while free testosterone levels remain unchanged [72]. DHT administration to male SOD1^{G93A} mice improved motor function and survival [73]. The loss in nuclear AR evident early in disease course prior to any MN loss, may suggest antecedent mechanisms contributing to MN vulnerability rather than a consequence of disease course.

In conclusion, a robust decrease in AR within MNs was evident throughout the CNS of male SOD1^{G93A} mice. In the lumbar α-MNs, a reduction in nuclear AR staining was evident prior to MN loss and may reflect earlier reports of dysregulated local androgen biosynthesis in the SOD1^{G93A} mouse. Unique subsets of MNs displaying high intensity AR did not appear to undergo degeneration in SOD1^{G93A} mice. We did not observe a universal correlation between AR expression and vulnerability in ALS through the CNS, likely reflecting the complexity and diversity across different MN populations and the mild influences of steroid hormone signalling on MN survival. Larger, more branched, spinal α-MN are potentially more sensitive to decreased AR signalling and further exploration of the functional impacts of altered AR in these MNs is warranted.

Table 1. Characterisation of AR staining intensity in the motor neuron subtypes and clusters within the central nervous system of male wildtype mice

Motor neuron population	Location	MN Classification	% AR positive (Mean ± SD)	Staining intensity	% change from WT
LVPN/CSMN	M1 cortex	Upper	94 ± 3	++/+++	ns
III (Oculomotor nucleus)	Brainstem	Lower - Somatic	49 ± 9	+	ns
IV (Trochlear nucleus)	Brainstem	Lower - Somatic	48 ± 15	+	ns
VI (Abducens nucleus)	Brainstem	Lower - Somatic	16 ± 13	-/+	ns
V (Trigeminal nucleus)	Brainstem	Lower - Branchial	68 ± 5	++	41 *
VII (Facial nucleus)	Brainstem	Lower - Branchial	69 ± 15	++	22 *
X (Dorsal nucleus of vagus nerve)	Brainstem	Lower - Visceral	86 ± 3	+++	ns
XII (Hypoglossal nucleus)	Brainstem	Lower - Somatic	74 ± 9	+/++	ns
Amb (Nucleus ambiguus)	Brainstem	Lower - Branchial/Visceral	91 ± 5	+++	ns
Cervical ventral horn	C1-8 spinal cord	Lower - Somatic	69 ± 5	++	54 *
Phrenic nuclei	C3-4 spinal cord	Lower - Somatic	79 ± 15	++	53 *
Lumbar ventral horn	L1-5 spinal cord	Lower - Somatic	81 ± 3	++	67 *
RDLN	L6 spinal cord	Lower - Somatic	75 ± 4	++	41 *
DLN	L6 spinal cord	Lower - Somatic	97 ± 6	+++	ns
VMN	L6 spinal cord	Lower - Somatic	100	++	60 *
SNB	L6 spinal cord	Lower - Somatic	100	+++	ns

Abbreviations: layer V pyramidal neuron (LVPN), corticospinal motor neuron (CSMN), retrodorsolateral nucleus (RDLN), dorsolateral nucleus (DLN), ventral medial nucleus (VMN), spinal nucleus of the bulbocavernosus (SNB)

* $P<0.05$ indicated a significant decrease compared to WT; ns = not significantly different by unpaired t-test.

Funding/acknowledgements

Funding for this project was provided by the Australian NHMRC (Project Grants 1104295, 1104299), Stafford Fox Medical Research Foundation, MND Research Institute of Australia (Ted Dimmick Memorial MND Research Grant). VM was supported by a MND Research Institute of Australia PhD Scholarship Top-Up Grant, NP was supported by a MND Research Institute of Australia Postdoctoral Fellowship, BT was supported by a NHMRC-ARC Dementia Research Leadership Fellowship 1137024.

Author contributions: Conceptualisation (VM), performed experiments (VM), analysed data (VM, MC), writing original draft (VM), review and editing (NP, CL, WC, BT), provided supervision (CL, WC, BT), funding acquisition (BT).

Declaration of Competing Interest

The authors have no conflict of interest to declare.

References

1. Taylor, J.P., R.H. Brown, Jr., and D.W. Cleveland, *Decoding ALS: from genes to mechanism.* Nature, 2016. **539**(7628): p. 197-206.
2. Lemon, R.N., *Descending pathways in motor control.* Annu Rev Neurosci, 2008. **31**: p. 195-218.
3. Haenggeli, C. and A.C. Kato, *Differential vulnerability of cranial motoneurons in mouse models with motor neuron degeneration.* Neurosci Lett, 2002. **335**(1): p. 39-43.
4. Sharma, R., et al., *Oculomotor dysfunction in amyotrophic lateral sclerosis: a comprehensive review.* Arch Neurol, 2011. **68**(7): p. 857-61.
5. Mannen, T., et al., *Preservation of a certain motoneurone group of the sacral cord in amyotrophic lateral sclerosis: its clinical significance.* J Neurol Neurosurg Psychiatry, 1977. **40**(5): p. 464-9.
6. Schellino, R., M. Boido, and A. Vercelli, *The Dual Nature of Onuf's Nucleus: Neuroanatomical Features and Peculiarities, in Health and Disease.* Front Neuroanat, 2020. **14**: p. 572013.
7. Hegedus, J., C.T. Putman, and T. Gordon, *Time course of preferential motor unit loss in the SOD1 G93A mouse model of amyotrophic lateral sclerosis.* Neurobiol Dis, 2007. **28**(2): p. 154-64.
8. Lalancette-Hebert, M., et al., *Gamma motor neurons survive and exacerbate alpha motor neuron degeneration in ALS.* Proc Natl Acad Sci U S A, 2016. **113**(51): p. E8316-E8325.
9. Swinnen, B. and W. Robberecht, *The phenotypic variability of amyotrophic lateral sclerosis.* Nat Rev Neurol, 2014. **10**(11): p. 661-70.
10. Ravits, J.M. and A.R. La Spada, *ALS motor phenotype heterogeneity, focality, and spread: deconstructing motor neuron degeneration.* Neurology, 2009. **73**(10): p. 805-11.
11. McCombe, P.A. and R.D. Henderson, *Effects of gender in amyotrophic lateral sclerosis.* Gend Med, 2010. **7**(6): p. 557-70.
12. Brown, R.H., Jr. and A. Al-Chalabi, *Amyotrophic Lateral Sclerosis.* N Engl J Med, 2017. **377**(16): p. 1602.
13. Chio, A., et al., *Phenotypic heterogeneity of amyotrophic lateral sclerosis: a population based study.* J Neurol Neurosurg Psychiatry, 2011. **82**(7): p. 740-6.
14. Kemppainen, J.A., et al., *Androgen receptor phosphorylation, turnover, nuclear transport, and transcriptional activation. Specificity for steroids and antihormones.* J Biol Chem, 1992. **267**(2): p. 968-74.
15. Nadal, M., et al., *Structure of the homodimeric androgen receptor ligand-binding domain.* Nat Commun, 2017. **8**: p. 14388.
16. Weiner, L.P., *Possible role of androgen receptors in amyotrophic lateral sclerosis. A hypothesis.* Arch Neurol, 1980. **37**(3): p. 129-31.
17. Sar, M. and W.E. Stumpf, *Androgen concentration in motor neurons of cranial nerves and spinal cord.* Science, 1977. **197**(4298): p. 77-9.
18. Ogata, A., et al., *Expression of androgen receptor in X-linked spinal and bulbar muscular atrophy and amyotrophic lateral sclerosis.* J Neurol Neurosurg Psychiatry, 1994. **57**(10): p. 1274-5.
19. La Spada, A.R., et al., *Androgen receptor gene mutations in X-linked spinal and bulbar muscular atrophy.* Nature, 1991. **352**(6330): p. 77-9.
20. Thomas, P.S., Jr., et al., *Loss of endogenous androgen receptor protein accelerates motor neuron degeneration and accentuates androgen insensitivity in a mouse model of X-linked spinal and bulbar muscular atrophy.* Hum Mol Genet, 2006. **15**(14): p. 2225-38.
21. Lieberman, A.P., et al., *Altered transcriptional regulation in cells expressing the expanded polyglutamine androgen receptor.* Hum Mol Genet, 2002. **11**(17): p. 1967-76.
22. McGrath, J.C., et al., *Guidelines for reporting experiments involving animals: the ARRIVE guidelines.* Br J Pharmacol, 2010. **160**(7): p. 1573-6.

23. Arlotta, P., et al., *Neuronal subtype-specific genes that control corticospinal motor neuron development in vivo.* Neuron, 2005. **45**(2): p. 207-21.
24. Huff, T. and D.T. Daly, *Neuroanatomy, Cranial Nerve 5 (Trigeminal)*, in *StatPearls*. 2021, StatPearls Publishing

25. Friese, A., et al., *Gamma and alpha motor neurons distinguished by expression of transcription factor Err3.* Proc Natl Acad Sci U S A, 2009. **106**(32): p. 13588-93.
26. Dulak, D. and I.A. Naqvi, *Neuroanatomy, Cranial Nerve 7 (Facial)*, in *StatPearls*. 2021, StatPearls Publishing

27. Morita-Isogai, Y., et al., *A distinct functional distribution of alpha and gamma motoneurons in the rat trigeminal motor nucleus.* Brain Struct Funct, 2017. **222**(7): p. 3231-3239.
28. Han, A.Y., S. Gupta, and B.G. Novitch, *Molecular specification of facial branchial motor neurons in vertebrates.* Dev Biol, 2018. **436**(1): p. 5-13.
29. Petko, B. and P. Tadi, *Neuroanatomy, Nucleus Ambiguus*, in *StatPearls*. 2021, StatPearls Publishing

30. Bacskai, T., et al., *Musculotopic organization of the motor neurons supplying the mouse hindlimb muscles: a quantitative study using Fluoro-Gold retrograde tracing.* Brain Struct Funct, 2014. **219**(1): p. 303-21.
31. Jordan, C.L., S.M. Breedlove, and A.P. Arnold, *Sexual dimorphism and the influence of neonatal androgen in the dorsolateral motor nucleus of the rat lumbar spinal cord.* Brain Res, 1982. **249**(2): p. 309-14.
32. Nijssen, J., L.H. Comley, and E. Hedlund, *Motor neuron vulnerability and resistance in amyotrophic lateral sclerosis.* Acta Neuropathol, 2017. **133**(6): p. 863-885.
33. Ragagnin, A.M.G., et al., *Motor Neuron Susceptibility in ALS/FTD.* Front Neurosci, 2019. **13**: p. 532.
34. Comley, L., et al., *Motor neurons with differential vulnerability to degeneration show distinct protein signatures in health and ALS.* Neuroscience, 2015. **291**: p. 216-29.
35. McLeod, V.M., et al., *Dysregulation of Steroid Hormone Receptors in Motor Neurons and Glia Associates with Disease Progression in ALS Mice.* Endocrinology, 2020. **161**(9).
36. Genc, B., et al., *Apical dendrite degeneration, a novel cellular pathology for Betz cells in ALS.* Sci Rep, 2017. **7**: p. 41765.
37. Genc, B., O. Gozutok, and P.H. Ozdinler, *Complexity of Generating Mouse Models to Study the Upper Motor Neurons: Let Us Shift Focus from Mice to Neurons.* Int J Mol Sci, 2019. **20**(16).
38. Ozdinler, P.H., et al., *Corticospinal motor neurons and related subcerebral projection neurons undergo early and specific neurodegeneration in hSOD1G(9)(3)A transgenic ALS mice.* J Neurosci, 2011. **31**(11): p. 4166-77.
39. Yasvoina, M.V., et al., *eGFP expression under UCHL1 promoter genetically labels corticospinal motor neurons and a subpopulation of degeneration-resistant spinal motor neurons in an ALS mouse model.* J Neurosci, 2013. **33**(18): p. 7890-904.
40. Lederer, C.W., et al., *Pathways and genes differentially expressed in the motor cortex of patients with sporadic amyotrophic lateral sclerosis.* BMC Genomics, 2007. **8**: p. 26.
41. Barrachina, M., et al., *Reduced ubiquitin C-terminal hydrolase-1 expression levels in dementia with Lewy bodies.* Neurobiol Dis, 2006. **22**(2): p. 265-73.
42. Choi, J., et al., *Oxidative modifications and down-regulation of ubiquitin carboxyl-terminal hydrolase L1 associated with idiopathic Parkinson's and Alzheimer's diseases.* J Biol Chem, 2004. **279**(13): p. 13256-64.
43. Oswald, M.J., et al., *Diversity of layer 5 projection neurons in the mouse motor cortex.* Front Cell Neurosci, 2013. **7**: p. 174.

44. Li, M., et al., *Testosterone has sublayer-specific effects on dendritic spine maturation mediated by BDNF and PSD-95 in pyramidal neurons in the hippocampus CA1 area.* Brain Res, 2012. **1484**: p. 76-84.
45. Cai, Y., et al., *Neuroprotective effects of testosterone metabolites and dependency on receptor action on the morphology of somatic motoneurons following the death of neighboring motoneurons.* Dev Neurobiol, 2017. **77**(6): p. 691-707.
46. Pike, C.J., et al., *Androgen cell signaling pathways involved in neuroprotective actions.* Horm Behav, 2008. **53**(5): p. 693-705.
47. Chio, A., et al., *ALS phenotype is influenced by age, sex, and genetics: A population-based study.* Neurology, 2020. **94**(8): p. e802-e810.
48. Katsuno, M., et al., *Pathogenesis and therapy of spinal and bulbar muscular atrophy (SBMA).* Prog Neurobiol, 2012. **99**(3): p. 246-56.
49. Kritzer, M., *The distribution of immunoreactivity for intracellular androgen receptors in the cerebral cortex of hormonally intact adult male and female rats: localization in pyramidal neurons making corticocortical connections.* Cereb Cortex, 2004. **14**(3): p. 268-80.
50. Clasca, F., P. Rubio-Garrido, and D. Jabaudon, *Unveiling the diversity of thalamocortical neuron subtypes.* Eur J Neurosci, 2012. **35**(10): p. 1524-32.
51. Bang, J., S. Spina, and B.L. Miller, *Frontotemporal dementia.* Lancet, 2015. **386**(10004): p. 1672-82.
52. Palmieri, A., et al., *Female gender doubles executive dysfunction risk in ALS: a case-control study in 165 patients.* J Neurol Neurosurg Psychiatry, 2015. **86**(5): p. 574-9.
53. Tobiansky, D.J., et al., *Androgen Regulation of the Mesocorticolimbic System and Executive Function.* Front Endocrinol (Lausanne), 2018. **9**: p. 279.
54. McHugh, D.J., et al., *Androgen-deprivation therapy, dementia, and cognitive dysfunction in men with prostate cancer: How much smoke and how much fire?* Cancer, 2018. **124**(7): p. 1326-1334.
55. Nimchinsky, E.A., et al., *Differential vulnerability of oculomotor, facial, and hypoglossal nuclei in G86R superoxide dismutase transgenic mice.* J Comp Neurol, 2000. **416**(1): p. 112-25.
56. Huppenbauer, C.B., et al., *Gonadal steroid attenuation of developing hamster facial motoneuron loss by axotomy: equal efficacy of testosterone, dihydrotestosterone, and 17-beta estradiol.* J Neurosci, 2005. **25**(16): p. 4004-13.
57. Tetzlaff, J.E., et al., *Motoneuron injury and repair: New perspectives on gonadal steroids as neurotherapeutics.* J Mol Neurosci, 2006. **28**(1): p. 53-64.
58. Yu, W.H. and M.C. Yu, *Acceleration of the regeneration of the crushed hypoglossal nerve by testosterone.* Exp Neurol, 1983. **80**(2): p. 349-60.
59. Yu, W.H. and C.G. Cao, *Muscle as the primary site for testosterone to promote survival of axotomized motoneurons.* Neuroreport, 1991. **2**(5): p. 258-60.
60. Kujawa, K.A., J.M. Jacob, and K.J. Jones, *Testosterone regulation of the regenerative properties of injured rat sciatic motor neurons.* J Neurosci Res, 1993. **35**(3): p. 268-73.
61. Fargo, K.N., et al., *Androgen regulation of axon growth and neurite extension in motoneurons.* Horm Behav, 2008. **53**(5): p. 716-28.
62. Moloney, E.B., F. de Winter, and J. Verhaagen, *ALS as a distal axonopathy: molecular mechanisms affecting neuromuscular junction stability in the presymptomatic stages of the disease.* Front Neurosci, 2014. **8**: p. 252.
63. Monks, D.A., E.L. O'Bryant, and C.L. Jordan, *Androgen receptor immunoreactivity in skeletal muscle: enrichment at the neuromuscular junction.* J Comp Neurol, 2004. **473**(1): p. 59-72.
64. Nichols, N.L., et al., *Intermittent hypoxia and stem cell implants preserve breathing capacity in a rodent model of amyotrophic lateral sclerosis.* Am J Respir Crit Care Med, 2013. **187**(5): p. 535-42.
65. Blanco, C.E., et al., *Exogenous testosterone treatment decreases diaphragm neuromuscular transmission failure in male rats.* J Appl Physiol (1985), 2001. **90**(3): p. 850-6.

66. Fogarty, M.J., et al., *Marked changes in dendritic structure and spine density precede significant neuronal death in vulnerable cortical pyramidal neuron populations in the SOD1(G93A) mouse model of amyotrophic lateral sclerosis.* Acta Neuropathol Commun, 2016. **4**(1): p. 77.
67. Fogarty, M.J., et al., *Motor Areas Show Altered Dendritic Structure in an Amyotrophic Lateral Sclerosis Mouse Model.* Front Neurosci, 2017. **11**: p. 609.
68. Fogarty, M.J., et al., *Size-dependent dendritic maladaptations of hypoglossal motor neurons in SOD1(G93A) mice.* Anat Rec (Hoboken), 2020.
69. Fargo, K.N. and D.R. Sengelaub, *Androgenic, but not estrogenic, protection of motoneurons from somal and dendritic atrophy induced by the death of neighboring motoneurons.* Dev Neurobiol, 2007. **67**(8): p. 1094-106.
70. Castelli, M.P., et al., *Regional distribution of 5alpha-reductase type 2 in the adult rat brain: an immunohistochemical analysis.* Psychoneuroendocrinology, 2013. **38**(2): p. 281-93.
71. Pozzi, P., et al., *Androgen 5-alpha-reductase type 2 is highly expressed and active in rat spinal cord motor neurones.* J Neuroendocrinol, 2003. **15**(9): p. 882-7.
72. Sawal, N., et al., *Dihydrotestosterone in Amyotrophic lateral sclerosis-The missing link?* Brain Behav, 2020. **10**(11): p. e01645.
73. Yoo, Y.E. and C.P. Ko, *Dihydrotestosterone ameliorates degeneration in muscle, axons and motoneurons and improves motor function in amyotrophic lateral sclerosis model mice.* PLoS One, 2012. **7**(5): p. e37258.

750 **Figure 1.**

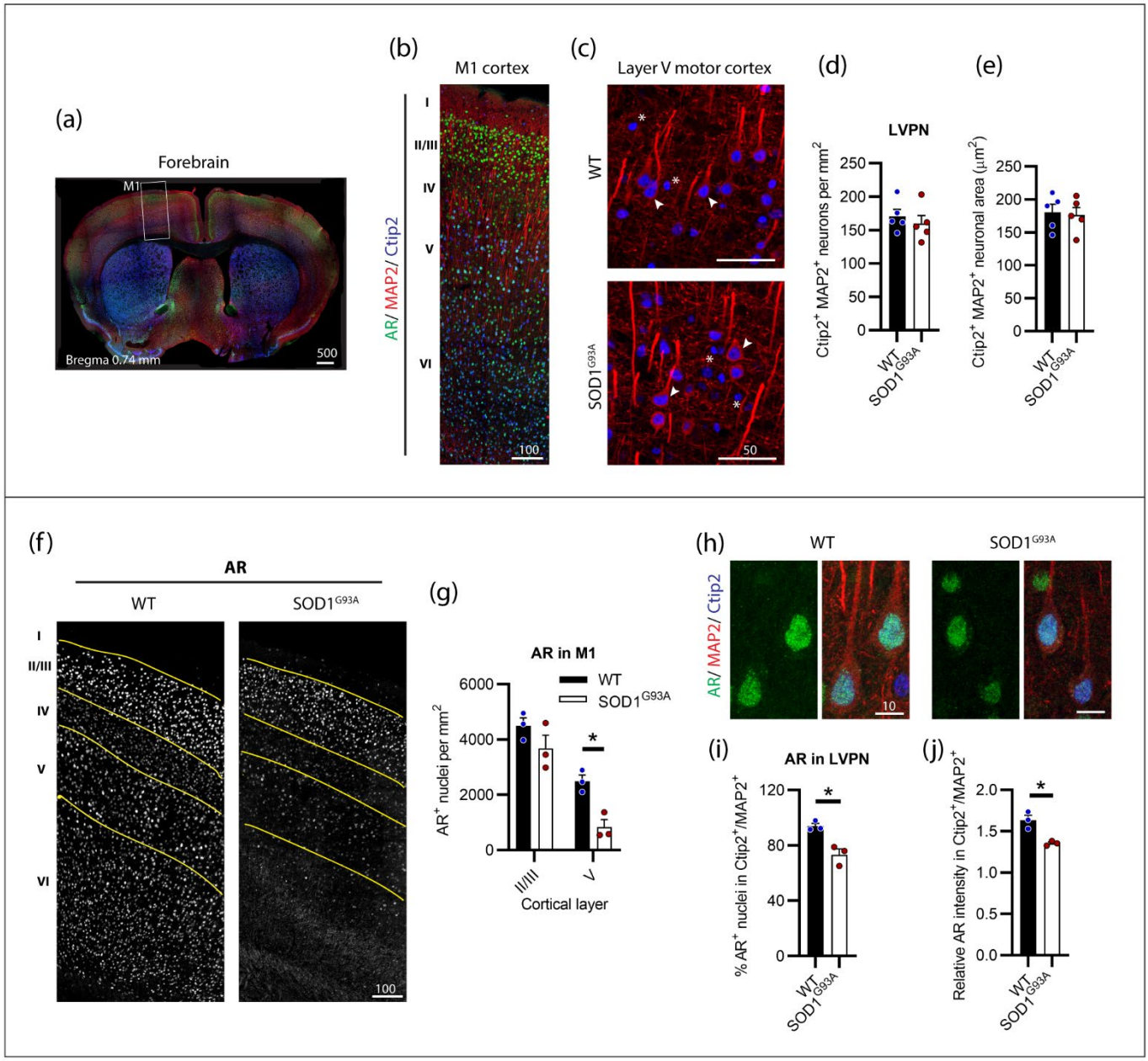

751 **Figure 1. Layer V projection neurons (LVPN) expressed high levels of AR and were preserved in**
752 **endstage SOD1^{G93A} male mice**. (a) Identification of primary motor cortex (M1) in mouse forebrain
753 coronal sections. (b) Layers of the M1 cortex identified by Ctip2 staining and MAP2 projection neurons
754 with AR nuclei observed throughout layers II-VI. (c) LVPN, including corticospinal motor neurons
755 (CSMN), were identified as larger MAP2 positive cell bodies and apical dendrites with Ctip2 positive
756 nuclei (indicated by arrows), smaller round Ctip2 nuclei (indicated by asterisk) were not counted as
757 CSMN. (d) Quantification of Ctip2^{+}/MAP2^{+} positive LVPN in WT and SOD1^{G93A} mice per unit area of
758 layer V and (e) somal area. Mean ± SEM, n=5 mice. (f) Representative images of AR^{+} staining by motor
759 cortex layer with (g) quantification of positive nuclei per unit area within layers II/III and V. * P<0.05
760 significantly different to WT male by two-way RM ANOVA with Sidak's multiple comparisons test
761 comparing genotype. (h) Representative images of AR^{+} nuclei identified in LVPN with (i) quantification
762 of AR^{+} population and (j) the mean intensity of AR nuclear signal relative to mean intensity of Ctip2^{+}
763 /MAP2^{+} neuron. * P<0.05 significantly different to WT male by unpaired t-test. Mean ± SEM, n=3 mice.
764 Scale bars = µm units.

765 **Figure 2.**

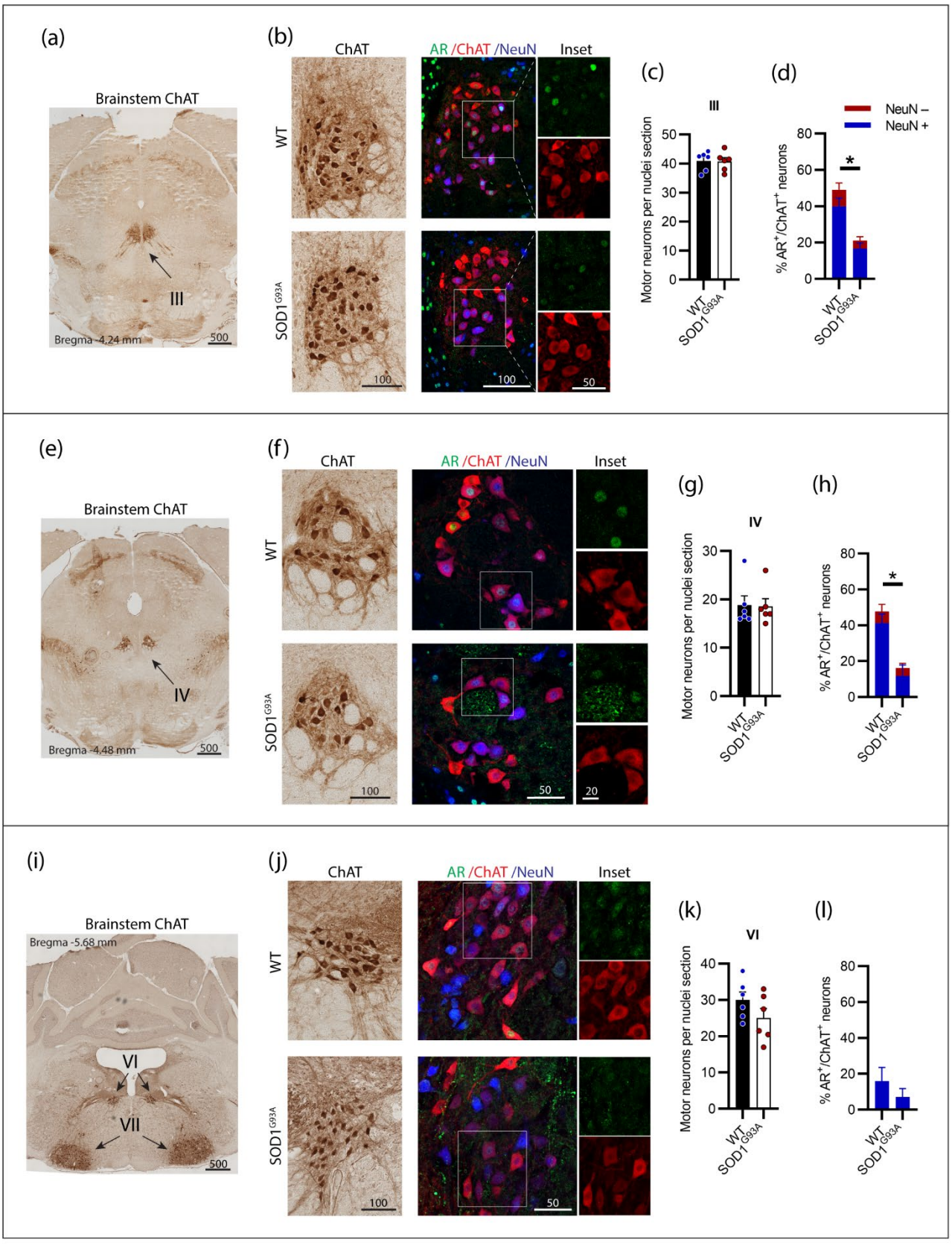
(a)
Brainstem ChAT
III
Bregma -4.24 mm
500
(b)
ChAT
AR /ChAT /NeuN
Inset
WT
SOD1G93A
100
100
50
(c)
III
Motor neurons per nuclei section
WT
SOD1G93A
(d)
NeuN –
NeuN +
% AR+/ChAT+ neurons
*
(e)
Brainstem ChAT
IV
Bregma -4.48 mm
500
(f)
ChAT
AR /ChAT /NeuN
Inset
100
50
20
(g)
IV
(h)
(i)
Brainstem ChAT
Bregma -5.68 mm
VI
VII
500
(j)
(k)
VI
(l)

Figure 2. Brainstem cranial nerve III (Oculomotor), IV (Trochlear) and VI (Abducent) motor neurons innervating the extraocular eye muscles were not lost in SOD1^{G93A} mice and displayed low level AR expression. (a) ChAT staining to identify cranial nerve III nuclei located medially within the midbrain. (b) Chromogenic ChAT labelling of nerve III motor neurons in WT and SOD1^{G93A} alongside immunofluorescent labelling of AR nuclei and NeuN within this ChAT positive population. (c) Quantification of chromogenic ChAT positive neurons within cranial nerve III sections of WT and SOD1^{G93A} mice and (d) quantification of AR positive staining with NeuN positive and negative proportions. (e) ChAT staining to identify cranial nerve IV nuclei located medially within the midbrain. (f) Chromogenic ChAT labelling of nerve IV motor neurons in WT and SOD1^{G93A} alongside immunofluorescent labelling of AR nuclei and NeuN within this population. (g) Quantification of chromogenic ChAT positive neurons within cranial nerve IV sections of WT and SOD1^{G93A} mice and (h) quantification of AR positive staining with NeuN positive and negative proportions in nerve IV motor neurons. (i) ChAT staining to identify cranial nerve VI nuclei located medially within the midbrain. (j) Chromogenic ChAT labelling of nerve VI in WT and SOD1^{G93A} alongside immunofluorescent labelling of AR nuclei and NeuN within this population. (k) Quantification of chromogenic ChAT positive neurons within cranial nerve IV sections of WT and SOD1^{G93A} mice and (l) quantification of AR positive staining with NeuN positive and negative proportions. Mean ± SEM, n=6 mice for ChAT cell counts, n=3 for AR quantification. * $P<0.05$ significantly different to WT male by unpaired t-test. Scale bars = µm units.

Figure 3.

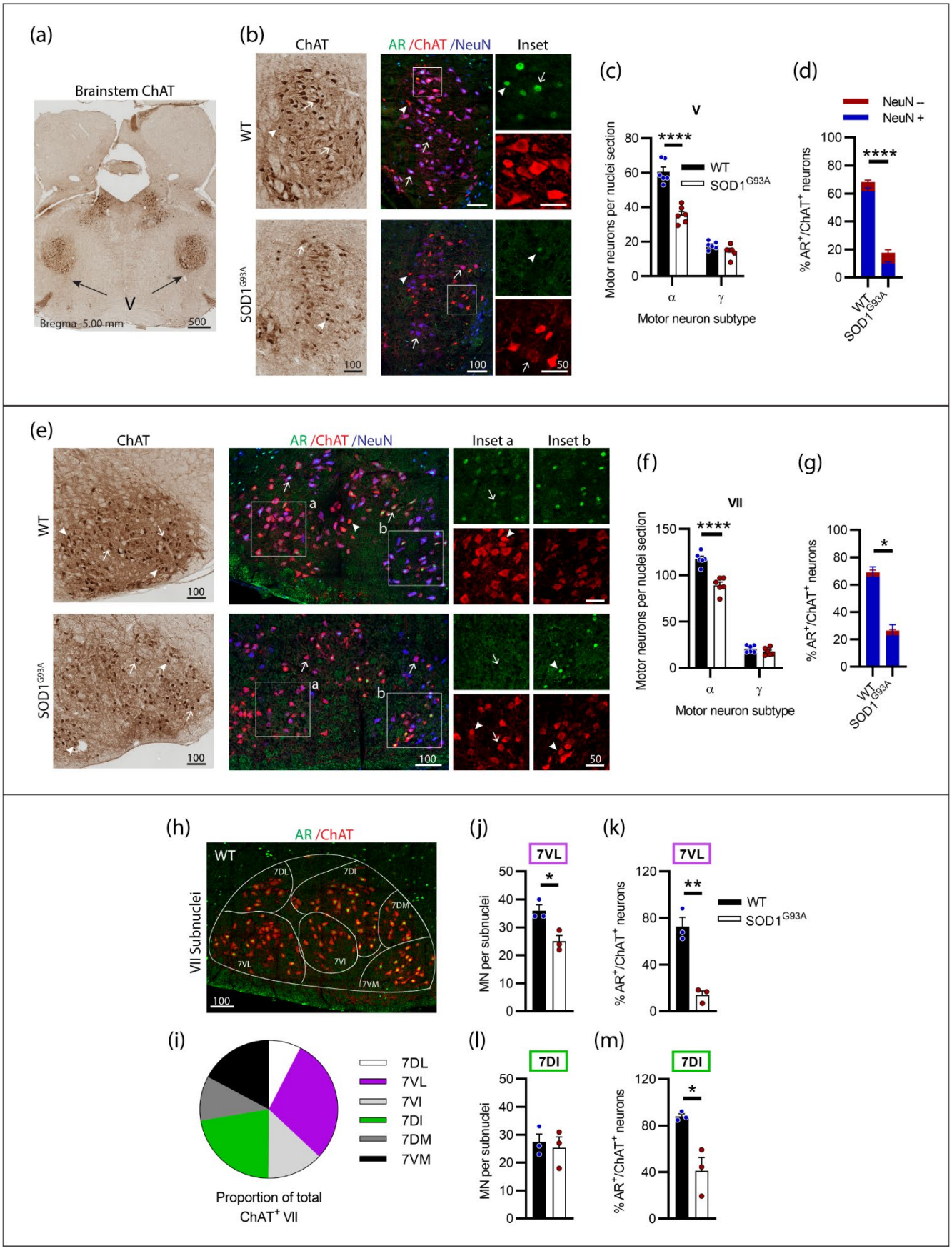
(a)
Brainstem ChAT
V
Bregma -5.00 mm
500
(b)
ChAT
AR /ChAT /NeuN
Inset
WT
SOD1G93A
100
100
100
50
(c)
V
Motor neurons per nuclei section
****
WT
SOD1G93A
α
γ
Motor neuron subtype
(d)
NeuN –
NeuN +
% AR+/ChAT+ neurons
****
WT
SOD1G93A
(e)
ChAT
AR /ChAT /NeuN
Inset a
Inset b
WT
SOD1G93A
a
b
100
100
100
50
(f)
VII
Motor neurons per nuclei section
****
α
γ
Motor neuron subtype
(g)
% AR+/ChAT+ neurons
*
WT
SOD1G93A
(h)
AR /ChAT
WT
VII Subnuclei
7DL
7DI
7DM
7VL
7VI
7VM
100
(i)
7DL
7VL
7VI
7DI
7DM
7VM
Proportion of total ChAT+ VII
(j)
7VL
MN per subnuclei
*
(k)
7VL
% AR+/ChAT+ neurons
**
WT
SOD1G93A
(l)
7DI
MN per subnuclei
(m)
7DI
% AR+/ChAT+ neurons
*

Figure 3. Brainstem cranial nerve V (Trigeminal) and VII (Facial) nuclei expressing moderate level of AR showed cell loss in endstage SOD1^{G93A} mice. (a) ChAT staining to identify cranial nerve V nuclei located laterally within the hindbrain. (b) Chromogenic ChAT labelling of nerve V in WT and SOD1^{G93A} alongside immunofluorescent labelling of AR nuclei within this ChAT positive population. (c) Quantification of chromogenic ChAT positive neurons within cranial nerve V sections of WT and SOD1^{G93A} mice based on size and morphology to distinguish alpha and gamma subpopulations alongside (d) quantification of AR positive staining with NeuN positive and negative proportions. Representative alpha and gamma motor neurons identified by arrows and arrow heads, respectively. (e) Chromogenic ChAT labelling of nerve VII in WT and SOD1^{G93A} alongside immunofluorescent labelling of AR nuclei and NeuN within this ChAT positive population. AR staining shows greater intensity in the medial subnucleus (inset b) compared to laterally located subnuclei (inset a). (f) Quantification of chromogenic ChAT positive neurons within cranial nerve VII sections of WT and SOD1^{G93A} mice alongside (g) quantification of AR positive staining with NeuN positive and negative proportions. (h) Division of CN VII motor neurons into subnuclei: dorsolateral (DL), ventrolateral (VL), ventral intermediate (VI), dorsal intermediate (DI), dorsomedial (DM) and ventromedial (VM) and (i) proportion of MNs making up each subnucleus. (j) Quantification of ChAT MNs in CN VII subnuclei 7VL in WT vs SOD1^{G93A} mice alongside (k) quantification of AR positive nuclei staining. (l) Quantification of ChAT MNs in CN VII subnuclei 7DI in WT vs SOD1^{G93A} mice alongside (m) quantification of AR positive nuclei staining. **** P<0.0001 significantly different to WT male by two-way ANOVA with Sidak's multiple comparisons test comparing genotype for ChAT quantification; mean ± SEM, n=6. * P<0.05, ** P<0.01, **** P<0.0001 significantly different to WT male by unpaired t-test for AR quantification and subnuclei quantification, mean ± SEM, n=3. Scale bars = µm units.

Figure 4.

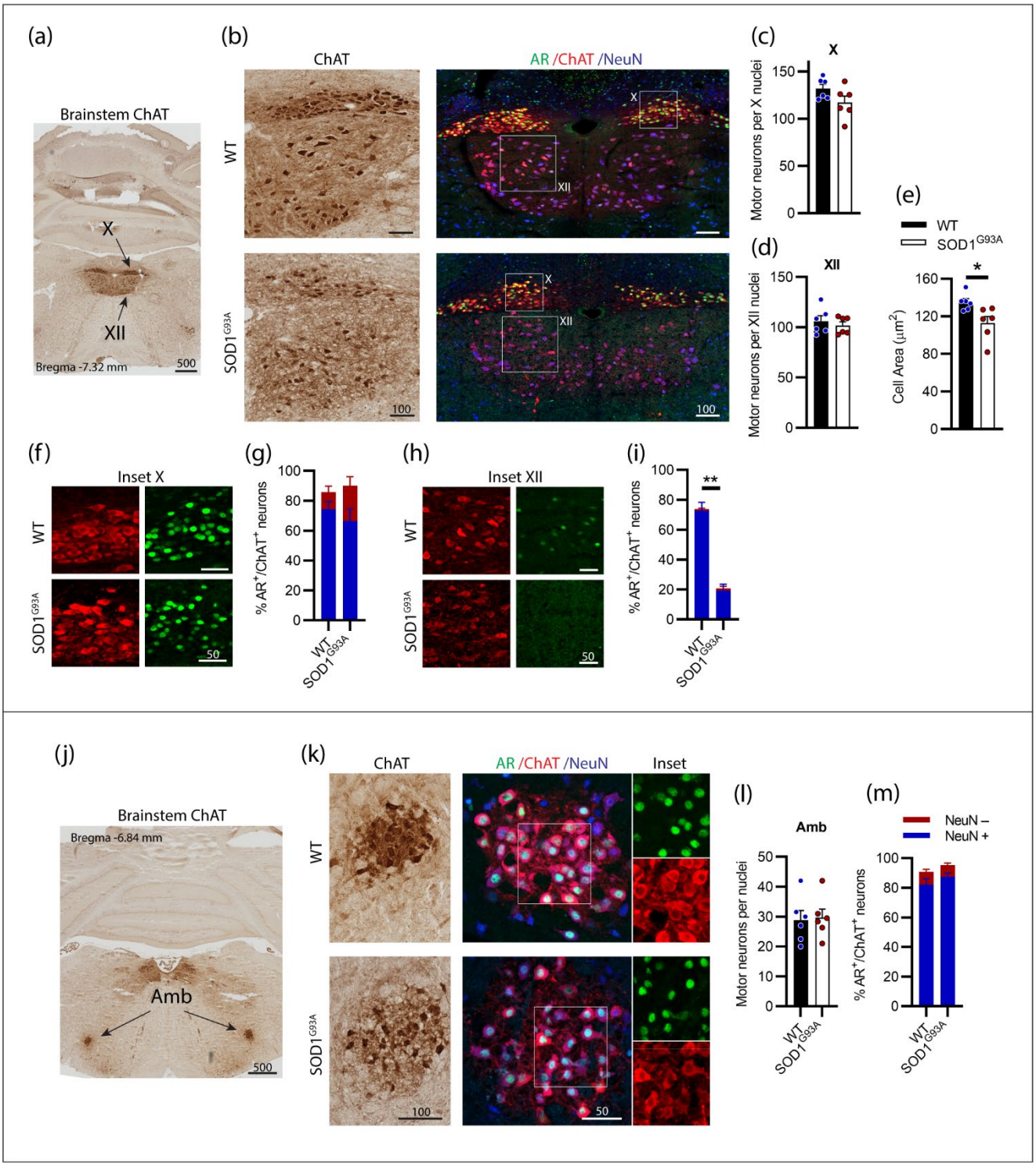
(a)
Brainstem ChAT
X
XII
Bregma -7.32 mm
500
(b)
ChAT
AR /ChAT /NeuN
WT
SOD1G93A
X
XII
100
(c)
X
Motor neurons per X nuclei
150
100
50
0
(d)
XII
Motor neurons per XII nuclei
150
100
50
0
(e)
WT
SOD1G93A
*
Cell Area (μm2)
160
120
80
40
0
(f)
Inset X
WT
SOD1G93A
50
(g)
% AR+/ChAT+ neurons
100
80
60
40
20
0
WT
SOD1G93A
(h)
Inset XII
WT
SOD1G93A
50
(i)
**
% AR+/ChAT+ neurons
100
80
60
40
20
0
WT
SOD1G93A
(j)
Brainstem ChAT
Bregma -6.84 mm
Amb
500
(k)
ChAT
AR /ChAT /NeuN
Inset
WT
SOD1G93A
100
50
(l)
Amb
Motor neurons per nuclei
50
40
30
20
10
0
WT
SOD1G93A
(m)
NeuN –
NeuN +
% AR+/ChAT+ neurons
100
80
60
40
20
0
WT
SOD1G93A

Figure 4. Brainstem cranial nerve X (Vagus) and ambiguus (Amb) motor neurons expressing high level of AR; and cranial nerve XII (Hypoglossal) motor neurons expressing moderate level of AR did not show cell loss in endstage SOD1^{G93A} mice. (a) ChAT staining to identify cranial nerve X and XII nuclei located medially within the hindbrain. (b) Chromogenic ChAT labelling of nerve X and XII in WT and SOD1^{G93A} alongside immunofluorescent labelling of AR nuclei and NeuN within these ChAT positive populations. (c) Quantification of chromogenic ChAT positive neurons in WT and SOD1^{G93A} CN X and (d) CN XII, alongside (g) cell body area in XII MNs. (f) AR staining shows greater intensity in the CN X nuclei (inset X) with (g) quantification of AR^{+} nuclei staining in NeuN$^{+/-}$ ChAT MNs. (h) AR staining in XII nuclei (inset XII) with (i) quantification of AR^{+} nuclei staining in NeuN$^{+/-}$ ChAT MNs. (j) ChAT staining to identify Amb nuclei located laterally within the hindbrain. (k) Chromogenic ChAT labelling of Amb nucleus in WT and SOD1^{G93A} alongside immunofluorescent labelling of AR nuclei and NeuN within this ChAT positive population. (l) Quantification of chromogenic ChAT positive neurons within Amb sections of WT and SOD1^{G93A} mice alongside (m) quantification of AR^{+} nuclei staining in NeuN$^{+/-}$ ChAT MNs. Mean ± SEM, n=6 mice for ChAT cell counts, n=3 for AR quantification. * $P<0.05$ significantly different to WT male by unpaired t-test. Scale bars = µm units.

Figure 5.

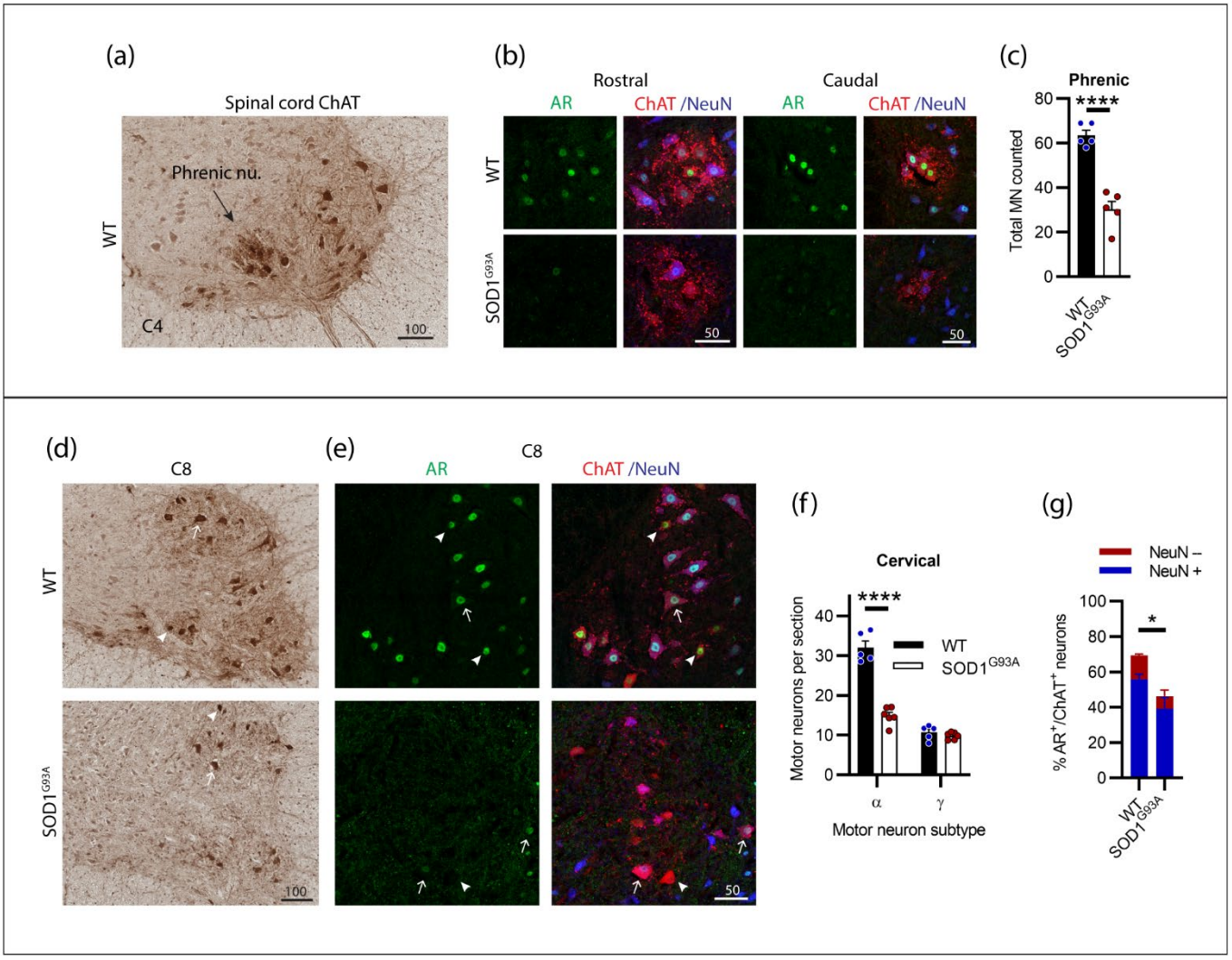

Figure 5. Cervical spinal cord motor neurons expressed consistent moderate levels of AR and showed extensive neurodegeneration in endstage SOD1^{G93A} mice. (a) ChAT staining in C4 spinal cord of WT mice to identify the phrenic nucleus located within the ventral horn of WT mice. (b) Representative immunofluorescent labelling of AR and NeuN within this ChAT positive MN population from a rostrally and caudally located section containing the phrenic motor column. (c) Quantification of chromogenic ChAT positive neurons the phrenic nuclei of C3-5 of WT and SOD1^{G93A}. Mean ± SEM, n=5 mice. **** P<0.0001 significantly different to WT male by Student's t-test. (d) ChAT staining in level C8 spinal with (e) immunofluorescent labelling of AR and NeuN. Alpha and gamma motor neurons identified by arrows and arrow heads, respectively. (f) Quantification of chromogenic ChAT positive neurons in the ventral horns of cervical spinal cord regions C1-8 of WT and SOD1^{G93A} using size and morphology to distinguish alpha and gamma subpopulations. Mean ± SEM, n=5 mice. **** P<0.0001 significantly different to WT male by two-way ANOVA with Sidak's multiple comparisons test comparing genotype. (g) Quantification of AR positive staining with NeuN positive and negative proportions. * P<0.05, significantly different to WT male by unpaired t-test for AR quantification, mean ± SEM, n=3. Scale bars = µm units.

839 **Figure 6.**

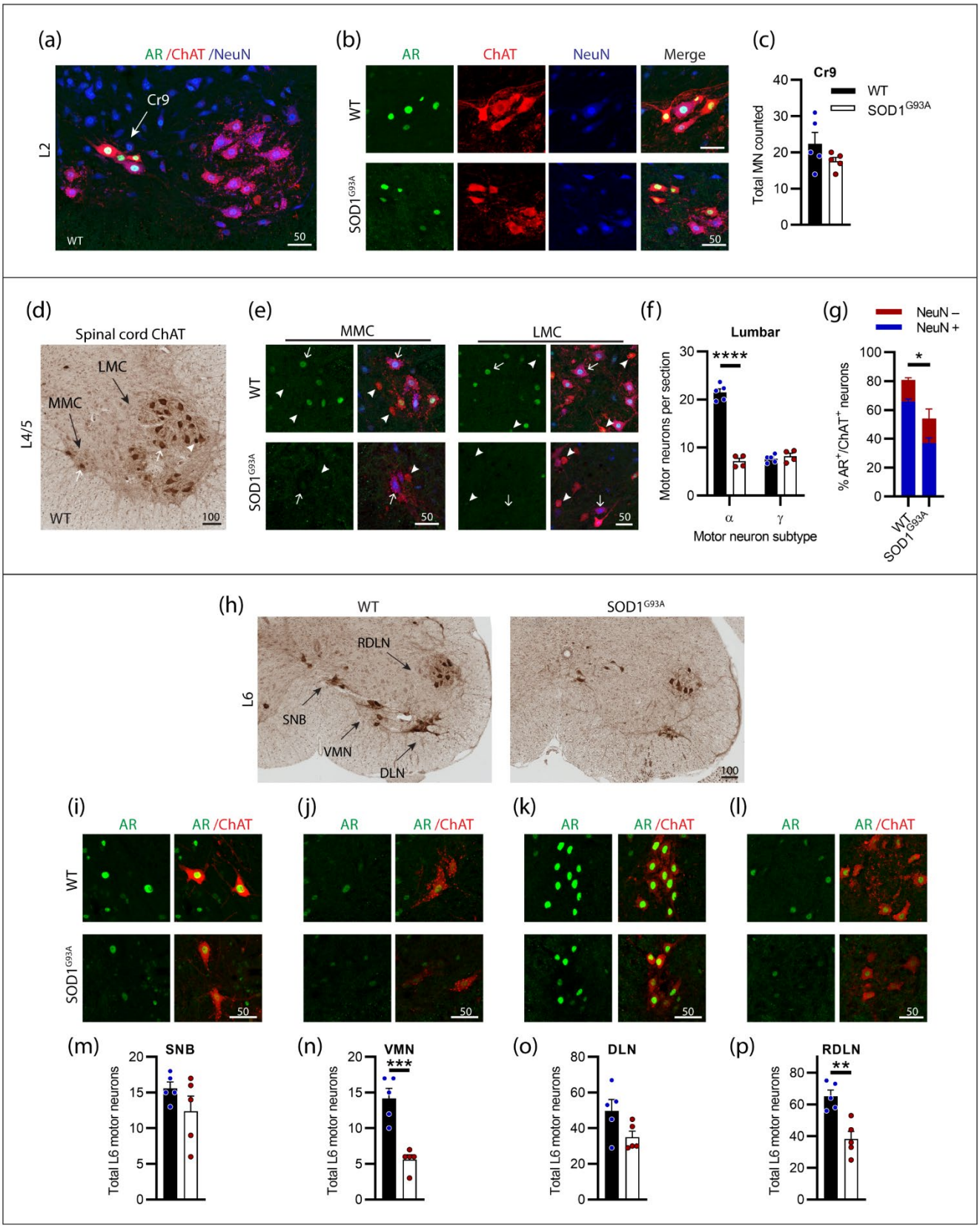
(a)
AR /ChAT /NeuN
Cr9
L2
WT
50
(b)
AR
ChAT
NeuN
Merge
WT
SOD1G93A
50
(c)
Cr9
WT
SOD1G93A
Total MN counted
(d)
Spinal cord ChAT
LMC
MMC
L4/5
WT
100
(e)
MMC
LMC
WT
SOD1G93A
50
(f)
Lumbar
****
Motor neurons per section
α
γ
Motor neuron subtype
(g)
NeuN –
NeuN +
*
% AR+/ChAT+ neurons
WT
SOD1G93A
(h)
WT
SOD1G93A
RDLN
SNB
VMN
DLN
L6
100
(i)
AR
AR /ChAT
WT
SOD1G93A
50
(j)
AR
AR /ChAT
50
(k)
AR
AR /ChAT
50
(l)
AR
AR /ChAT
50
(m)
SNB
Total L6 motor neurons
(n)
VMN
***
Total L6 motor neurons
(o)
DLN
Total L6 motor neurons
(p)
RDLN
**
Total L6 motor neurons

Figure 6. Lumbar spinal cord motor neurons expressed heterogenous levels of AR and showed the greatest loss in endstage SOD1^{G93A} mice with evidence of high AR expressing resistant populations. (a) AR, ChAT and NeuN staining of from ~L2 spinal cord ventral horn of WT mice to identify a subpopulation of high AR expressing cremaster (Cr9) motor neurons. (b) Representative images of Cr9 motor neurons present in both WT and SOD1^{G93A} within rostral lumbar regions which show mixed NeuN expression. (c) Quantification of Cr9 MN populations in fluorescent-stained images of L1-2 of WT and SOD1^{G93A} male mice. Mean ± SEM, n=5 mice. (d) ChAT staining in level L4/5 of spinal cord of WT mice with motor neurons clustered into a median motor column (MMC) and lateral motor column (LMC). (e) Immunofluorescent labelling of AR and NeuN in ChAT-stained motor neurons from the MMC (left panel) and LMC (right panel) regions of WT and SOD1^{G93A} spinal cord. Alpha and gamma motor neurons identified by arrows and arrow heads, respectively. (f) Quantification of chromogenic ChAT positive neurons in the ventral horns of lumbar spinal cord regions L1-5 of WT and SOD1^{G93A} using size and morphology to distinguish alpha and gamma subpopulations. Mean ± SEM, n=5 mice. **** P<0.0001 significantly different to WT male by two-way RM ANOVA with Sidak's multiple comparisons test comparing genotype. (g) Quantification of AR positive staining with NeuN positive and negative proportions. Mean ± SEM, n=3; * P<0.05, significantly different to WT male by unpaired t-test. (h) Chromogenic ChAT staining in L6 spinal cord of WT and SOD1^{G93A} mice showing sexually dimorphic motor neuron populations including spinal nucleus of bulbocavernosus (SNB), (ventromedial nucleus (VMN), dorsolateral nucleus (DLN) and retrodorsolateral nucleus (RDLN). Immunofluorescent labelling of AR in ChAT^{+} motor neuron nuclei within: (i) SNB, (j) VMN, (k) DLN and (l) RDLN of L6 male spinal cords of WT with SOD1^{G93A} with quantification of chromogenic ChAT counts provided below for (m) SNB, (n) VMN, (o) DLN and (p) RDLN. Mean ± SEM, n=5 mice. ** P<0.01, ***P<0.001 significantly different to WT male by unpaired t-test. Scale bars = μm units.

Figure 7.

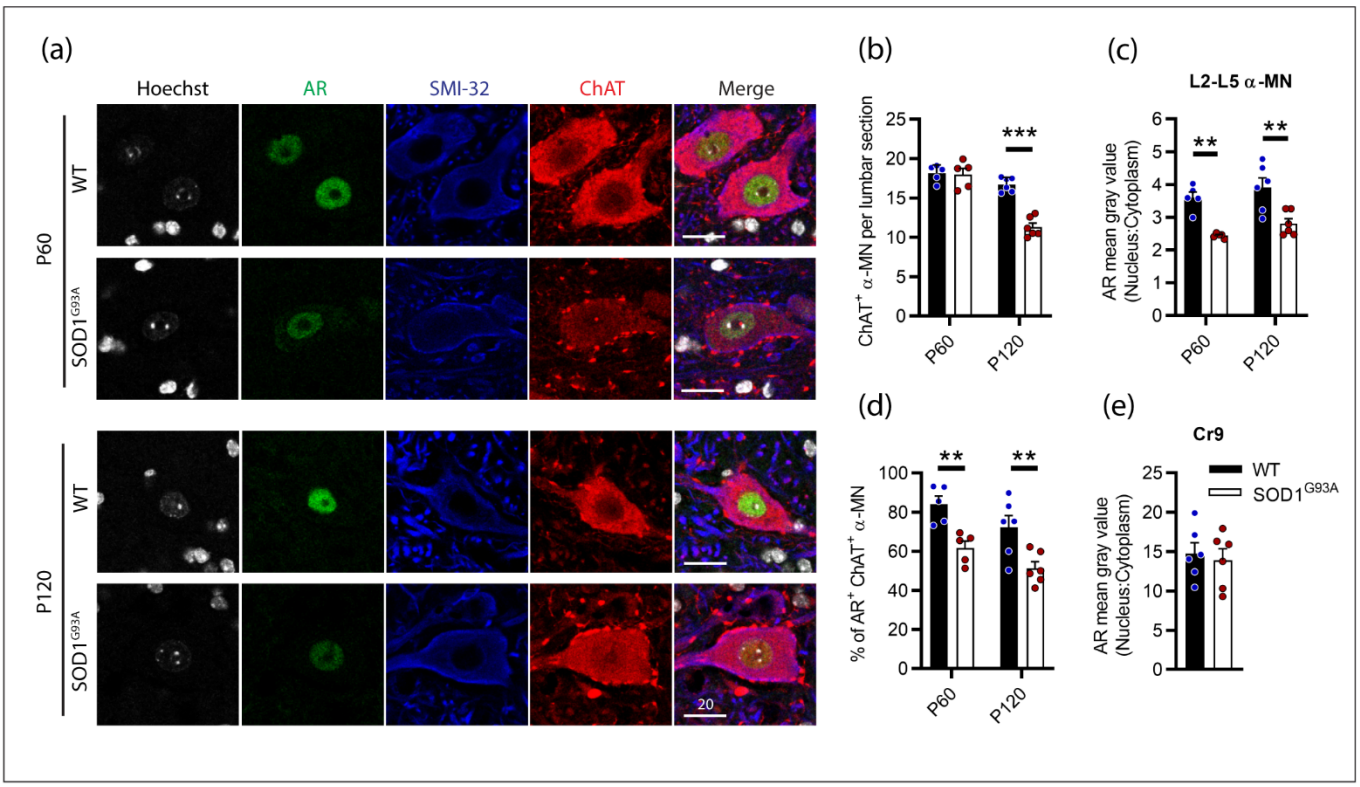

Figure 7. Androgen receptor nuclear staining was decreased in SOD1^{G93A} male mice lumbar motor neurons from pre-symptomatic (P60) age compared to wildtype mice. (a) AR nuclear staining identified in ChAT and SMI-32 positive α-MNs, scale bar = 20 µm. (b) Quantification of ChAT positive α-MNs per section in the lumbar spinal cord of P60 and P120, WT and SOD1G93A mice alongside, (c) measured by mean grey value in L2-5 α-MNs. (d) Percentage of ChAT positive α-MNs with detectable nuclear AR staining. (e) Quantification of nuclear to cytoplasmic AR staining intensity the highly AR expressing cremaster (Cr9) population in L2 from P120 mice. Data represent mean ± SEM, n=5-6 mice per group. ** *P*<0.01, *** *P*<0.001, significantly different to WT male by two-way ANOVA with Sidak's multiple comparisons test comparing genotype.

Chapter 4. Early downregulation in skeletal muscle androgen receptor occurs in SOD1^{G93A} mice with dual effects on neurotrophic support

4.1. Manuscript in preparation

This short manuscript has been prepared for submission to Muscle & Nerve

Early downregulation in skeletal muscle androgen receptor occurs in SOD1^{G93A} mice with dual effects on neurotrophic support

Victoria M. McLeod[1], Nirma D. Perera[1], Wah C. Boon[1], Bradley J. Turner[1,2,*]

[1]*Florey Institute of Neuroscience and Mental Health, University of Melbourne, Parkville, VIC 3052, Australia.*

[2]*Perron Institute for Neurological and Translational Science, Queen Elizabeth Medical Centre, Nedlands, WA 6150, Australia*

* Corresponding author

Bradley J. Turner

Florey Institute of Neuroscience and Mental Health

University of Melbourne

30 Royal Parade

Parkville, VIC, Australia, 3052

Tel: +61 3 9035 6521, Fax: +61 3 9035 3107

Email: bradley.turner@florey.edu.au

Keywords: androgen receptor, skeletal muscle, SOD1^{G93A} mouse, amyotrophic lateral sclerosis, neurotrophism

Abbreviations: androgen receptor (AR), androgen receptor knock out (ARKO), amyotrophic lateral sclerosis (ALS), brain derived neurotrophic factor (BDNF), calcitonin gene-related peptide (CGRP), ciliary neurotrophic factor (CNTF), 5α-dihydrotestosterone (DHT), glial cell-derived neurotrophic factor (GDNF), GDNF family receptor alpha-1 (GFRα1), insulin-like growth factor 1 (IGF-1), insulin-like growth factor 2 (IGF-2), motor neurons (MN), nerve growth factor (NGF), neuromuscular junction (NMJ), neurotrophin-4 (NTF4), neurotrophic factors (NTF), quantitative reverse transcription polymerase chain reaction (qRT-PCR), superoxide dismutase 1 (SOD1), transforming growth factor beta 1 (TGF-β1), vascular endothelial growth factor (VEGF)

Abstract

Background: Androgens are considered to have anabolic and trophic functions in skeletal muscle. Here, we explore androgen receptor (AR) changes in skeletal muscle of $SOD1^{G93A}$ mice and the potential impact of AR on transcriptional regulation of neurotrophic factors.

Methods: Pre-symptomatic (P60) and symptomatic (P120) $SOD1^{G93A}$ mouse gastrocnemius muscle was studied for AR transcript and immunohistochemical protein expression. Expression profiles of gastrocnemius and lumbar transcripts from AR knockout (ARKO), $SOD1^{G93A}$, and flutamide-treated $SOD1^{G93A}$ mice were examined by qRT-PCR.

Results: A decrease in nuclear AR alongside decreased AR transcript was observed in the gastrocnemius from P60 age $SOD1^{G93A}$ male mice. Multiple neurotrophic factors influenced by AR, were also dysregulated in $SOD1^{G93A}$ skeletal muscle at P60. ARKO mice showed reduced IGF-1 expression and upregulation in BDNF and GDNF receptor transcript. AR antagonism in $SOD1^{G93A}$ male mice elevated BDNF transcript after prolonged treatment.

Conclusions: The dysregulation of AR in skeletal muscle of $SOD1^{G93A}$ male mice may have dual effects in the regulation of neurotrophic support.

Introduction

Amyotrophic lateral sclerosis (ALS) is a neurodegenerative disease resulting from death of motor neurons (MNs) and atrophy of skeletal muscle through denervation [1]. The $SOD1^{G93A}$ transgenic mouse remains the most utilised preclinical model accurately reflecting many ALS clinical and pathogenic mechanisms [2]. With hindlimb paralysis most prominent in this mouse, it accurately reflects the dying back phenomena [3] which proposes that the destruction of the neuromuscular junction (NMJ) in muscle occurs prior to degeneration of MNs [1]. As specific muscle derived neurotrophic factor (NTF) delivery was neuroprotective in the $SOD1^{G93A}$ mouse [4, 5], preservation of the NMJ presents an attractive therapeutic target.

Androgen receptors (AR) are widely expressed nuclear steroid hormone receptors which regulate target gene transcription via activation by androgens, primarily testosterone and dihydrotestosterone (DHT). Androgens are known to exhibit anabolic actions in skeletal muscle. Androgen action in the sexually dimorphic, pelvic levator ani muscle, is well studied, whereby AR activation robustly induces insulin-like growth factor 1 (IGF-1) [6, 7] and brain derived neurotrophic factor (BDNF) [8] expression, promoting muscle hypertrophy and neuroprotection to innervating spinal nucleus of bulbocavernosus (SNB) MNs. However, evidence for muscle-driven AR stimulated NTF protection to MNs, remains largely limited to the highly androgen sensitive SNB system [9, 10]. Limb musculature is largely unresponsive to AR-mediated hypertrophy although androgens mediate muscle strength [6, 11]. Androgen-sensitivity of MNs can be enhanced through enrichment of AR in target-muscle, as demonstrated in quadriceps innervating MNs [12].

Therapeutic interventions targeting AR impact skeletal muscle. We previously described hindlimb muscle atrophy but no detrimental effect on MN survival in $SOD1^{G93A}$ male mice treated with AR antagonist, flutamide [13]. Conversely, chronic DHT treatment increased skeletal muscle IGF-1 and IGF-2 mRNA, preserving innervation, and protecting MNs [14]. We have previously reported that AR is decreased in $SOD1^{G93A}$ male mouse spinal cord MNs with disease progression [15]. Here, we investigated the AR changes in $SOD1^{G93A}$ skeletal muscle compared to WT mice. Using additional muscle from flutamide-treated $SOD1^{G93A}$ mice and ARKO mice we explored the potential impacts on neurotrophic support to innervating MNs.

Methods

Animals

All animal experiments were approved by the institution animal ethics committee (approval #15-060-FINMH & #16-001-FINMH) and conducted in accordance with the Australian NHMRC published code of practice. Transgenic SOD1^{G93A} mice (stock number 004435) were sourced from Jackson Laboratory (Bar Harbor, ME, USA) and maintained on a C57BL/6J background. ARKO were generated as previously detailed [16]. Flutamide treatment was administered as previously described [13]. Gastrocnemius muscle and lumbar spinal cord were collected and processed as previously described [13, 15]. See supplementary material for detailed methods.

Immunohistochemistry

Gastrocnemius muscle sections (12 µm) were stained for AR as previously described [13]. Images were acquired across a single muscle cross-section, traversing the muscle belly, on a Leica SP8 confocal microscope at 20x magnification. Each image was comprised of a 10x 1µm Z-stack and 5 images were collected per mouse (n=5 mice per genotype). The number of Hoechst positive nuclei and AR positive nuclei per image were determined by semi-quantitative particle counting using ImageJ.

qRT-PCR

RNA extraction from muscle and spinal cord tissue, and subsequent qRT-qPCR was performed and analysed as previously described [13, 15]. Primer sequences and detailed methods are provided in Supplementary Information, Table S1.

Results

Androgen receptor is downregulated in SOD1^{G93A} gastrocnemius muscle

To determine extent of muscle atrophy, we measured gastrocnemius cross-sectional area. At P120, symptomatic SOD1^{G93A} cross-sectional area was significantly decreased by ~50%, while only a ~20% decrease was observed at P60, not significantly different to WT (Figure 1a). Muscle satellite cells, identified by PAX7 nuclear stain, are considered to be quiescent stem cells of the muscle, responding to injury or regenerative demands. We identified 2.7% of muscle nuclei were PAX7-positive in P120 WT mice. In line with an anticipated response to muscle atrophy, a 63% increase in PAX7^{+} nuclei was

found in P60 SOD1^{G93A} muscle and a 46% increase at P120 compared to WT (Supplementary Information, Figure S1). AR transcript levels were consistently lower in SOD1^{G93A} gastrocnemius at both P60 and P120, with a greater than 50% reduction in AR mRNA compared to WT (Figure 1b). Myocyte nuclei were identified by Hoechst DNA stain (Figure 1c) and were significantly increased with disease progression in SOD1^{G93A} muscle by 54 and 92%, at P60 and P120, respectively, indicating rapid myogenesis (Figure 1d). While the density of myocyte nuclei increased per mm^2, AR positive nuclei number remained constant over disease course (Figure 1e). This resulted in a decreased % AR$^+$ nuclei in SOD1^{G93A} muscle with ~25-30% being positive in SOD1^{G93A} mice vs. ~50% of nuclei in WT muscle (Figure 1f).

Neurotrophic factor levels are dysregulated in SOD1^{G93A} skeletal muscle

We next determined the SOD1^{G93A} disease-mediated alterations in various growth factors, and proteins associated with androgen activity (Figure 2). Growth factors IGF-1, IGF-2 and VEGF were all robustly downregulated by 40-50% in P60 SOD1^{G93A} gastrocnemius and maintained at reduced levels by symptomatic age (Figure 2a,b,d). Classical neurotrophins, NGF and NTF4, were downregulated by 61% and 70%, respectively, in contrast to BDNF which was unchanged over disease course (Figure 2c,e,f). The most striking change was glial cell-derived neurotrophic factor (GDNF) showing a 22-fold upregulation in P60 SOD1^{G93A} (Figure 2h). TGF-β1 is a secreted cytokine indicative of muscle atrophy, shown to be upregulated in muscle by anabolic steroid, nandrolone, at SOD1^{G93A} disease onset [17]. We observed an elevation in TGF-β1 in P60 SOD1^{G93A} mice (Figure 2j).

IGF-1, BDNF and GFRA1 are differentially altered in AR knockout skeletal muscle

A global deletion of AR in male ARKO mice downregulated IGF-1 mRNA in gastrocnemius muscle by 33% compared to WT mice at P60 (Figure 2a). Similarly, downregulation in IGF-1 occurred in the SOD1^{G93A} mouse at P60 (Figure 2a). Conversely, ARKO mice showed a 2-fold elevation in BDNF transcript and a 50% elevation in GDNF receptor, GFRα1, transcript (Figure 2c,i). BDNF expression can be regulated by estrogens acting via the estrogen receptor (ER) [18]. Therefore, we measured ERα transcript in ARKO gastrocnemius. A trend toward elevation (*P*=0.0996; Supplementary Information, Figure S2) was evident in ARKO muscle compared to WT, hence, this could only in part explain the altered BDNF level. No changes to mRNA expression of these NTFs or their receptors were observed in the lumbar spinal cords of P60 SOD1^{G93A} mice (Supplementary Information, Figure S3).

AR antagonism in SOD1^{G93A} mice elevates BDNF in symptomatic male skeletal muscle

To explore if AR antagonism in SOD1^{G93A} mice further altered IGF-1, VEGF and BDNF, we chronically administered flutamide from P60 as previously described [13]. In male SOD1^{G93A} mice, BDNF was elevated by 45% in P120 flutamide treated mice compared to untreated controls (Figure 3c), whereas IGF-1 and VEGF levels remained comparable across treatment time course. No changes to mRNA expression of these NTFs were observed in the lumbar spinal cords of P120 SOD1^{G93A} male or female flutamide treated mice (Supplementary Information, Figure S4).

Discussion

We report a loss of AR in hindlimb skeletal muscle at P60 age, a timepoint when muscle atrophy is occurring but prior to any motor neuron loss in SOD1^{G93A} male mice. Skeletal muscle groups are differentially responsive to the action of androgens, possibly a direct influence of AR presence; pelvic levator ani muscle in mice contain 74% AR^{+} myonuclei; less responsive extensor digitorum longus contains only 7% AR^{+} myonuclei [19]; quadriceps contains 51% AR^{+} [20], similar to our reported ~50% AR^{+} myonuclei in gastrocnemius muscle. Due to the dynamic changes in muscle composition occurring in SOD1^{G93A} diseased muscle (myofiber atrophy and loss alongside rapid myogenesis), it is difficult to determine whether the downregulation in AR is due to losses in existing myonuclei or production of AR deficient myonuclei. Close to 90% of the muscle satellite cells are AR^{+} [20]. MacKrell *et al*. determined that AR signalling was critical for efficient satellite cell activation into myogenesis, responsible for promoting regeneration and repair mechanisms [7]. Satellite cells from SOD1^{G93A} male mice show reduced proliferative capacity [21], reflecting an impairment which could be imparted by the loss in AR observed in the current study. Further investigation into the mechanism and cell-types responsible for the loss in AR as well as implications to the SOD1^{G93A} disease course are required.

BDNF expression is downregulated in skeletal muscle of spinal-bulbar muscular atrophy mice [22], a MN neurodegenerative disease, caused by an expansion mutation in AR. While we observed no change in BDNF transcript levels in SOD1^{G93A} mice, an elevation was observed in SOD1^{G93A} males following chronic AR antagonism, which was associated with accelerated disease onset and exacerbated muscle pathology [11]. Upregulation of BDNF also occurred in ARKO mice. This is in contrast to the anticipated response, with androgen promoting BDNF expression in healthy quadriceps muscle [8]. BDNF expression shows differential time-dependent responses in gastrocnemius following sciatic nerve axotomy, as well as regulation by corticosteroids such as glucocorticoids [23]. ARKO mice exhibit hypertrophic adrenal glands and elevated glucocorticoid

levels [24] which may be responsible for the elevated BDNF. In SOD1^{G93A}, BDNF levels may be altered via alternate mechanisms in response to the enhanced muscle atrophy observed in P120 flutamide-treated muscle [13]. The inherent reduced AR level in SOD1^{G93A} muscle compared to WT, potentially minimises its responsiveness to androgens. Therefore, changes in growth factor expression such as decreased in IGF-1, are not observed upon antagonism of AR by flutamide. Further exploration into muscle-related transcription targets, regulated through androgens and AR enhancement, especially within the context of ALS, would be beneficial to build on the preliminary evidence we report here showing reduced AR signalling in muscle of SOD1^{G93A} male mice.

Acknowledgements

This projected was assisted by funding from the Australian NHMRC (Project Grants 1104295, 1104299), Stafford Fox Medical Research Foundation, MND Research Institute of Australia (Ted Dimmick Memorial MND Research Grant). VM received support from an MND Research Institute of Australia PhD Scholarship Top-Up Grant, NP is the recipient of an MND Research Institute of Australia Postdoctoral Fellowship, BT was supported by an NHMRC-ARC Dementia Research Leadership Fellowship 1137024.

Conflict of Interest

The authors have no conflict of interest to disclose.

Ethical Publication Statement

We confirm that we have read the Journal's position on issues involved in ethical publication and affirm that this report is consistent with those guidelines.

References

1. Kiernan, M.C., et al., *Amyotrophic lateral sclerosis.* Lancet, 2011. **377**(9769): p. 942-55.
2. Gurney, M.E., et al., *Motor neuron degeneration in mice that express a human Cu,Zn superoxide dismutase mutation.* Science, 1994. **264**(5166): p. 1772-5.
3. Fischer, L.R., et al., *Amyotrophic lateral sclerosis is a distal axonopathy: evidence in mice and man.* Exp Neurol, 2004. **185**(2): p. 232-40.
4. Dobrowolny, G., et al., *Muscle expression of a local Igf-1 isoform protects motor neurons in an ALS mouse model.* J Cell Biol, 2005. **168**(2): p. 193-9.
5. Li, W., et al., *Muscle-derived but not centrally derived transgene GDNF is neuroprotective in G93A-SOD1 mouse model of ALS.* Exp Neurol, 2007. **203**(2): p. 457-71.
6. Chambon, C., et al., *Myocytic androgen receptor controls the strength but not the mass of limb muscles.* Proc Natl Acad Sci U S A, 2010. **107**(32): p. 14327-32.
7. MacKrell, J.G., et al., *Molecular targets of androgen signaling that characterize skeletal muscle recovery and regeneration.* Nucl Recept Signal, 2015. **13**: p. e005.
8. Verhovshek, T., L.M. Rudolph, and D.R. Sengelaub, *Brain-derived neurotrophic factor and androgen interactions in spinal neuromuscular systems.* Neuroscience, 2013. **239**: p. 103-14.
9. Xu, J., et al., *Blockade of endogenous neurotrophic factors prevents the androgenic rescue of rat spinal motoneurons.* J Neurosci, 2001. **21**(12): p. 4366-72.
10. Cary, G.A. and A.R. La Spada, *Androgen receptor function in motor neuron survival and degeneration.* Phys Med Rehabil Clin N Am, 2008. **19**(3): p. 479-94, viii.
11. Widmer, C.G. and J. Morris-Wiman, *Limb, respiratory, and masticatory muscle compartmentalization: developmental and hormonal considerations.* Prog Brain Res, 2010. **187**: p. 63-80.
12. Huguenard, A.L., et al., *Overexpression of androgen receptors in target musculature confers androgen sensitivity to motoneuron dendrites.* Endocrinology, 2011. **152**(2): p. 639-50.
13. McLeod, V.M., et al., *Androgen receptor antagonism accelerates disease onset in the SOD1(G93A) mouse model of amyotrophic lateral sclerosis.* Br J Pharmacol, 2019. **176**(13): p. 2111-2130.
14. Yoo, Y.E. and C.P. Ko, *Dihydrotestosterone ameliorates degeneration in muscle, axons and motoneurons and improves motor function in amyotrophic lateral sclerosis model mice.* PLoS One, 2012. **7**(5): p. e37258.
15. McLeod, V.M., et al., *Dysregulation of Steroid Hormone Receptors in Motor Neurons and Glia Associates with Disease Progression in ALS Mice.* Endocrinology, 2020. **161**(9).
16. McLeod, V.M., et al., *Exploring germline recombination in Nestin-Cre transgenic mice using floxed androgen receptor.* Genesis, 2020: p. e23390.
17. Galbiati, M., et al., *The anabolic/androgenic steroid nandrolone exacerbates gene expression modifications induced by mutant SOD1 in muscles of mice models of amyotrophic lateral sclerosis.* Pharmacol Res, 2012. **65**(2): p. 221-30.
18. Sohrabji, F., R.C. Miranda, and C.D. Toran-Allerand, *Identification of a putative estrogen response element in the gene encoding brain-derived neurotrophic factor.* Proc Natl Acad Sci U S A, 1995. **92**(24): p. 11110-4.
19. Monks, D.A., E.L. O'Bryant, and C.L. Jordan, *Androgen receptor immunoreactivity in skeletal muscle: enrichment at the neuromuscular junction.* J Comp Neurol, 2004. **473**(1): p. 59-72.
20. Sinha-Hikim, I., et al., *Androgen receptor in human skeletal muscle and cultured muscle satellite cells: up-regulation by androgen treatment.* J Clin Endocrinol Metab, 2004. **89**(10): p. 5245-55.
21. Manzano, R., et al., *Altered in vitro proliferation of mouse SOD1-G93A skeletal muscle satellite cells.* Neurodegener Dis, 2013. **11**(3): p. 153-64.
22. Halievski, K., et al., *Disease Affects Bdnf Expression in Synaptic and Extrasynaptic Regions of Skeletal Muscle of Three SBMA Mouse Models.* Int J Mol Sci, 2019. **20**(6).

246 23. Funakoshi, H., et al., *Differential expression of mRNAs for neurotrophins and their receptors*
247 *after axotomy of the sciatic nerve.* J Cell Biol, 1993. **123**(2): p. 455-65.
248 24. Miyamoto, J., et al., *The pituitary function of androgen receptor constitutes a glucocorticoid*
249 *production circuit.* Mol Cell Biol, 2007. **27**(13): p. 4807-14.

250

251

Figure 1.

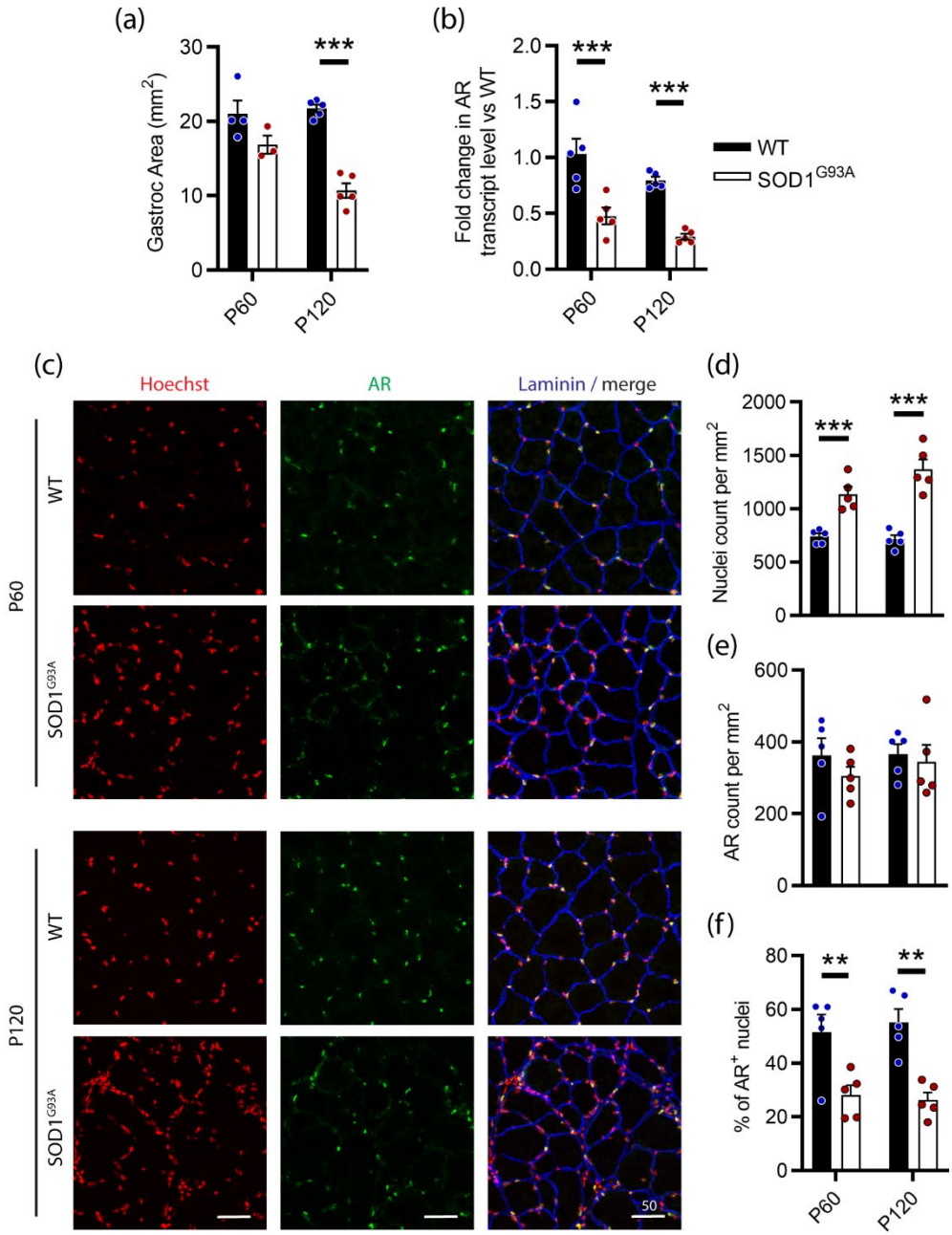

Figure 1. AR transcript and immunohistochemical analysis in gastrocnemius muscle from pre-symptomatic (P60) and symptomatic (P120) WT and SOD1^{G93A} transgenic male mice. (a) Gastrocnemius muscle cross-sectional area. (b) Quantification of AR transcript levels relative to P60 WT group. (c) AR nuclear staining identified in muscle cross section, scale bar = 50 µm. (d) Quantification of Hoechst stained and (e) AR positive nuclei per unit area of muscle cross-section. (f) AR positive staining expressed as a % of total nuclei. Data represent mean ± SEM, n=3-5 mice per group. ** *P*<0.01, *** *P*<0.001, significantly different to WT male by two-way ANOVA with Sidak's multiple comparisons test comparing genotype.

Figure 2.

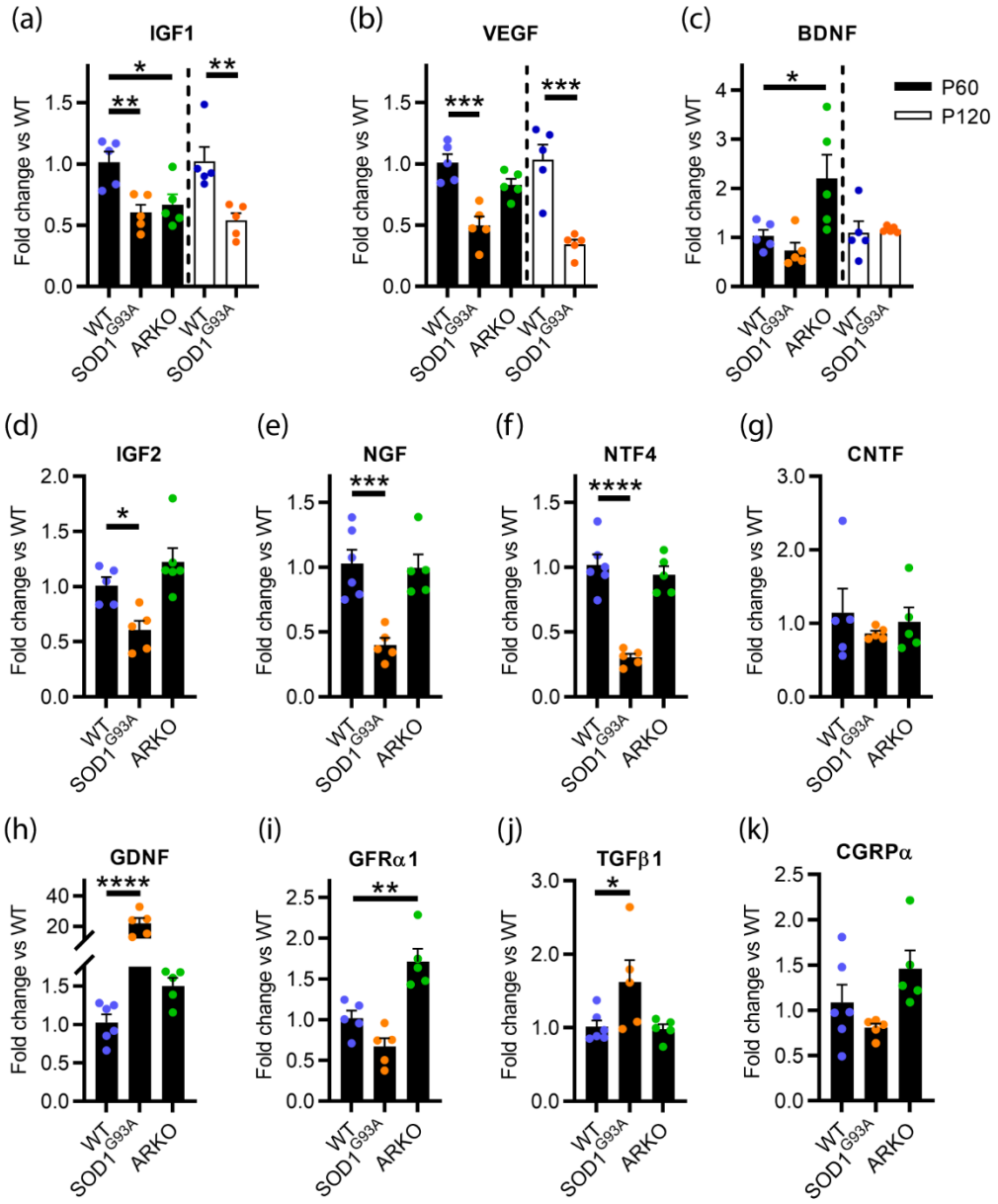

Figure 2. Analysis of mRNA transcripts in gastrocnemius muscle from pre-symptomatic (P60) and symptomatic (P120) WT, SOD1^{G93A} and AR knockout male mice. qRT-PCR analysis of (a) IGF-1, (b) VEGF, and (C) BDNF in P60 SOD1^{G93A} and ARKO mice compared to WT and P120 SOD1^{G93A} compared to WT, data analysed separately as indicated by dashed line. qRT-qPCR analysis of (d) IGF-2, (e) NGF, (f) NTF4, (g) CNTF, (h) GDNF, (i) GDNF receptor, (j) TGF-β1, and (k) CGRPα in P60 SOD1^{G93A} and ARKO mice compared to WT. Data represent mean ± SEM, n=5 mice per group. * P<0.05, ** P<0.01, *** P<0.001, **** P<0.0001, significantly different to WT male by one-way ANOVA with Dunnett's multiple comparison test for P60 data or unpaired t-test for P120 data.

274 **Figure 3.**

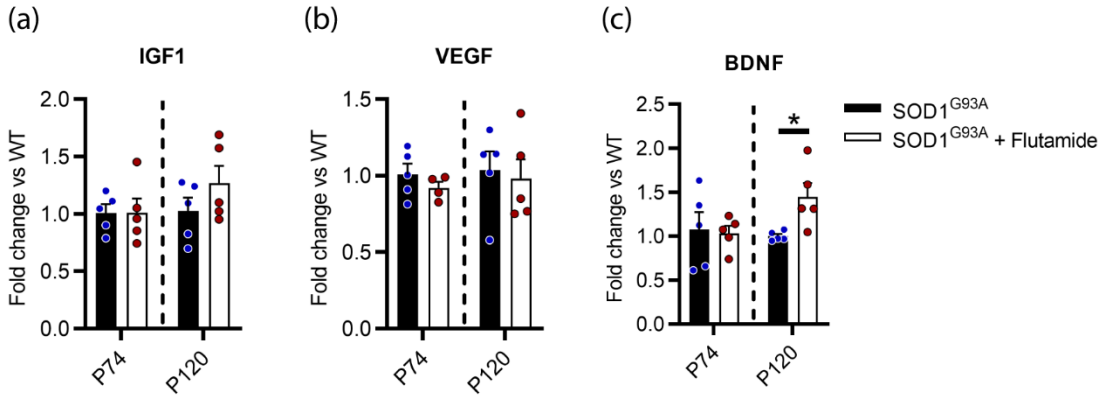

275 **Figure 3. Analysis of mRNA transcripts in gastrocnemius muscle from flutamide treated SOD1^{G93A}**
276 **mice compared to control SOD1^{G93A} mice**. qRT-PCR analysis of (a) IGF-1, (b) VEGF, and (C) BDNF in
277 male SOD1^{G93A} at P74 and P120 following continuous flutamide (4.7 mg/day) treatment from P60
278 compared to placebo control mice. Data represent mean ± SEM, n=5 mice per group. * *P*<0.05,
279 significantly different to WT by unpaired t-test.

280

Supplementary Material

Early downregulation in skeletal muscle androgen receptor occurs in SOD1^{G93A} mice with dual effects on neurotrophic support

Victoria M. McLeod[1], Nirma D. Perera[1], Wah C. Boon[1], Bradley J. Turner[1,2,*]

[1]*Florey Institute of Neuroscience and Mental Health, University of Melbourne, Parkville, VIC 3052, Australia.*

[2]*Perron Institute for Neurological and Translational Science, Queen Elizabeth Medical Centre, Nedlands, WA 6150, Australia*

Extended methods

Animals

All mice genotypes were maintained on a C57BL/6J background, in standard SPF-housing with free-access to standard rodent chow and water. For assessment of AR level and transcript levels of IGF-1, BDNF and VEGF, SOD1^{G93A} transgenic male mice and litter matched WT mice were aged to P60 and P120 for tissue collection of gastrocnemius muscle and lumbar spinal cord. (n=5 mice per group). ARKO mice were aged to P60 for transcript assessment in gastrocnemius muscle and lumbar spinal cord (n=5). Due to *Ar* having X-chromosome inheritance and infertility issues of the ARKO and female SOD1^{G93A} mice, generating an ARKO x SOD1^{G93A} mouse model was not possible. For this reason we used chronic AR antagonism to study inhibition of AR signalling in SOD1^{G93A} mice. Flutamide treated mice have been previously described [2], briefly at P60, male and female SOD1^{G93A} mice were implanted with a chronic slow release flutamide capsule, and gastrocnemius and lumbar tissue was collected at both P74 (14 days post-treatment) and at P120 (n=5 mice per group).

Immunohistochemistry

Fresh gastrocnemius muscle was snap frozen in Tissue-Tek O.C.T embedding media (Sakura Finetek, CA) and stored at -80°C prior to sectioning. The cross-sectional image of the gastrocnemius muscle belly was acquired at 20x magnification using tiled acquisition on a Leica DMLB2 microscope and area measured using ImageJ software. For chromogenic detection of PAX7, muscle sections were fixed in 4% paraformaldehyde for 10 min and then antigen retrieval was performed by baking slides at 95ºC in citrate buffer for 10 min. Endogenous peroxidase was quenched in 0.5% hydrogen peroxide and tissue permeabilised in 0.3% triton-X in PBS. Sections were blocked using animal-free blocking reagent (Cell Signalling Technology, Cat# 15019) for 1 h at room temperature and primary antibody against PAX7 supernatant (1:5, DSHB Cat# pax7, RRID:AB_528428) incubated at 4ºC for 48 h in SignalStain® antibody diluent (Cell Signalling Technology, Cat# 8112). SignalStain® Boost IHC Detection Reagent (CST, Cat# 8125) was used as a secondary detection reagent and DAB colorimetric reaction performed using SignalStain® DAB Substrate Kit (CST, Cat# 8059). Images were acquired on a Leica DMLB2 microscope.

qRT-PCR

Gastrocnemius and lumbar tissue was processed as previously described [1,2] from n=5-6 mice per genotype. For SOD1^{G93A} vs. WT vs. ARKO male mice tissue was collected at P60; some additional transcripts were compared between SOD1^{G93A} vs. WT in symptomatic P120 mice. For flutamide-treated SOD1^{G93A} mice, comparisons to placebo control SOD1^{G93A} mice were conducted at P74 and P120 in both male and female cohorts. *Hprt1* housekeeping gene was used in lumbar spinal cord tissue and for within SOD1^{G93A} mouse muscle comparisons. *PPIA* was used for muscle comparison between wildtype and transgenic mice.

Table S1. Primer sequences

Gene ID	Target protein	Forward sequence 5'-3'	Reverse sequence 5'-3'	Previous reference
Ar	AR	GTGAAATGGGACCTTGGATG	GCCAGAAGCTTCATCTCCAC	[1]
Igf1	IGF-1	TGGATGCTCTTCAGTTCGTG	GCAACACTCATCCACAATGC	
Vegfa	VEGF	CACGACAGAAGGAGAGCAGA	ACACAGGACGGCTTGAAGAT	
Bdnf	BDNF	TGGCTGACACTTTTGAGCAC	CAAAGGCACTTGACTGCTGA	
Igf2	IGF-2	CGCTTCAGTTTGTCTGTTCG	GGGGTGGCACAGTATGTCTC	
Ngf	NGF	ACCACAGCCACAGACATCAA	GCACCCACTCTCAACAGGAT	
Ntf4	Neurotrophin 4	TCCCCTGCGTCAGTACTTCT	TTGCATTCTGAGAGCCAGTG	
Cntf	CNTF	TGGCTAGCAAGGAAGATTCG	CATCTCACTCCAGCGATCAG	
Gdnf	GDNF	TGGGCTATGAAACCAAGGAG	CAACATGCCTGGCCTACTTT	
Gfra1	GDNF receptor α1	AGAACGAGAGAGGCCCAACT	GGCAGTCTGCGTAGTTCTCC	
Tgfb1	TGF-β1	TGCGCTTGCAGAGATTAAAA	CGTCAAAAGACAGCCACTCA	[2]
Calca	CGRPα	TGGTTGTCAGCATCTTGCTC	CAGCAGGCGAACTTCTTCTT	
Esr1	ERα	TGCAATGACTATGCCTCTGG	CTCCGGTTCTTGTCAATGGT	[1]
Nrn1	Neuritin	GGGCTTTTCAGACTGTTTGC	TAAGAGCTGTGACCGTGCAG	
Ntrk2	TrkB	CGAACCTGCAGATACCCAAT	CCAACGTCCCAGTACAAGGT	
Cntfr	CNTF receptor	CTGTTTCCACCGTGACTCCT	AAGCCCTTGGGGTAAGTGTT	
Hprt1	HPRT1	GATCAGTCAACGGGGGACAT	CATTTTGGGGCTGTACTGCTT	[2]
PPIA	Cyclophilin A	CTTGGGCCGCGTCTCCTTC	TGCCGCCAGTGCCATTAT	[3]

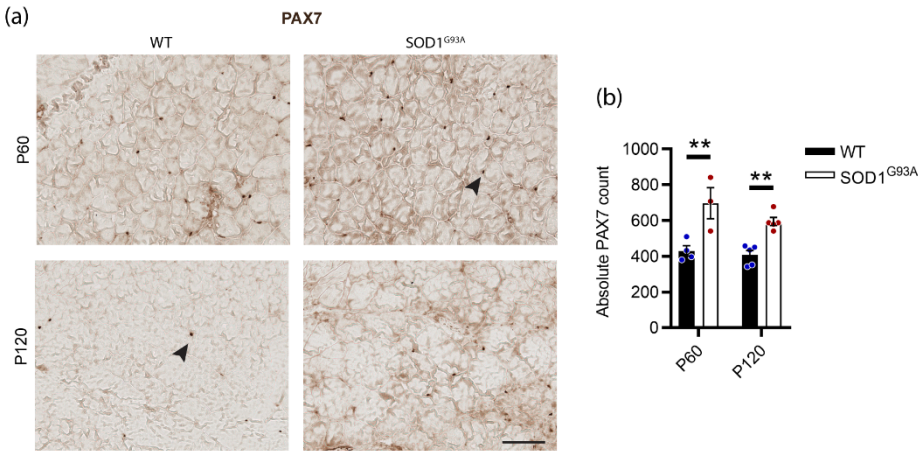

Figure S1. PAX7 immunohistochemical analysis in gastrocnemius muscle of WT and SOD1^{G93A} mice. (a) PAX7 nuclear staining (arrow heads) identified in the nuclei of muscle cross section in P60 and P120 male mice. Scale bar = 50 µm. (b) Quantification of PAX7 in muscle cross section. Data represent mean ± SEM, n=3-5 mice per group. ** P<0.01, significantly different to WT male by two-way ANOVA with Sidak's multiple comparison test comparing genotype.

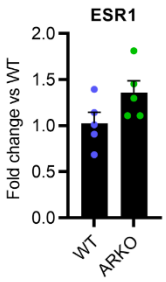

Figure S2. Analysis of ERα mRNA transcript in gastrocnemius
qRT-PCR analysis of ESR1 in wiltype vs. AR knockout mice at age P60. Data represent mean ± SEM, n=5 mice per group. P=0.0996 by unpaired t-test

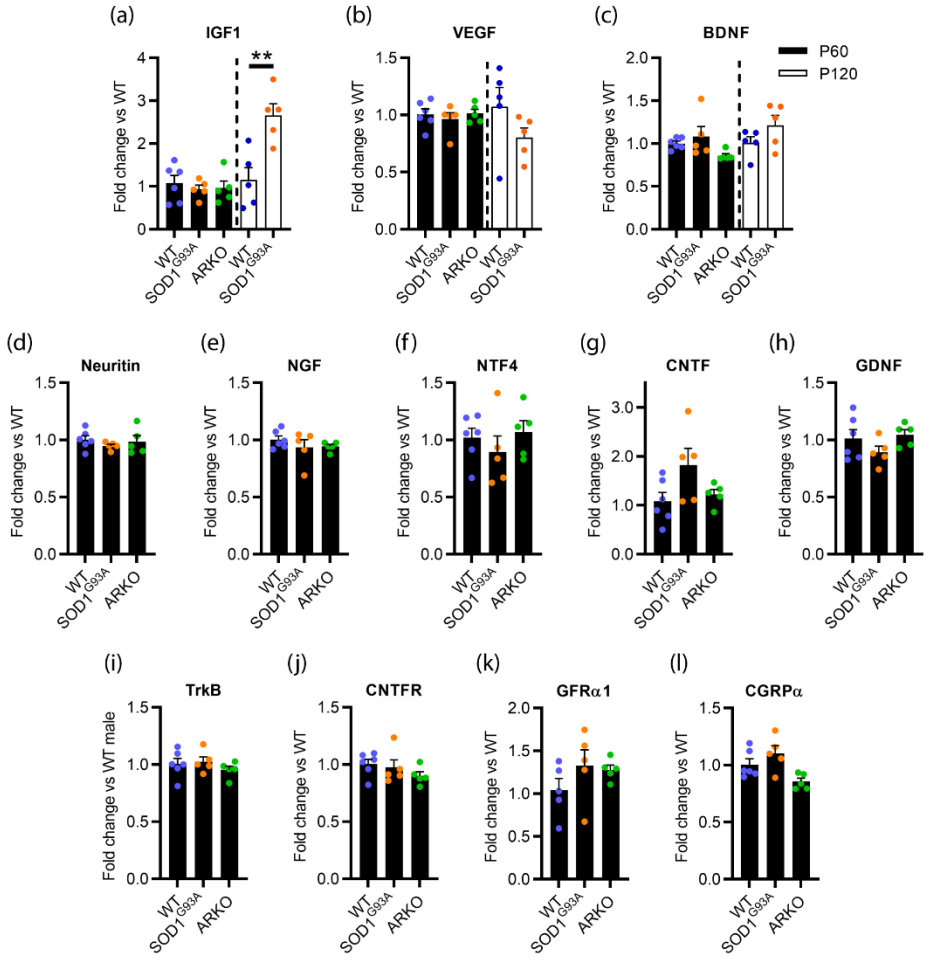

Figure S3. Analysis of mRNA transcripts in lumbar spinal cord from presymptomatic (P60) and symptomatic (P120) WT, SOD1^{G93A} and AR knockout male mice. qRT-PCR analysis of (a) insulin-like growth factor 1 (IGF-1), (b) vascular endothelial growth factor (VEGF), and (C) brain derived neurotrophic factor (BDNF) in P60 SOD1^{G93A} and ARKO mice and P120 SOD1^{G93A} compared to respective WT, data analysed separately as indicated by dashed line. qRT-qPCR analysis of (d) neuritin, (e) nerve growth factor (NGF), (f) neurotrophin-4 (NTF4), (g) ciliary neurotrophic factor (CNTF), (h) glial cell-derived neurotrophic factor (GDNF), (i) tropomyosin receptor kinase B (TrkB), (j) CNTF receptor, (k) GDNF receptor and (l) calcitonin gene-related peptide alpha (CGRPα) in P60 SOD1^{G93A} and ARKO mice compared to WT. Data represent mean ± SEM, n=5 mice per group. ** P<0.01, significantly different to WT unpaired t-test.

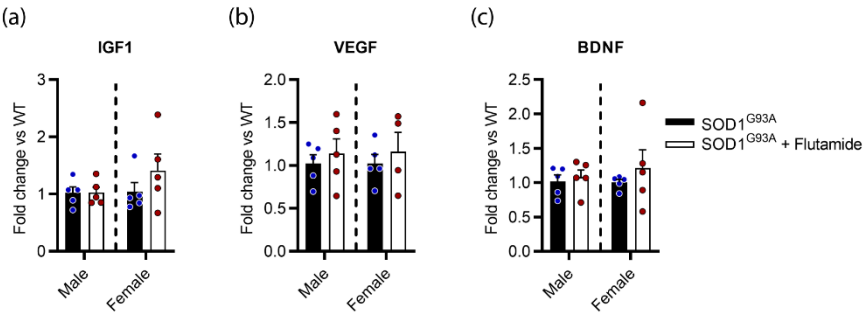

Figure S4. Analysis of mRNA transcripts in lumbar spinal cord from P120 flutamide treated SOD1^{G93A} mice compared to control mice. qRT-PCR analysis of (a) IGF-1, (b) VEGF, and (C) BDNF in male and female SOD1^{G93A} treated from P60 age with flutamide (4.7 mg/day) compared to placebo control. Data represent mean ± SEM, n=5 mice per group.

References

1. McLeod, V.M., et al., *Dysregulation of Steroid Hormone Receptors in Motor Neurons and Glia Associates with Disease Progression in ALS Mice.* Endocrinology, 2020. **161**(9).
2. McLeod, V.M., et al., *Androgen receptor antagonism accelerates disease onset in the SOD1(G93A) mouse model of amyotrophic lateral sclerosis.* Br J Pharmacol, 2019. **176**(13): p. 2111-2130.
3. Boon, W.C., et al., *Hippocampal NMDA receptor subunit expression and watermaze learning in estrogen deficient female mice.* Brain Res Mol Brain Res, 2005. **140**(1-2): p. 127-32.

Chapter 5. Androgen receptor antagonism accelerates disease onset in the SOD1^{G93A} mouse model of amyotrophic lateral sclerosis

Received: 17 October 2018 | Revised: 25 January 2019 | Accepted: 20 February 2019

DOI: 10.1111/bph.14657

RESEARCH PAPER

Androgen receptor antagonism accelerates disease onset in the SOD1^{G93A} mouse model of amyotrophic lateral sclerosis

Victoria M. McLeod[1] | Chew L. Lau[1] | Mathew D.F. Chiam[1] | Thusitha W. Rupasinghe[2] | Ute Roessner[2] | Elvan Djouma[3] | Wah C. Boon[1] | Bradley J. Turner[1]

[1] Florey Institute of Neuroscience and Mental Health, University of Melbourne, Parkville, VIC, Australia

[2] Metabolomics Australia, School of BioSciences, University of Melbourne, Melbourne, VIC, Australia

[3] Department of Physiology, Anatomy and Microbiology, La Trobe University, Bundoora, VIC, Australia

Correspondence
Bradley J. Turner, Florey Institute of Neuroscience and Mental Health, University of Melbourne, 30 Royal Parade, Parkville, VIC 3052, Australia.
Email: bradley.turner@florey.edu.au

Funding information
Motor Neurone Disease Research Institute of Australia (MNDRIA), Grant/Award Number: 1557; National Health and Medical Research Council (NHMRC), Grant/Award Numbers: 1104295 and 1104299; Mr Tony Gray; Pratt Foundation; Stafford Fox Medical Research Foundation

Background and Purpose: Amyotrophic lateral sclerosis (ALS) is a fatal neurodegenerative disease typically more common in males, implicating androgens in progression of both patients and mouse models. Androgen effects are mediated by androgen receptor which is highly expressed in spinal motor neurons and skeletal muscles. To clarify the role of androgen receptors in ALS, we therefore examined the effect of androgen receptor antagonism in the SOD1^{G93A} mouse model.

Experimental Approach: The androgen receptor antagonist, flutamide, was administered to presymptomatic SOD1^{G93A} mice as a slow-release subcutaneous implant (5 mg·day^{-1}). Testosterone, flutamide, and metabolite levels were measured in blood and spinal cord tissue by LC–MS–MS. Effects on disease onset and progression were assessed using motor function tests, survival, muscle, and neuropathological analyses.

Key Results: Flutamide was metabolised to 2-hydroxyflutamide achieving steady-state plasma levels across the study duration and reached the spinal cord at pharmacologically active concentrations. Flutamide treatment accelerated disease onset and locomotor dysfunction in male SOD1^{G93A} mice, but not female mice, without affecting survival. Analysis of hindlimb muscles revealed exacerbation of myofibre atrophy in male SOD1^{G93A} mice treated with flutamide, although motor neuron pathology was not affected.

Conclusion and Implications: The androgen receptor antagonist accelerated disease onset in male SOD1^{G93A} mice, leading to exacerbated muscle pathology, consistent with a role of androgens in modulating disease severity, sexual dimorphism, and peripheral pathology in ALS. These results also demonstrate a key contribution of skeletal muscle pathology to disease onset, but not outcome, in this mouse model of ALS.

1 | INTRODUCTION

Amyotrophic lateral sclerosis (ALS) is a fatal adult onset neurodegenerative disorder characterised by the loss of upper (motor cortex) and lower (brainstem and spinal cord) motor neurons, ultimately resulting in respiratory paralysis and death typically within 3–5 years following diagnosis (Brown & Al-Chalabi, 2017). ALS pathophysiology encompasses both cell and non-cell autonomous mechanisms, the latter involving centrally (astrocytes, microglia, and oligodendrocytes) and peripherally (Schwann cells, skeletal myocytes, and T-cells) acting contributors to motor neuron survival (Taylor, Brown, & Cleveland, 2016). The origins and trajectory of motor neuron loss within the CNS have become one of the most contested topics in ALS research. Two main

Abbreviations: ALS, amyotrophic lateral sclerosis; DHT, dihydrotestosterone; HF, 2-hydroxyflutamide; SBMA, spinal and bulbar muscular atrophy

theories have emerged: the "dying-forward" hypothesis which proposes that upper motor neurons initially die, promoting the death of their monosynaptic connections, the lower motor neurons in the spinal cord through **glutamate** toxicity (Geevasinga, Menon, Ozdinler, Kiernan, & Vucic, 2016); and second, the "dying-back" hypothesis whereby the disease starts in the lower motor neurons with the destruction of the neuromuscular junction (NMJ) and retraction of axons preceding cell death (Moloney, de Winter, & Verhaagen, 2014).

ALS shows sexual dimorphism in incidence, age of onset, and anatomical site of onset, with males usually having higher incidence, earlier age of onset, and presenting with spinal onset symptoms, as opposed to bulbar onset (McCombe & Henderson, 2010). While this evidence is largely based on cohorts of sporadic ALS patients, accounting for 90% of the disease, other evidence suggests a male predominance in familial ALS patients with SOD1 mutations (Kim et al., 2007) and *C9orf72* repeat expansions (Rooney et al., 2017). Sex-related effects are reproduced in the $SOD1^{G93A}$ mouse model of ALS with males showing earlier disease onset with decreased survival, depending on the background strain (Pfohl, Halicek, & Mitchell, 2015). Furthermore, $TDP\text{-}43^{A315T}$ male mice have earlier disease onset and death, compared to females (Hatzipetros et al., 2014). Collectively, this evidence implicates hormonal influences, particularly androgens, in ALS pathogenesis.

Androgens, primarily **testosterone** and **dihydrotestosterone** (DHT), exert their biological effects through activation of the **androgen receptor**, a nuclear steroid receptor involved in the regulation of target gene transcription. Androgen receptor function is important to the survival, growth, and maintenance of both skeletal muscle and motor neurons (Cary & La Spada, 2008; Fargo, Galbiati, Foecking, Poletti, & Jones, 2008; Rana, Lee, Zajac, & MacLean, 2014). Androgens promote neurite outgrowth in cultured motor neurons (Marron et al., 2005) and promote recovery from facial nerve crush injury (Kujawa, Emeric, & Jones, 1991), as well as spinal and cranial nerve axotomy in vivo (Fargo et al., 2008). The polyglutamine disorder, spinal and bulbar muscular atrophy (SBMA), arises from a CAG repeat expansion mutation in the *AR* gene and leads to selective lower motor neuron death (Beitel, Alvarado, Mokhtar, Paliouras, & Trifiro, 2013; La Spada, Wilson, Lubahn, Harding, & Fischbeck, 1991), emphasizing the importance of androgen receptor signalling for motor neuron health.

However, the role of androgens in ALS, whether detrimental or protective, remains unclear. Castration of male $SOD1^{G93A}$ mice to deplete circulating androgens does not modify disease onset or survival (Aggarwal et al., 2014; Sheean et al., 2015), most likely due to persisting androgen production from adrenal glands, arguing for more systemic approaches to block androgen receptor signalling. In male $SOD1^{G93A}$ mice, administration of DHT was neuroprotective and improved survival (Yoo & Ko, 2012), while conversely, treatment with the anabolic steroid **nandrolone** worsened the phenotype in castrated $SOD1^{G93A}$ mice (Aggarwal et al., 2014). However, there have been no studies of the effects of antiandrogens in ALS to date.

Here, we examine the effects of **flutamide** treatment on disease onset, progression, and pathology in $SOD1^{G93A}$ mice. Flutamide is classified as a first-generation nonsteroidal antiandrogen therapy primarily used in the treatment of prostate cancer. Its mechanism of action as a competitive androgen receptor antagonist negates the effects mediated by testosterone and DHT. Flutamide is a low MW drug, well absorbed following oral and subcutaneous administration and is rapidly metabolised by the liver **CYP1A2** enzyme (Matsuzaki et al., 2006) to its biologically active form, 2-**hydroxyflutamide** (HF). In our experiments, flutamide administered to presymptomatic $SOD1^{G93A}$ mice accelerated onset of disease and locomotor deficits in males, but not females, without affecting survival. Moreover, flutamide worsened muscle atrophy at gene expression and histological levels in treated male $SOD1^{G93A}$ mice, suggesting that impaired androgen receptor signalling is detrimental in ALS.

What is already known

- Testosterone and dihydrotestosterone are key androgens that exert biological effects via activation of androgen receptors.
- Flutamide is a competitive androgen receptor antagonist that displaces androgen binding.

What this study adds

- This study demonstrates that flutamide treatment accelerates disease onset and muscle atrophy in ALS mice.
- Antagonism of androgen receptors reveals muscle wasting contributes to disease onset, but not outcome.

What is the clinical significance

- These findings suggest a potential protective role of androgens in modulating disease severity in ALS.

2 | METHODS

2.1 | Animals

All animal care and experimental procedures complied with the Australian National Health and Medical Research Council published Code of Practice and was approved by the Florey Institute of Neuroscience and Mental Health Animal Ethics Committee (approval number 15-060-FINMH). Animal studies are reported in compliance with the ARRIVE guidelines (Kilkenny, Browne, Cuthill, Emerson, & Altman, 2010; McGrath, Drummond, McLachlan, Kilkenny, & Wainwright, 2010) and with the recommendations made by the *British Journal of Pharmacology*. All human embryonic stem cell (hESC) experimentation was approved by the Biomedical Science Human Ethics Advisory Group, University of Melbourne (approval number 1647041.1).

2.2 | Androgen receptor luciferase reporter assay in hESC-derived motor neurons

H9 hESCs (RRID:CVCL_9773; Thomson et al., 1998) were differentiated into spinal motor neurons as previously described (Du et al., 2015) with modifications. Briefly, at 5 and 6 days in vitro (DIV), culture medium was supplemented with 50-ng·ml^{-1} GDF11, and SB431543 was removed. Stage 4 (from 19 DIV) medium was changed to BrainPhys® Neuronal Medium (STEMCELL Technologies, Melbourne, Australia). HB9^{+} and ChAT^{+} mature motor neurons for this differentiation protocol have been previously quantified and reported by our laboratory (Perera et al., 2017). Here, we confirm the expression of specific motor neuron markers ChAT and HB9, as well as androgen receptors, as detailed under the relevant experimental sections below.

At 19 DIV (Stage 4, Day 1), motor neuron spheres were gently dissociated using accutase digestion and transfected with a 1:1 DNA ratio of human androgen receptor construct and luciferase androgen receptor reporter construct (assay optimisation can be found in Figure S1) using the Neon® Transfection System (Life Technologies, Australia). Briefly, 96-well plates were coated 24 hr prior to cell plating with poly-L-ornithine (0.01% w/v), followed by laminin (20 µg·ml^{-1}) and fibronectin (5 µg·ml^{-1}) with overnight incubation at 37°C. The cell suspension containing 5-µg DNA/3.75 × 10^{6} cells was electroporated using a double 1,400 V, 20-ms pulse protocol and plated at 1.5 × 10^{5} cells per well in BrainPhys® medium with **Y7632**, a RHO/ROCK pathway inhibitor. At 24 hr post-transfection, Y-27632 was removed by full medium change, and cells were treated in duplicate wells with increasing concentrations (variable range from 0.1 nM to 100 µM) of testosterone, DHT, flutamide or HF alone, or flutamide in combination with 10-nM DHT or 50-nM testosterone. Drug stocks were prepared in ethanol with a 0.1% (v/v) final ethanol concentration in treatment medium. At 16 hr drug post-treatment, luciferase activity was measured using a Dual-Glo® Luciferase Assay System following the manufacturer's protocol and luminescence detected on a POLARstar Omega Microplate reader (BMG Labtech, Melbourne, Australia). Experiments were repeated in three independent cell differentiations. Firefly luminescence values were normalised against the *Renilla* luciferase construct which acted as an internal control for construct expression, and the response relative to untreated controls was determined. To compare androgen receptor activation, data were fitted to a log (agonist) versus response curve (Y = Bottom+(Top − Bottom)/[1+10$^{(\text{Log EC50} - X)}$]) with bottom constraint set to 1.0 (GraphPad Prism 7, La Jolla, CA, USA). Likewise, to assess effectiveness of androgen receptor antagonism, data were fitted to a log (antagonist) versus response curve (Y = Bottom+(Top − Bottom)/[1+10$^{(X - \text{Log IC50})}$]) with top constraint set to 1.0 and bottom constraint >0.

2.3 | Immunocytochemistry

The antibody-based procedures used in this study comply with the recommendations made by the *British Journal of Pharmacology* (Alexander et al., 2018). Cells at 19 DIV as stated above were plated onto glass coverslips of 1.5 thickness (Marienfield-Superior, Germany) in 48-well plates following coating with poly-L-ornithine, laminin, and fibronectin as detailed above. At Stage 4, Day 3, approximately 48 hr following plating, cells were fixed for 10 min in 4% paraformaldehyde and washed twice in DPBS. Cells were blocked in 10% normal donkey serum with 0.1% (v/v) Triton-X 100 in 0.1-M PBS and incubated overnight at 4°C in the following primary antibodies: rabbit anti-ChAT (1:500, Millipore Cat# AB143, RRID:AB_2079760), sheep anti-ChAT (1:300, Abcam Cat# ab18736, RRID:AB_2244867), chicken anti-β III tubulin (1:500, Abcam Cat# ab107216, RRID:AB_10899689), mouse anti-HB9 (5 µg·ml^{-1}, DSHB Cat# MNR2, RRID:AB_2314625), mouse anti-SMI-32 (1:1,000, BioLegend Cat# 801702, RRID:AB_2715852), and rabbit anti-androgen receptor (1:200, Cell Signaling Technology Cat# 5153, RRID:AB_10691711) in antibody diluent 5% (v/v) normal donkey serum with 0.1% (v/v) Triton-X 100 in 0.1-M PBS. Cells were incubated in the following secondary antibodies in the same diluent for 2 hr at room temperature: anti-rabbit Alexa Fluor®-488 (1:400, Jackson ImmunoResearch Labs Cat# 711-545-152, RRID:AB_2313584), anti-goat DyLight®-550 (1:400, Thermo Fisher Scientific Cat# SA5-10087, RRID:AB_2556667), anti-chicken Cy™3 (1:200, Jackson ImmunoResearch Labs Cat# 703-165-155, RRID:AB_2340363), and anti-mouse F(ab')$_2$ fragment Alexa Fluor®-647 (1:400, Jackson ImmunoResearch Labs Cat# 715-606-151, RRID:AB_2340866) followed by 10-min incubation in 1-µg·ml^{-1} Hoechst 33342 nuclear stain (LifeTech, Cat# H1399). Cells were imaged at 40× magnification on a Leica SP8 confocal microscope.

2.4 | Animals and drug administration

Transgenic SOD1^{G93A} mice (B6.Cg-Tg (SOD1*G93A)1Gur/J line, stock number 004435, RRID:IMSR_JAX:004435) were purchased from the Jackson Laboratory (Bar Harbor, ME, USA). This model was used for experiments as it remains the only validated mouse model of ALS for preclinical study according to the ALS Therapy Development Institute and reproduces much of the pathogenesis and pathology of clinical disease. The colony was maintained on a C57BL/6 background at the Florey Institute of Neuroscience and Mental Health Core Animal Services under specific pathogen-free conditions. Experimental animals were group housed in microisolator caging under standard 12-hr light–dark conditions with access to food and water ad libitum. At postnatal day 60 (P60), male and female SOD1^{G93A} mice were randomised to receive either flutamide or placebo control via surgically implanted subcutaneous slow-release drug pellets (100 mg per 21-day release; Innovative Research of America, Sarasota, FL, USA). Group sizes were based on the recommended preclinical study guidelines of the ALS Therapy Development Institute (Scott et al., 2008). Briefly, mice were anaesthetised with isoflurane, and drug pellets were inserted laterally under the skin of the upper back via an incision at the back of the neck. A single dose of meloxicam (3 mg·kg^{-1}, s.c. above the hindlimb) was given prior to incision to manage post-operative pain. Pellets were surgically replaced every 21 days until mice reached

clinical endpoint or a specified tissue collection time point. Serial blood collection (50–200 µl) was performed by submandibular bleed prior to drug administration and every 28 days until clinical endpoint. This part of the study was performed unblinded due to the distinctive yellow colour of flutamide and excreted metabolites, compared to the drug-void placebo pellet. Animals were killed with a lethal dose of sodium pentobarbitone (100 mg·kg^{-1}, i.p.), and (a) organs were collected, weighed, and snap frozen in dry ice, (b) the animal was transcardially perfused with 0.1-M PBS and tissue collected and snap frozen for LC–MS–MS analysis, or (c) the animal was transcardially perfused with 0.1-M PBS followed by 4% paraformaldehyde in 0.1-M PB with 1–2 hr post-fix and cryoprotected in a sucrose gradient 10%, 20%, and 30% in PBS for up to 5 days prior to snap freezing in isopentane cooled in dry ice.

2.5 | Behavioural and survival analyses

Mice were assessed weekly from treatment initiation for body weight change and motor performance. Motor coordination and function were determined on a Rota-Rod 47600 (Ugo Basile, Italy) with training as previously described (Perera et al., 2017). Mice were placed on an accelerating rod (4–40 r.p.m.) over a 5-min period. An average of two trials was conducted over a 1-hr period, and latency to fall was recorded for each animal. The appearance of disease onset was retrospectively determined using the age of maximal body weight which is a reliable and objective measure of muscle denervation onset, as previously described (Turner et al., 2014). Clinical endpoint criteria for survival analysis in SOD1^{G93A} mice were defined as the onset of paralysis in hindlimbs and/or the cumulative loss of 20% peak body weight. One female mouse from the flutamide treatment group was found dead without previous signs of clinical endstage and was excluded from survival analysis.

2.6 | Testosterone, flutamide, and metabolite assessment in plasma

At blood collection, EDTA (2.5 µmol per tube) was used as an anticoagulant, and plasma was isolated by centrifugation at 1,150 *g* for 10 min following collection and stored at −80°C. For extraction of total testosterone and flutamide, plasma aliquots of 25 µl were vortexed for 1 min in 200 µl of methyl tert-butyl ether (MTBE) containing 100 pg·ml^{-1} of 17α-hydroxyprogesterone-d_8 used as an internal standard. Following 10-min centrifugation at 21,000 *g*, the supernatant was collected, and the process was repeated on the remaining aqueous fraction. Combined supernatants were dried down using a rotary evaporator under 200 mbar, and pellets were reconstituted in 100 µl of 50/50 (v/v) acetonitrile and water.

Testosterone, flutamide, and flutamide metabolites (Tevell et al., 2006) were analysed by UHPLC-MS-MS coupled to an Agilent 6490 triple quadrupole with an Agilent 6490 triple quadrupole (QqQ) mass spectrometer. LC was performed on an Agilent UHPLC system equipped with a 1290 Infinity II pump, degasser, an autosampler, and a temperature-controlled column compartment. Chromatographic separation for testosterone, flutamide, and flutamide metabolites was achieved on an Agilent Poroshell 120 C18 (2.1 µm, 1.8 id × 100 mm) column connected with a guard column. The column oven temperature was maintained at 35°C, and the injection volume was set to 10 µl. A gradient mobile phase consisting of 1-mM ammonium fluoride in water (A) and methanol (B), at a flow rate of 0.25 ml·min^{-1}, was used.

Quantitation of the target analytes was performed in multiple reaction monitoring mode on an Agilent Jet Stream/ESI source in dual (positive and negative) modes. The specific multiple reaction monitoring transitions for testosterone, flutamide, HF, 4-nitro-3-(trifluoromethyl)-aniline (Flu-1), and 17α-hydroxyprogesterone-d_8 (internal standard) were monitored (20-ms dwell time per transition) at *m/z* 289.1 > 108.8, 275 > 204.8, 291 > 204.8, 205 > 204.8, and 339 > 100.1, respectively. All analyses were quantified using retention times and the ratios of selected precursor and product ions with those of standards. Data analysis was performed using Agilent Mass Hunter software (version B. 07.1, RRID:SCR_015040). Total testosterone in plasma was calculated based on solvent standards adjusted for extraction and processing recovery from plasma spiked standards, with a limit of quantitation at 27 pg·ml^{-1} (details are provided in the Supporting Information). Flutamide and metabolites, HF, and Flu-1 concentrations were determined based on a blank plasma spiked standard curve (Tables S2–S4).

2.7 | Testosterone, flutamide, and metabolite assessment in spinal cord

In animals treated for 2 weeks with either placebo or flutamide, ~30 mg of frozen spinal cord tissue was homogenised in 500 µl of ice-cold MTBE containing 100 pg·ml^{-1} of internal standard. Samples were placed in Lysing Matrix D, 2-ml tubes (MP Biomedicals, Australia) and homogenised in a Precellys® 24 homogeniser with cryolysis cooling (Bertin Technologies, France) using the 6,800 r.p.m., 3 × 30-s programme at −10°C. Homogenates were centrifuged at 21,000 *g* for 10 min, supernatant was removed, and pellet fraction was vortexed for 1 min in a second 500-µl internal standard containing aliquot of MTBE and centrifuged. Pooled supernatants were dried down and resuspended in 100 µl of 50/50 (v/v) acetonitrile and water before analysis by UHPLC–MS–MS as described above. Total testosterone, flutamide, HF, and Flu-1 concentrations were determined in tissue based on solvent and blank tissue spiked standards and presented as ng·g^{-1} tissue amounts.

2.8 | Protein extraction and immunoblot analysis

Cells were lysed in Triton-X lysis buffer (20-mM Tris-Cl, 150-mM NaCl, and 1% Triton-X 100) containing protease and phosphatase inhibitor cocktail tablets (Roche) for 20 min on ice. Supernatants obtained following centrifugation (21,000 *g* for 20 min at 4°C) were quantified for protein using the Direct Detect® IR Spectrometer (Millipore). For tissue, gastrocnemius muscle was firstly pulverised

mechanically in liquid nitrogen prior to processing for biochemical assays. Spinal cord and muscle tissue were homogenised by sonication in ice-cold RIPA buffer (50-mM Tris-Cl, pH 7.4, 150-mM NaCl, 0.1% SDS, 1% sodium deoxycholate, and 1% Triton-X 100) with the addition of protease and phosphatase inhibitor cocktail tablets. Sonication was conducted at 50% amplitude (Q55 Sonicator, Sonica, Newtown, CT, USA) with brief pulses applied over 10–15 s until tissue particulates were no longer visible and samples incubated on ice for 20 min before centrifugation at 21,000 *g* for 20 min at 4°C. Supernatants from tissue were collected and quantified for total protein using the BCA assay according to the manufacturer's protocol (Pierce® BCA assay kit, Thermo Fisher, Cat# 23225). Protein lysates were denatured by boiling in Laemmli buffer containing 2% (v/v) β-mercaptoethanol, and 50-µg protein was separated by electrophoresis on 4–20% Mini-PROTEAN® TGX Stain-Free™ gels for cell lysate or 4–15% Criterion™ TGX Stain-Free™ gels for tissue lysate (Bio-Rad Laboratories, NSW, Australia) and transferred onto PVDF membrane at 25 V for 16 min using a Trans-Blot® Turbo™ Transfer System (Bio-Rad). Total protein transferred onto membrane was imaged on a ChemiDoc™ MP Imaging System (Bio-Rad Laboratories) prior to blocking with 5% low-fat milk powder in TBST for 1 hr at room temperature and probed with rabbit primary antibody against androgen receptors (1:1,000 unpurified, Abcam, Cat# ab133273, RRID:AB_11156085), or antibody against human androgen receptors (1:1,000) and anti-HB9 antibody (1:50), both detailed above, using a SignalBoost™Immunoreaction Enhancer Kit (Merck Millipore, Cat# 407207) overnight at 4°C. Detection of mouse androgen receptors by immunoblotting was validated using testis tissue and androgen receptor knockout tissue as a positive and negative control, respectively. Membranes were probed with StarBright™ Blue 700 goat anti-rabbit secondary antibody (1:5,000, Bio-Rad, Cat# 12004161, RRID:AB_2721073) and DyLight 800 goat anti-mouse secondary antibody (1:5,000, Bio-Rad, Cat# STAR117D800GA, RRID: AB_10845157) for 1 hr at room temperature and imaged on a ChemiDoc™ MP. Primary antibody diluents were used sequentially up to three times for immunoblotting. For analysis, background adjusted total androgen receptor band intensity was normalised against background adjusted total lane protein intensity using Image Lab 6.0 software (Bio-Rad, www.bio-rad.com/en-au/product/image-lab-software, RRID:SCR_014210). Average group values were then expressed fold relative to averaged control group values (expressed as 1.0) to interpret any changes in protein abundance occurring in flutamide-treated animals.

2.9 | RNA extraction and qPCR analysis

RNA was extracted from cell cultures using the RNeasy Mini Kit (Qiagen, Cat# 74104) and from 30-mg gastrocnemius muscle using RNeasy Fibrous Tissue Mini Kit (Qiagen, Cat# 74704) according to the manufacturer's protocol with homogenisation of tissue using the TissueLyserLT (Qiagen) for 5 min at 50 Hz. cDNA was reverse transcribed using iScript™ Reverse Transcription Supermix (Bio-Rad, Cat# 1708841) under the following PCR conditions: 5 min at 25°C, 30 min at 42°C, and 5 min at 85°C. qPCR was performed using SsoAdvanced™ Universal SYBR® Green Supermix (Bio-Rad, Cat# 1725270), and 20-µl reaction volume containing 400 nM of each primer was run using CFX Manager™ 3.1 software (RRID: SCR_003375) provided with a CFX96™ Touch Real-Time PCR Detection System (Bio-Rad). Primers were designed using Primer3 v0.4.0 design tool (http://bioinfo.ut.ee/primer3-0.4.0/, RRID:SCR_003139) to cover majority of RefSeq transcript variants (UCSC Genome Browser, http://genome.ucsc.edu/, RRID:SCR_005780) as described in Table 1. Samples were run in triplicate, and data were expressed in Ct values normalised to *Gapdh* or *Hprt1* housekeeping gene for cells and tissue, respectively, and fold change between control and treated groups determined using the $2^{-\Delta\Delta Ct}$ method. Validation of *Gapdh* as the most viable housekeeping gene for comparisons across undifferentiated embryonic stem cell to mature motor neurons can be found in Table S1.

TABLE 1 Primer sequences

Gene name	Species	Forward primer	Reverse primer
Chat	Human	5′-TTTTGTGAGAGCCGTGACTG-3′	5′-GTCAATGGCCATCCCTGTTA-3′
Isl1	Human	5′-CGCCTTGCAGAGTGACATAG-3′	5′-AGGACTGGCTACCATGCTGT-3′
Mnx1	Human	5′-GCACCAGTTCAAGCTCAACA-3′	5′-CTTTTTGCTGCGTTTCCATT-3′
Gapdh	Human	5′-CTGACTTCAACAGCGACACC-3′	5′-CCCTGTTGCTGTAGCCAAAT-3′
Tgfb1	Mouse	5′-TGCGCTTGCAGAGATTAAAA-3′	5′-CGTCAAAAGACAGCCACTCA-3′
Myog	Mouse	5′-CAGTGAATGCAACTCCCACA-3′	5′-CTGTCCACGATGGACGTAAG-3′
Myod1	Mouse	5′-TACAGTGGCGACTCAGATGC-3′	5′-TAGTAGGCGGTGTCGTAGCC-3′
Chrng (nAChRγ)	Mouse	5′-GCAGGCAGTATTGGAGAAGC-3′	5′-ACGAGCCATGAGGTTACAGG-3′
Ncam1	Mouse	5′-CAGCAGTGAACCGTATTGGA-3′	5′-TCTGGCTCATCAAACTGCAC-3′
Musk	Mouse	5′-CTACCCTCAGCCCGAGATTT-3′	5′-TGTCTTCCACGCTCAGAATG-3′
Hprt1	Mouse	5′-GATCAGTCAACGGGGGACAT-3′	5′-CATTTTGGGGCTGTACTGCTT-3′

Note. nAChRγ: nicotinic ACh receptor γ.

2.10 | Spinal cord immunohistochemistry and image quantification

Lumbar spinal cord tissue was cryosectioned at 20 µm with 1:10 series mounted onto poly-L-lysine coated slides. For androgen receptor staining, antigen retrieval was performed by baking slides for 2 hr at 95°C in citrate buffer (10-mM citric acid, pH 6.0). Sections were blocked in 6% (v/v) normal donkey serum in 0.3% (v/v) Triton-X 100 in 0.1-M PBS for 1 hr at room temperature. An additional endogenous avidin–biotin blocking step (Endogenous Avidin/Biotin Blocking Kit, Abcam, Cat# ab64212) was performed according to the manufacturer's protocol. Primary antibodies including rabbit anti-androgen receptor (1:100 unpurified, Abcam, Cat# ab133273), goat anti-ChAT (1:100, Millipore, Cat# AB144P, RRID:AB_2079751), rat anti-GFAP (1:500, Zymed, Cat# 13-0300), and rat anti-CD11b (1:100, Bio-Rad, Cat# MCA711, RRID:AB_321292) were prepared in 2% (v/v) normal donkey serum in 0.3% (v/v) Triton-X 100 in 0.1-M PBS for a single use 48-hr incubation at 4°C. An additional 3-hr incubation at room temperature with donkey biotinylated-anti-rabbit (1:100, Jackson ImmunoResearch Cat# 711-065-152, RRID:AB_2340593) was included to amplify the detection of androgen receptors. Secondary antibodies were incubated for 2 hr at room temperature in the same antibody diluent, including streptavidin Alexa Fluor®-488 (1:200, Jackson ImmunoResearch Cat# 016-540-084, RRID:AB_2337249), anti-goat DyLight®-550 (1:200), and anti-rat Alexa Fluor®-647 (1:200, Jackson ImmunoResearch, Cat# 712-605-153, RRID:AB_2340694). For quantification of androgen receptors, staining for androgen receptors, detectable in the nucleus of ChAT-expressing motor neurons, was counted through L1–6 spinal cord ventral horns (~40 sections per mouse). Quantification of ChAT-positive motor neurons was determined by counting and averaging 10 sections (equivalent to 10 ventral horn pairs) selected at equally spaced intervals spanning L1–6 under 20× magnification. GFAP-positive astrocyte and CD11b-positive microglia images were acquired at 40× magnification with Z-stacked fields taken at 0.54 µm per step through an 8-µm stack (i.e., 15 images stacked together). An average of 10 fields were counted from separate ventral horns selected at equally spaced intervals spanning L1–6 and expressed as cells·mm^{-2} area. All images were captured by the Zeiss AxioObserver Z1 (Carl Zeiss Pty Ltd, North Ryde, Australia).

2.11 | Muscle immunohistochemistry and image quantification

Unperfused gastrocnemius muscle was collected and embedded in OCT prior to snap freezing in isopentane cooled over dry ice. Cross sections of 12 µm, one in 12 series, were slide mounted and dried for 1 hr at room temperature and either stored at −80°C or processed for immunostaining. Slides were drop fixed in neutral-buffered formalin for 10 min and rinsed in PBS. Sections were processed as described in previous setting without antigen-retrieval step for androgen receptor staining. For quantification of androgen receptor staining, sections were co-incubated with anti-androgen receptor (as above) and rat anti-laminin (1:200, Abcam, Cat# ab11576, RRID:AB_298180) for 48 hr at 4°C. Secondary antibody incubation was as described above, followed by 15-min incubation in 1-µg·ml^{-1} Hoechst 33342 nuclear stain. A series of five randomly selected images were taken from a single muscle cross section per animal, with treatment group blinding at 40× magnification on a Zeiss AxioObserver Z1, and total nuclei were determined by semi-automated particle analysis using ImageJ software (RRID:SCR_003070) followed by manual counting of androgen receptor positive nuclei. For analysis of fibre cross-sectional area, sections were immunolabelled with rabbit anti-laminin (1:500, Abcam, Cat# ab11575, RRID:AB_298179) to delineate the basement membrane, followed by anti-rabbit secondary as detailed above. Semi-automated analysis was performed using ImageJ software following the methodology described previously by Tyagi, Beqollari, Lee, Walker, and Bannister (2017), including a slight modification to the macro to allow fibres within the range of 100–20,000 µm^2 to be captured. A total of five randomly selected fields of view were taken at 20× magnification and averaged as representation of the gastrocnemius cross section, allowing ~800–1,000 fibres to be quantified per animal. NMJ staining was performed on 4% PFA perfused tissue with 24- to 48-hr cryoprotection in 20% sucrose in 0.1-M PB before rapid freezing in OCT. Fibres were longitudinally cryosectioned at 50 µm, one in six series, and slide mounted prior to staining. Sections were permeabilised in 2% Triton-X 100 in PBS for 30 min, followed by blocking in 5% normal donkey serum/3% BSA with 1% Triton-X 100 in PBS for 1 hr at room temperature. Primary antibody incubation with anti-neurofilament heavy chain (1:500, Abcam, Cat# ab8135, RRID:AB_306298) and anti-synaptophysin (1:200, Abcam, Cat# ab32594, RRID:AB_778204) was conducted overnight at 4°C in diluent containing 2% donkey serum/3% BSA/1% Triton-X 100 in PBS. Triplicate 15-min wash steps were followed by a 2-hr incubation in anti-rabbit DyLight®-550 secondary antibody (1:200, Thermo Fisher Scientific Cat# SA5-10039, RRID:AB_2556619) and 488-conjugated α-bungarotoxin (1:1,000, LifeTech, Cat# B13422). Images were acquired at 20× magnification on a Leica SP8 confocal microscope with Z-stacked fields taken at 2 µm per step through 20-µm stack (i.e., 10 images stacked together). An average of 10 fields were imaged per animal allowing approximately 100 NMJs to be analysed as fully innervated, partially innervated, or denervated.

2.12 | Data and statistical analyses

The data and statistical analyses comply with the recommendations on experimental design and analysis in pharmacology (Curtis et al., 2018). All analyses were performed using GraphPad Prism 7.0 software (San Diego, CA, USA, RRID:SCR_002798) and data presented as mean ± *SEM*. Survival of flutamide- and control-treated mice was compared using log-rank (Mantel–Cox) test with median values reported. Western blot data, ages to peak body weight and rotarod activity, motor neuron, and glial cell counts were analysed using two-way ANOVA with Fisher's least significant difference test for planned comparisons between control and flutamide or male and female where *F*

value indicated a significant difference ($P < 0.05$). Tissue weight, plasma testosterone concentrations over time, and myofibre diameter frequency in males were analysed by two-way ANOVA with Fisher's least significant difference test comparing control with flutamide group at each time interval or fibre diameter, respectively, where F value indicated a significant treatment difference. All other comparisons between control- and flutamide-treated means were using two-tailed Student's t test. In cases where a parametric test could not be used as significantly different variances occurred between groups, a Mann–Whitney test was used to compare control and flutamide group means. Only statistically significant data are reported for means including $n = 5$ with $P < 0.05$ taken as statistical significance.

2.13 | Materials

Stem cell reagents including Accutase™, BrainPhys™ neuronal medium, and Y-27632 were purchased from STEMCELL Technologies (VIC, Australia), Gibco™ natural mouse laminin protein was from Life Technologies (VIC, Australia), human fibronectin was from In Vitro Technologies (VIC, Australia), poly-L-ornithine 0.01% solution was from Sigma-Aldrich (NSW, Australia), and recombinant human GDF-11 was from Lonza (VIC, Australia). Testosterone, 5α-androstan-17β-ol-3-one (5α-DHT), flutamide, HF, 4-nitro-3-(trifluoromethyl) aniline, and 17α-hydroxyprogesterone-d8 were purchased from Sigma-Aldrich (Australia). Human ARQ24 androgen receptor plasmid (Simeoni et al., 2000) was kindly donated by Professor Angelo Poletti (University of Milan, Italy). Cignal Androgen Receptor Reporter (luc) Kit was purchased from Qiagen (VIC, Australia), and Dual-Glo® Luciferase Assay System was supplied by Promega Australia (NSW, Australia). Meloxicam animal analgesic was supplied by Troy Laboratories (NSW, Australia). Roche cOmplete™ Mini Protease Inhibitor Cocktail and PhosSTOP™ tablets were purchased from Sigma-Aldrich.

2.14 | Nomenclature of targets and ligands

Key protein targets and ligands in this article are hyperlinked to corresponding entries in http://www.guidetopharmacology.org, the common portal for data from the IUPHAR/BPS Guide to PHARMACOLOGY (Harding et al., 2018), and are permanently archived in the Concise Guide to PHARMACOLOGY 2017/18 (Alexander, Cidlowski et al., 2017; Alexander, Fabbro et al., 2017; Alexander, Kelly et al., 2017; Alexander, Peters et al., 2017).

3 | RESULTS

3.1 | Implantable flutamide pellets result in steady-state flutamide and hydroxyflutamide plasma levels and pharmacologically active concentrations in the spinal cord

We first established effective concentrations of flutamide to block androgen-induced activation of androgen receptors in vitro to extrapolate to spinal cord in vivo. hESC-derived motor neurons were validated for expression of motor neuron-specific markers at both transcript and protein levels (Figure 1a–e) including ChAT and HB9. These data were in line with previous quantification of this differentiation protocol by our laboratory where we reported 80% and 69% neurons positive for ChAT and HB9, respectively (Perera et al., 2017). hESC-derived motor neurons also expressed endogenous androgen receptors which were elevated by DHT treatment (Figure 1d) and were predominantly nuclear, as expected (Figure 1f). hESC-derived motor neurons expressing an androgen receptor-activated luciferase reporter showed concentration-dependent responses to the androgen receptor agonists, testosterone and DHT (Figure 1g). DHT showed a 10-fold greater potency, compared to testosterone, with maximal activation occurring from 10 to 100 nM, respectively. This reflects previous androgen receptor binding and potency data (Gao, Bohl, & Dalton, 2005). The flutamide metabolite, HF, showed weak agonist activity at high concentrations 10–100 μM in the absence of androgen receptor agonist, as previously described (Culig et al., 1999; Figure 1g). Flutamide revealed poor antagonist activity and was only effective at a single high dose concentration of 100 μM with HF showing dose-dependent inhibition of androgen receptor activation with a 50- to 100-fold higher pA_2, compared to flutamide (Figure 1h,i). Based on the IC_{50} (provided in Figure 1), an 11-fold and 36-fold molar excess of HF would be required to block 50% androgen receptor activation by 50-nM testosterone (Figure 1h) or 10-nM DHT (Figure 1i), respectively. For full androgen receptor inhibition, approximately 200-fold and 1,000-fold molar excess of HF would be anticipated to inhibit testosterone and DHT, respectively, based on maximal inhibitory responses achieved at 10-μM HF in hESC-derived motor neurons.

Next, male $SOD1^{G93A}$ mice were implanted with slow-release placebo control or flutamide pellets from postnatal day 60 (P60) using a dose regimen (5 mg·day^{-1}, s.c.) effective in mouse models of SBMA (Renier et al., 2014). Importantly, this dose of flutamide does not affect body weight and motor function in wild-type mice (Renier et al., 2014). Plasma levels of testosterone, flutamide, and its metabolites were first serially measured in implanted mice. Antagonism of androgen receptors in the hypothalamic gonadotropin-releasing hormone neurons results in disinhibition of androgen production via the HPG axis and systemic testosterone release by the testes (Figure S2). We confirmed a significant early elevation in circulating testosterone levels in response to flutamide treatment with a 6-fold increase, compared to control mice observed at P74 or 2 weeks post-treatment initiation (Figure 2a). A 2.5-fold elevation in testosterone levels persisted in flutamide-treated mice at P88 or 4 weeks post-treatment initiation. Circulating testosterone levels were comparable in flutamide and control male mice from P116 onwards. Over the course of the study, flutamide was maintained at a steady-state plasma concentration of approximately 100 ng·ml^{-1}, with metabolites HF at approximately 50-fold higher level and pharmacologically inactive, Flu-1, maintained at 10-fold lower plasma concentration, relative to flutamide (Figure 2b). The levels of testosterone and drug in spinal

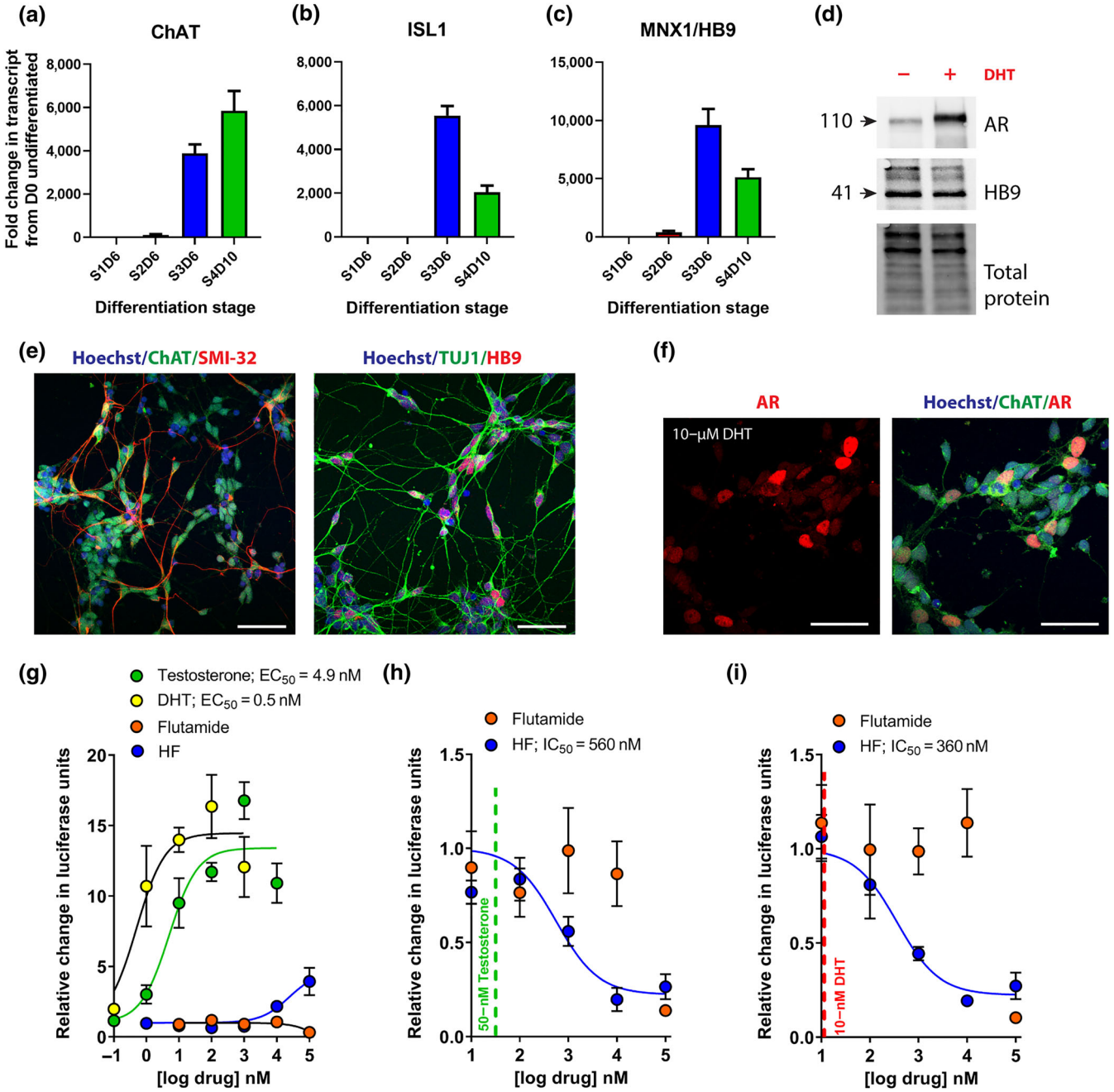

FIGURE 1 Agonist and antagonist dose responses of the luciferase androgen receptor reporter assay in human embryonic stem cell-derived motor neurons. qRT-PCR analysis of (a) ChAT, (b) ISL1, and (c) MNX1/HB9 expression various stages of the differentiation (Stages 1–4) compared to undifferentiated cells at Day 0. (d) Western blot confirming HB9 protein expression and androgen receptor (AR) expression in experimental motor neurons in the presence or absence of 10-μM DHT. (e) Immunocytochemistry confirming the expression of mature neuronal (TUJ1 and SMI-32) and motor neuron-specific (ChAT and HB9) markers in experimental motor neurons. Scale bar = 50 μm. (f) Expression of androgen receptors in motor neurons showing nuclear localisation in the presence of 10-μM DHT. Scale bar = 50 μm. (g) Activation of androgen receptors following 16-hr treatment with testosterone, DHT, flutamide, and HF over a 0.1- to 10^5-nM concentration range with the EC_{50} indicated where applicable. (h) Activation of androgen receptors following 16-hr co-treatment with testosterone and increasing concentrations of antagonist with IC_{50} value indicated for HF. Green dotted line indicates the basal 50-nM testosterone concentration. (i) Activation of androgen receptors following 16-hr co-treatment with DHT and increasing concentrations of antagonist with IC_{50} value indicated for HF. Red dotted line indicates the basal 10-nM DHT concentration. Data are presented as mean ± *SEM*, *n* = 3 independent experiments

cord tissue at 2 weeks post-treatment reflected systemic circulating levels (Figure 2c). Importantly, there was a ~250-fold molar excess of HF in spinal cord relative to testosterone, consistent with effective displacement of testosterone for androgen receptor binding and activation based on the hESC-derived motor neuron androgen receptor activation assay.

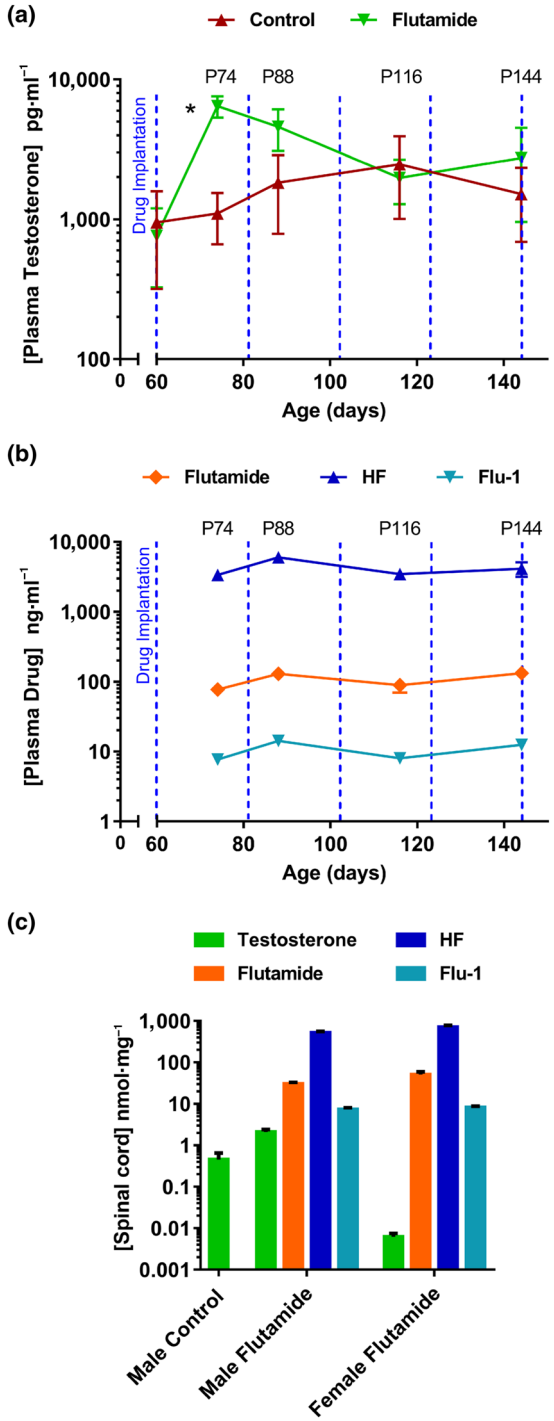

FIGURE 2 Testosterone, flutamide, and metabolite concentrations in plasma and spinal cord of male SOD1^{G93A} mice treated with either a placebo control or a flutamide-releasing s.c. implant from postnatal day 60 (P60). (a) Plasma testosterone levels in control- and flutamide-treated male mice from pre-implant to endstage of disease (n = 5–14 mice per group). *P < 0.05, significantly different to control; two-way ANOVA with Fisher's least significant difference test. (b) Plasma flutamide, HF, and Flu-1 levels in plasma of flutamide-treated male mice from 14 days post-implant (P74) to endstage of disease (n = 5–10 mice per group). Blue lines indicate when a 21-day slow-release pellet was implanted. (c) Spinal cord testosterone, flutamide, HF, and Flu-1 drug levels after 14 days post-treatment (P74) in male and female mice (n = 5 mice per group). Data represent mean ± *SEM*

3.2 | Flutamide decreases prostate and seminal vesicle weights in male SOD1^{G93A} mice

The prostate and seminal vesicles (SVs) are highly responsive to circulating androgens with weights reflecting circulating testosterone levels (van Roijen et al., 1997). Given that flutamide treatment elevates circulating testosterone levels, SV weight in the current study reflected the systemic effects of flutamide antagonism of androgen receptors. SV weight showed a significant 30% reduction following 2 weeks of flutamide treatment (P74) and a 50% reduction at 2 months post-treatment (P120; Figure 3a,b). Systemic androgen receptor antagonism was also reflected in flutamide-treated male prostate weights, with a significant 30–40% reduction, compared to control males at P74 and P120 (Figure 3c). While the testis is responsible for testosterone production and regulation from the HPG feedback system, we confirmed no change in testis weight over the duration of treatment (Figure 3d), in line with previous studies (Marchetti & Labrie, 1988).

3.3 | Flutamide reduces androgen receptor levels in skeletal muscle and spinal cord of male SOD1^{G93A} mice

We next determined androgen receptor expression in skeletal muscle and spinal cord in response to flutamide treatment in SOD1^{G93A} mice. Androgen receptors were detected in both male and female gastrocnemius muscles and spinal cord as a single ~110-kDa monomer (Figure 4a). As expected, androgen receptor levels were consistently and significantly ~50% lower in females, than males, in both skeletal muscle and spinal cord. Gastrocnemius muscle androgen receptor protein levels were similar in gastrocnemius muscles, irrespective of treatment at P74 (Figure 4a,b). Androgen receptor protein levels were reduced in male mice treated with flutamide at P120, although not statistically significant (Figure 4c,d). In spinal cord, androgen receptor levels were significantly decreased by 23% in male flutamide-treated mice, compared to control male mice at P74 (Figure 4e,f). In contrast, Androgen receptor expression in female spinal cord was not affected by flutamide treatment at P74. Lastly, Androgen receptor protein accumulation was again similarly decreased, although not statistically significant, in spinal cords of flutamide-treated male animals, compared to untreated male mice at P120 (Figure 4g,h).

To determine whether the nuclear translocation of androgen receptors was affected by flutamide in skeletal muscle and spinal cord, we examined the subcellular distribution of androgen receptors in male SOD1^{G93A} mice at P120 (Figure 4i–m). In concert with immunoblotting results in gastrocnemius muscle, there was a significant 50% reduction in the number of androgen receptor-positive myonuclei in flutamide-treated males, compared to controls (Figure 4j), which was independent of the total number of nuclei present in the muscle (Figure 4k). Flutamide treatment did not significantly affect the percentage of androgen receptor-positive nuclei in ChAT^{+} motor neurons in the spinal cord (Figure 4l) with approximately 15% of total motor

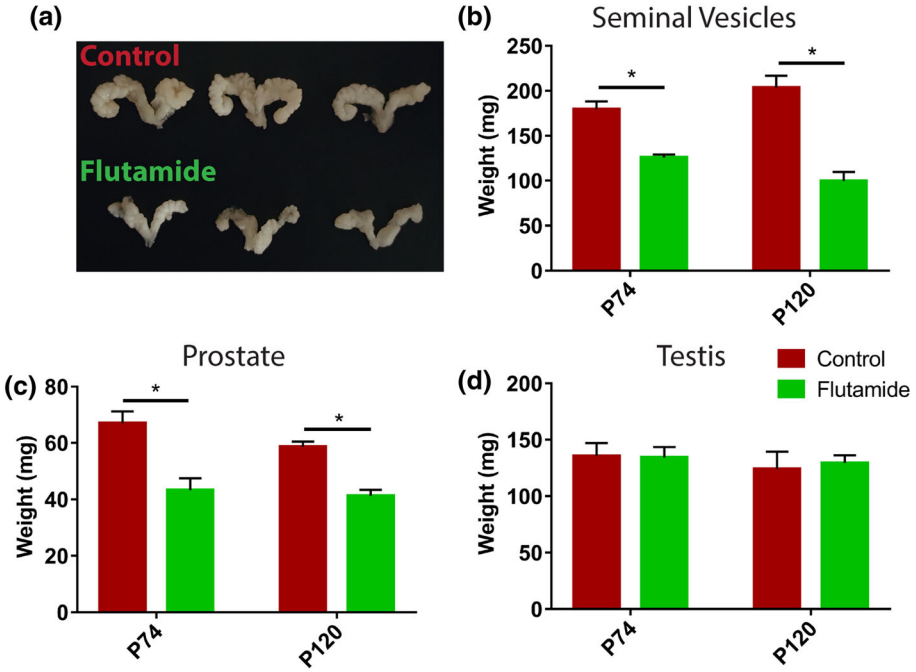

FIGURE 3 Effect of chronic flutamide treatment on the weights of male sex organs in SOD1^{G93A} mice. (a) Representative images of seminal vesicles at postnatal day 120 (P120). (b) Seminal vesicle weights at P74 and P120. *P < 0.05 significantly different from control; two-way ANOVA with Fisher's least significant difference test. (c) Prostate weights. *P < 0.05 significantly different from control; two-way ANOVA with Fisher's least significant difference test. (d) Testis weights. Data represent mean ± *SEM*, n = 5 mice per group

neurons showing androgen receptor-immunoreactive nuclei in both flutamide- and control-treated mice (Figure 4m); total ChAT^{+} motor neuron counts are reported in Figure 8b. Androgen receptor immunoreactivity was largely undetectable in gastrocnemius myocytes and spinal cord motor neurons of female mice (data not shown).

3.4 | Flutamide treatment accelerates disease onset and motor dysfunction in male SOD1^{G93A} mice

The effect of flutamide treatment on disease onset, progression, and survival was next assessed in SOD1^{G93A} mice. The mean disease onset, determined by the age of weight loss onset, was significantly hastened by 19 days in flutamide-treated male mice, compared to control males (Figure 5a). Flutamide did not affect disease initiation in female mice, compared to control females. Flutamide did not show a significant reduction in the absolute body weights of male and female mice compared to their control counterparts, although male mice showed a significant interaction effect between treatment and time by two-way ANOVA (Figure S3A,B). A comparison of locomotor function at disease onset in flutamide-treated males revealed a significant treatment interaction effect with a deficit in rotarod test performance, compared to control males (Figure 5b). There was no effect of flutamide on locomotor function of female mice at disease onset. Neither male nor female mice showed a significant treatment interaction with declining locomotor function over the duration of the disease (Figure S3C,D).

Kaplan–Meier analysis of disease onset showed a median onset of disease of 84 days in flutamide-treated male mice and of 112 days in control male mice (not significantly different; P = 0.06, determined by the log-rank [Mantel–Cox] test; Figure 5c). Median survival, determined by the time to reach hindlimb paralysis onset, was comparable in flutamide (159 days) and control male mice (155 days; Figure 5e). Kaplan–Meier analysis of median disease onset in females revealed no difference in flutamide (116 days) and control mice (119 days; Figure 5d). The median lifespans of flutamide (161 days) and control female mice (160.5 days) were also similar (Figure 5f). Thus, flutamide affects disease onset, but not outcome, specifically in male SOD1^{G93A} mice.

3.5 | Flutamide exacerbates hindlimb muscle atrophy in male SOD1^{G93A} mice

To address how flutamide accelerates disease onset and motor deficits in male SOD1^{G93A} mice, we examined skeletal muscle for atrophy markers. In SOD1^{G93A} mice, the up-regulation of transcripts for TGF-β1, myogenin (MYOG), and myoblast determination protein 1 (MyoD) in skeletal muscle reflects atrophy (Galbiati et al., 2012). In the gastrocnemius muscle of male mice at P120, flutamide caused a significant ~1.5-fold up-regulation of atrophy markers TGF-β1 (Figure 6a), MYOG (Figure 6b), and MyoD (Figure 6c), compared to controls. In contrast, there was no significant change in expression of atrophy markers in gastrocnemius muscle of female SOD1^{G93A} mice with flutamide treatment, with exception of MyoD which was down-

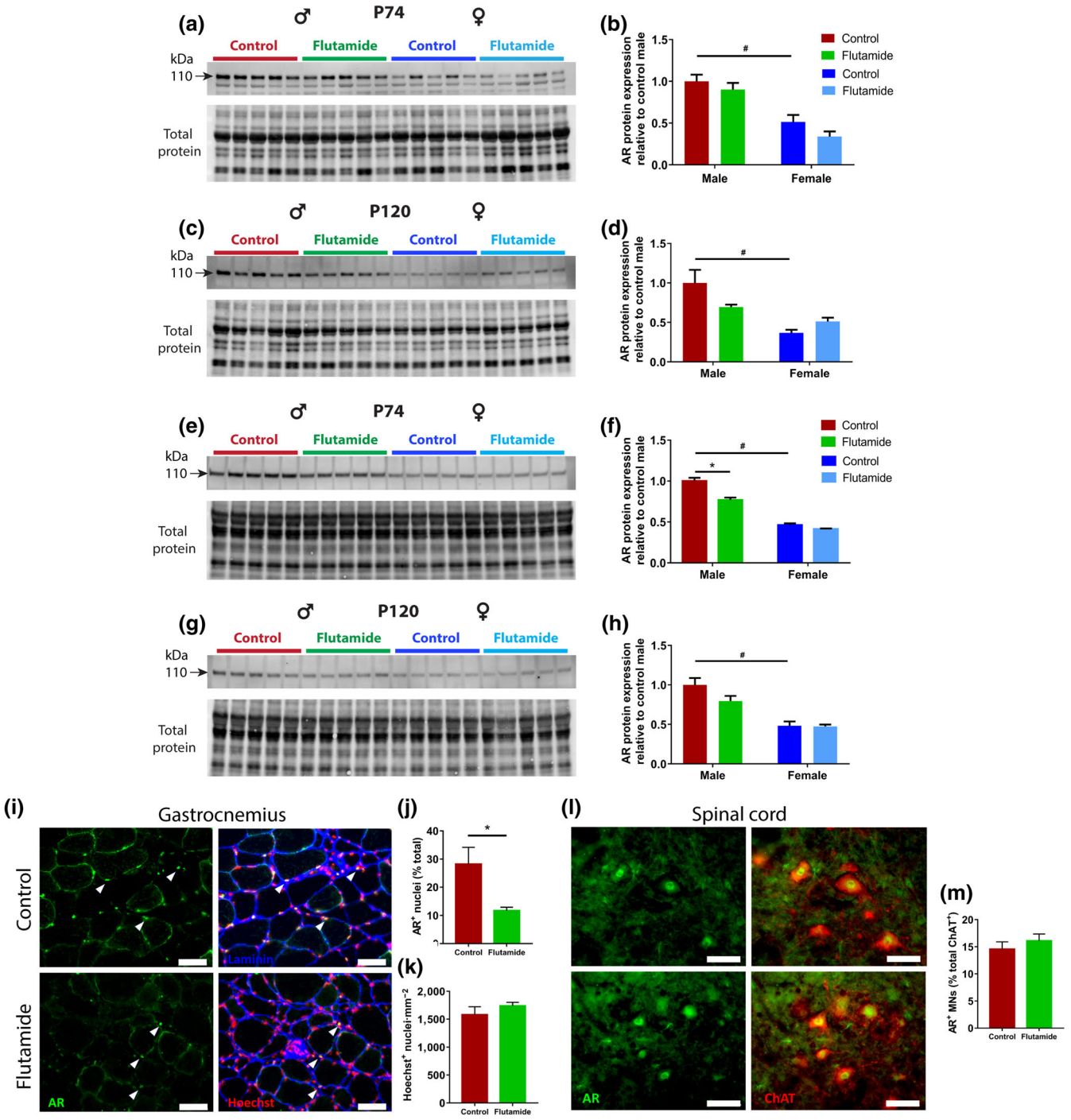

FIGURE 4 Expression of androgen receptor protein and cellular distribution in skeletal muscle and spinal cord from control- and flutamide-treated male and female SOD1^{G93A} mice. (a) Immunoblot analysis of androgen receptors in gastrocnemius muscle relative to total protein levels at postnatal day 74 (P74) and (c) P120. Quantification of androgen receptor levels relative to male control group is shown for (b) P74 and (d) P120. $^{\#}P < 0.05$, significantly different to male counterpart; two-way ANOVA with Fisher's least significant difference (LSD) test comparing sex effect. (e) Immunoblot analysis of androgen receptors in spinal cord relative to total protein at P74 and (g) P120. Quantification of androgen receptor levels relative to male control group is shown for (f) P74 and (h) P120. $^{\#}P < 0.05$, significantly different to male counterpart; two-way ANOVA with Fisher's LSD test comparing sex. $^{*}P < 0.05$, significantly different to male control; two-way ANOVA with Fisher's LSD test comparing treatments. (i) Immunohistochemical analysis of androgen receptors in gastrocnemius muscle of male mice at P120. Androgen receptor-positive nuclei are indicated by arrowheads. Gastrocnemius myocyte nuclei were identified by positive Hoechst labelling with quantification for (j) androgen receptor-positive nuclei and (k) total nuclei. $^{*}P < 0.05$, significantly different to control; Mann–Whitney test. (l) Immunohistochemical analysis of androgen receptors in lumbar spinal cords of male mice at P120. Ventral horn motor neurons identified by ChAT immunolabelling with (m) quantification of androgen receptor-positive nuclei in ChAT-positive motor neurons shown. Data represent mean ± *SEM*, $n = 5$ mice per group. Scale bar = 50 μm

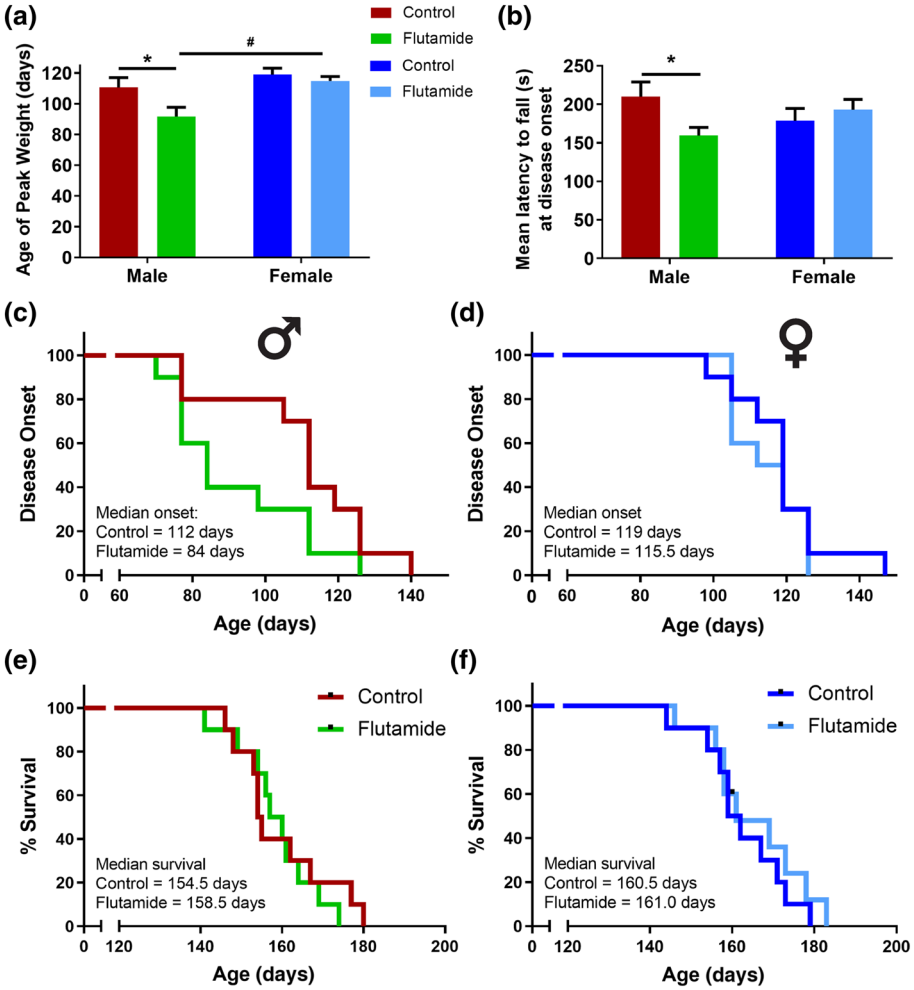

FIGURE 5 Flutamide treatment accelerates disease onset and motor dysfunction in male SOD1^{G93A} mice. (a) Mean disease onset determined by body weight loss onset was significantly advanced in male mice receiving flutamide, compared to male control. $^{*}P < 0.05$, significantly different to control; $^{\#}P < 0.05$, significantly different to male counterpart; two-way ANOVA with Fisher's least significant difference test comparing treatment and sex. (b) Rotarod function at the time of disease onset was significantly impaired in male mice treated with flutamide, compared to male controls. $^{*}P < 0.05$, significantly different to control; two-way ANOVA with Fisher's least significant difference test comparing treatment. (c, d) Kaplan–Meier curves of age at which mice showed onset of disease and (e, f) age to reach endstage of disease defined by hindlimb paralysis in flutamide and control male and female mice. Data represent mean ± *SEM*, $n = 10$ mice per group

regulated by ~0.3-fold (Figure 6d–f). To correlate up-regulation of these muscle atrophy markers with muscle pathology in male mice, we analysed myofibre cross-sectional properties in gastrocnemius muscles at P120 (Figure 6g). Fibre number per area unit quantified was significantly increased by 20% per in flutamide-treated male mice, relative to control males (Figure 6h). Importantly, there was a significant 24% reduction in the mean fibre cross-sectional area in flutamide-treated males, compared to controls (Figure 6i). The minimum Feret diameter, which minimises the potential impact of oblique tissue sectioning, was also significantly lower by 12% in flutamide-treated males, compared to controls (Figure 6j). A stratification of muscle fibre diameters showed that flutamide-treated males had a significantly greater frequency of fibres with a cross-sectional area ≤1,000 μm^2 and less fibres ≥4,000 μm^2 (Figure 6k). These findings collectively suggest that flutamide may exacerbate the clinical phenotype of male SOD1^{G93A} mice by promoting disease progression and/or skeletal muscle wasting.

3.6 | Effects of flutamide on denervation and motor neuron survival in male SOD1^{G93A} mice

The effects of flutamide on neuropathology was next examined in male SOD1^{G93A} mice. Denervation of muscle fibres by motor neuron terminals alters the expression of several genes within the muscle tissue. A switch in the composition of nicotinic ACh receptors (nAChRs) from α to γ subunits, elevation in **neural cell adhesion molecule (NCAM1)**, and **muscle-specific kinase (MuSK)** are key markers of denervation (Aare et al., 2016). In flutamide-treated male mice, there was no significant difference in **nAChR γ** subunits or MuSK transcript levels in gastrocnemius muscle, although a significant 1.3-fold increase in NCAM1 levels occurred, compared to control males (Figure 7a–c). Morphological innervation was also examined in longitudinal sections of gastrocnemius muscles collected from male mice. Innervation was determined by the colocalisation of the muscle motor endplate labelled with α-bungarotoxin and the motor neuron synaptic terminals

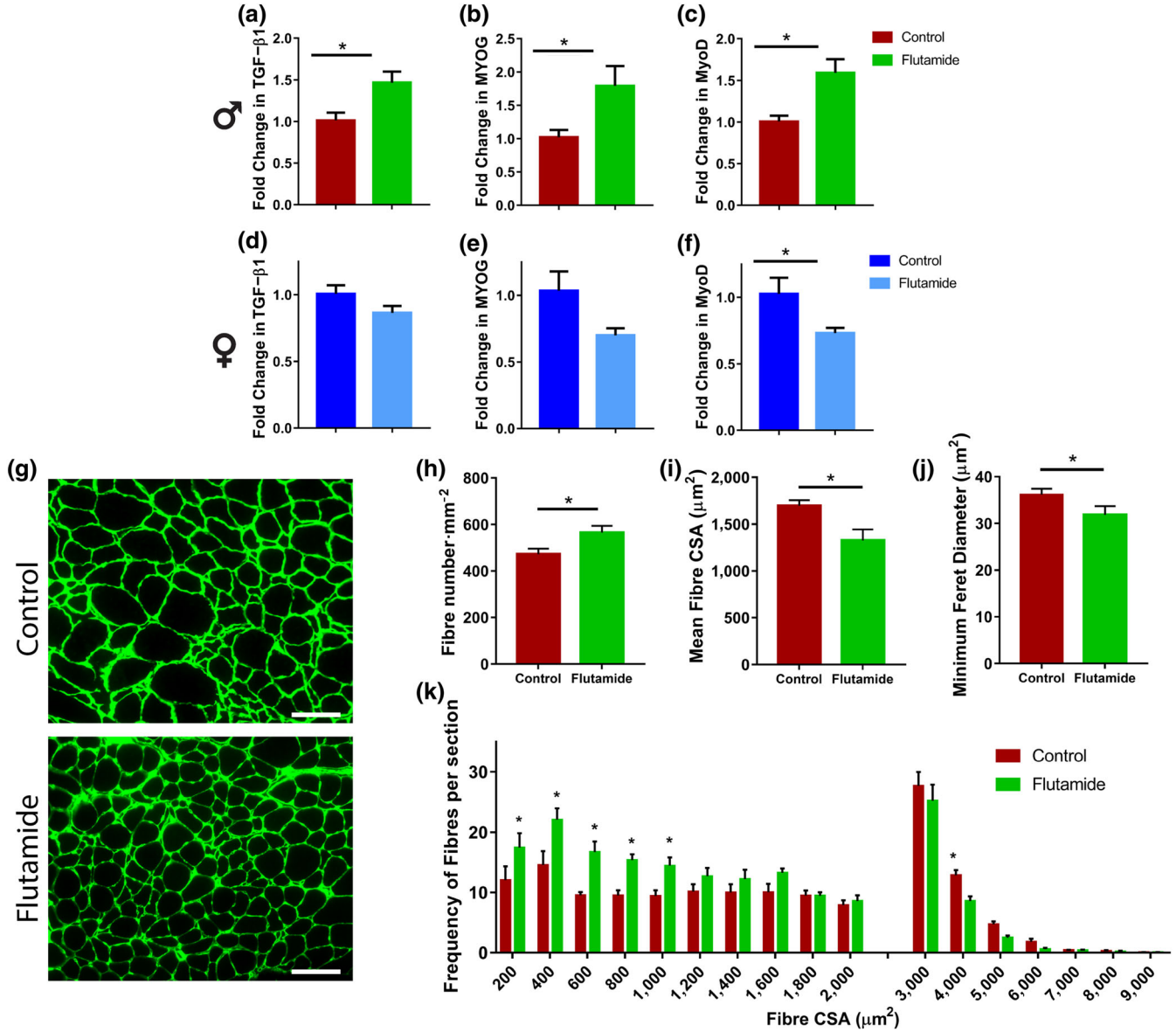

FIGURE 6 Flutamide treatment aggravates hindlimb skeletal muscle atrophy in male SOD1^{G93A} mice. qRT-PCR analysis of (a) TGF-β1, (b) myogenin, and (c) MyoD mRNA levels in gastrocnemius muscles of male mice at postnatal day 120 (P120). qRT-PCR analyses of (d) TGF-β1, (e) myogenin, and (f) MyoD mRNA levels in gastrocnemius muscles of female mice at P120. *$P < 0.05$, significantly different to control ; Student's *t* test or Mann–Whitney test where unequal variance was indicated. (g) Photomicrograph of gastrocnemius muscle cross sections with laminin immunohistochemistry. Scale bar = 100 μm. Quantification of (h) fibre number per unit of area, (i) mean cross-sectional area (CSA) of measured fibres, and (j) mean minimum Feret diameter of measured fibres. *$P < 0.05$, significantly different to control; Student's *t* test. (k) The distribution of measured fibre CSAs in flutamide-treated males, compared to control treated. *$P < 0.05$, significantly different to control; two-way ANOVA using repeated measures with Fisher's least significant difference test comparing treatment. Data represent mean ± *SEM*, $n = 5$ mice per group

labelled with synaptophysin (Figure 7d). There was a trend towards increased denervation in muscles of flutamide-treated males, compared to control males, although this was not significant (Figure 7e).

3.7 | Effects of flutamide on motor neuron survival and glial cell activation in male SOD1^{G93A} mice

The effects of flutamide on spinal cord pathology were next evaluated in male SOD1^{G93A} mice. ChAT-positive motor neurons were counted across spinal cord region L1-L6. No significant treatment-related changes were observed, although a sex-specific difference revealed that motor neuron counts were significantly higher in flutamide-treated males, compared to flutamide-treated female mice (Figure 8a,b). Astrocyte activation assessed by GFAP immunohistochemistry in spinal cord was similar in flutamide and control mice; however, GFAP-positive cell counts were lower in control female mice, compared to control males (Figure 8c,d). Microgliosis shown by CD11b immunohistochemistry was also similar in flutamide and control mice, irrespective of sex (Figure 8e,f). Thus, flutamide treatment

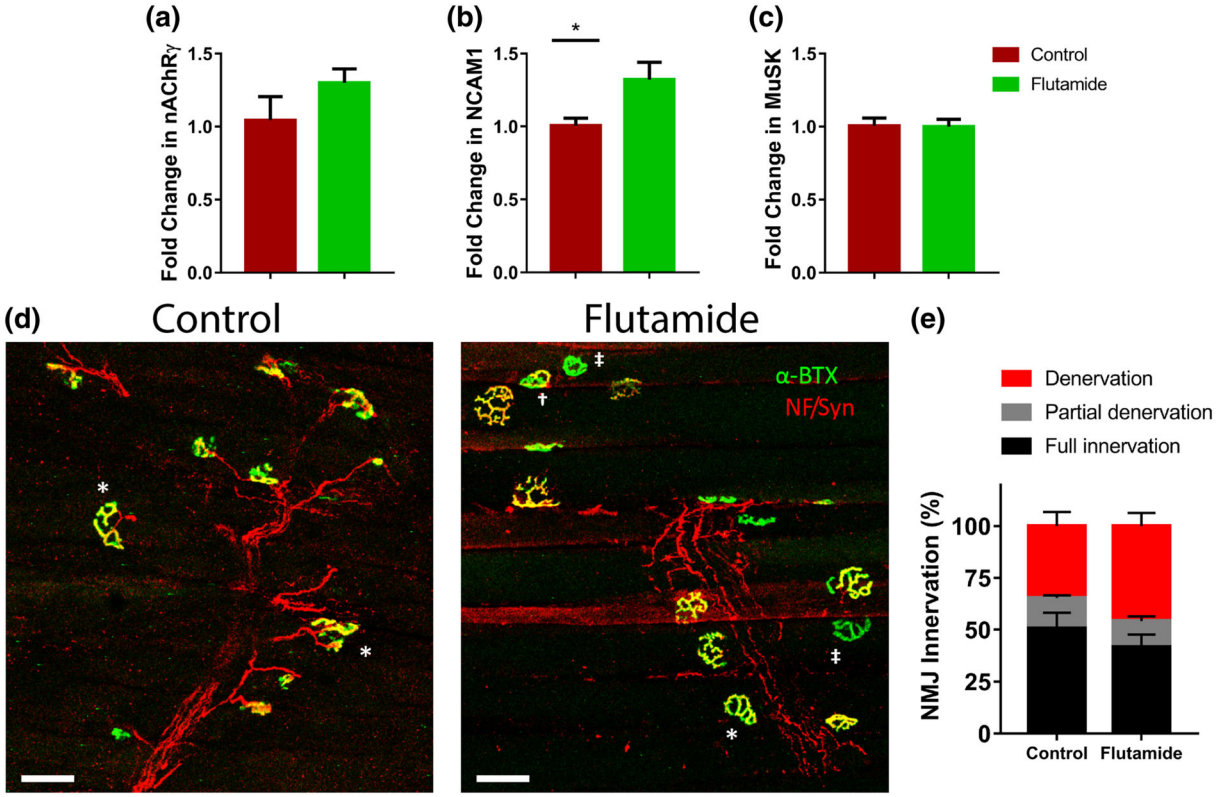

FIGURE 7 Effect of flutamide treatment on hindlimb skeletal muscle denervation in male SOD1^{G93A} mice. qRT-PCR analysis of (a) nAChRγ, (b) NCAM1, and (c) MuSK mRNA levels in gastrocnemius muscle of flutamide- and control-treated mice at postnatal day 120 (P120). *P < 0.05, significantly different to control; Student's t test. (d) Histochemical staining of neuromuscular junctions (NMJs) within the gastrocnemius muscle; postsynaptic motor endplates labelled with α-bungarotoxin (BTX) and immunolabelling of presynaptic nerves (NF) and nerve terminals (Syn). *denotes full innervation, †represents partial innervation, and ‡shows denervated endplates. Scale bar = 50 μm. (e) Quantification of innervated, partially denervated, and fully denervated endplates (n = 4 mice per group)

promotes skeletal muscle pathology, but not central pathology, in this mouse model of ALS.

4 | DISCUSSION

There is clear epidemiological, genetic, and biological evidence for a key role of androgens and androgen receptor signalling in ALS. First, ALS is more common in males with an earlier age of onset in both male patients and mouse models, implicating androgen influences in disease (McCombe & Henderson, 2010). Second, mutations in androgen receptors cause lower motor neuron loss in SBMA which shows some pathological overlap with ALS, suggesting that defects in androgen receptors can trigger motor neuron degeneration (Beitel et al., 2013; Cortes & La Spada, 2014). Lastly, administration of androgens to SOD1^{G93A} mice ameliorates disease progression (Yoo & Ko, 2012). Our study is the first to assess the effects of antiandrogen treatment on a mouse model of ALS to clarify the contribution of androgen receptor signalling. Chronic administration of the androgen receptor antagonist, flutamide, to presymptomatic SOD1^{G93A} mice accelerated disease onset and motor dysfunction in male mice, with a concomitant exacerbation of hindlimb skeletal muscle pathology. Interestingly, flutamide worsened peripheral, but not central, pathology in male SOD1^{G93A} mice, reflecting the contribution of skeletal muscle pathology to disease onset and outcome in this mouse model of ALS.

We employed a dose of flutamide which had been effective in three different mouse models of SBMA (Renier et al., 2014). Importantly, this flutamide dose does not affect body weights or locomotor function in wild-type mice (Renier et al., 2014), allowing us to distinguish mutant SOD1-specific effects from effects on general physiology. This sustained-release pellet preparation was estimated to release ~4.7 mg of drug per day over 21 days, thereby exposing mice to a dose of ~180–230 mg·kg^{-1} based on weight distributions. Limited studies have determined the pharmacokinetics of flutamide in mice, which is critical in providing effective drug antagonism of androgen receptors to compete with local androgens for receptor binding. A single oral dose of 20-mg·kg^{-1} flutamide administered to mice yielded a peak plasma concentration below 0.5 μg·ml^{-1} for flutamide and 4.5 μg·ml^{-1} for HF (Matsuzaki et al., 2006). Based on this, Renier et al. (2014) estimated that the sustained-release flutamide formulation would generate serum levels of approximately 30 μg·ml^{-1} which is 300-fold higher than the 0.1-μg·ml^{-1} measured plasma steady-state concentrations in this current study. As flutamide has a short $t_{1/2}$ in vivo due to its rapid metabolism to HF in the liver, in addition to undergoing first-pass metabolism following oral administration (Schulz, Schmoldt, Donn, & Becker, 1988), making

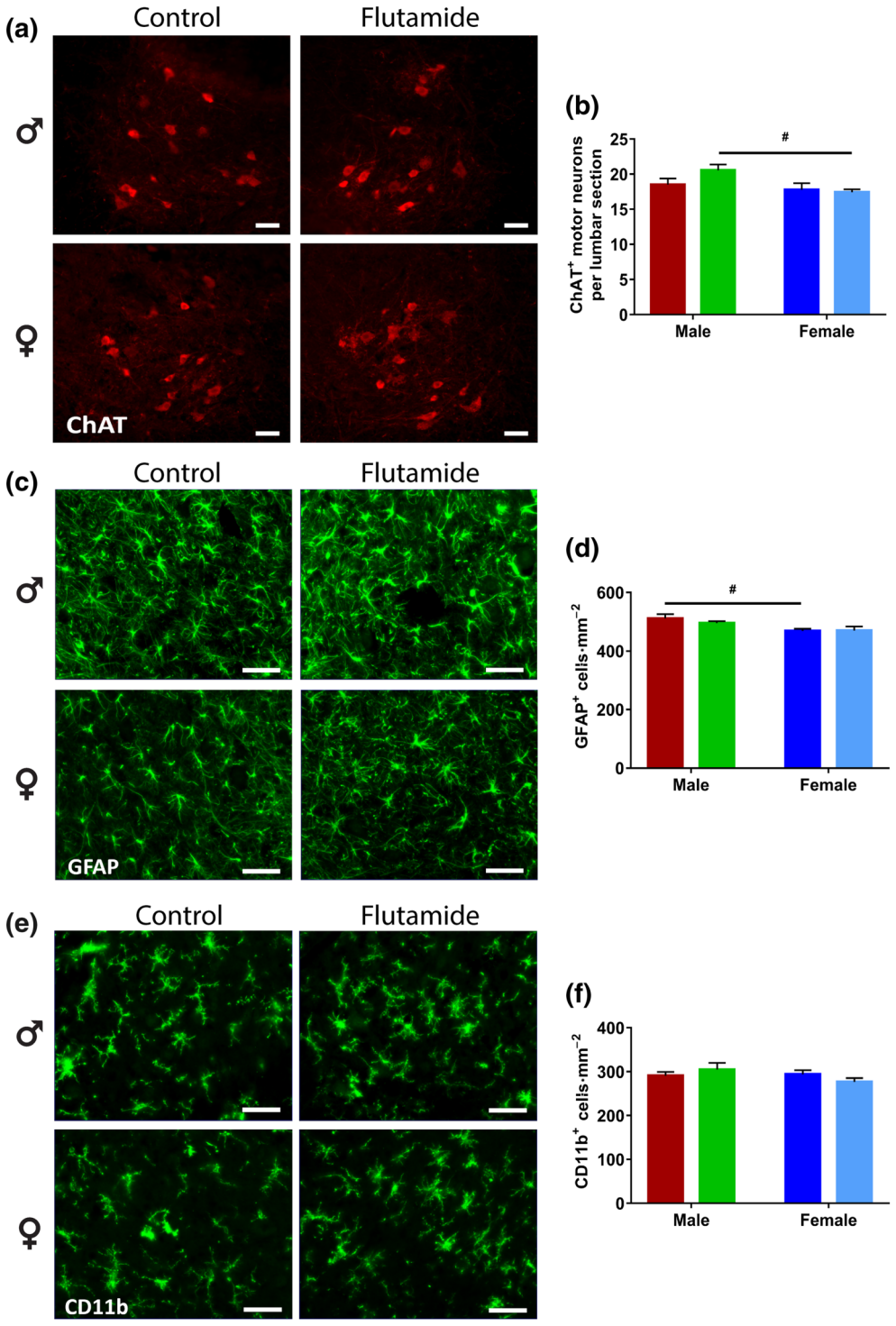

FIGURE 8 Effects of flutamide treatment on motor neuron and glial cell pathology in lumbar spinal cord ventral horns of SOD1^{G93A} mice at postnatal day 120 (P120). (a) Representative immunostaining of ChAT-positive motor neurons with (b) quantification. $^{\#}P < 0.05$, significantly different to male counterpart; two-way ANOVA with Fisher's least significant difference test comparing sex effect. (c) Representative immunostaining of GFAP-positive astrocytes with (d) quantification of astrocytes. $^{\#}P < 0.05$, significantly different to male counterpart; two-way ANOVA with Fisher's least significant difference test comparing sex effect. (e) Representative immunostaining of CD11b-positive microglia with (f) quantification of microglial cell counts. Data represent mean ± *SEM*, $n = 5$ mice per group. Scale bars = 50 μm

predictions based on single oral doses limited. Indeed, the steady-state plasma levels of HF were approximately 50 times higher than parent compound in the current study. This is similar to the human pharmacokinetics that show consistently higher levels of both metabolites, HF and Flu-1, compared to parent compound (Aizawa et al., 2003; Asade, Prizont, Muino, & Tessler, 1991), and in rats where HF reaches 70-fold higher tissue concentrations compared to flutamide (Neri, 1989). In contrast to human data, the metabolite

Flu-1 was lower than that of flutamide and may reflect differences between human and rodent metabolism.

Evidence of systemic antagonism of androgen receptors was reflected by significantly reduced prostate and SV weights of flutamide-treated male SOD1^{G93A} mice. The relationship between the mechanism of action of flutamide and its effect on both androgen receptor protein stability and nuclear translocation has been a subject of debate. In an SBMA mouse model receiving 1.8 mg of flutamide every second day, SV and prostate showed reduced weights, with no effect on androgen receptor levels in spinal cord or muscle (Katsuno et al., 2003). Flutamide administered at efficacious levels by a continuous slow-release formulation showed reductions in both soluble androgen receptor levels in spinal cord and muscle and decreased mutant androgen receptor aggregates only in muscle (Renier et al., 2014). In the current study, plasma and spinal cord levels of testosterone following 2 weeks of flutamide administration were elevated, compared to control mice, similar to those observed in SBMA models (Renier et al., 2014). Likewise, we confirmed a decrease in the levels of soluble androgen receptors in the spinal cord of these mice, indicative of flutamide-induced reduction in androgen receptor protein stability.

In muscle tissue, androgen receptors are expressed in some mature myofibres but more extensively in the mesenchymal precursor satellite cells (Sinha-Hikim, Taylor, Gonzalez-Cadavid, Zheng, & Bhasin, 2004), whereby androgens promote myogenesis and differentiation into mature skeletal muscle tissue. In ALS, skeletal muscle undergoes both intrinsic metabolic disturbances, as well as degeneration in response to denervation. Denervation of the gastrocnemius muscle is reportedly detectable as early as P50 in SOD1^{G93A} mice (Frey et al., 2000) before symptoms are obvious. In response, myogenesis occurs to replace the lost myofibres (Pun, Santos, Saxena, Xu, & Caroni, 2006), and the satellite cell marker, PAX7, is up-regulated in presymptomatic SOD1^{G93A} mice (Manzano et al., 2011). Satellite cells also showed an intrinsic loss in proliferative capacity in SOD1^{G93A} mice (Manzano et al., 2013). Hence, there is strong evidence for a potential role for androgen receptors in early ALS pathogenesis. This was confirmed in the current study, as we show that flutamide can accelerate disease onset and motor deficits in male mice, with concomitant exacerbation in myofibre atrophy. Castration in SOD1^{G93A} mice has shown to both induce muscle hypotrophy (Yoo & Ko, 2012) and have no effect on clinical parameters (Aggarwal et al., 2014) and may reflect influences from the genetic background of mice on the transgene (Pfohl et al., 2015). To date, castration has consistently failed to modify disease onset or survival in male SOD1^{G93A} mice (Aggarwal et al., 2014; Sheean et al., 2015; Yoo & Ko, 2012). The reasons for the lack of effect seen in these studies, compared to our study showing exacerbated disease onset may be complex. For instance, castration may disrupt the source and production of other steroid hormones such as estrogen which is produced from testosterone metabolism, as well as the testis being a source of androstenedione and progesterone (Murphy & O'Shaughnessy, 1991). Their influences on disease progression cannot be discounted. In gonadally intact mice, androgens may also signal via alternative pathways, for example, the membrane-located androgen receptors which function as GPCRs, rather than androgen receptors in the nucleus, activating the classical genomic pathway (Pi & Quarles, 2012; Wang, Liu, & Cao, 2014).

Many experimental therapies tested over the past decade, which have specifically targeted muscle pathology in ALS, have been unsuccessful in modifying survival in ALS rodent models. Muscle-targeted expression of the transcriptional coactivator, PPARγ coactivator-1α, in SOD1^{G37R} mice improved mitochondrial biogenesis, muscle atrophy, and function but did not impact upon disease onset, muscle innervation, motor neuron, or glial cell pathology (Da Cruz et al., 2012). Skeletal muscle or CNS-restricted **IGF-1** overexpression did not change disease onset or motor neuron survival in SOD1^{G93A} mice (Messi, Clark, Prevette, Oppenheim, & Delbono, 2007), in contrast to an earlier study which showed positive effects of muscle-specific IGF-1 expression on survival (Dobrowolny et al., 2005). Blocking the effect of myostatin, a muscle growth inhibitor, increased muscle mass and strength in both SOD1^{G93A} mice and rats, with no change in disease onset or survival (Holzbaur et al., 2006). A robust delay in disease onset occurred in SOD1^{G93A} mice overexpressing the antioxidant-regulating transcription factor, **nuclear factor erythroid 2-related factor 2,** specifically in vulnerable fast type II myofibres; however, no change in survival was observed (Vargas et al., 2013). Taken together, these studies demonstrate that while muscle-targeted therapies may have a modulatory influence on disease progression and in many cases muscle atrophy, they are most often unable to halt motor neuron loss, the underlying cause of hindlimb paralysis or clinical endstage in these mice. Alternatively, muscle-derived therapies or delivery strategies, which specifically target preservation of NMJ structure and motor axons, present more promising approaches to extend survival in SOD1^{G93A} mice, as supported by benefits of MuSK stimulation, a receptor kinase important in NMJ maintenance (Cantor et al., 2018) and muscle delivery of retrogradely transported neurotrophic growth factors (Acsadi et al., 2002; Azzouz et al., 2004; Kaspar, Llado, Sherkat, Rothstein, & Gage, 2003; Pun et al., 2006).

The recent evidence that myopathic features in SBMA strongly play a role in driving disease processes (Cortes et al., 2014) has once again raised questions about the potential role of skeletal muscle in non-cell autonomous mechanisms in other motor neuron degenerative disorders, including ALS (Cortes & La Spada, 2014). Similar to muscle-restricted expression of polyQ-expanded androgen receptor-causing disease phenotype in SBMA, muscle-restricted overexpression of SOD1^{G93A} was able to induce muscle atrophy and dysfunction through oxidative stress (Dobrowolny et al., 2008), identifying muscle as a primary target in ALS. However, other studies which used several approaches to specifically target SOD1^{G93A} transgene in the skeletal muscle showed no therapeutic survival benefits (Miller et al., 2006; Towne, Raoul, Schneider, & Aebischer, 2008). A more recent study by Dobrowolny et al. (2015) showed that muscle-specific SOD1^{G93A} transgene expression was able to modulate transcript expression in the spinal cords of mice supporting the notion that muscle signalling is able to regulate the function of surrounding nerves. IGF-1 has consistently been of interest as a mediator of this relationship between muscle and motor neuron, as discussed previously as muscle-targeted

therapy in ALS, a muscle-specific IGF-1 isoform administered to an SBMA mouse model delayed disease onset and improved survival by targeting the mutant androgen receptor protein via the **Akt** signalling pathway (Palazzolo et al., 2009).

Our findings that androgen receptor antagonism exacerbates the phenotype of male SOD1^{G93A} mice support other studies manipulating androgens in this mouse model. Administration of DHT was shown to attenuate skeletal muscle atrophy and motor neuron degeneration and improve the clinical phenotype of SOD1^{G93A} mice (Yoo & Ko, 2012), and this effect was attributed to elevated production of IGF-1 in muscle which provided neurotrophic support to motor neurons. The effect of DHT is in contrast to that of nandrolone, a synthetic anabolic steroid, which when given to castrated SOD1^{G93A} mice, exacerbated disease onset and hastened death, in spite of hypertrophic effects on muscle (Aggarwal et al., 2014). The key difference between nandrolone and testosterone is their transcriptional gene targets with nandrolone having a myotrophic:androgenic ratio of ~11:1 compared to that of testosterone at ~1:1 (Kicman, 2008). Additionally, nandrolone suppresses the production of endogenous testosterone; therefore, the potential of androgen therapies to modify ALS disease processes may be better focused on the enhancement of androgenic effects to motor neurons, rather than the anabolic effects in the muscle tissue alone.

In conclusion, the present study demonstrates for the first time that administration of an antiandrogen, flutamide, accelerates disease onset and motor deficits in male SOD1^{G93A} mice. As evidenced by exacerbated muscle wasting in symptomatic stages of disease, this is likely a reflection of peripherally mediated effects where androgen receptor signalling is affecting secondary disease mechanisms. Our study is consistent with a role of androgens in modulating disease severity and sexual dimorphism in ALS.

ACKNOWLEDGEMENTS

We thank Assoc. Prof. Clare Parish and Dr Jon Niclis for providing H9 cells and expertise on differentiations. Funding for this project was provided by the Australian National Health and Medical Research Council (NHMRC) (Project Grants 1104295 and 1104299), Stafford Fox Medical Research Foundation, Motor Neurone Disease Research Institute of Australia (MNDRIA) Research Institute of Australia (Ted Dimmick Memorial MND Research Grant), Pratt Foundation, and Mr Tony Gray. V.M. was supported by an MNDRIA PhD Scholarship Top-Up Grant Scholarship Top-Up Grant, and B.T. was supported by an NHMRC-ARC Dementia Research Leadership Fellowship.

CONFLICT OF INTEREST

The authors declare no conflicts of interest.

AUTHOR CONTRIBUTIONS

B.J.T. conceived the study. B.J.T., W.C.B., and C.L.L. provided supervision. V.M.M. conducted all mouse efficacy studies, biochemical and histological analysis, and interpretation with assistance from M.D.C. C.L.L. generated hESC-derived motor neurons. T.W.R. and U.R. performed LC–MS–MS analysis. C.L.L., W.C.B., and E.D. assisted in data interpretation. V.M.M. and B.J.T. wrote manuscript with all authors contributing to edits. All authors approved the final version.

DECLARATION OF TRANSPARENCY AND SCIENTIFIC RIGOUR

This Declaration acknowledges that this paper adheres to the principles for transparent reporting and scientific rigour of preclinical research as stated in the *BJP* guidelines for Design & Analysis, Immunoblotting and Immunochemistry, and Animal Experimentation, and as recommended by funding agencies, publishers, and other organisations engaged with supporting research.

ORCID

Elvan Djouma https://orcid.org/0000-0002-7414-6278
Bradley J. Turner https://orcid.org/0000-0001-6580-7655

REFERENCES

Aare, S., Spendiff, S., Vuda, M., Elkrief, D., Perez, A., Wu, Q., … Hepple, R. T. (2016). Failed reinnervation in aging skeletal muscle. *Skeletal Muscle*, *6*, 29. https://doi.org/10.1186/s13395-016-0101-y

Acsadi, G., Anguelov, R. A., Yang, H., Toth, G., Thomas, R., Jani, A., … Shy, M. E. (2002). Increased survival and function of SOD1 mice after glial cell-derived neurotrophic factor gene therapy. *Human Gene Therapy*, *13*, 1047–1059. https://doi.org/10.1089/104303402753812458

Aggarwal, T., Polanco, M. J., Scaramuzzino, C., Rocchi, A., Milioto, C., Emionite, L., … Pennuto, M. (2014). Androgens affect muscle, motor neuron, and survival in a mouse model of SOD1-related amyotrophic lateral sclerosis. *Neurobiology of Aging*, *35*, 1929–1938. https://doi.org/10.1016/j.neurobiolaging.2014.02.004

Aizawa, Y., Ikemoto, I., Kishimoto, K., Wada, T., Yamazaki, H., Ohishi, Y., … Ueda, M. (2003). Flutamide-induced hepatic dysfunction in relation to steady-state plasma concentrations of flutamide and its metabolites. *Molecular and Cellular Biochemistry*, *252*, 149–156. https://doi.org/10.1023/A:1025560513308

Alexander, S. P. H., Cidlowski, J. A., Kelly, E., Marrion, N. V., Peters, J. A., Faccenda, E., … CGTP Collaborators. (2017). The Concise Guide to PHARMACOLOGY 2017/18: Nuclear hormone receptors. *British Journal of Pharmacology*, *174*(Suppl 1), S208–S224. https://doi.org/10.1111/bph.13880

Alexander, S. P. H., Fabbro, D., Kelly, E., Marrion, N. V., Peters, J. A., Faccenda, E., … CGTP Collaborators. (2017). The Concise Guide to PHARMACOLOGY 2017/18: Enzymes. *British Journal of Pharmacology*, *174*, S272–S359. https://doi.org/10.1111/bph.13877

Alexander, S. P. H., Kelly, E., Marrion, N. V., Peters, J. A., Faccenda, E., Harding, S. D., … CGTP Collaborators (2017). The Concise Guide to PHARMACOLOGY 2017/18: Other proteins. *British Journal of Pharmacology*, *174*, S1–S16. https://doi.org/10.1111/bph.13882

Alexander, S. P. H., Peters, J. A., Kelly, E., Marrion, N. V., Faccenda, E., Harding, S. D., … CGTP Collaborators. (2017). The Concise Guide to PHARMACOLOGY 2017/18: Ligand-gated ion channels. *British Journal of Pharmacology*, *174*, S130–S159. https://doi.org/10.1111/bph.13879

Alexander, S. P. H., Roberts, R. E., Broughton, B. R. S., Sobey, C. G., George, C. H., Stanford, S. C., … Ahluwalia, A. (2018). Goals and practicalities of immunoblotting and immunohistochemistry: A guide for submission to the British Journal of Pharmacology. *British Journal of Pharmacology*, *175*, 407–411. https://doi.org/10.1111/bph.14112

Asade, R. H., Prizont, L., Muino, J. P., & Tessler, J. (1991). Steady-state hydroxyflutamide plasma levels after the administration of two dosage forms of flutamide. *Cancer Chemotherapy and Pharmacology*, *27*, 401–405. https://doi.org/10.1007/BF00688866

Azzouz, M., Ralph, G. S., Storkebaum, E., Walmsley, L. E., Mitrophanous, K. A., Kingsman, S. M., … Mazarakis, N. D. (2004). VEGF delivery with retrogradely transported lentivector prolongs survival in a mouse ALS model. *Nature*, *429*, 413–417. https://doi.org/10.1038/nature02544

Beitel, L. K., Alvarado, C., Mokhtar, S., Paliouras, M., & Trifiro, M. (2013). Mechanisms mediating spinal and bulbar muscular atrophy: Investigations into polyglutamine-expanded androgen receptor function and dysfunction. *Frontiers in Neurology*, *4*, 53.

Brown, R. H. Jr., & Al-Chalabi, A. (2017). Amyotrophic lateral sclerosis. *The New England Journal of Medicine*, *377*, 1602.

Cantor, S., Zhang, W., Delestree, N., Remedio, L., Mentis, G. Z., & Burden, S. J. (2018). Preserving neuromuscular synapses in ALS by stimulating MuSK with a therapeutic agonist antibody. *eLife*, *7*. https://doi.org/10.7554/eLife.34375

Cary, G. A., & La Spada, A. R. (2008). Androgen receptor function in motor neuron survival and degeneration. *Physical Medicine and Rehabilitation Clinics of North America*, *19*, 479–494 viii. https://doi.org/10.1016/j.pmr.2008.03.002

Cortes, C. J., & La Spada, A. R. (2014). Motor neuron degeneration in spinal and bulbar muscular atrophy is a skeletal muscle-driven process: Relevance to therapy development and implications for related motor neuron diseases. *Rare Diseases*, *2*, e962402. https://doi.org/10.4161/2167549X.2014.962402

Cortes, C. J., Ling, S. C., Guo, L. T., Hung, G., Tsunemi, T., Ly, L., … la Spada, A. R. (2014). Muscle expression of mutant androgen receptor accounts for systemic and motor neuron disease phenotypes in spinal and bulbar muscular atrophy. *Neuron*, *82*, 295–307. https://doi.org/10.1016/j.neuron.2014.03.001

Culig, Z., Hoffmann, J., Erdel, M., Eder, I. E., Hobisch, A., Hittmair, A., … Klocker, H. (1999). Switch from antagonist to agonist of the androgen receptor bicalutamide is associated with prostate tumour progression in a new model system. *British Journal of Cancer*, *81*, 242–251. https://doi.org/10.1038/sj.bjc.6690684

Curtis, M. J., Alexander, S., Cirino, G., Docherty, J. R., George, C. H., Giembycz, M. A., … Ahluwalia, A. (2018). Experimental design and analysis and their reporting II: updated and simplified guidance for authors and peer reviewers. *British Journal of Pharmacology*, *175*, 987–993. https://doi.org/10.1111/bph.14153

Da Cruz, S., Parone, P. A., Lopes, V. S., Lillo, C., McAlonis-Downes, M., Lee, S. K., … Cleveland, D. W. (2012). Elevated PGC-1α activity sustains mitochondrial biogenesis and muscle function without extending survival in a mouse model of inherited ALS. *Cell Metabolism*, *15*, 778–786.

Dobrowolny, G., Aucello, M., Rizzuto, E., Beccafico, S., Mammucari, C., Boncompagni, S., … Musarò, A. (2008). Skeletal muscle is a primary target of SOD1G93A-mediated toxicity. *Cell Metabolism*, *8*, 425–436. https://doi.org/10.1016/j.cmet.2008.09.002

Dobrowolny, G., Bernardini, C., Martini, M., Baranzini, M., Barba, M., & Musaro, A. (2015). Muscle expression of $SOD1^{G93A}$ modulates microRNA and mRNA transcription pattern associated with the myelination process in the spinal cord of transgenic mice. *Frontiers in Cellular Neuroscience*, *9*, 463.

Dobrowolny, G., Giacinti, C., Pelosi, L., Nicoletti, C., Winn, N., Barberi, L., … Musarò, A. (2005). Muscle expression of a local Igf-1 isoform protects motor neurons in an ALS mouse model. *The Journal of Cell Biology*, *168*, 193–199. https://doi.org/10.1083/jcb.200407021

Du, Z. W., Chen, H., Liu, H., Lu, J., Qian, K., Huang, C. L., … Zhang, S.-C. (2015). Generation and expansion of highly pure motor neuron progenitors from human pluripotent stem cells. *Nature Communications*, *6*, 6626. https://doi.org/10.1038/ncomms7626

Fargo, K. N., Galbiati, M., Foecking, E. M., Poletti, A., & Jones, K. J. (2008). Androgen regulation of axon growth and neurite extension in motoneurons. *Hormones and Behavior*, *53*, 716–728. https://doi.org/10.1016/j.yhbeh.2008.01.014

Frey, D., Schneider, C., Xu, L., Borg, J., Spooren, W., & Caroni, P. (2000). Early and selective loss of neuromuscular synapse subtypes with low sprouting competence in motoneuron diseases. *The Journal of Neuroscience*, *20*, 2534–2542. https://doi.org/10.1523/JNEUROSCI.20-07-02534.2000

Galbiati, M., Onesto, E., Zito, A., Crippa, V., Rusmini, P., Mariotti, R., … Poletti, A. (2012). The anabolic/androgenic steroid nandrolone exacerbates gene expression modifications induced by mutant SOD1 in muscles of mice models of amyotrophic lateral sclerosis. *Pharmacological Research*, *65*, 221–230. https://doi.org/10.1016/j.phrs.2011.12.001

Gao, W., Bohl, C. E., & Dalton, J. T. (2005). Chemistry and structural biology of androgen receptor. *Chemical Reviews*, *105*, 3352–3370. https://doi.org/10.1021/cr020456u

Geevasinga, N., Menon, P., Ozdinler, P. H., Kiernan, M. C., & Vucic, S. (2016). Pathophysiological and diagnostic implications of cortical dysfunction in ALS. *Nature Reviews. Neurology*, *12*, 651–661. https://doi.org/10.1038/nrneurol.2016.140

Harding, S. D., Sharman, J. L., Faccenda, E., Southan, C., Pawson, A. J., Ireland, S., … NC-IUPHAR (2018). The IUPHAR/BPS Guide to PHARMACOLOGY in 2018: Updates and expansion to encompass the new guide to IMMUNOPHARMACOLOGY. *Nucleic Acids Research*, *46*, D1091–D1106. https://doi.org/10.1093/nar/gkx1121

Hatzipetros, T., Bogdanik, L. P., Tassinari, V. R., Kidd, J. D., Moreno, A. J., Davis, C., … Perrin, S. (2014). C57BL/6J congenic Prp-TDP43A315T mice develop progressive neurodegeneration in the myenteric plexus of the colon without exhibiting key features of ALS. *Brain Research*, *1584*, 59–72. https://doi.org/10.1016/j.brainres.2013.10.013

Holzbaur, E. L., Howland, D. S., Weber, N., Wallace, K., She, Y., Kwak, S., … Walsh, F. S. (2006). Myostatin inhibition slows muscle atrophy in rodent models of amyotrophic lateral sclerosis. *Neurobiology of Disease*, *23*, 697–707. https://doi.org/10.1016/j.nbd.2006.05.009

Kaspar, B. K., Llado, J., Sherkat, N., Rothstein, J. D., & Gage, F. H. (2003). Retrograde viral delivery of IGF-1 prolongs survival in a mouse ALS model. *Science*, *301*, 839–842. https://doi.org/10.1126/science.1086137

Katsuno, M., Adachi, H., Doyu, M., Minamiyama, M., Sang, C., Kobayashi, Y., … Sobue, G. (2003). Leuprorelin rescues polyglutamine-dependent phenotypes in a transgenic mouse model of spinal and bulbar muscular atrophy. *Nature Medicine*, *9*, 768–773. https://doi.org/10.1038/nm878

Kicman, A. T. (2008). Pharmacology of anabolic steroids. *British Journal of Pharmacology*, *154*, 502–521. https://doi.org/10.1038/bjp.2008.165

Kilkenny, C., Browne, W., Cuthill, I. C., Emerson, M., & Altman, D. G. (2010). Animal research: Reporting in vivo experiments: The ARRIVE guidelines. *British Journal of Pharmacology*, *160*, 1577–1579.

Kujawa, K. A., Emeric, E., & Jones, K. J. (1991). Testosterone differentially regulates the regenerative properties of injured hamster facial motoneurons. *The Journal of Neuroscience*, *11*, 3898–3906. https://doi.org/10.1523/JNEUROSCI.11-12-03898.1991

Kim, H. Y., Ki, C. S., Koh, S. H., Park, K. H., Sunwoo, I. N., & Kim, S. H. (2007). Clinical characteristics of familial amyotrophic lateral sclerosis with a Phe20Cys mutation in the SOD1 gene in a Korean family.

Amyotrophic Lateral Sclerosis, *8*, 73–78. https://dio.org/10.1080/17482960701223154

La Spada, A. R., Wilson, E. M., Lubahn, D. B., Harding, A. E., & Fischbeck, K. H. (1991). Androgen receptor gene mutations in X-linked spinal and bulbar muscular atrophy. *Nature*, *352*, 77–79. https://doi.org/10.1038/352077a0

Manzano, R., Toivonen, J. M., Calvo, A. C., Olivan, S., Zaragoza, P., Rodellar, C., … Osta, R. (2013). Altered in vitro proliferation of mouse SOD1-G93A skeletal muscle satellite cells. *Neurodegenerative Diseases*, *11*, 153–164. https://doi.org/10.1159/000338061

Manzano, R., Toivonen, J. M., Olivan, S., Calvo, A. C., Moreno-Igoa, M., Munoz, M. J., … Osta, R. (2011). Altered expression of myogenic regulatory factors in the mouse model of amyotrophic lateral sclerosis. *Neurodegenerative Diseases*, *8*, 386–396. https://doi.org/10.1159/000324159

Marchetti, B., & Labrie, F. (1988). Characteristics of flutamide action on prostatic and testicular functions in the rat. *Journal of Steroid Biochemistry*, *29*, 691–698. https://doi.org/10.1016/0022-4731(88)90170-7

Marron, T. U., Guerini, V., Rusmini, P., Sau, D., Brevini, T. A., Martini, L., & Poletti, A. (2005). Androgen-induced neurite outgrowth is mediated by neuritin in motor neurones. *Journal of Neurochemistry*, *92*, 10–20. https://doi.org/10.1111/j.1471-4159.2004.02836.x

Matsuzaki, Y., Nagai, D., Ichimura, E., Goda, R., Tomura, A., Doi, M., & Nishikawa, K. (2006). Metabolism and hepatic toxicity of flutamide in cytochrome P450 1A2 knockout SV129 mice. *Journal of Gastroenterology*, *41*, 231–239. https://doi.org/10.1007/s00535-005-1749-y

McCombe, P. A., & Henderson, R. D. (2010). Effects of gender in amyotrophic lateral sclerosis. *Gender Medicine*, *7*, 557–570. https://doi.org/10.1016/j.genm.2010.11.010

McGrath, J. C., Drummond, G. B., McLachlan, E. M., Kilkenny, C., & Wainwright, C. L. (2010). Guidelines for reporting experiments involving animals: The ARRIVE guidelines. *British Journal of Pharmacology*, *160*, 1573–1576. https://doi.org/10.1111/j.1476-5381.2010.00873.x

Messi, M. L., Clark, H. M., Prevette, D. M., Oppenheim, R. W., & Delbono, O. (2007). The lack of effect of specific overexpression of IGF-1 in the central nervous system or skeletal muscle on pathophysiology in the G93A SOD-1 mouse model of ALS. *Experimental Neurology*, *207*, 52–63. https://doi.org/10.1016/j.expneurol.2007.05.016

Miller, T. M., Kim, S. H., Yamanaka, K., Hester, M., Umapathi, P., Arnson, H., … Kaspar, B. K. (2006). Gene transfer demonstrates that muscle is not a primary target for non-cell-autonomous toxicity in familial amyotrophic lateral sclerosis. *Proceedings of the National Academy of Sciences of the United States of America*, *103*, 19546–19551. https://doi.org/10.1073/pnas.0609411103

Moloney, E. B., de Winter, F., & Verhaagen, J. (2014). ALS as a distal axonopathy: Molecular mechanisms affecting neuromuscular junction stability in the presymptomatic stages of the disease. *Frontiers in Neuroscience*, *8*, 252.

Murphy, L., & O'Shaughnessy, P. J. (1991). Testicular steroidogenesis in the testicular feminized (Tfm) mouse: Loss of 17α-hydroxylase activity. *The Journal of Endocrinology*, *131*, 443–449. https://doi.org/10.1677/joe.0.1310443

Neri, R. (1989). Pharmacology and pharmacokinetics of flutamide. *Urology*, *34*, 19–21 discussion 46-56. https://doi.org/10.1016/0090-4295(89)90230-6

Palazzolo, I., Stack, C., Kong, L., Musaro, A., Adachi, H., Katsuno, M., … Pennuto, M. (2009). Overexpression of IGF-1 in muscle attenuates disease in a mouse model of spinal and bulbar muscular atrophy. *Neuron*, *63*, 316–328. https://doi.org/10.1016/j.neuron.2009.07.019

Perera, N. D., Sheean, R. K., Lau, C. L., Shin, Y. S., Beart, P. M., Horne, M. K., & Turner, B. J. (2017). Rilmenidine promotes MTOR-independent autophagy in the mutant SOD1 mouse model of amyotrophic lateral sclerosis without slowing disease progression. *Autophagy*, 1–18.

Pfohl, S. R., Halicek, M. T., & Mitchell, C. S. (2015). Characterization of the contribution of genetic background and gender to disease progression in the SOD1 G93A mouse model of amyotrophic lateral sclerosis: A meta-analysis. *Journal of Neuromuscular Diseases*, *2*, 137–150. https://doi.org/10.3233/JND-140068

Pi, M., & Quarles, L. D. (2012). GPRC6A regulates prostate cancer progression. *Prostate*, *72*, 399–409. https://doi.org/10.1002/pros.21442

Pun, S., Santos, A. F., Saxena, S., Xu, L., & Caroni, P. (2006). Selective vulnerability and pruning of phasic motoneuron axons in motoneuron disease alleviated by CNTF. *Nature Neuroscience*, *9*, 408–419. https://doi.org/10.1038/nn1653

Rana, K., Lee, N. K., Zajac, J. D., & MacLean, H. E. (2014). Expression of androgen receptor target genes in skeletal muscle. *Asian Journal of Andrology*, *16*, 675–683. https://doi.org/10.4103/1008-682X.122861

Renier, K. J., Troxell-Smith, S. M., Johansen, J. A., Katsuno, M., Adachi, H., Sobue, G., … Jordan, C. L. (2014). Antiandrogen flutamide protects male mice from androgen-dependent toxicity in three models of spinal bulbar muscular atrophy. *Endocrinology*, *155*, 2624–2634. https://doi.org/10.1210/en.2013-1756

Rooney, J., Fogh, I., Westeneng, H. J., Vajda, A., McLaughlin, R., Heverin, M., … Hardiman, O. (2017). C9orf72 expansion differentially affects males with spinal onset amyotrophic lateral sclerosis. *Journal of Neurology, Neurosurgery, and Psychiatry*, *88*, 281.

Schulz, M., Schmoldt, A., Donn, F., & Becker, H. (1988). The pharmacokinetics of flutamide and its major metabolites after a single oral dose and during chronic treatment. *European Journal of Clinical Pharmacology*, *34*, 633–636. https://doi.org/10.1007/BF00615229

Scott, S., Kranz, J. E., Cole, J., Lincecum, J. M., Thompson, K., Kelly, N., … Heywood, J. A. (2008). Design, power, and interpretation of studies in the standard murine model of ALS. *Amyotrophic Lateral Sclerosis*, *9*, 4–15. https://doi.org/10.1080/17482960701856300

Sheean, R. K., Weston, R. H., Perera, N. D., D'Amico, A., Nutt, S. L., & Turner, B. J. (2015). Effect of thymic stimulation of CD4+ T cell expansion on disease onset and progression in mutant SOD1 mice. *Journal of Neuroinflammation*, *12*, 40. https://doi.org/10.1186/s12974-015-0254-3

Simeoni, S., Mancini, M. A., Stenoien, D. L., Marcelli, M., Weigel, N. L., Zanisi, M., … Poletti, A. (2000). Motoneuronal cell death is not correlated with aggregate formation of androgen receptors containing an elongated polyglutamine tract. *Human Molecular Genetics*, *9*, 133–144. https://doi.org/10.1093/hmg/9.1.133

Sinha-Hikim, I., Taylor, W. E., Gonzalez-Cadavid, N. F., Zheng, W., & Bhasin, S. (2004). Androgen receptor in human skeletal muscle and cultured muscle satellite cells: Up-regulation by androgen treatment. *The Journal of Clinical Endocrinology and Metabolism*, *89*, 5245–5255. https://doi.org/10.1210/jc.2004-0084

Taylor, J. P., Brown, R. H. Jr., & Cleveland, D. W. (2016). Decoding ALS: From genes to mechanism. *Nature*, *539*, 197–206. https://doi.org/10.1038/nature20413

Tevell, A., Lennernas, H., Jonsson, M., Norlin, M., Lennernas, B., Bondesson, U., & Hedeland, M. (2006). Flutamide metabolism in four different species in vitro and identification of flutamide metabolites in human patient urine by high performance liquid chromatography/tandem mass spectrometry. *Drug Metabolism and Disposition*, *34*, 984–992.

Thomson, J. A., Itskovitz-Eldor, J., Shapiro, S. S., Waknitz, M. A., Swiergiel, J. J., Marshall, V. S., & Jones, J. M. (1998). Embryonic stem cell lines derived from human blastocysts. *Science*, *282*, 1145–1147. https://doi.org/10.1126/science.282.5391.1145

Towne, C., Raoul, C., Schneider, B. L., & Aebischer, P. (2008). Systemic AAV6 delivery mediating RNA interference against SOD1: Neuromuscular transduction does not alter disease progression in fALS mice. *Molecular Therapy*, *16*, 1018–1025. https://doi.org/10.1038/mt.2008.73

Turner, B. J., Alfazema, N., Sheean, R. K., Sleigh, J. N., Davies, K. E., Horne, M. K., & Talbot, K. (2014). Overexpression of survival motor neuron improves neuromuscular function and motor neuron survival in mutant SOD1 mice. *Neurobiology of Aging*, *35*, 906–915. https://doi.org/10.1016/j.neurobiolaging.2013.09.030

Tyagi, S., Beqollari, D., Lee, C. S., Walker, L. A., & Bannister, R. A. (2017). Semi-automated analysis of mouse skeletal muscle morphology and fiber-type composition. *Journal of Visualized Experiments*, *126*, e56024. https://doi.org/10.3791/56024

van Roijen, J. H., Ooms, M. P., Weber, R. F., Brinkmann, A. O., Grootegoed, J. A., & Vreeburg, J. T. (1997). Comparison of the response of rat testis and accessory sex organs to treatment with testosterone and the synthetic androgen methyltrienolone (R1881). *Journal of Andrology*, *18*, 51–61.

Vargas, M. R., Burton, N. C., Kutzke, J., Gan, L., Johnson, D. A., Schafer, M., … Johnson, J. A. (2013). Absence of Nrf2 or its selective overexpression in neurons and muscle does not affect survival in ALS-linked mutant hSOD1 mouse models. *PLoS ONE*, *8*, e56625. https://doi.org/10.1371/journal.pone.0056625

Wang, C., Liu, Y., & Cao, J. M. (2014). G protein-coupled receptors: Extranuclear mediators for the non-genomic actions of steroids. *International Journal of Molecular Sciences*, *15*, 15412–15425. https://doi.org/10.3390/ijms150915412

Yoo, Y. E., & Ko, C. P. (2012). Dihydrotestosterone ameliorates degeneration in muscle, axons and motoneurons and improves motor function in amyotrophic lateral sclerosis model mice. *PLoS ONE*, *7*, e37258. https://doi.org/10.1371/journal.pone.0037258

SUPPORTING INFORMATION

Additional supporting information may be found online in the Supporting Information section at the end of the article.

How to cite this article: McLeod VM, Lau CL, Chiam MDF, et al. Androgen receptor antagonism accelerates disease onset in the SOD1^{G93A} mouse model of amyotrophic lateral sclerosis. *Br J Pharmacol*. 2019;176:2111–2130. https://doi.org/10.1111/bph.14657

Supplementary Material:

Androgen receptor antagonism accelerates disease onset and exacerbates muscle atrophy in the SOD1^{G93A} mouse model of amyotrophic lateral sclerosis

Victoria M. McLeod[1], Chew L. Lau[1], Mathew D.F. Chiam[1], Thusitha W. Rupasinghe[2], Ute Roessner[2], Elvan Djouma[3], Wah C. Boon[1], Bradley J. Turner[1,*]

[1]*Florey Institute of Neuroscience and Mental Health, University of Melbourne, Parkville, VIC 3052, Australia.*

[2]*Metabolomics Australia, School of BioSciences, University of Melbourne, VIC 3010 Australia*

[3]*Department of Physiology, Anatomy and Microbiology, La Trobe University, VIC 3086 Australia*

* Corresponding author

Bradley J. Turner

Florey Institute of Neuroscience and Mental Health

University of Melbourne

30 Royal Parade

Parkville, VIC, Australia, 3052

Tel: +61 3 9035 6521, Fax: +61 3 9035 3107

Email: bradley.turner@florey.edu.au

Validation of AR luciferase reporter assay

Methods

Human wild-type AR (hAR) construct was kindly donated by Prof. Angelo Poletti (University of Milan) and transformed in XL10-Gold ultracompetent cells (Agilent Technologies) and amplified in NZY^{+} broth according to manufactures protocol (Agilent Tech) followed by plasmid DNA extraction and purification using PureLink™ HiPure Plasmid Filter (Invitrogen, Australia). In order to optimise the co-expression of hAR and AR reporter conditions were validated using three ratios of hAR in combination with AR reporter, negative or positive control constructs for 24h followed by 16h treatment with 10nM DHT to assess AR activation.

Results

A 1:1 mass ratio of hAR:reporter construct DNA gave a maximal increase of 6-fold relative luciferase output upon treatment with DHT with no response seen in the negative control.

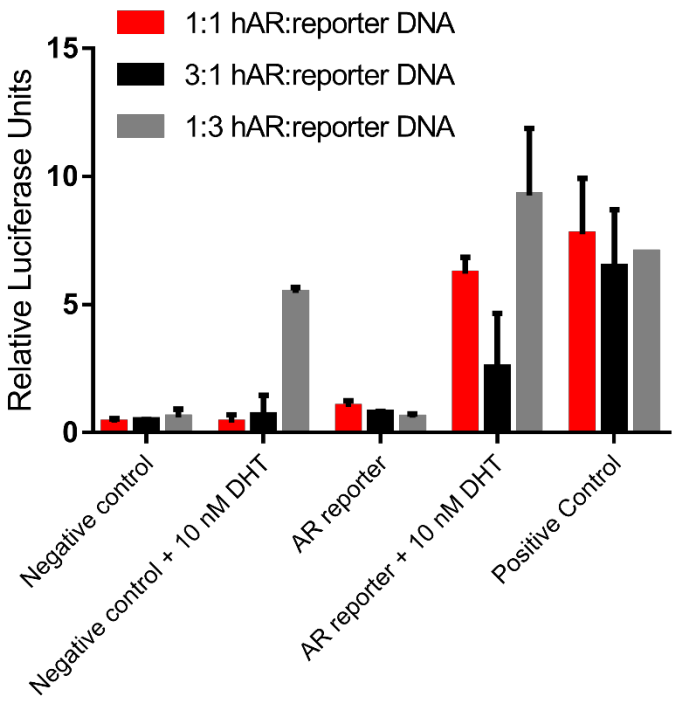

Figure S1. Dual Luciferase assay response of transfected hESC-derived motor neurons with various construct combinations normalized to huAR:AR reporter (1:1) untreated.

Validation of Housekeeping genes (HKGs) during hESC differentiation into mature motor neurons

Methods

Samples and cDNA were prepared and qPCR conducted as previously described on n=3 differentiations to generate a Ct value for 4 commonly used housekeeping genes. Primer sequences were as follows: *B2M*: Forward 5'- GTGCTCGCGCTACTCTCTCT-3', Reverse 5'- TTCAATGTCGGATGGATGAA-3', *RPS18*: Forward 5'- TGTGGTGTTGAGGAAAGCAG-3', Reverse 5'- TTGTACTGGCGTGGATTCTG-3', *Hprt1*: Forward 5'- GCTGAGGATTTGGAAAGGGTG-3', Reverse 5'- GCTACAATGTGATGGCCTCC-3'.

Table S1. Threshold cycle (C_T): Values of average, standard deviation and coefficient of variation for HKGs

C_T	B2M	GAPDH	RPS18	Hprt1
Stage 1 Day 0	21.95	15.16	15.52	21.53
Stage 1 Day 6	22.52	15.16	15.05	22.82
Stage 2 Day 6	22.31	16.09	15.68	23.70
Stage 3 Day 6	22.52	16.46	16.78	25.11
Stage 4 Day 10	19.30	16.35	17.35	23.98
Max-Min	3.22	1.30	2.31	3.58
Mean	21.72	15.84	16.08	23.43
Std Deviation	1.37	0.64	0.96	1.34
Coefficient of Variation (%)	6.33	4.03	5.95	5.72

Validation of Testosterone and Flutamide by LC-MS-MS

Testosterone standards were prepared over 1-10000 pg/ml range in 50/50 acetonitrile/water. For quantification (Table S1 and S2) a low-range standard curve (5-100 pg/ml) and mid-range standard curve (100-10000 pg/ml) were validated using nonlinear regression, four parametric logistic standard curves (SigmaPlot 14.0, Systat Software Inc., San Jose, CA). Plasma and tissue standards were prepared from pooled sample (containing basal level testosterone) by spiking known concentrations of testosterone and internal standard to adjust for processing and extraction efficiency. The LOQ for plasma testosterone was ~27 pg/ml with 75% processing recovery. The LOQ was ~16 pg/g testosterone in spinal cord tissue with 68% processing recovery.

Table S2. Low-range Testosterone Solvent Standards

Standard (pg/ml)	**5**	**25**	**100**
n (curves)	3	3	3
% CV	13.1	6.7	0.3
% Accuracy	91.4 ± 4.0	96.6 ± 3.4	99.4 ± 0.3

Table S3. Mid-range Testosterone Solvent Standards

Standard (pg/ml)	**100**	**1000**	**10000**
n (curves)	3	3	3
% CV	11.5	14.8	1.7
% Accuracy	87.7 ± 9.2	89.9 ± 12.2	99.0 ± 1.7

Flutamide standards were prepared and validated over 0.5-500 ng/ml linear range by spiking into blank plasma (Table S3). The LOQ in plasma was set at 0.5 ng/ml which is below the detectable range across samples and 1.7 ng/g in spinal cord. The processing recovery in plasma based on flutamide solvent standards was 97%. Metabolite, 2-hydroxyflutamide and Flu-1, standards were prepared in 50:50 acetonitrile and validated against flutamide for correct peak detection and quantitative response. The LOQ of 2-hydroxyflutamide and Flu-1 in plasma was 2.25 ng/ml and 1.4 ng/ml, respectively, and 7.5 and 4.6 ng/g in spinal cord tissue, respectively.

Table S4. Flutamide in Plasma Standards

Standard (ng/ml)	**0.5**	**10**	**500**
n (curves)	3	3	3
% CV	15.2	14.6	0.17
% Accuracy	87.2 ± 3.3	86.7 ± 1.6	99.9 ± 0.1

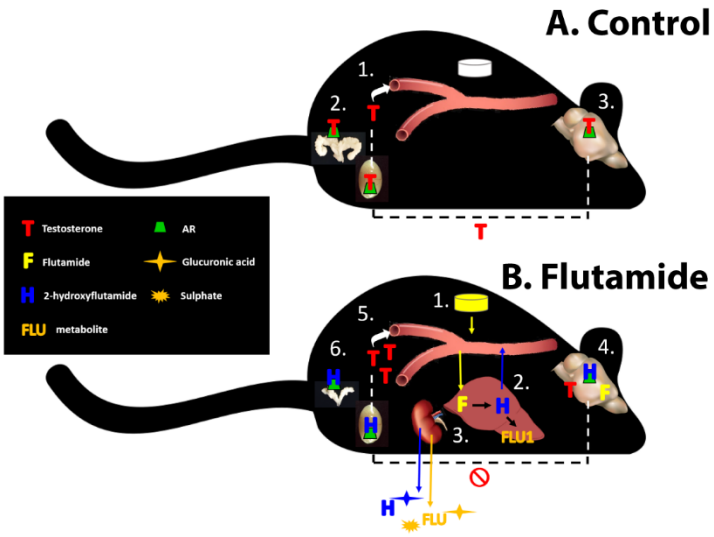

Figure S2. Schematic of systemic testosterone regulation in male mice and the impact of flutamide administration. (A) In control mice, testosterone is mainly produced by the testes (1), where it binds to androgen receptors (AR) to mediate healthy function of male secondary sex organs such as the seminal vesicles (2) and binds to AR located in the hypothalamus (3) which signals via a negative feedback loop to inhibit testosterone production. (B) In flutamide treated mice, drug is implanted under the skin, subcutaneously released and absorbed into the systemic bloodstream (1), and metabolised into HF and then Flu-1 in the liver and reabsorbed back into the systemic bloodstream (2), and further cleared via subsequent metabolism by the kidneys (3). Flutamide and HF readily cross the blood-brain-barrier where they preferentially bind to hypothalamic AR (4) causing disinhibition of feedback regulation, resulting in increased testosterone production by the testes (5). Systemic effects of AR antagonism decrease the weight of male secondary sex organs (6).

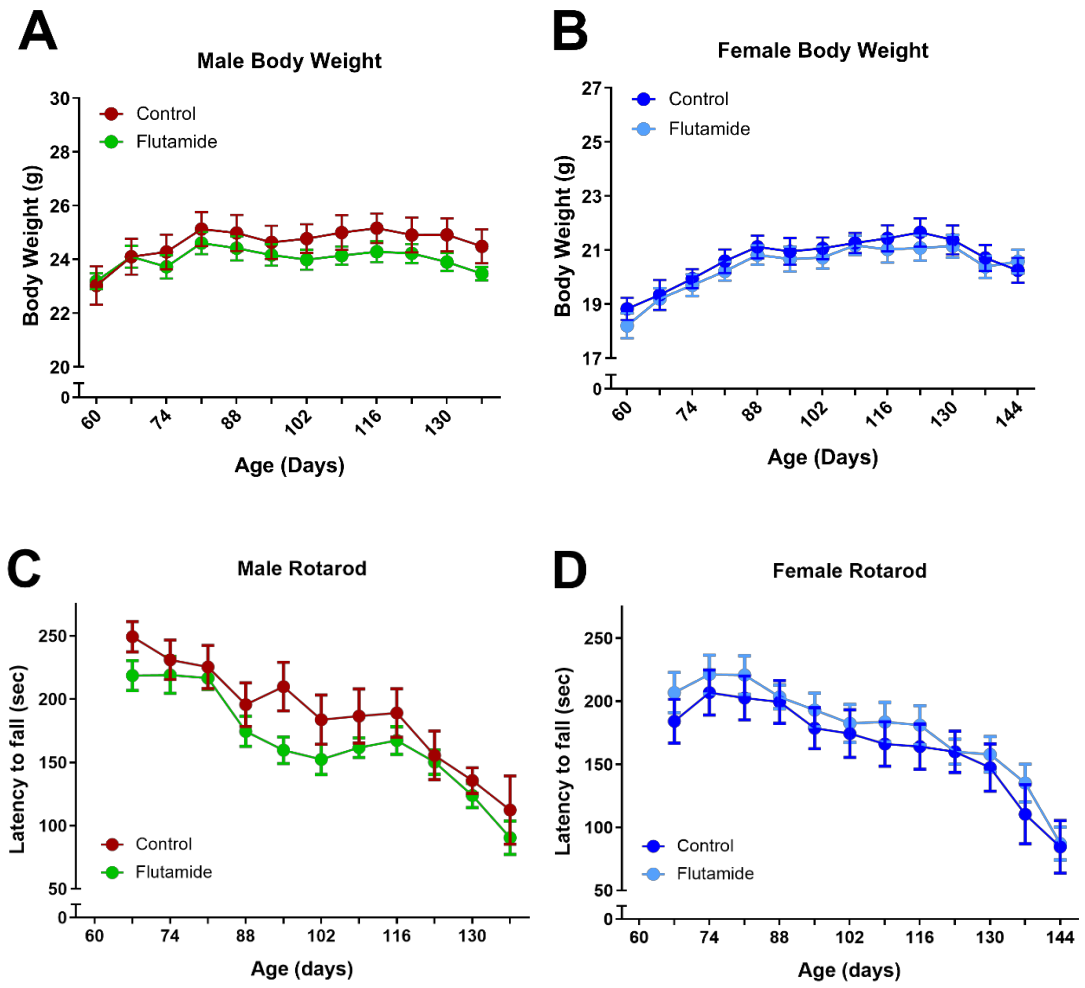

Figure S3. Absolute body weight measurements and rotarod performance of control and flutamide treated SOD1^{G93A} mice.

Body weights of male (A) and female (B) control vs fluamide treated mice from treatment initiation at 60 days of age to late symptomatic stage. Latency to fall on rotarod motor function test in male (C) and female (B) control vs flutamde mice. Data represent mean ± SEM, n=10 mice per group.

Chapter 6. Dissociation of disease onset, progression and sex differences from androgen receptor levels in a mouse model of amyotrophic lateral sclerosis

scientific reports

Check for updates

OPEN

Dissociation of disease onset, progression and sex differences from androgen receptor levels in a mouse model of amyotrophic lateral sclerosis

Doris Tomas[1,3], Victoria M. McLeod[1,3], Mathew D. F. Chiam[1], Nayomi Wanniarachchillage[1], Wah C. Boon[1] & Bradley J. Turner[1,2]✉

Amyotrophic lateral sclerosis (ALS) is an adult-onset neurodegenerative disorder caused by loss of motor neurons. ALS incidence is skewed towards males with typically earlier age of onset and limb site of onset. The androgen receptor (AR) is the major mediator of androgen effects in the body and is present extensively throughout the central nervous system, including motor neurons. Mutations in the AR gene lead to selective lower motor neuron degeneration in male spinal bulbar muscular atrophy (SBMA) patients, emphasising the importance of AR in maintaining motor neuron health and survival. To evaluate a potential role of AR in onset and progression of ALS, we generated SOD1^{G93A} mice with either neural AR deletion or global human AR overexpression. Using a Cre-LoxP conditional gene knockout strategy, we report that neural deletion of AR has minimal impact on the disease course in SOD1^{G93A} male mice. This outcome was potentially confounded by the metabolically disrupted Nestin-Cre phenotype, which likely conferred the profound lifespan extension observed in the SOD1^{G93A} double transgenic male mice. In addition, overexpression of human AR produced no benefit to disease onset and progression in SOD1^{G93A} mice. In conclusion, the disease course of SOD1^{G93A} mice is independent of AR expression levels, implicating other mechanisms involved in mediating the sex differences in ALS. Our findings using Nestin-Cre mice, which show an inherent metabolic phenotype, led us to hypothesise that targeting hypermetabolism associated with ALS may be a more potent modulator of disease, than AR in this mouse model.

Amyotrophic lateral sclerosis (ALS) is a fatal progressive neurodegenerative disorder in which upper and lower motor neurons die, leading to muscle atrophy and ultimately respiratory failure[1]. ALS shows increased incidence, a younger age and predominantly limb onset in males[2–4]. Higher incidence of ALS has been identified among professional athletes and soccer players[5–8] which could be linked to higher prenatal testosterone exposure[9–11]. The biological actions of androgens are mediated by the androgen receptor (AR), a nuclear steroid hormone receptor expressed within tissues throughout the body including the central nervous system (CNS)[12]. The adult onset neurodegenerative disorder, spinal bulbar muscular atrophy (SBMA), is caused by trinucleotide repeat expansions in the *AR* gene, resulting in selective lower motor neuron degeneration in males[13]. This evidence supports a pivotal role for androgens and AR in motor neuron health.

Animal models of ALS reflect the sex differences observed clinically[14,15]. The mutant superoxide dismutase 1 (SOD1^{G93A}) mouse is the most well characterised and commonly used model of ALS[16]. Studies into the mechanisms by which sex influences ALS have to date, largely focused on manipulation of hormones. Firstly, castration in male SOD1^{G93A} mice does not modify disease course[17,18]. Several confounds to castration exist. It may lead to the disruption of other hormone sources and steroidogenesis pathways, such as progesterone and estrogens. Alternatively, the adrenal glands provide another source of androgens[19]. Blockade of AR by the anti-androgen,

[1]Florey Institute of Neuroscience and Mental Health, University of Melbourne, 30 Royal Parade, Parkville, VIC 3052, Australia. [2]Perron Institute for Neurological and Translational Science, Queen Elizabeth Medical Centre, Nedlands, WA 6150, Australia. [3]These authors contributed equally: Doris Tomas and Victoria M. McLeod. ✉email: bradley.turner@florey.edu.au

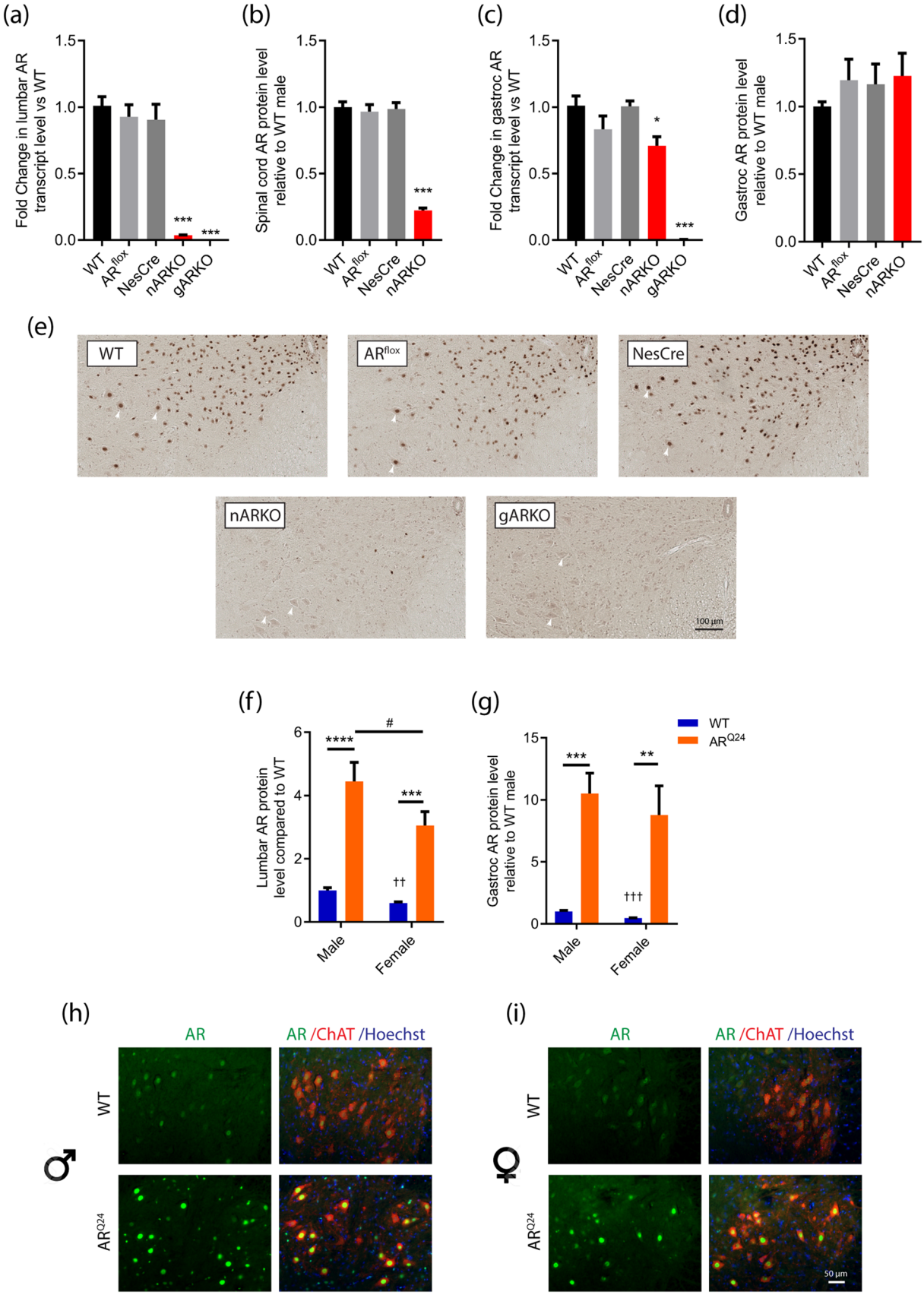
(a)
Fold Change in lumbar AR transcript level vs WT
1.5
1.0
0.5
0.0
***
***
WT
AR flox
NesCre
nARKO
gARKO
(b)
Spinal cord AR protein level relative to WT male
1.5
1.0
0.5
0.0
***
WT
AR flox
NesCre
nARKO
(c)
Fold Change in gastroc AR transcript level vs WT
1.5
1.0
0.5
0.0
*
***
WT
AR flox
NesCre
nARKO
gARKO
(d)
Gastroc AR protein level relative to WT male
1.5
1.0
0.5
0.0
WT
AR flox
NesCre
nARKO
(e)
WT
AR flox
NesCre
nARKO
gARKO
100 µm
(f)
Lumbar AR protein level compared to WT
6
4
2
0
#
****
***
††
Male
Female
(g)
WT
AR Q24
Gastroc AR protein level relative to WT male
15
10
5
0
***
**
†††
Male
Female
(h)
AR
AR /ChAT /Hoechst
♂
WT
AR Q24
(i)
AR
AR /ChAT /Hoechst
♀
WT
AR Q24
50 µm

◂**Figure 1.** Validation of AR expression in spinal cord and skeletal muscle of nARKO and AR^{Q24} mice. **(a)** AR transcript and **(b)** protein levels in nARKO spinal cord, compared to control genotypes. **(c)** AR transcript and **(d)** protein levels in nARKO gastrocnemius muscle, compared to control genotypes at 2 months age. Data represents mean ± SEM, n = 5 mice per group. * $P < 0.05$, *** $P < 0.001$, **** $P < 0.0001$ by one-way ANOVA with Dunnett's multiple comparison test comparing all genotypes to WT. Full-length blots are presented in Supplementary Fig. 1a,b. **(e)** AR immunohistochemical staining in the ventral horn spinal cord of nARKO mice, compared with control genotypes, at 6 months age. Representative motor neurons indicated by white arrowheads. **(f)** AR protein expression in the lumbar spinal cord and **(g)** gastrocnemius muscle of male and female AR^{Q24} transgenic mice, relative to male WT levels at 3 months age. Data represents mean ± SEM, n = 6 mice per group. **$P < 0.01$, ***$P < 0.001$, ****$P < 0.0001$ by two-way ANOVA with Sidak's multiple comparisons test comparing genotype effect; $^{\#}P < 0.05$ by two-way ANOVA with Sidak's multiple comparisons test comparing sex effect. $^{\dagger\dagger}P < 0.01$, $^{\dagger\dagger\dagger}P < 0.001$ compared to WT male by unpaired t-test. Full-length blots are presented in Supplementary Fig. S1c,d. **(h)** AR immunostaining in the lumbar spinal cord of male and **(i)** female WT and AR^{Q24} mice. Motor neurons are identified by positive ChAT staining.

flutamide, exacerbated muscle atrophy and induced an earlier disease onset in male $SOD1^{G93A}$ mice[20]. Administration of the androgen, dihydrotestosterone (DHT), was neuroprotective in $SOD1^{G93A}$ male mice[21], while the anabolic steroid nandrolone was detrimental[22]. These studies highlight the differential actions and tissue-selectivity of biological and synthetic androgens. Lastly, evidence supports prenatal testosterone exposure potentially having an early impact on motor neuron vulnerability in later life[9], whereas most of the studies conducted in $SOD1^{G93A}$ mice manipulate AR signalling systems from adulthood at a time when disease onset occurs.

Here, we have used genetic manipulation of AR to study its impact throughout the lifespan of $SOD1^{G93A}$ mice. Despite the compelling evidence for androgen influences in ALS, neither selective neural deletion nor global overexpression of AR modified the disease course of male $SOD1^{G93A}$ mice. The Cre-LoxP conditional knockout strategy we employed to selectively delete AR from neurons and glia, used the Nestin-Cre (NesCre) mouse which inherently displays an altered metabolic phenotype. When crossed with $SOD1^{G93A}$ mice, NesCre inadvertently delayed disease onset and extended survival, revealing that targeting hypermetabolism associated with ALS may be a more effective modulator of disease than sex hormones in this mouse model.

Results

Androgen receptor is efficiently and selectively deleted in spinal cord of nARKO mice. We first used a Cre-LoxP system in mice to obtain CNS-conditional deletion of AR. The NesCre transgenic expresses Cre-recombinase under the rat nestin promotor and enhancer, resulting in AR deletion from neuronal and glial precursor cells[23]. AR transcript was abolished by 96% of wild-type (WT) levels in neural AR knockout (nARKO) spinal cord (Fig. 1a) with a corresponding 78% depletion of AR protein (Fig. 1b, S1a). Gastrocnemius muscle revealed a 30% reduction in AR transcript (Fig. 1c) with no change in AR protein level detected in nARKO mice (Fig. 1d, S1b). In lumbar spinal cord, nuclear AR was not detected in ventral horn motor neurons of nARKO mice which was comparable to the global knockout (gARKO) mouse (Fig. 1e). All 3 genotypes WT, AR^{flox} and Nes-Cre expressed AR abundantly in nuclei of motor neurons in the spinal cord (Fig. 1e). Organ weight analysis showed consistently increased spleen (0.061 ± 0.007 g vs. 0.078 ± 0.014 g; $P = 0.035$) and seminal vesicle (0.12 ± 0.035 g vs. 0.24 ± 0.053 g; $P < 0.0001$) weights in nARKO mice compared to NesCre controls, and reduced testis weights (0.16 ± 0.012 g vs. 0.12 ± 0.009 g $P = 0.0002$) from 2 months age onwards (Table S1). Increased seminal vesicle weights reflect elevated testosterone levels, a commonly observed concomitant of neuronal AR deletion models due to disruption of the hypothalamic-pituitary–gonadal (HPG) axis[24,25]. The AR^{flox} mouse line, used in the current studies, was modified to remove a neomycin resistance cassette[26] which interfered in AR gene function in several previous AR floxed models[27,28]. There is no known observable interference from loxP insertions in this mouse, confirmed by our assessment of long-term growth curves, major organ weights and AR quantification being indistinguishable from WT mice (Fig. 1a, 2a, S1, Table S1).

AR is robustly overexpressed in motor neurons and skeletal muscle of AR^{Q24} male and female mice. The AR^{Q24} mouse expresses 5 copies of the WT human AR transgene driven by the chicken β-actin promoter[29]. In lumbar spinal cord, total AR protein levels were increased 4.4-fold in male AR^{Q24} mice, compared to WT controls, while in females this was slightly lower at threefold increase (Fig. 1f, S1c). In gastrocnemius muscle, total AR protein level was elevated 10.5-fold in male AR^{Q24} mice, compared to WT controls (Fig. 1g, S1d). In AR^{Q24} females, AR was increased 8.8-fold compared to WT male mice. Male vs. female WT levels were not significantly different using two-way ANOVA analysis due to the dominating effect of the AR^{Q24} levels. When analysed separately, female WT mice had 40% less AR in lumbar spinal cord compared to males and 54% less AR in gastrocnemius, consistent with our previous study[20]. AR protein overexpression was reflected in ventral horn spinal cord immunohistochemistry (Fig. 1h,i), where nuclear AR staining was substantially greater in $ChAT^{+}$ motor neurons of AR^{Q24} male and female spinal cord, as well as appearing in the smaller nuclei of surrounding cell populations. Organ weights were comparable between male AR^{Q24} and WT controls, except for decreased skeletal muscle weight observed in AR^{Q24} mice (Table S2).

Neural AR deletion and global AR overexpression have a detrimental effect on survival of male mice. Male mice carrying the NesCre transgene displayed significant growth retardation over 24 months, compared to WT males, while AR^{flox} males displayed no overt impairments in growth and body weight (Fig. 2a). This has been reported previously in NesCre transgenic mice which have mild hypopituitarism and growth

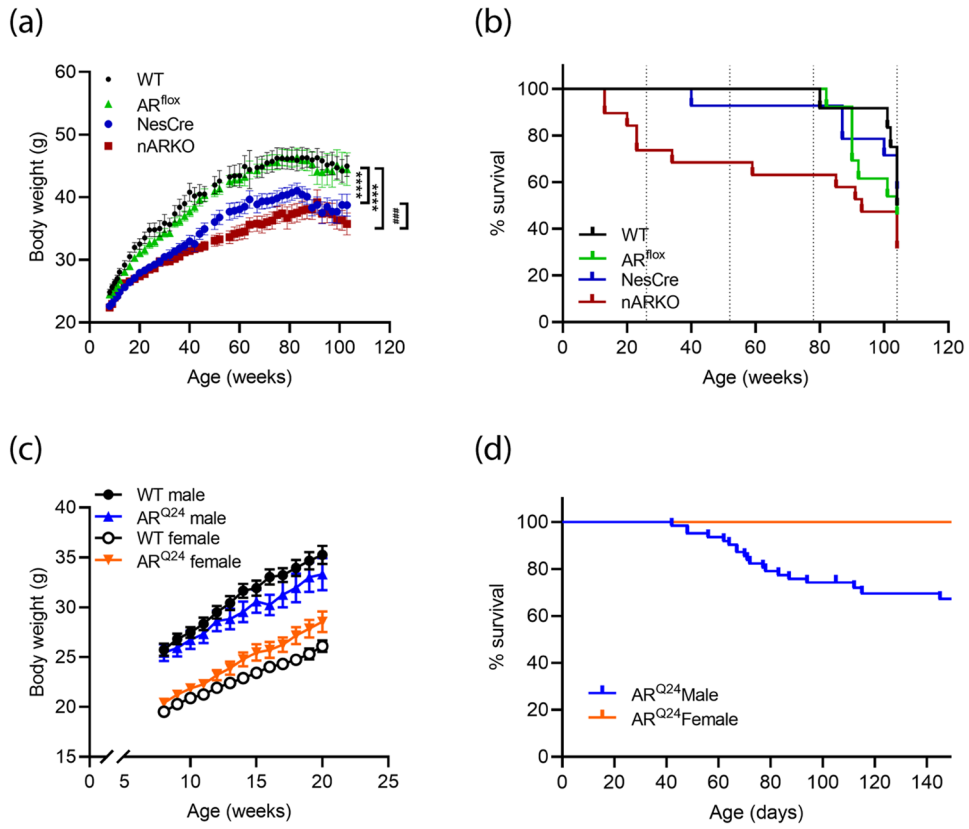

Figure 2. Impact of neural AR deletion and global AR overexpression on male mouse survival. **(a)** Body weight analysis of AR^{flox} x NesCre cross mice over 24 months. Mean ± SEM, n = 11–13 mice per group. **** P < 0.0001 vs WT; ### P < 0.001 vs NesCre by mixed-effects analysis with Tukey's multiple comparison test for main genotype effect. **(b)** Kaplan–Meier curves of AR^{flox} x NesCre cross mouse survival over 24 months; n = 12 WT; n = 13 AR^{flox}; n = 14 NesCre; n = 10 nARKO. **(c)** Body weight analysis of WT and AR^{Q24} mice to P150. Mean ± SEM, n = 12–14 mice per group. (d) Kaplan–Meier curves of AR^{Q24} transgenic mouse survival over 150 days; n = 62 males.

hormone deficiency[30]. Body weight growth was further reduced in nARKO mice, compared to NesCre, revealing a requirement of AR for weight gain. Mice reached maximal weights of 49 ± 5.1 g, 49 ± 5.5 g, 43 ± 4.8 g and 39 ± 6.0 g for WT, AR^{flox}, NesCre and nARKO male mice, respectively. At 6 months of age, little difference in organ weights were observed between NesCre and nARKO mice, other than increased prostate weight (0.08 ± 0.01 g vs. 0.13 ± 0.05 g; $P = 0.0132$) and previously mentioned spleen, seminal vesicle and testis differences (Table S1). Off-target AR deletion was evident in kidney, skeletal muscle and heart tissue in 6-month old nARKO mice (Fig S2), and elevated liver AR transcript and protein levels were apparent through secondary mechanisms with no genomic deletion of AR evident (Fig S2). Spontaneous deaths occurred in nARKO mice from 13 weeks (3 months) of age onward, with 8/10 mice showing no signs of ill-health prior to death (Fig. 2b). In this study cohort, 6/19 mice reached 24 months of age without appreciable weight loss, adverse events or evidence of abnormal gross pathology. Control genotypes began losing mice beyond 18 months of age, typically due to general poor health and weight decline. Mice reaching 24 months of age with no evidence of poor health included 6/12, 6/13 and 8/14 mice for WT, AR^{flox} and NesCre groups, respectively (Fig. 2b). Aged nARKO mice showed significant enlargement of the prostate up to 6-fold, compared to NesCre controls (0.108 ± 0.016 g vs. 0.681 ± 0.179 g; $P < 0.0001$ for nARKO and NesCre mice, respectively. Table S1). No other differences in gross organ pathology were notable.

We analysed the effects of AR overexpression in male and female mice (Fig. 2c). A slight downward weight trend in AR^{Q24} males and upward trend in AR^{Q24} females was observed, compared to WT counterparts. This genotype effect was only found to be significant in females when analysed by repeated measures two-way ANOVA ($F_{(1,22)} = 5.056$; $P = 0.0349$). Unexpectedly, sudden deaths were observed in approximately one third of male AR^{Q24} mice by 150 days (Fig. 2d). These mice frequently showed a sudden rapid weight gain prior to death, indicative of fluid retention. Cardiac hypertrophy was evident on post-mortem inspection and was confirmed as the cause of death by external veterinary pathology. The occurrence of these deaths appear to coincide with rising circulating testosterone levels which we have previously reported in mice from P60-P150 age[31]. The heart weight of remaining healthy AR^{Q24} mice did not show a difference, compared to control WT mice, indicating incomplete penetrance of this phenotype in AR^{Q24} male mice (Supplementary material Fig S3a). Previously, this

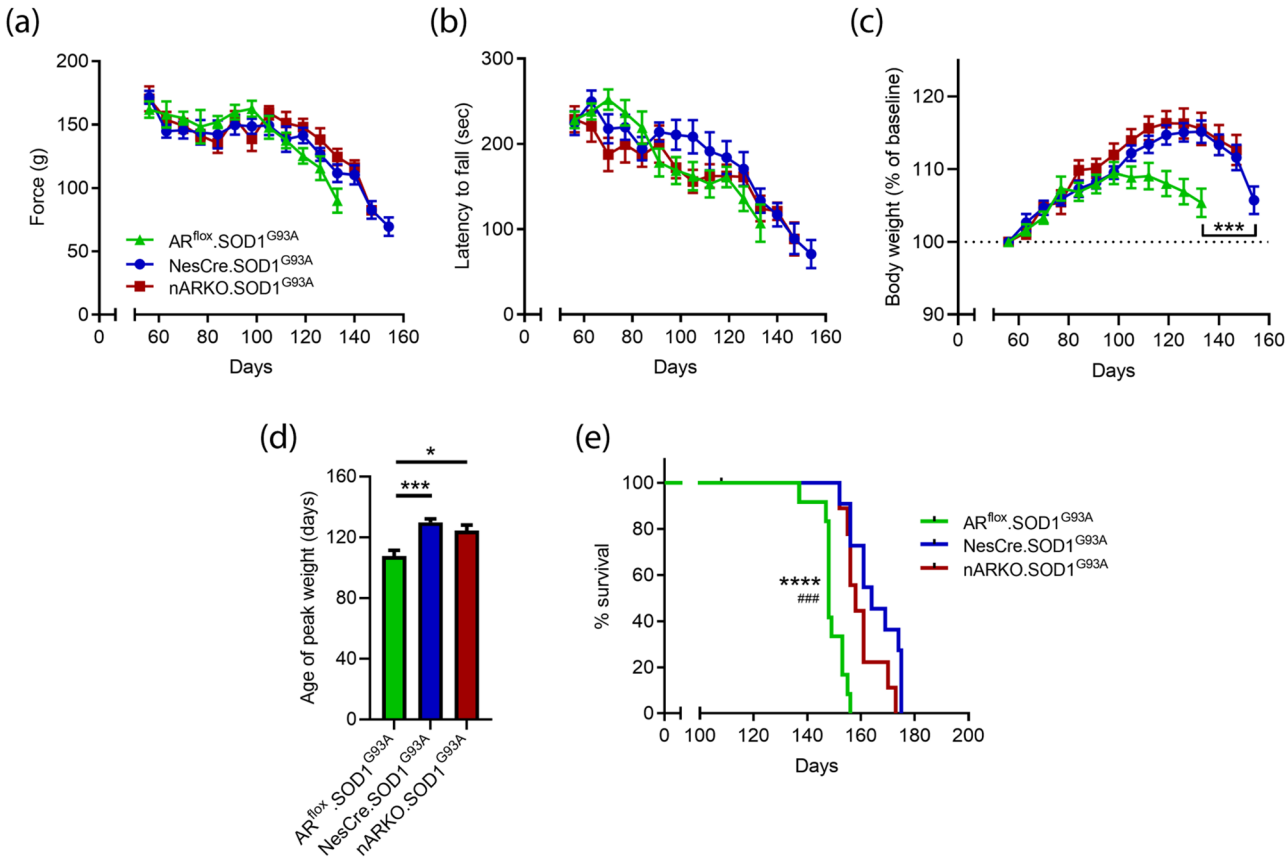

Figure 3. Neural deletion of AR does not alter disease course in SOD1^{G93A} male mice. Motor function assessment by **(a)** four limb grip strength and **(b)** rotarod performance. **(c)** Body weight analysis of AR^{flox} x NesCre x SOD1^{G93A} cross mice over disease course; ***$P < 0.001$ vs. NesCre:SOD1^{G93A} by two-way ANOVA with Tukey's multiple comparison test comparing main genotype effect. **(d)** Age in weeks when peak weight occurred; $P < 0.001$ by one-way ANOVA with Dunnett's multiple comparison test comparing all genotypes to NesCre:SOD1^{G93A}. **(e)** Kaplan–Meier curves show reduced survival in AR^{flox}:SOD1^{G93A} compared to NesCre:SOD1^{G93A} (****$P < 0.0001$) and nARKO:SOD1^{G93A} ($^{###}P < 0.001$). All values presented as mean ± SEM; n = 9–12 mice per group.

genotype was backcrossed onto the C57BL/6 J genetic background and spontaneous deaths were not described in the phenotype[29]. Notably, the current B6D2 mixed background exhibits greater heart weight than C57BL/6 J counterparts (0.22 ± 0.03 g vs. 0.12 ± 0.01 g; Fig S3), hence AR effects on cardiac phenotype may be exacerbated in mice on the B6D2 background. Likewise, nARKO heart weights were not different to NesCre controls throughout their lifespan (Fig S3b).

Neural deletion of AR does not alter disease course in SOD1^{G93A} male mice. After establishing the effects of AR ablation in non-diseased mice, we next determined the impact of AR ablation in the CNS, on the phenotype of male transgenic SOD1^{G93A} mice. SOD1^{G93A} mice were generated with nARKO, AR^{flox} or NesCre transgenes. A comparison of limb muscle strength (Fig. 3a) and locomotor function (Fig. 3b) revealed no overt genotype differences. Body weight analysis showed an earlier symptomatic decline in the AR^{flox}:SOD1^{G93A} genotype from 105 days onwards ($P = 0.0002$; Fig. 3c). Age of peak body weight was used to retrospectively assess disease onset (Fig. 3d). Onset was 108 ± 13 days in the AR^{flox}:SOD1^{G93A} group, in line with a previous recent assessment conducted on identical SOD1^{G93A} mice from within our laboratory, reporting onset at 110 ± 20 days using this method[20]. NesCre:SOD1^{G93A} mice showed a delay in disease onset by 22 days, compared to AR^{flox}:SOD1^{G93A} ($P < 0.0001$) reaching peak body weight at 130 ± 8 days. nARKO:SOD1^{G93A} disease onset was slightly earlier than NesCre:SOD1^{G93A} mice at 124 ± 11 days, although this 6-day difference was not statistically significant ($P = 0.4623$). NesCre:SOD1^{G93A} and nARKO:SOD1^{G93A} mice showed a 16 and 10 day median survival extension, respectively, compared to AR^{flox}:SOD1^{G93A} (Fig. 3e). nARKO:SOD1^{G93A} mice showed a modest reduction in median survival by 6 days, compared to NesCre:SOD1^{G93A} which approached statistical significance ($P = 0.07$) by the log-rank test. Taken together, the NesCre phenotype appears to be driving the survival extension in SOD1^{G93A} male mice.

Overexpression of AR does not influence disease parameters in SOD1^{G93A} mice. With evidence that neither deletion of AR from neurons, nor peripheral AR antagonism[20] are capable of modifying disease outcome in SOD1^{G93A} mice we turned to an overexpression model. The effects of global AR overexpression were

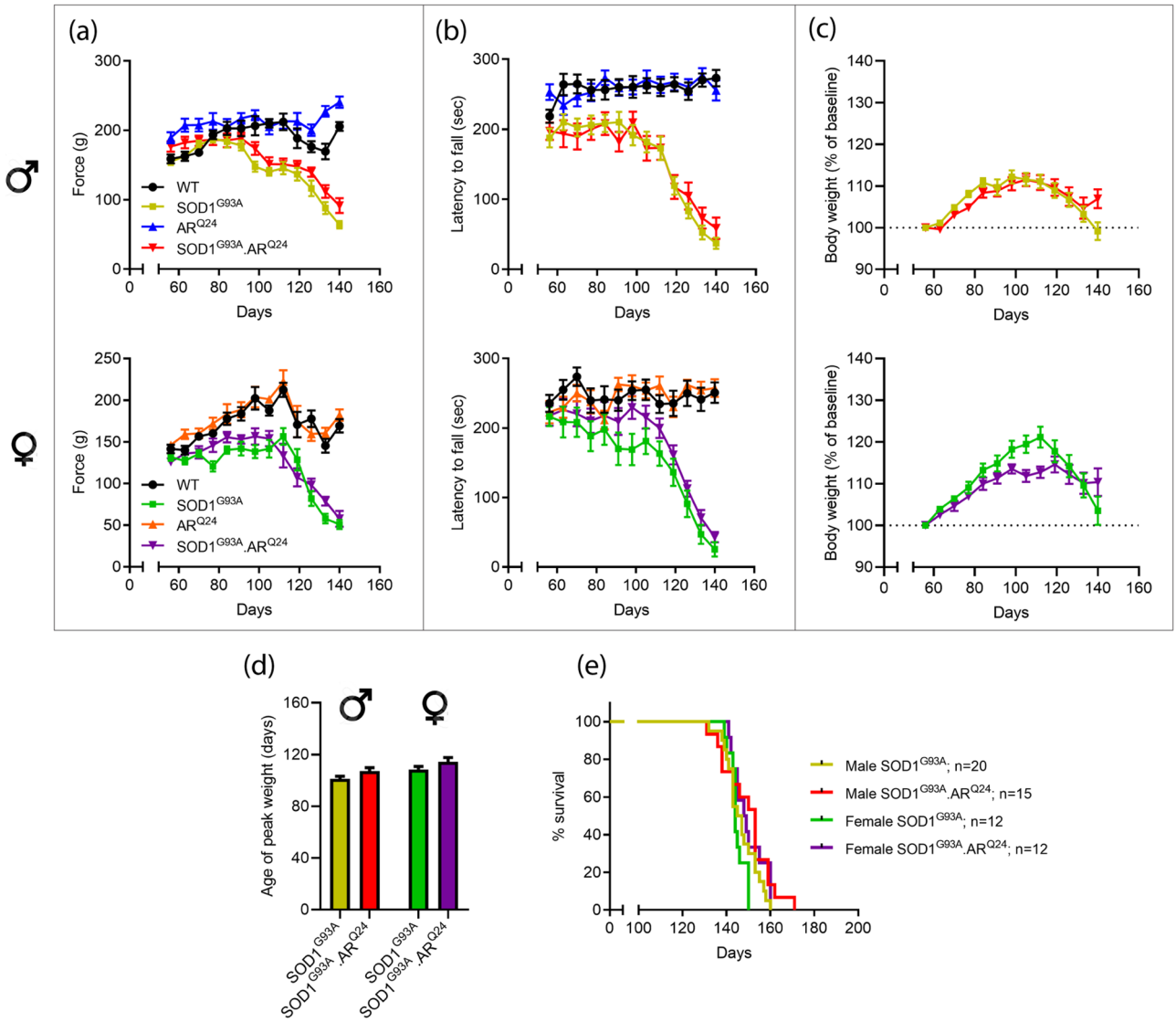

Figure 4. Global overexpression of AR does not influence disease progression and survival in SOD1^{G93A} mice. Motor function assessment by **(a)** four limb grip strength and **(b)** rotarod performance and **(c)** body weight analysis of AR^{Q24} x SOD1^{G93A} cross male and female mice over disease course. **(d)** Age in weeks when peak weight occurred in males and female. **(e)** Kaplan–Meier curves showing comparable survival in SOD1^{G93A}:AR^{Q24} mice compared to SOD1^{G93A} mice. All values presented as mean ± SEM; n = 12–20 mice per group.

evaluated in SOD1^{G93A} mice. SOD1^{G93A} mice were crossed with AR^{Q24} mice, giving rise to WT, SOD1^{G93A}, AR^{Q24} and SOD1^{G93A}:AR^{Q24} genotypes. Muscle strength showed comparable decline in SOD1^{G93A} and SOD1^{G93A}:AR^{Q24} mice with consistent performance maintained in aged-matched non-disease counterparts, AR^{Q24} and WT mice (Fig. 4a). In SOD1^{G93A} male mice, the onset of decline in grip strength was 89 ± 9 days compared to 103 ± 12 days in female mice (P = 0.0006 by unpaired t-test, Fig S4a). AR overexpression did not have a significant effect on the onset of decline in grip strength in SOD1^{G93A} mice, with onset occurring at 95 ± 10 days and 102 ± 11 days in SOD1^{G93A}:AR^{Q24} male and female mice, respectively. Similar trends were observed in locomotor performance (Fig. 4b) with the onset of decline in function occurring at 102 ± 10 days compared to 110 ± 7 days in male and female SOD1^{G93A} mice, respectively (P = 0.0221 by unpaired t-test, Fig S4b). Again, AR overexpression did not have an effect on disease onset determined by locomotor performance, occurring at 107 ± 9 days and 106 ± 9 days in SOD1^{G93A}:AR^{Q24} male and female mice, respectively. Comparable weight declines were apparent between SOD1^{G93A} and SOD1^{G93A}:AR^{Q24} genotypes (Fig. 4c). Age of peak body weight showed a significant effect of sex ($F_{(1,56)} = 7.82$; $P = 0.0071$) and genotype ($F_{(1,56)} = 5.24$; $P = 0.0258$) on disease onset when analysed by two-way ANOVA (Fig. 4d). Multiple comparisons did not reveal significant intergroup differences. Separate analysis of male vs. female SOD1^{G93A} mice again revealed males had a significantly earlier disease onset compared to female mice (P = 0.0271 by unpaired t-test, Fig S4c), showing a consistent trend across multiple methods of determining disease onset in SOD1^{G93A} mice. The median lifespan of male SOD1^{G93A} mice (146 days) was comparable to SOD1^{G93A}:AR^{Q24} mice (153 days) ($P = 0.1494$). Likewise, in females, no survival differences were apparent, with median survival of 144 vs. 149 days for SOD1^{G93A} and SOD1^{G93A}:AR^{Q24} mice, respectively ($P = 0.0810$; Fig. 4e).

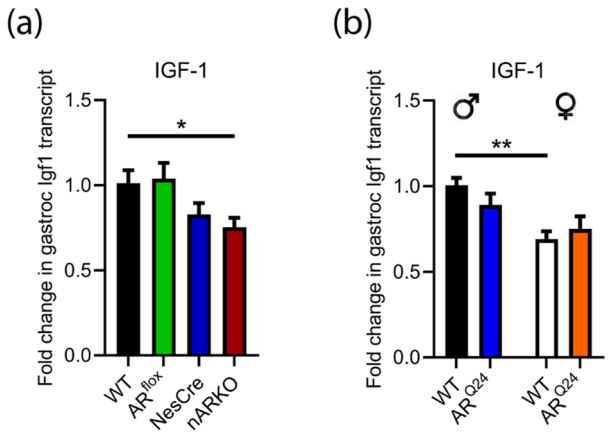

Figure 5. AR expression levels do not drive an alteration in skeletal muscle IGF-1 transcript. **(a)** IGF-1 transcript levels in gastrocnemius muscle of AR^{flox} x NesCre male mice at 2 months age. Data represents mean ± SEM, n = 5 mice per group. *P < 0.05 by one-way ANOVA with Dunnett's multiple comparison test comparing all genotypes to WT. **(b)** IGF-1 transcript levels in gastrocnemius muscle of male and female AR^{Q24} mice compared to WT at 3 months age. Data represents mean ± SEM, n = 6 mice per group. **P < 0.01 by two-way ANOVA with Sidak's multiple comparisons test comparing sex effect.

Changes in AR expression do not drive an alteration in skeletal muscle IGF-1 transcript. Insulin-like growth factor 1 (IGF-1) is a known transcriptional target of skeletal muscle AR[32] and mediates local trophic effects[33] and neuroprotective actions in motor neurons[34]. IGF-1 expression in muscle was not altered in AR^{flox} mice, whereas it appears to be downregulated in the NesCre mice by 17% compared to WT (Fig. 5a). While nARKO mice were significantly downregulated by 25% compared to WT males, there is no difference when compared to NesCre controls (Fig. 5a). Interestingly, there was no effect of overexpressing AR on muscle IGF-1 expression (Fig. 5b). A sex effect is observed ($F_{(1,56)} = 5.24$; $P = 0.0258$) with female WT mice showing a 30% reduction in IGF-1 transcript compared to WT males, indicating that androgen levels rather than AR levels, dictate regulation of IGF-1.

Discussion

We have explored the impact of genetic manipulation of AR on motor performance, growth and survival in healthy and diseased mice. To selectively delete AR within the CNS, we crossed the floxed AR mouse with the NesCre mouse which expresses Cre-recombinase in neural progenitor cells. Neural AR deletion did not show significant impacts upon disease progression and survival of $SOD1^{G93A}$ transgenic mice compared to NesCre controls. The introduction of the NesCre transgene to $SOD1^{G93A}$ mice profoundly increased survival by 16 days, compared to those carrying the phenotypic benign AR^{flox} transgene. Overexpression of AR did not modify disease progression and survival in $SOD1^{G93A}$ male or female mice. However, both AR deletion and overexpression models negatively influenced the survival of non-diseased male mice with incomplete penetrance.

The widespread presence of AR and systemic testosterone action throughout the body make it difficult to isolate tissue-specific impacts of AR signalling. Deletion of AR from the CNS results in disruptions to the HPG axis regulating testosterone release, resulting in elevated circulating testosterone levels[25,35]. In a calcium/calmodulin-dependent protein kinase IIα (CaMKIIα)-iCre driven ARKO mouse, testosterone levels were increased 2-fold and seminal vesicle weight increased 4-fold[25]. In nARKO mice, 2 to 4-fold elevations in circulating testosterone have been reported[24,35], reflecting the ~ 2-fold increased seminal vesicle weight in our study. The NesCre driver line also reportedly has activity outside of the intended target, causing further potential confounds[36,37]. Therefore, the implications of altered AR signalling in the periphery of nARKO mice cannot be discounted. In gastrocnemius muscle, we report no net change to AR protein level in nARKO mice, despite a 30% reduction in AR transcript level. This could be due to altered local androgen levels affecting AR protein turnover[31]. In myocyte-specific KO mice, AR was not found to contribute to androgen-mediated hypertrophy in gastrocnemius or other limb muscles, although it negatively impacted muscle strength[38,39]. Conversely, we have previously reported that systemic administration of the AR competitive antagonist, flutamide, promoted muscle atrophy and enhanced disease onset, without altering survival in $SOD1^{G93A}$ male mice[20]. Interestingly, restricted overexpression of WT AR in muscle had a detrimental effect, with mice developing a neurodegenerative phenotype similar to SBMA models[40]. Our global overexpression model, which expresses human WT AR, decreased gastrocnemius muscle weight, mildly reduced body weight in non-disease males, and had no influence on disease progression in $SOD1^{G93A}$ mice. The reason for the discrepancies observed between these overexpressing models could be the different promotors used to drive transgene expression. In the skeletal muscle-specific model, AR^{Q22} expression was driven by α-actin which is far more abundant in muscle compared to β-actin[41], used to drive global AR expression in the current study. It is possible that the level of AR in muscle in the former model prompted a toxic gain of function. In models of SBMA it has been shown that expression of the polyglutamine expanded AR in muscle alone, is capable of driving neurological components of the disease. Males have an earlier disease

onset in both mouse models and clinical ALS, with denervation and muscle atrophy among the earliest pre-symptomatic pathologies of the disease[42]. Further exploration of the role of skeletal muscle AR in driving disease onset in ALS models is warranted.

The perturbation of AR signalling outside of the CNS in these models is likely responsible for the negative survival effects observed in non-disease models. This is especially relevant for the AR^{Q24} overexpression model where sudden death appeared to be the result of cardiac hypertrophy. The role of androgens in human cardiovascular disease is contradictory. The risk of cardiovascular disease is higher in males than females, which could indicate a negative impact of AR signalling. Likewise, androgens acting via AR impair recovery of cardiac function after ischemia–reperfusion injury[43] and promote chronic kidney disease[44]. Conversely, lower testosterone levels in ageing males correlates with greater cardiovascular disease mortality[45]. In global ARKO models, mice exhibit increased atherosclerosis, higher circulating cholesterol and increased development of cardiac fibrosis, as reviewed by Chang and colleagues[46]. In nARKO mice, we observed genetic deletion of AR within both kidney and heart tissue. This age-dependence and contradictory role of AR in cardiovascular disease is reflected in our survival data in AR genetic models. Deaths in nARKO mice, typically occurred beyond 5 months of age; in AR^{Q24} mice this occurred much earlier coinciding with rising circulating testosterone levels.

We have previously reported that AR is depleted in the lumbar spinal cords of male $SOD1^{G93A}$ mice[31]. In light of this finding, further abolishment of AR signalling, through AR deletion, may have limited impact on disease course and survival. We did observe a mild 6-day reduction in median survival of nARKO:$SOD1^{G93A}$ males, compared to NesCre:$SOD1^{G93A}$ males, although not significant. A higher prenatal testosterone exposure associates with ALS[9]. This contrasts to evidence that early postnatal testosterone administration is neuroprotective against cortical injury in adult rodents[47]. In NesCre mice, Cre-LoxP recombination is reported to have occurred throughout the CNS by E15.5[36]. This is prior to the first testosterone surge, occurring between E17-19 in rodents[48]. Therefore, we anticipate that the direct effects of early prenatal testosterone exposure on neurons is sufficiently abolished in nARKO:$SOD1^{G93A}$ mice and has minimal impact on adult disease course. The levels of testosterone in AR^{Q24} mice have not been reported. No change in testosterone levels were evident in a CMV-promoter driven AR overexpression model[49]. It therefore seems unlikely that dysregulation in testosterone production and reduced AR signalling is responsible for the lack of effect observed in the $SOD1^{G93A}$:AR^{Q24} model. Quantification of skeletal muscle IGF-1 transcript, a known AR transcriptional target, was not altered by AR overexpression. A lower level of the transcript was observed in female WT mice, implicating local androgens as driving transcript levels independent of AR level. This is supported by evidence that exogenous administration of DHT to male $SOD1^{G93A}$ mice, significantly upregulated IGF-1 transcript in tibialis anterior muscle[21].

In the current study we did not observe AR-mediated alteration in disease onset or outcome in $SOD1^{G93A}$ mice. While we cannot rule out that model limitations confounded the ability to detect an underlying role for AR, it is also possible that other factors are mediating the sex-specific differences in ALS. Estrogen receptors (ER) are abundantly expressed by motor neurons and all glial cell populations in the lumbar spinal cord of $SOD1^{G93A}$ mice[31]. Exogenous estradiol has potent anti-inflammatory actions and provides neuroprotection to motor neurons when administered to male $SOD1^{G93A}$ mice[50]. Exogenous progesterone, stimulated autophagy in the spinal cord of male $SOD1^{G93A}$ mice, delaying disease onset and extending survival[51]. Ovariectomy in female $SOD1^{G93A}$ mice did not impact disease onset, but accelerated disease progression[52]. Together, these studies present a strong case for estrogens and progesterone having multiple neuroprotective and disease modifying actions in $SOD1^{G93A}$ mice. Alternatively, it is possible that sex chromosome effects could be mediating sex differences in ALS, independently of gonadal hormones[53]. For example, in multiple sclerosis and autoimmune disease, differential methylation of the X-chromosome gene, Foxp3, has been identified in T lymphocytes; possibly resulting from X-chromosome imprinting[54,55]. In Parkinson's disease, the expression of Y chromosome gene, SRY, is upregulated and promotes nigrostriatal degeneration[56]. This may contribute to the male bias of the disease.

The NesCre mouse has been described as having a metabolic phenotype[37] caused by the ectopic expression of the human growth hormone gene in the hypothalamus[57]. This causes a decrease in growth hormone regulating hormone (GHRH) release by mouse hypothalamic neurosecretory neurons. In turn this leads to a 70–80% reduction in growth hormone (GH) release by the anterior pituitary[30]. Likewise, the pituitary hormones prolactin (PRLH) and thyroid stimulating hormone (TSH) were similarly decreased. GH is responsible for promoting growth, hence, the observed impairment in weight gain in the NesCre mice. GH operates to stimulate lipid and carbohydrate metabolism acting primarily on the adipose/fat tissue and liver. We have summarised the disrupted energy metabolism effects described for NesCre transgenic mice in Fig S5. Notably, a 50% reduction in liver IGF-1 transcript, a major target of GH action, was observed[57]. Most of these actions, including increased leptin production, increased insulin sensitivity and higher adiposity[58], act to promote energy storage. Additionally, the reduced TSH production by the pituitary and resulting thyroid hormone deficiency would be expected to contribute to a hypometabolic state[59] in the NesCre mouse.

Hypermetabolism, defined by increased resting energy expenditure, is a well described early phenomenon in ALS patients. It does not appear to correlate with age, sex or BMI[60], although clearly associates with poor prognosis[61]. Likewise, hypermetabolism is also an early pre-symptomatic feature of disease in $SOD1^{G93A}$ mice[62–65]. The mechanisms leading to hypermetabolism in the $SOD1^{G93A}$ mice appear to be highly complex and have only recently begun to be unravelled. A GH deficiency and decrease in IGF-1 signalling were evident in advanced symptomatic $SOD1^{G93A}$, reflecting clinical ALS[62]. Further studies revealed GH secretions fluctuate with disease course showing an elevation coinciding with onset of disease[65]. The authors suggested this to be a response to denervation, in an attempt to stimulate muscle repair through IGF-1 upregulation. We show decreased IGF-1 transcript in skeletal muscle of NesCre mice, therefore, this pathway unlikely presents the mechanism of neuroprotection when crossed with $SOD1^{G93A}$ mice. Skeletal muscle plays a major role in determining systemic metabolic rate[66] and seems a likely contributor to metabolic dysfunction in ALS. In $SOD1^{G93A}$ mice an increase in fatty acid oxidation occurs in muscle, reflecting a switch toward the used of lipids as a primary fuel source

in peripheral tissues[64,67]. In NesCre mice, increased lipid uptake and storage occurs and may counteract the dysregulation in energy source occurring in SOD1^{G93A} mice (Fig S5). This is supported by evidence of lifespan extension in SOD1^{G93A} mice when crossed with a transgenic harbouring a Dynein *Cra* mutation; the latter causing defective lipolysis and increased lipid stores[68]. The resulting double transgenic mice showed an increased adiposity and restoration in the use of carbohydrate energy sources. More recently, impaired glucose homeostasis was shown in symptomatic SOD1^{G93A} mice[69]. This was characterised by two major defects: increased glucose uptake, independent of altered insulin sensitivity; and impaired glucagon signalling, the pancreatic hormone stimulating conversion of liver glycogen to glucose. NesCre mice have been shown to have dysregulated insulin and glucose sensitivity, presenting another potential mechanism to counter SOD1^{G93A} hypermetabolism.

In conclusion, we demonstrate here that genetic perturbations to AR levels in mice can have detrimental impacts on male mice, although, these do not exacerbate or alter the disease course in SOD1^{G93A} mice. Furthermore, AR manipulation alone may be insufficient to modulate disease with circulating and local tissue hormone levels likely to be the driving force behind sex differences in ALS. Finally, the altered metabolism in NesCre mice has inadvertently provided striking evidence that combating early hypermetabolism in SOD1^{G93A} is likely a key target in modulation of ALS progression.

Methods

Animals. All experiments on mice were conducted in accordance with the Australian National Health and Medical Research Council published Code of Practice and approved by the Florey Institute of Neuroscience and Mental Health Animal Ethics Committee (approval numbers 16-001-FINMH and 17-074-FINMH). The study was carried out in compliance with the ARRIVE guidelines. Transgenic SOD1^{G93A} mice (B6.Cg-Tg(SOD1*G93A)1Gur/J line; stock number 004435), AR^{flox} mice[26] (B6.129S1-Ar$^{tm2.1Reb}$/J line, stock number 018450) and Nestin-Cre (NesCre) mice[23] (B6.Cg-Tg(Nes-cre)1Kln/J line, stock number 003771) were purchased from the Jackson Laboratory (Bar Harbor, ME, USA) were maintained on a C57BL/6J background. Transgenic AR^{Q24} mice[29] (B6D2-Tg(CAG-AR*24Q)5-5Sobu; stock number RBRC00827) were purchased from RIKEN BioResource Centre and maintained on a B6D2 background.

To generate conditional neural ARKO mice, heterozygous female AR$^{fl/wt}$ mice were crossed with male NesCre$^{+/-}$ to generate four litter-matched male genotypes; non-transgenic WT, AR^{fl}, NesCre$^{+/-}$ and AR^{fl}:NesCre$^{+/-}$ (nARKO). To generate constitutive ARKO mice for negative control tissue, AR$^{fl/wt}$:NesCre$^{+/-}$ double heterozygous transgenic females were bred with male mice giving rise to AR null males (gARKO) through germline recombination, as previously described[70]. Given the high frequency of germline recombination in female AR$^{fl/wt}$:NesCre$^{+/-}$ breeders[70] it was not viable to pair with SOD1^{G93A} male breeders. Male SOD1^{G93A} mice were crossed with female NesCre$^{+/-}$ to generate male SOD1^{G93A}:NesCre$^{+/-}$ transgenic mice. Due to SOD1^{G93A} and NesCre transgenes being located on chromosome 12, in male SOD1^{G93A}:NesCre$^{+/-}$, these two transgenes were segregated during meiosis and not inherited together in F1 progeny. We acquired a unique transgenic male SOD1^{G93A}:NesCre$^{+/-}$ through chance breeding whereby the SOD1^{G93A} and NesCre$^{+/-}$ became linked to chromosome 12 through homologous recombination. These mice were crossed with AR$^{fl/wt}$ heterozygous females to produce AR^{wt}:NesCre$^{+/-}$:SOD1^{G93A} (NesCre:SOD1^{G93A}) and AR^{fl}: NesCre$^{+/-}$:SOD1^{G93A} triple transgenic male (nARKO:SOD1^{G93A}) littermates. A parallel breeding strategy was set up where SOD1^{G93A} mice were crossed with AR$^{fl/wt}$ heterozygous females to generate AR^{fl}:SOD1^{G93A} males (AR^{flox}:SOD1^{G93A}).

To generate AR overexpressing SOD1^{G93A} mice, female AR^{Q24} heterozygous mice were crossed with male SOD1^{G93A} to generate four litter-matched male genotypes; non-transgenic WT, SOD1^{G93A}, AR^{Q24} and SOD1^{G93A}:AR^{Q24}. The mice were a mixed isogenic F1 background.

Animals were group-housed under standard 12 h light–dark conditions with access to standard rodent chow and water. At 2, 3 or 6 months of age, animals were killed by lethal dose of sodium pentobarbitone (100 mg/kg, i.p.) and organs collected, weighed and snap frozen in dry-ice. For immunohistochemistry, mice were cardiac perfused with 0.1 M PBS followed by 4% paraformaldehyde, sucrose cryoprotected and snap freezing in isopentane as previously described[31].

RT-qPCR. Spinal cord and gastrocnemius muscle were prepared and RNA extractions performed as previously described[20,31]. Brain, liver, kidney, gastrocnemius and heart tissue from NesCre and nARKO mice were mechanically pulverised using liquid nitrogen prior to processing for DNA, RNA and protein extraction. Genomic DNA (gDNA) was extracted from tissue samples overnight using PureLink Genomic DNA Mini Kit (Invitrogen) according to manufacturer's protocol. Primer sequences for gDNA were: *Ar^{ex1}* forward 5′- AAG CAG GTA GCT CTG GGA CA -3′, *Ar^{ex1}* reverse 5′- GAG CCA GCG GAA AGT TGT AG -3′; and internal control *DAG1* forward 5′- CCA AGG AGC AGA TCA TAG GGC -3′, *DAG1* reverse 5′- AGA GCA TTG GAG AAG GCA GG -3′. For RNA extraction tissue was homogenised in QIAzol Lysis Reagent (Qiagen, Cat# 79306) using the TissueLyserLT (Qiagen) for 5 min at 50 Hz and RNA containing phase isolated using chloroform prior to further purification using RNeasy Mini Kit following manufacturer's protocol. Primer sequences for RNA were: *Ar* forward 5′- GTG AAA TGG GAC CTT GGA TG -3′, *Ar* reverse 5′- GCC AGA AGC TTC ATC TCC AC -3′; *Igf1* forward 5′- TGG ATG CTC TTC AGT TCG TG -3′, *Igf1* reverse 5′- GCA ACA CTC ATC CAC AAT GC -3′; and internal control *Hprt1* forward 5′- GAT CAG TCA ACG GGG GAC AT -3′, *Hprt1* reverse 5′- CAT TTT GGG GCT GTA CTG CTT -3′. RT-qPCR was performed as previously described[20] and samples analysed in triplicate with Ct values normalized to the housekeeping gene. Fold change between WT control and transgenic groups was determined using the $2^{-\Delta\Delta Ct}$ method.

Western blotting. Spinal cord and gastrocnemius muscle were prepared and protein extractions performed as previously described[20,31]. Brain, liver, kidney and heart tissue was homogenised by sonication (50% ampli-

tude pulses applied over 10–15 s) in ice-cold RIPA buffer (50 mM Tris–Cl, pH 7.4, 150 mM NaCl, 0.1% SDS, 1% sodium deoxycholate and 1% Triton-X 100) containing protease and phosphatase inhibitor cocktail tablets. Protein lysates were denatured and electrophoresed through 4–15% Criterion TGX Stain-Free gels (Bio-Rad Laboratories, NSW, Australia) or 4–20% Mini-PROTEAN TGX Stain-Free gels (for brain, liver, kidney and heart supernatants) and transferred onto PVDF membrane using a Trans-Blot Turbo Transfer System (Bio-Rad) as previously described[20,31]. Blots were probed overnight at 4 °C with rabbit primary antibody against AR (1:1000, Abcam, cat# ab133273, RRID:AB_11156085) in SignalBoost Immunoreaction Enhancer (Merck Millipore, Cat# 407207) followed by 1 h room temperature incubation with StarBright Blue 700 goat anti-rabbit secondary antibody (1:5000, Bio-Rad, Cat# 12004161, RRID:AB_2721073). For analysis, background adjusted AR band intensity was normalised to total lane protein intensity using Image Lab 6.0 software (Bio-Rad, www.bio-rad.com/en-au/product/image-lab-software, RRID:SCR_014210). Average group values were then expressed fold relative to averaged WT control group values (expressed as 1.0).

Immunohistochemistry. Lumbar spinal cord was cryosectioned at 20 µm and slide mounted onto poly-L-lysine coated glass slides. Citrate antigen retrieval was performed as previously described[31]. For fluorescent detection immunostaining was performed as previously described[31] with the following primary antibodies: rabbit anti-AR (1:200, Abcam, Cat# ab133273) and goat anti-ChAT (1:200, Millipore, Cat# AB144P, RRID:AB_2079751). The following secondary antibodies were incubated for 2 h at room temperature; donkey biotinylated-anti-rabbit (1:200, Jackson ImmunoResearch Cat# 711-065-152, RRID:AB_2340593), streptavidin Alexa Fluor-488 (1:200, Jackson ImmunoResearch Cat# 016-540-084, RRID:AB_2337249) and anti-goat DyLight-550 (1:200, Thermo Fisher Scientific Cat# SA5-10087, RRID:AB_2556667). Hoechst 33342 (Invitrogen) DNA stain was incubated for 15 min at 1 µg/ml. All images were captured on a Zeiss AxioObserver Z1 (Carl Zeiss Pty Ltd, North Ryde, Australia). For chromogenic DAB detection, sections were blocked for 15 min in 0.5% hydrogen peroxide in PBS and 1 h at room temperature in animal-free blocking reagent (Cell Signalling Technology, Cat# 15019). Rabbit anti-AR (as described above) was incubated at 4 °C for 48 h in SignalStain antibody diluent (Cell Signaling Technology, Cat# 8112). SignalStain Boost IHC Detection Reagent (HRP, rabbit) (Cell Signaling Technology, Cat# 8114) was used as secondary detection and DAB colorimetric reaction performed using SignalStain DAB Substrate Kit (Cell Signaling Technology, Cat# 8059). Images were acquired on a Leica DMLB2 microscope.

Behavioural analyses and survival assessment. For aging of AR^{flox} x NesCre mouse cohorts (n = 12–19 from 2 months age onwards), animals were weighed fortnightly until 24 months of age. Mice reaching endpoint criterion included decline in physical condition and/or progressive non-recoverable weight loss amounting to 20% of peak weight. The survival of male AR^{Q24} mice was determined across a cohort of 62 mice to age 150 days. In $SOD1^{G93A}$ mouse survival studies mice were weighed once weekly and assessed for motor function. Locomotion was assessed using an accelerating rotarod (Rota-Rod 47600, Ugo Basile, Italy) as previously reported[20]. Muscular strength was assessed using a grip strength meter (BIO-G53, Bioseb, US). Mice were suspended by the tail and lowered onto a slanted metal grid until all four paws briefly made contact. Mice were then pulled from the mesh grid in parallel to the attached force transducer in a rapid, smooth and continuous motion. Force was measured in grams and an average of five successive pulls was reported for each mouse. The appearance of disease onset was determined retrospectively using the age of maximal body weight. Clinical endpoint for survival was defined as onset of paralysis in the hindlimbs and/or a cumulative loss of 20% peak body weight. In the AR^{flox} x NesCre x $SOD1^{G93A}$ cohort, n = 9–13 mice per group reached clinical endpoint and were included in the dataset. Once mouse from nARKO group died at 108 days prior to any symptom onset and was included as a censored value. In the AR^{Q24} x $SOD1^{G93A}$ cohort group sizes included in survival data analysis were n = 20 male $SOD1^{G93A}$, n = 15 male $SOD1^{G93A}$:AR^{Q24}, n = 12 female $SOD1^{G93A}$ and n = 12 female $SOD1^{G93A}$:AR^{Q24}.

Data analyses and statistics. Transcript, western blot, tissue weight and peak body weight data from AR^{flox} x NesCre cross mice were analysed by one-way ANOVA with Dunnett's multiple comparison comparing each genotype against WT. Western blot and peak body weight data from AR^{Q24} mice were analysed by two-way ANOVA with Sidak's multiple comparison test for sex and genotype effects where F-value indicated a significant effect ($P < 0.05$). Cumulative body weight gain plots were analysed by either mixed-effects analysis (for 24 month aged mice) or two-way ANOVA with repeated measures and Tukey's multiple comparison test for main genotype effect. Survival data was analysed by Log-rank (Mantel-Cox) test. All other single genotype comparisons were performed using two-tailed Student's t-test. Statistical analysis were performed using GraphPad Prism 8.3 (San Diego, CA, USA) and data presented as mean ± SEM unless otherwise stated.

Received: 10 December 2020; Accepted: 30 March 2021
Published online: 29 April 2021

References

1. Taylor, J. P., Brown, R. H. Jr. & Cleveland, D. W. Decoding ALS: From genes to mechanism. *Nature* **539**, 197–206 (2016).
2. McCombe, P. A. & Henderson, R. D. Effects of gender in amyotrophic lateral sclerosis. *Gend. Med.* **7**, 557–570 (2010).
3. Rooney, J. *et al.* C9orf72 expansion differentially affects males with spinal onset amyotrophic lateral sclerosis. *J. Neurol. Neurosurg. Psychiatry* **88**, 281 (2017).

4. Trojsi, F. *et al.* Comparative analysis of C9orf72 and sporadic disease in a large multicenter ALS population: The effect of male sex on survival of C9orf72 positive patients. *Front. Neurosci.* **13**, 485 (2019).
5. Blecher, R. *et al.* Contact sports as a risk factor for amyotrophic lateral sclerosis: A systematic review. *Global Spine J.* **9**, 104–118 (2019).
6. Scarmeas, N., Shih, T., Stern, Y., Ottman, R. & Rowland, L. P. Premorbid weight, body mass, and varsity athletics in ALS. *Neurology* **59**, 773–775 (2002).
7. Visser, A. E. *et al.* Multicentre, cross-cultural, population-based, case-control study of physical activity as risk factor for amyotrophic lateral sclerosis. *J. Neurol. Neurosurg. Psychiatry* **89**, 797–803 (2018).
8. Beghi, E. Are professional soccer players at higher risk for ALS?. *Amyotroph. Lateral Scler. Frontotemp. Degener.* **14**, 501–506 (2013).
9. Vivekananda, U. *et al.* Low index-to-ring finger length ratio in sporadic ALS supports prenatally defined motor neuronal vulnerability. *J. Neurol. Neurosurg. Psychiatry* **82**, 635–637 (2011).
10. Manning, J. T., Morris, L. & Caswell, N. Endurance running and digit ratio (2D:4D): Implications for fetal testosterone effects on running speed and vascular health. *Am. J. Hum. Biol.* **19**, 416–421 (2007).
11. Giffin, N. A., Kennedy, R. M., Jones, M. E. & Barber, C. A. Varsity athletes have lower 2D:4D ratios than other university students. *J. Sports Sci.* **30**, 135–138 (2012).
12. Hardiman, O. *et al.* Amyotrophic lateral sclerosis. *Nat. Rev. Dis. Primers* **3**, 17071 (2017).
13. La Spada, A. R., Wilson, E. M., Lubahn, D. B., Harding, A. E. & Fischbeck, K. H. Androgen receptor gene mutations in X-linked spinal and bulbar muscular atrophy. *Nature* **352**, 77–79 (1991).
14. Pfohl, S. R., Halicek, M. T. & Mitchell, C. S. Characterization of the contribution of genetic background and gender to disease progression in the SOD1 G93A mouse model of amyotrophic lateral sclerosis: A meta-analysis. *J. Neuromuscul. Dis.* **2**, 137–150 (2015).
15. Hatzipetros, T. *et al.* C57BL/6J congenic Prp-TDP43A315T mice develop progressive neurodegeneration in the myenteric plexus of the colon without exhibiting key features of ALS. *Brain Res.* **1584**, 59–72 (2014).
16. Turner, B. J. & Talbot, K. Transgenics, toxicity and therapeutics in rodent models of mutant SOD1-mediated familial ALS. *Prog. Neurobiol.* **85**, 94–134 (2008).
17. Sheean, R. K. *et al.* Effect of thymic stimulation of CD4+ T cell expansion on disease onset and progression in mutant SOD1 mice. *J. Neuroinflamm.* **12**, 40 (2015).
18. Hayes-Punzo, A. *et al.* Gonadectomy and dehydroepiandrosterone (DHEA) do not modulate disease progression in the G93A mutant SOD1 rat model of amyotrophic lateral sclerosis. *Amyotroph. Lateral Scler.* **13**, 311–314 (2012).
19. Mostaghel, E. A. *et al.* Contribution of adrenal glands to intratumor androgens and growth of castration-resistant prostate cancer. *Clin. Cancer Res.* **25**, 426–439 (2019).
20. McLeod, V. M. *et al.* Androgen receptor antagonism accelerates disease onset in the SOD1(G93A) mouse model of amyotrophic lateral sclerosis. *Br. J. Pharmacol.* **176**, 2111–2130 (2019).
21. Yoo, Y. E. & Ko, C. P. Dihydrotestosterone ameliorates degeneration in muscle, axons and motoneurons and improves motor function in amyotrophic lateral sclerosis model mice. *PLoS ONE* **7**, e37258 (2012).
22. Aggarwal, T. *et al.* Androgens affect muscle, motor neuron, and survival in a mouse model of SOD1-related amyotrophic lateral sclerosis. *Neurobiol. Aging* **35**, 1929–1938 (2014).
23. Tronche, F. *et al.* Disruption of the glucocorticoid receptor gene in the nervous system results in reduced anxiety. *Nat. Genet.* **23**, 99–103 (1999).
24. Raskin, K. *et al.* Conditional inactivation of androgen receptor gene in the nervous system: Effects on male behavioral and neuroendocrine responses. *J. Neurosci.* **29**, 4461–4470 (2009).
25. Davey, R. A. *et al.* Androgen action via the androgen receptor in neurons within the brain positively regulates muscle mass in male mice. *Endocrinology* **158**, 3684–3695 (2017).
26. Chakraborty, P. *et al.* Androgen-dependent sertoli cell tight junction remodeling is mediated by multiple tight junction components. *Mol. Endocrinol.* **28**, 1055–1072 (2014).
27. Holdcraft, R. W. & Braun, R. E. Androgen receptor function is required in Sertoli cells for the terminal differentiation of haploid spermatids. *Development* **131**, 459–467 (2004).
28. MacLean, H. E. *et al.* A floxed allele of the androgen receptor gene causes hyperandrogenization in male mice. *Physiol. Genomics* **33**, 133–137 (2008).
29. Katsuno, M. *et al.* Testosterone reduction prevents phenotypic expression in a transgenic mouse model of spinal and bulbar muscular atrophy. *Neuron* **35**, 843–854 (2002).
30. Galichet, C., Lovell-Badge, R. & Rizzoti, K. Nestin-Cre mice are affected by hypopituitarism, which is not due to significant activity of the transgene in the pituitary gland. *PLoS ONE* **5**, e11443 (2010).
31. McLeod, V.M., *et al.* Dysregulation of steroid hormone receptors in motor neurons and glia associates with disease progression in ALS mice. *Endocrinology* **161**(2020).
32. Wu, Y. *et al.* Identification of androgen response elements in the insulin-like growth factor I upstream promoter. *Endocrinology* **148**, 2984–2993 (2007).
33. Yoshida, T. & Delafontaine, P. Mechanisms of IGF-1-mediated regulation of skeletal muscle hypertrophy and atrophy. *Cells* **9** (2020).
34. Kaspar, B. K., Llado, J., Sherkat, N., Rothstein, J. D. & Gage, F. H. Retrograde viral delivery of IGF-1 prolongs survival in a mouse ALS model. *Science* **301**, 839–842 (2003).
35. Juntti, S. A. *et al.* The androgen receptor governs the execution, but not programming, of male sexual and territorial behaviors. *Neuron* **66**, 260–272 (2010).
36. Dubois, N. C., Hofmann, D., Kaloulis, K., Bishop, J. M. & Trumpp, A. Nestin-Cre transgenic mouse line Nes-Cre1 mediates highly efficient Cre/loxP mediated recombination in the nervous system, kidney, and somite-derived tissues. *Genesis* **44**, 355–360 (2006).
37. Harno, E., Cottrell, E. C. & White, A. Metabolic pitfalls of CNS Cre-based technology. *Cell Metab.* **18**, 21–28 (2013).
38. Ophoff, J. *et al.* Androgen signaling in myocytes contributes to the maintenance of muscle mass and fiber type regulation but not to muscle strength or fatigue. *Endocrinology* **150**, 3558–3566 (2009).
39. Chambon, C. *et al.* Myocytic androgen receptor controls the strength but not the mass of limb muscles. *Proc. Natl. Acad. Sci. U S A* **107**, 14327–14332 (2010).
40. Monks, D. A. *et al.* Overexpression of wild-type androgen receptor in muscle recapitulates polyglutamine disease. *Proc. Natl. Acad. Sci. U S A* **104**, 18259–18264 (2007).
41. Kee, A. J., Gunning, P. W. & Hardeman, E. C. Diverse roles of the actin cytoskeleton in striated muscle. *J. Muscle Res. Cell Motil.* **30**, 187–197 (2009).
42. Dupuis, L. & Loeffler, J. P. Neuromuscular junction destruction during amyotrophic lateral sclerosis: insights from transgenic models. *Curr. Opin. Pharmacol.* **9**, 341–346 (2009).
43. Wang, M. *et al.* Both endogenous and exogenous testosterone decrease myocardial STAT3 activation and SOCS3 expression after acute ischemia and reperfusion. *Surgery* **146**, 138–144 (2009).
44. Verzola, D. *et al.* Androgen-mediated apoptosis of kidney tubule cells: role of c-Jun amino terminal kinase. *Biochem. Biophys. Res. Commun.* **387**, 531–536 (2009).

45. Yeap, B.B., Dwivedi, G., Chih, H.J. & Reid, C. Androgens and cardiovascular disease in men. In *Endotext* (eds. Feingold, K.R., *et al.*) (South Dartmouth, 2000).
46. Chang, C., Yeh, S., Lee, S. O. & Chang, T. M. Androgen receptor (AR) pathophysiological roles in androgen-related diseases in skin, bone/muscle, metabolic syndrome and neuron/immune systems: Lessons learned from mice lacking AR in specific cells. *Nucl. Recept. Signal* **11**, e001 (2013).
47. Forgie, M. L. & Kolb, B. Manipulation of gonadal hormones in neonatal rats alters the morphological response of cortical neurons to brain injury in adulthood. *Behav. Neurosci.* **117**, 257–262 (2003).
48. Weisz, J. & Ward, I. L. Plasma testosterone and progesterone titers of pregnant rats, their male and female fetuses, and neonatal offspring. *Endocrinology* **106**, 306–316 (1980).
49. Swift-Gallant, A., Coome, L. A., Ramzan, F. & Monks, D. A. Nonneural androgen receptors affect sexual differentiation of brain and behavior. *Endocrinology* **157**, 788–798 (2016).
50. Heitzer, M. *et al.* Administration of 17beta-estradiol improves motoneuron survival and down-regulates inflammasome activation in male SOD1(G93A) ALS mice. *Mol. Neurobiol.* **54**, 8429–8443 (2017).
51. Kim, J., Kim, T. Y., Cho, K. S., Kim, H. N. & Koh, J. Y. Autophagy activation and neuroprotection by progesterone in the G93A-SOD1 transgenic mouse model of amyotrophic lateral sclerosis. *Neurobiol. Dis.* **59**, 80–85 (2013).
52. Groeneveld, G. J. *et al.* Ovariectomy and 17beta-estradiol modulate disease progression of a mouse model of ALS. *Brain Res.* **1021**, 128–131 (2004).
53. Snell, D. M. & Turner, J. M. A. Sex chromosome effects on male-female differences in mammals. *Curr. Biol.* **28**, R1313–R1324 (2018).
54. Voskuhl, R. R., Sawalha, A. H. & Itoh, Y. Sex chromosome contributions to sex differences in multiple sclerosis susceptibility and progression. *Mult. Scler.* **24**, 22–31 (2018).
55. Golden, L.C., *et al.* Parent-of-origin differences in DNA methylation of X chromosome genes in T lymphocytes. *Proc. Natl. Acad. Sci. U S A* (2019).
56. Lee, J. *et al.* Sex-specific neuroprotection by inhibition of the Y-chromosome gene, SRY, in experimental Parkinson's disease. *Proc. Natl. Acad. Sci. U S A* **116**, 16577–16582 (2019).
57. Declercq, J. *et al.* Metabolic and behavioural phenotypes in nestin-cre mice are caused by hypothalamic expression of human growth hormone. *PLoS ONE* **10**, e0135502 (2015).
58. Briancon, N., McNay, D. E., Maratos-Flier, E. & Flier, J. S. Combined neural inactivation of suppressor of cytokine signaling-3 and protein-tyrosine phosphatase-1B reveals additive, synergistic, and factor-specific roles in the regulation of body energy balance. *Diabetes* **59**, 3074–3084 (2010).
59. Mullur, R., Liu, Y. Y. & Brent, G. A. Thyroid hormone regulation of metabolism. *Physiol. Rev.* **94**, 355–382 (2014).
60. Bouteloup, C. *et al.* Hypermetabolism in ALS patients: an early and persistent phenomenon. *J. Neurol.* **256**, 1236–1242 (2009).
61. Steyn, F. J. *et al.* Hypermetabolism in ALS is associated with greater functional decline and shorter survival. *J. Neurol. Neurosurg. Psychiatry* **89**, 1016–1023 (2018).
62. Steyn, F. J. *et al.* Impairments to the GH-IGF-I axis in hSOD1G93A mice give insight into possible mechanisms of GH dysregulation in patients with amyotrophic lateral sclerosis. *Endocrinology* **153**, 3735–3746 (2012).
63. Pharaoh, G. *et al.* Metabolic and stress response changes precede disease onset in the spinal cord of mutant SOD1 ALS mice. *Front. Neurosci.* **13**, 487 (2019).
64. Scaricamazza, S., *et al.* Skeletal-muscle metabolic reprogramming in ALS-SOD1(G93A) mice predates disease onset and is a promising therapeutic target. *iScience* **23**, 101087 (2020).
65. Steyn, F. J. *et al.* Growth hormone secretion is correlated with neuromuscular innervation rather than motor neuron number in early-symptomatic male amyotrophic lateral sclerosis mice. *Endocrinology* **154**, 4695–4706 (2013).
66. Zurlo, F., Larson, K., Bogardus, C. & Ravussin, E. Skeletal muscle metabolism is a major determinant of resting energy expenditure. *J. Clin. Invest.* **86**, 1423–1427 (1990).
67. Fergani, A. *et al.* Increased peripheral lipid clearance in an animal model of amyotrophic lateral sclerosis. *J. Lipid Res.* **48**, 1571–1580 (2007).
68. Fergani, A. *et al.* A mutation in the dynein heavy chain gene compensates for energy deficit of mutant SOD1 mice and increases potentially neuroprotective IGF-1. *Mol. Neurodegener.* **6**, 26 (2011).
69. McDonald, T.S., Kumar, V., Fung, J.N., Woodruff, T.M. & Lee, J.D. Glucose clearance and uptake is increased in the SOD1_{G93A} mouse model of amyotrophic lateral sclerosis through an insulin-independent mechanism. bioRxiv:2020.2008.2002.233411 (2020).
70. McLeod, V.M., Cuic, B., Chiam, M.D.F., Lau, C.L. & Turner, B.J. Exploring germline recombination in Nestin-Cre transgenic mice using floxed androgen receptor. *Genesis*, e23390 (2020).

Author contributions

D.T. and V.M. coordinated and performed experiments and analysed data. V.M. wrote the manuscript. M.C. and N.W. assisted in experiments and analysis. W.B. and B.T. provided supervision and BT conceived the study idea. All authors contributed to and approved the final manuscript.

Funding

Funding for this project was provided by the Australian NHMRC (Project Grants 1104295, 1104299), Stafford Fox Medical Research Foundation, MND Research Institute of Australia (Ted Dimmick Memorial MND Research Grant). VM was supported by a MND Research Institute of Australia PhD Scholarship Top-Up Grant, BT was supported by an NHMRC-ARC Dementia Research Leadership Fellowship (1137024).

Competing interests

The authors declare no competing interests.

Additional information

Supplementary Information The online version contains supplementary material available at https://doi.org/10.1038/s41598-021-88415-0.

Correspondence and requests for materials should be addressed to B.J.T.

Reprints and permissions information is available at www.nature.com/reprints.

Publisher's note Springer Nature remains neutral with regard to jurisdictional claims in published maps and institutional affiliations.

Supplementary Material

Dissociation of disease onset, progression and sex differences from androgen receptor levels in a mouse model of amyotrophic lateral sclerosis

Doris Tomas[1], Victoria M. McLeod[1], Mathew D.F. Chiam[1], Nayomi Wanniarachchillage[1], Wah C. Boon[1], Bradley J. Turner[1,*]

[1]*Florey Institute of Neuroscience and Mental Health, University of Melbourne, Parkville, VIC 3052, Australia.*

Table S1. Tissue weights of AR^{flox}:NesCre transgenic mice

	WT	AR^{flox}	NesCre	nARKO	gARKO
2 months old	(g)	(g)	(g)	(g)	(g)
Liver	1.13 ± 0.20	1.08 ± 0.21	1.03 ± 0.20	1.01 ± 0.17	1.04 ± 0.07
Kidney	0.338 ± 0.030	0.347 ± 0.041	0.261 ± 0.039 **	0.265 ± 0.043 **	0.252 ± 0.021 ***
Heart	0.136 ± 0.017	0.131 ± 0.014	0.119 ± 0.010	0.117 ± 0.027	0.114 ± 0.011
Lung	0.145 ± 0.005	0.145 ± 0.007	0.129 ± 0.014	0.133 ± 0.020	0.156 ± 0.020
Spleen	0.077 ± 0.010	0.081 ± 0.014	0.061 ± 0.007	0.078 ± 0.014 ††	0.096 ± 0.004 * ††††
Pancreas	0.189 ± 0.048	0.195 ± 0.019	0.180 ± 0.029	0.158 ± 0.036	0.121 ± 0.011 **
Gastrocnemius	0.137 ± 0.007	0.134 ± 0.010	0.116 ± 0.010 *	0.105 ± 0.018 ****	0.111 ± 0.007 **
Thymus	0.047 ± 0.006	0.058 ± 0.008 *	0.050 ± 0.006	0.040 ± 0.006	0.086 ± 0.009 ****
Seminal Vesicles	0.143 ± 0.019	0.121 ± 0.044	0.119 ± 0.035	0.237 ± 0.053 *** †††	
Testis	0.176 ± 0.020	0.161 ± 0.021	0.159 ± 0.012	0.117 ± 0.009 **** †††	0.014 ± 0.003 **** ††††
Prostate	0.053 ± 0.007	0.045 ± 0.006	0.045 ± 0.012	0.061 ± 0.015	
6 months old					
Liver			1.34 ± 0.10	1.36 ± 0.15	
Kidney			0.327 ± 0.028	0.338 ± 0.053	
Heart			0.149 ± 0.011	0.162 ± 0.024	
Lung			0.163 ± 0.022	0.170 ± 0.015	
Spleen			0.072 ± 0.007	0.086 ± 0.010 ††	
Pancreas			0.166 ± 0.027	0.151 ± 0.032	
Gastrocnemius			0.147 ± 0.011	0.140 ± 0.007	
Thymus			0.059 ± 0.009	0.052 ± 0.016	
Seminal Vesicles			0.283 ± 0.046	0.731 ± 0.197 ††††	
Testis			0.187 ± 0.019	0.139 ± 0.013 ††††	
Prostate			0.081 ± 0.010	0.129 ± 0.048 †	
24 months old					
Heart	0.200 ± 0.049	0.174 ± 0.023	0.170 ± 0.019	0.143 ± 0.017	
Testis	0.180 ± 0.025	0.182 ± 025	0.180 ± 0.032	0.094 ± 0.019 *** †††	
Prostate	0.100 ± 0.016	0.099 ± 0.020	0.108 ± 0.016	0.681 ± 0.179 **** ††††	

Mean ± SD, n=4-8. * P<0.05, ** P<0.01, *** P<0.001, **** P<0.0001 compared to WT; † P<0.05, †† P<0.01, ††† P<0.001, †††† P<0.0001 compared to NesCre

Table S2. Tissue weights of AR^{Q24} transgenic mice

	WT male	AR^{Q24} male	WT female	AR^{Q24} female
3 months old	(g)	(g)	(g)	(g)
Liver	1.61 ± 0.16	1.63 ± 0.23	1.20 ± 0.14 **	1.20 ± 0.19
Kidney	0.565 ± 0.085	0.518 ± 0.080	0.311 ± 0.037 ****	0.346 ± 0.023
Heart	0.216 ± 0.028	0.218 ± 0.028	0.148 ± 0.020 ***	0.148 ± 0.016
Lung	0.204 ± 0.017	0.299 ± 0.157	0.168 ± 0.014	0.167 ± 0.042
Spleen	0.081 ± 0.019	0.084 ± 0.018	0.073 ± 0.011	0.086 ± 0.016
Pancreas	0.196 ± 0.038	0.170 ± 0.024	0.134 ± 0.025 **	0.167 ± 0.042
Gastrocnemius	0.161 ± 0.022	0.134 ± 0.008 **	0.118 ± 0.010 ****	0.125 ± 0.011
Thymus	0.041 ± 0.010	0.032 ± 0.007	0.056 ± 0.005 **	0.046 ± 0.008
Seminal Vesicles	0.294 ± 0.040	0.316 ± 0.058		
Testis	0.195 ± 0.038	0.205 ± 0.019		
Prostate	0.084 ± 0.023	0.090 ± 0.008		
Ovary			0.018 ± 0.002	0.027 ± 0.003 ###

Mean ± SD, n=6. ** P<0.01, *** P<0.001, ****P<0.0001 compared to WT male; ### P<0.001 compared to WT female

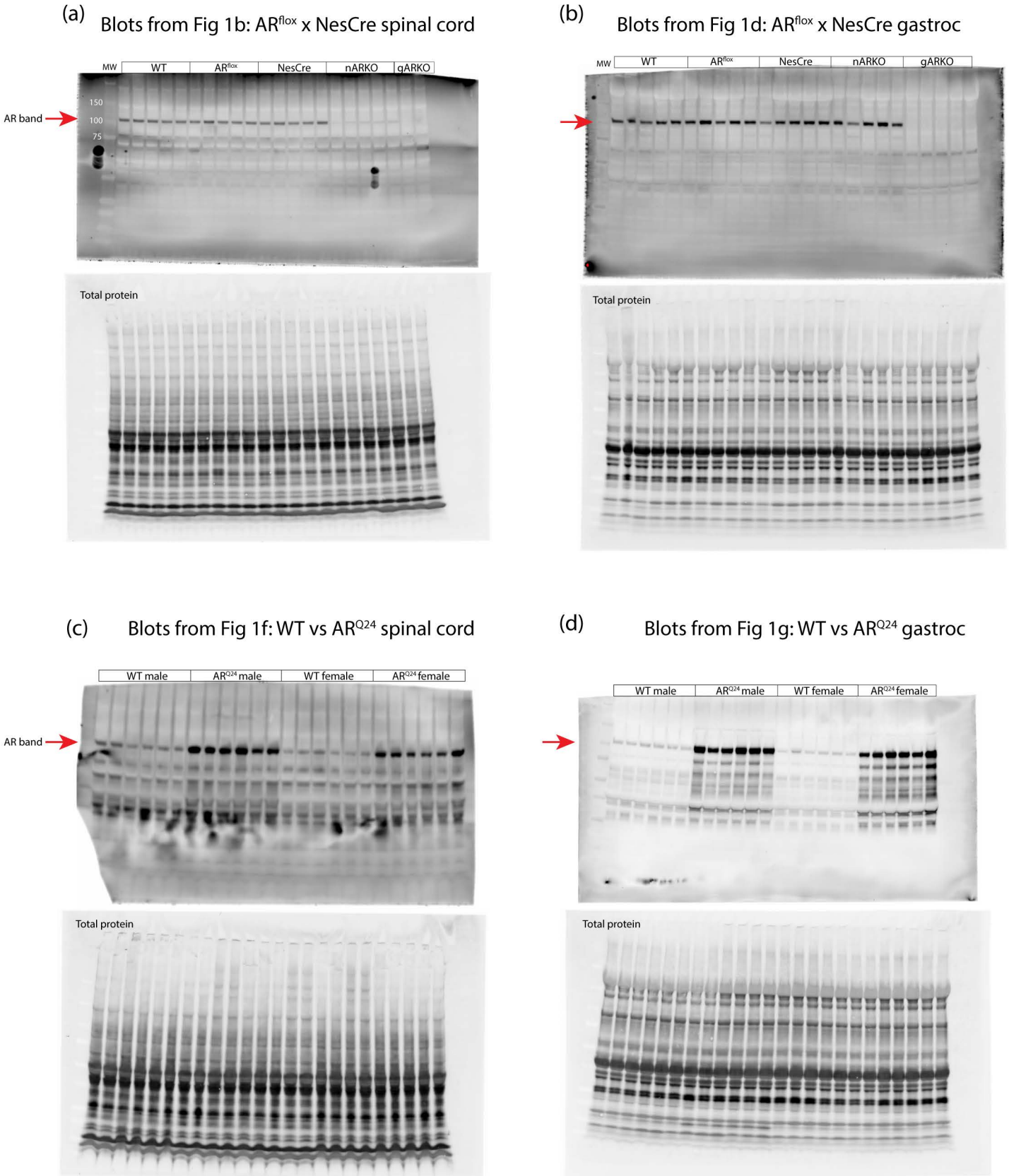

Figure S1. Western blots of spinal cord and gastrocnemius tissue AR (110 kDa) and total protein of data presentened in Figure 1. (a) AR in the spinal cord tissue and (b) gastrocnemius of progeny from AR^{flox} x NesCre crossed mice. (c) AR in the spinal cord and (d) gastrocnemius of overexpressing ARQ24 mice compared to their wildtype counterparts.

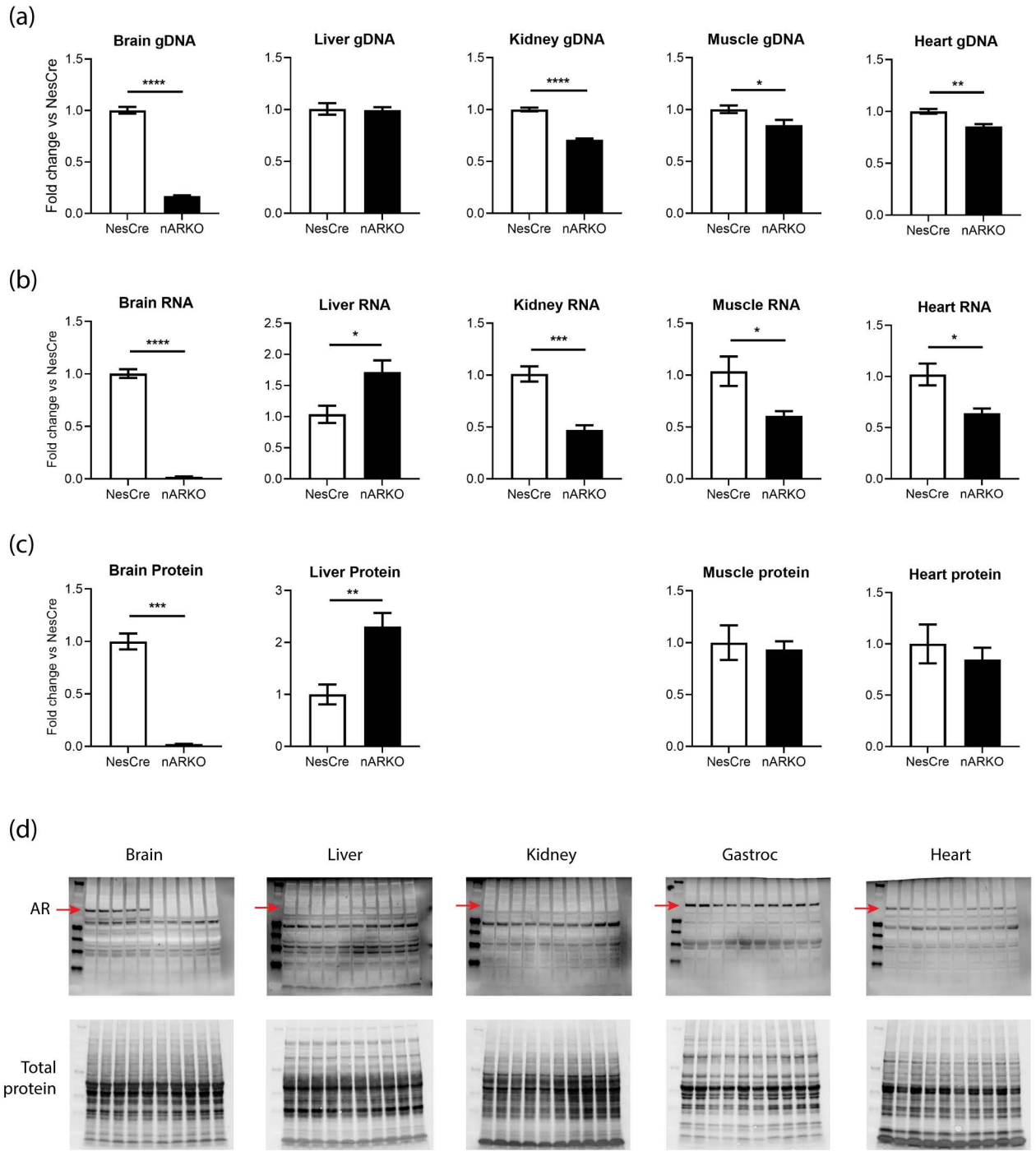

Figure S2. AR deletion in the neuronal ARKO mouse tissues compared to NesCre controls in 6 month old mice at the level of (a) genomic DNA, (b) RNA and (c) protein. (d) Western blots of AR (110 kDa) and total protein in tissues (note accurate levels of AR could not be detected in kidney tissue).

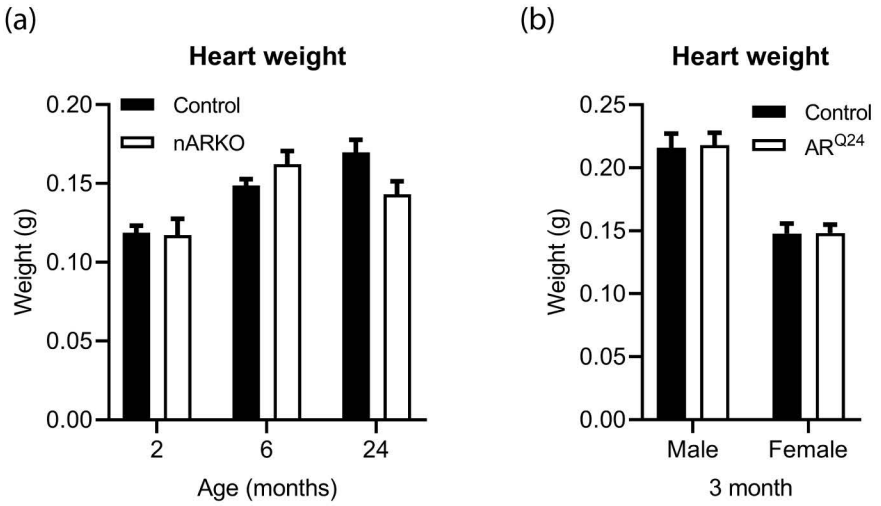

Figure S3. Heart weights of (a) nARKO males at 2, 6 and 24 months age compared to NesCre controls (n=4-8 mice per group) and male and female ARQ24 transgenic mice at 3 months compared to WT controls (n= 6-8 mice per group). Mean ± SEM.

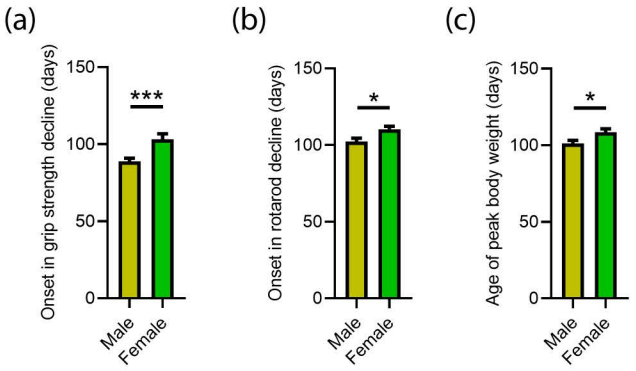

Figure S4. Comparison of disease onset between male and female SOD1^{G93A} mice measured by (a) decline in grip strength, (b) decline in locomotor performance and (c) age of peak body weight. Data represents mean ± SEM (n=≥12). * P<0.05, *** P<0.001 by unpaired t-test.

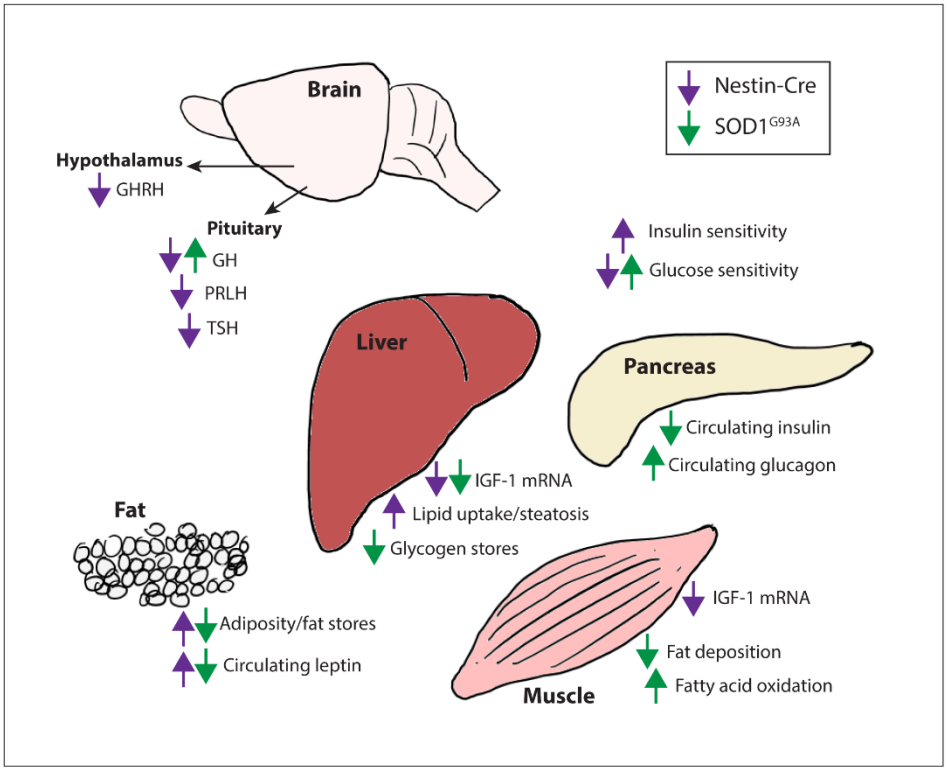

Figure S5. Central and peripheral changes contributing to the altered metabolic condition in Nestin-Cre and SOD1^{G93A} mice. Growth-hormone releasing hormone (GHRH), growth hormone (GH), prolactin releasing hormone (PRLH), thyroid stimulating hormone (TSH).

Chapter 7. General Discussion

7.1. SOD1^{G93A} males have reduced AR expression in spinal motor neurons

AR is present throughout the body, including the CNS, where it is abundant in neurons such as MNs. In Chapter 2, overall changes in AR were assessed at transcript, protein and cellular levels within the lumbar spinal cord of SOD1^{G93A} male and female mice over disease course. This was conducted in parallel with the other major sex steroid hormone receptors ERα, ERβ and PR, to provide for the first time a comprehensive characterisation of changes to steroid hormone systems in the SOD1^{G93A} mouse model. This study highlighted several major findings: 1) the abundance of ER in glial cell populations at comparable levels in male and female mice, supporting prior evidence that estrogens provide anti-inflammatory and immunomodulatory effects in neurodegeneration, including ALS [75, 236]; 2) AR was more abundant in male spinal cord, compared to females, and showed a disease-dependent reduction in protein levels within SOD1^{G93A} males. Together, these two findings support a mechanism by which sexual dimorphism may occur in SOD1^{G93A} mice. Males appear to exhibit a dual reduction in neurotrophic support, compared to females, through the combination of a) lower spinal cord E2 concentrations conferring limited ER-mediated signalling and b) a reduction in AR-induced signalling conferred by loss in AR protein and potentially local androgens.

AR is abundant throughout the spinal cord, with high intensity immunoreactivity in both the dorsal grey commissure and the dorsal horn [237]. It is also differentially expressed across MN populations within the CNS. Chapter 3 attempted to address these issues by focusing on characterising AR levels specifically within MNs which may be diluted upon examining whole tissue sections, such as lumbar spinal cord and bulk brain sections. A key finding in this chapter was that vulnerable spinal motor neurons innervating skeletal musculature, such as hindlimb and diaphragm, show a moderate level of AR in healthy male mice and this is extensively reduced in SOD1^{G93A}-mediated disease. Not only is AR lost from MNs with disease progression, but it appears to be an early event commencing prior to the loss of any motor neurons. Given that a downregulation in AR transcript did not accompany the decreased AR protein expression in male spinal cord, we rationalised that it is likely altered local androgen metabolism responsible for this loss in nuclear AR. Several lines of evidence support this theory. Firstly, we showed that in both endogenous AR expressing myocyte cell line and hESC-derived motor neurons, the application of non-aromatisable, DHT, increased AR protein levels, without altering AR transcript, through stabilisation of the protein through ligand-binding. This androgen-induced stabilisation has been previously described, and occurs independently of nuclear localisation, with more rapid ligand dissociation leading to AR degradation and translating to a loss in AR function *in vivo* [238]. With little evidence that circulating T levels are impaired in male SOD1^{G93A} mice, and AR protein levels maintained in both the testis and prostate, a more localised disease-specific dysregulation in androgen metabolism is feasible. Secondly, we showed that SRD5A2 transcript levels in the SOD1^{G93A} male spinal cord are decreased. Due to a lack of available antibodies, it was not possible to confirm 5α-R type II protein levels in the SOD1^{G93A} mouse or locality to MNs, however, a well-established body of evidence supports the notion that 5α-R type II has a high affinity for androgens and is predominantly expressed by ventral horn motor neurons and pyramidal neurons within the CNS [97, 239]. 5α-R type II expression is regulated by sterol regulatory element binding protein 2 (SREBP2) [240]. These proteins are transcription factors responsible for the regulation of sterol biosynthesis pathways and cholesterol

metabolism [241] and are upregulated in the absence of sterols. Cholesterol homeostasis is known to be dysregulated in the SOD1^{G93A} mouse and male ALS patients [242-245] and appears to be an early event prior to clinical symptom onset in rodent models. A reported increase in sterol presence within the spinal cords of SOD1^{G93A} mice [244], likely suppresses local SREBP activation and subsequent 5α-R type II production. This in turn would lead to a loss of T conversion to DHT particularly in the spinal motor neurons and pyramidal neurons comprising layer V motor cortex, reducing AR stability in these neurons.

In support of disrupted localised androgen metabolism in ALS, administration of exogenous DHT to male SOD1^{G93A} mice effectively extended survival through protection of muscle against atrophy, maintenance of NMJs and improved MN survival [82]. In a recent analysis of androgen levels in the CSF of ALS patients, free T was unchanged while DHT was lower than control patients [51]. However, the cause and consequence of CSF levels of DHT is unclear. The authors hypothesised a mechanism based on substrate deficiency – that a decrease in free T in the CNS occurs due to "testosterone resistance" of the blood-brain-barrier to T uptake in ALS. In turn, a reduction in the conversion of T to DHT in the CNS supposedly leads to disinhibition of HPG negative feedback loop at the anterior pituitary, resulting in elevated LH and T levels in ALS. This hypothesis has several flaws. Firstly, there is a lack of mechanistic evidence to support the theory. Secondly, it is largely based on outdated findings of steroid hormone profiling, superseded by more accurate bioassays [246, 247]. Thirdly, it is largely not supported by current clinical evidence of increased circulating T and LH levels in ALS patients [50, 248], as well as the study's own findings that free T levels in the CSF are unchanged. The conversion of T to DHT is a tightly regulated intracellular activity within specific androgen-responsive tissues and is considered largely independent of circulating DHT levels [249]. Circulating DHT levels do decrease following 5α-R inhibitor therapy due to a decreased leakage from the peripheral tissues [249]. Therefore, it could be expected that reduced CSF levels of DHT reflect reduced leakage from neural tissue as a result of enzyme deficiency, rather than substrate deficiency. This supports the findings of the current thesis where a reduction in 5α-R type II enzyme in male SOD1^{G93A} mice in disease affected tissues of the CNS, rather than a global enzyme deficiency.

AR in skeletal muscle targets is known to modulate androgen sensitivity of the innervating MNs [207, 208]. Chapter 4 sought to identify if decreased AR was confined to the CNS tissue or perhaps associates with MN targets. Like MNs, muscle cells in gastrocnemius also showed a loss of AR, in this case evident at both the transcript and protein levels. AR protein expression in the testis and prostate was maintained in SOD1^{G93A} male mice, and no evidence of reduced systemic T production as measured by total circulating plasma concentrations, as well as seminal vesicle weight, was reported in Chapter 1. Therefore, it appears that the loss in AR is confined to the motor unit, although a widespread assessment of other AR-expressing tissues was not explored in this thesis. The mechanism of the decreased AR levels in skeletal muscle is unknown. Muscle does not express 5α-R type II (confirmed by analysis conducted in the present studies) and utilises T as the primary source of androgen, most likely owing to its superior anabolic properties. AR transcript levels were also decreased in SOD1^{G93A} muscle and an increase in myonuclei void of AR protein were evident, pointing to a possible mechanism of impaired myogenesis and regeneration.

Future studies are required to investigate the mechanism behind the decreased AR described in Chapters 2-4 of this thesis. It would be valuable to confirm if there are localised changes in 5α-R type I and II enzymes within the spinal cord, particularly within the ventral horn MNs. RNAscope® technology would be of interest to compliment the current qPCR data on whole lumbar homogenates. The generation of sensitive monoclonal antibodies for these proteins would also overcome limitations in being able to localise changes in these enzymes at a protein level. While a preliminary screen of the major sex steroid hormones within whole spinal cord homogenates was conducted in chapter 2 of this thesis, mass spectrometry analysis of sterols and steroid hormone precursors in both the lumbar and skeletal muscle from SOD1^{G93A} mice would be of interest. These studies would shed some light on whether AR dysfunction in ALS, is a downstream consequence of disrupted sterol biosynthesis and metabolic pathways.

7.2. Role of AR in modulation of disease outcome in SOD1^{G93A} males

Systemic administration of the AR antagonist, flutamide, was conducted in Chapter 5 to address the shortcomings of castration models which ineffectively eliminate all androgen sources and alternative synthesis and pathways. The main outcome from this work was that AR inhibition had a significant impact on skeletal muscle pathology, exacerbating atrophy and disease onset in male SOD1^{G93A} mice, however this ultimately had no impact on the disease outcome. In line with other muscle targeted therapies in SOD1^{G93A} mice, without actions in preserving the neuromuscular junction, trophism on muscle alone is ineffective [250, 251]. In a study by Yoo and Ko [82], where chronically administering DHT to SOD1^{G93A} was protective in male mice, the authors claim the increase in IGF-1 in skeletal muscle as the mechanism of neuroprotection to motor neurons via retrograde transport. This certainly has merits given that viral IGF-1 therapy administered to muscle of SOD1^{G93A} mice is potent to survival extension [216], and findings from Chapter 4 indicating that IGF-1 transcript is decreased in both male SOD1^{G93A} and ARKO mouse gastrocnemius muscle. It is also reported in Chapter 4 that IGF-1 is increased in the spinal cord of symptomatic SOD1^{G93A} male mice and that chronic flutamide treatment had no effects of IGF-1 transcript levels in either the spinal cord or gastrocnemius muscle. It seems likely that local spinal cord sources of IGF-1 may be upregulated in response to disease progression. All neuronal and glial cells are capable of IGF-1 production [252] and IGF-1 immunoreactivity has been observed in astrocytes, Schwann cells, muscle fibres and MN soma and axons in ALS patients [253]. In SOD1^{G93A} mice, microglia are a known source of IGF-1 upregulation in the lumbar spinal cord [254]. In light of the contributions of data in this thesis; both AR and IGF-1 are downregulated in SOD1^{G93A} muscle, it supports the mechanism that DHT therapy targets the depleted muscle AR pool, stimulating local production of IGF-1 [255], which in turn is responsible for the elevated hypertrophy in muscle fibres [256]. With IGF-1 levels already elevated in SOD1^{G93A} cord, it seems less likely that muscle-derived IGF-1 delivery was the neuroprotective mechanism, but perhaps DHT is having a direct effect on MNs which are potentially deficient in DHT as a result of disease. To date, there is little direct evidence of robust IGF-1 regulation mediated by AR in MNs.

To more robustly determine if neural AR influences male disease course in chapter 6 a double transgenic mouse was created in which AR was deleted from neural progenitor cells in male SOD1^{G93A} mice. AR was deleted from

neurons and glial cells using the Nestin-Cre mouse line. An unfortunate consequence of this study was the undesired phenotype of the Nestin-Cre mouse having a more profound impact on SOD1^{G93A} survival which overshadowed the main aim of isolating an AR-driven influence on neural tissue. A clear trend is noticeable in male SOD1^{G93A} nARKO mice towards reduced survival, however, it is likely that the phenotype imparted by Nestin-Cre transgene is a more potent regulator of survival which could abolish in part some of the impact of AR deletion. Likewise, AR signalling is also involved in various metabolic functions [129, 257] and could overlap with Nestin-Cre effects, masking the phenotypic effects in the CNS. Future studies which would better address this issue could be to employ a Cre-driver line under a lower motor neuron promotor. Cre recombinase is expressed from P5 under control of the ChAT promotor [258] or alternatively at E9.5 under the motor neuron and pancreas homeobox 1 (MNX1) promotor [259]. Due to high MNX1 expression in the pancreas and other endocrine tissues, this may confound its use in exploring the role of AR in motor neurons. The ChAT cre driver line presents an attractive approach to robustly delete AR from the lower MNs in the SOD1^{G93A} mouse. This approach has been successfully used to delete EphA4 tyrosine kinase receptor from MNs in SOD1^{G93A} mice [260]. In addition, AR would not be deleted from neurons involved in the HPG regulatory control of testosterone production.

With the apparent decrease in AR observed centrally and peripherally in SOD1^{G93A} mice, Chapter 6 also explored the impact of systemic overexpression of human AR in an attempt to circumvent these observed losses. Increasing AR globally did not have an impact on disease onset or survival in male and female SOD1^{G93A} mice. One consideration is that the elevation in AR protein present did not translate to elevated AR signalling in desired tissues. The level of circulating or local androgens may be decreased in response to disturbances of AR in neurosecretory cells of the HPG feedback system. This would potentially diminish an increase to AR signalling through increased AR expression. Analysis of muscle IGF-1 levels between WT and AR^{Q24} mice, only showed a statistical difference between male and female WT mice, possibly indicating that hormone levels rather than receptor levels are critical in mediating disease modifying responses and sex differences. However, the detrimental impacts on the cardiovascular system in male AR^{Q24} mice, would argue that global AR signalling is increased. Several other considerations with this model could be: AR had opposing effects in different tissues which resulted in no net effect in altering SOD1^{G93A} disease course; or there is an optimal level of AR and androgens to induce positive effects and exceeding this could lead to detrimental side effects. As evidenced from an efficacy study in male SOD1^{G93A} mice, administering daily intraperitoneal progesterone at doses of 2 mg/kg, 4 mg/kg and 8 mg/kg; only the 4 mg/kg dose extended survival by 10 days, while the other doses were no different to vehicle [83]. To future understand these complexities, future studies could employ selective overexpression of AR to skeletal muscle or lower motor neurons. Additionally, dose-ranging studies exploring the optimisation of overexpression levels of AR, in conjunction with systemic androgens would be beneficial.

7.3. Exercise - the missing link?

Athleticism and physical exercise have long been associated with possible increased risk of ALS [261, 262]. Prenatal testosterone exposure links athletic ability and increased risk of developing ALS [52]. The hypertrophic actions of androgens on muscle usually requires interaction with exercise [263]. These findings raise the question about whether androgens and ALS may be associated via exercise prompting further evidence to be explored in this section. The impact of exercise in ALS has remained controversial and its effects may be differential depending on the type, intensity, duration and frequency of the engaged activity. This is certainly reflected in investigations in the $SOD1^{G93A}$ mouse. Mild to moderate daily exercise, such as forced treadmill running, was found to significantly extend survival in males only [264, 265], with one study only observing a survival extension in females [266]. However, in the latter study the mice were on a mixed B6SJL x BALB/c background which potentially contributed to the unexpected effect. Conversely, in cases where prolonged or high intensity exercise was imparted, survival was shortened in male transgenic mice [267, 268]. Clearly, sex and exercise, could be factors in ALS risk. The potential influence of exercise on disease process and risk factors is far-reaching with involvement in regulating body mass index, mitochondrial and antioxidant capacity, and neurotrophic effects in CNS though enhancement of neurogenesis [269, 270].

Resistance exercise in humans increases AR transcript and protein expression in skeletal muscle, alongside IGF-1 [271, 272], and both have been shown to interact to induce muscle hypertrophy [273]. AR is also increased in type II muscle fibres following resistance exercise [274] and in response to electrical stimulation in rats [275]. It is possible that in ALS muscle, the denervation and reduced stimulation, which occurs early in $SOD1^{G93A}$ disease pathogenesis, replicates the reverse effect leading to downregulation of AR transcript. Exogenous T regulates AR expression in response to stressors such as energy deficit [276]. Skeletal muscle in $SOD1^{G93A}$ mice and ALS patients shows bioenergetic defects, even prior to denervation [277]. Therefore, an alternative mechanism is that the enhanced energy expenditure and hypermetabolism in $SOD1^{G93A}$ muscle may be disrupting regulation of AR transcription, resulting in the downregulation observed in Chapter 4. Mild exercise can also increase SRD5A1, SRD5A2 and AR mRNA expression in the hippocampus, irrespective of castration, increasing local DHT production [278].

Exercise increases the production of several potent neurotrophic factors: BDNF [279], NGF [280, 281] and IGF-1 [282]. These neurotrophic factors interact with androgen signalling to modulate MN functions either directly or via their muscle targets. Androgens upregulate BDNF and its receptor, TrkB, in both SNB MNs [283, 284], as well as other somatic MNs [284, 285]. Androgens also upregulate BDNF in quadriceps muscle and decrease expression in BC/LA muscles [284]. AR activation has been shown in the latter to regulate BDNF protein levels in innervating SNB MNs. Androgen-BDNF interactions alter MN morphology and stimulate neuroprotection/regeneration following axonal injury [286]. The effects of AR on IGF-1 synthesis in muscle are well established and discussed numerously throughout this thesis. The androgen response element was identified in the *Igf1* gene promoter, confirming it is a direct transcriptional target of AR [287]. IGF-1 has reciprocal effects on AR function, stimulating AR signalling by increasing co-activators [288] or inhibiting co-repressors [289]. IGF-1 can also stimulate Akt phosphorylation of AR which interferes with androgen binding,

decreasing AR activation [290]. The NGF receptor, TrkA, interacts with ligand-activated AR, coordinating the androgen-NGF signalling pathway stimulating neuritogenesis (Figure 1.2) [120, 291]. DHT upregulates neuritin expression and stimulates neurite extension in MNs [170]. Taken together, there is evidence for stimulation of AR and neurotrophic factor production through exercise. This may enhance or facilitate the androgen interaction with these neurotrophic factors to promote neuroprotective actions on MNs. The exogenous administration of BDNF and IGF-1 in ALS patients did not translate to a clinical benefit, despite their known potent neuroprotective actions on MNs. This is potentially due to stability issues and impenetrable to blood brain barrier uptake. A better understanding of neurotrophic factor perturbations and their regulation *in vivo* could improve their application as therapies.

7.4. Limitations & considerations

Use of the SOD1^{G93A} mouse model to explore potential pathogenic mechanisms in ALS is not without limitations. The overexpression of the human WT SOD1 transgene has a contribution to the disease and the SOD1^{G93A} mutation only represents 2% of overall ALS cases. The SOD1^{G93A} mouse does, however, robustly develop adult-onset motor neuron degeneration, recapitulating the majority of clinical pathologies and disease mechanisms observed in both familial and sporadic ALS. Several major shortcomings in this model limit its validity in modelling clinical ALS. It does not exhibit any pathological TDP-43 inclusions which are evident in almost all sALS patients, as well as other human neurodegenerative conditions [292]. As an extension of this, the SOD1^{G93A} model does not possess defective RNA missplicing, comparable to the levels observed in alternative ALS models and ALS patients [293]. This may limit the possibility to capture an interaction between AR and RNA binding proteins implicated in clinical ALS. For example, fused in sarcoma (FUS) protein was found to be a co-regulator of AR expression in prostate cancer cells [294]; and alopecia, resulting from elevated DHT levels in hair follicles, was associated with a single nucleotide polymorphism in TDP-43 in ALS [295]. Lastly, while this model reflects well the "dying back" hypothesis, whereby disease initiates with disrupted neuromuscular connectivity followed by death of LMNs, it does not present with significant UMN loss by endstage as reported in Chapter 3 findings from this thesis. Another limitation in the translatability of mice models to clinical ALS is, they do not have an inherent susceptibility to develop neurodegeneration to the same capacity as humans. For example, to replicate clinical ALS pathology in mice requires expression of ~25 copies of the mutant SOD1^{G93A} gene. Mice do not have an expanded or polymorphic AR polyglutamine tract [296] and require insertion of human AR with CAG repeats far longer than those which cause clinical SBMA, to replicate the disease pathology.

Another point for consideration is the studies conducted in this thesis used male and female gonadally intact SOD1^{G93A} mice on the C57BL/6 genetic background. This genetic background appears to minimise the sex-effect on disease onset and survival observed on other backgrounds, such as the SJL [59]. Subtle effects on disease onset, in combination with the aggressive disease course in the SOD1^{G93A}, it is not unreasonable that the interventions to alter AR function alone did not translate to marked disease modifications. Disruption to sex steroid hormone signalling pathways can have downstream impacts. Blocking or deleting androgen action on the HPG axis causes loss in feedback mechanisms regulating T production [88]. While many studies use

castration and steroid supplementation as a way around this [297], it does not reflect the normal biological situation of cyclical hormone production and regulation. Using *in vivo* models is hampered by such limitations. In both chapter 5 and 6, the inhibition of androgen-responsive neurons in the hypothalamus, led to increased T production by the testis and most likely increased peripheral AR activation. Therefore, it is possible that such effects counteracted some of the action to block or genetically delete AR in discrete cell populations. An alternative approach to chapters 5, would be using a drug alternative to flutamide which does not cross the blood brain barrier. This would determine peripheral only effects and eliminate the central effects of elevated T production. For example a similar drug, bicalutamide, does not result in serum elevations of LH and T, compared to flutamide [298]. In line with this drug approach, an AR genetic deletion, restricted to muscle specific cell populations would be interesting to build on the current findings in this thesis. Finally, it would also be of interest to further characterise AR expression across different muscle groups and myofiber types in $SOD1^{G93A}$ mice compared to WT controls, and MN populations innervating select skeletal muscles. This would build on the preliminary findings of chapters 3 and 4, which show inherent downregulation of AR in the $SOD1^{G93A}$.

7.5. Clinical considerations

To date, evidence for dysregulation of AR and androgen involvement in clinical ALS has not been widely explored. Most studies have been conducted on patient cohorts much too small to draw any robust conclusions, including measurement of circulating and CSF androgens and detection of AR gene polymorphisms [50, 155]. Human *AR* is subject to genetic variations not reflected in mouse *Ar*, for example, there is no polyQ repeat expansion in mice [296]. The potential contributions of undiscovered alterations in the function of AR in human ALS can therefore not be ruled out as a contributing risk factor.

Targeting steroid hormones or hormone replacement is not without substantial risk due to their off-target effects. As observed in postmenopausal women, hormone replacement therapy associated with a worse ALS prognosis. ALS is largely a disease of aging [299] - therefore hormones as age-dependent modifiers must also be considered. The use of exogenous androgens for clinical applications is limited due to their detrimental systemic effects, primarily on the cardiovascular system and prostate [300]. The development of selective androgen receptor modulators (SARMs) could be a way to target and activate AR within specific tissues of interest. This approach has been particularly successful in developing analogous selective estrogen receptor modulators (SERMs), which are now showing promise as therapies for neurological diseases, including traumatic brain injury, stroke and Parkinson's disease [301]. Unfortunately, the development of SARMs has not been as successful. While improved targeting effects, these have largely fallen short in providing robust evidence of clinically beneficial improvements to gain approval as enhancers of muscle mass and bone deposition [302]. For patients, currently diagnosed with ALS, there is no clear evidence to suggest that hormone-replacement therapy with either estrogens, or androgens, is recommended to provide any beneficial effect. In fact, it is often the off-target effects of these therapies that may be detrimental, considering the age of the patient and the potential for other comorbidities. It is anticipated that future work into the mechanisms behind sex-differences in ALS will help greatly understand the heterogeneity of the disease and provide better stratification of patients into clinical

trials, help tailor therapies to patients and could also provide insight into dietary and exercise recommendations for patients.

7.6. Concluding remarks

This thesis explored the potential dysregulation of AR in ALS. While clear sex-specific differences are evident in ALS, as well as other neurodegenerative diseases and brain disorders, disentangling the exact mechanisms of hormonal influences proves difficult. One major finding of this thesis is that there is an inherent decrease in AR present in the CNS, particularly in motor neurons, and skeletal muscle, early in the disease course of $SOD1^{G93A}$ male mice. Further investigations into the mechanisms leading to this loss in AR would be beneficial to confirm its involvement as a pathogenic contributor or a consequence of other disease processes. The second major finding of this thesis is that AR antagonism, neural AR deletion and AR overexpression are not able to alter disease outcome in male $SOD1^{G93A}$ mice. This work contributes to a growing body of evidence that androgen-based manipulations in this mouse model of ALS, alone, have minimal impact. Future studies should focus on exploring these effects in alternative ALS models and the influence of AR manipulation in combination with other modifiers of disease such as exercise and metabolic dysfunction.

Bibliography

1. Hardiman, O., et al., *Amyotrophic lateral sclerosis.* Nat Rev Dis Primers, 2017. **3**: p. 17071.
2. McCombe, P.A. and R.D. Henderson, *Effects of gender in amyotrophic lateral sclerosis.* Gend Med, 2010. **7**(6): p. 557-70.
3. Weiner, L.P., *Possible role of androgen receptors in amyotrophic lateral sclerosis. A hypothesis.* Arch Neurol, 1980. **37**(3): p. 129-31.
4. Sar, M. and W.E. Stumpf, *Androgen concentration in motor neurons of cranial nerves and spinal cord.* Science, 1977. **197**(4298): p. 77-9.
5. La Spada, A.R., et al., *Androgen receptor gene mutations in X-linked spinal and bulbar muscular atrophy.* Nature, 1991. **352**(6330): p. 77-9.
6. Ogata, A., et al., *Expression of androgen receptor in X-linked spinal and bulbar muscular atrophy and amyotrophic lateral sclerosis.* J Neurol Neurosurg Psychiatry, 1994. **57**(10): p. 1274-5.
7. Jones, T.M., R. Yu, and J.P. Antel, *Response of patients with amyotrophic lateral sclerosis to testosterone therapy: endocrine evaluation.* Arch Neurol, 1982. **39**(11): p. 721-2.
8. Bruson, A., et al., *CAG repeat length in androgen receptor gene is not associated with amyotrophic lateral sclerosis.* Eur J Neurol, 2012. **19**(10): p. 1373-5.
9. Cary, G.A. and A.R. La Spada, *Androgen receptor function in motor neuron survival and degeneration.* Phys Med Rehabil Clin N Am, 2008. **19**(3): p. 479-94, viii.
10. Fargo, K.N., et al., *Neuroprotective actions of androgens on motoneurons.* Front Neuroendocrinol, 2009. **30**(2): p. 130-41.
11. Mangelsdorf, D.J., et al., *The nuclear receptor superfamily: the second decade.* Cell, 1995. **83**(6): p. 835-9.
12. Laudet, V., et al., *Evolution of the nuclear receptor gene superfamily.* EMBO J, 1992. **11**(3): p. 1003-13.
13. Brown, R.H., Jr. and A. Al-Chalabi, *Amyotrophic Lateral Sclerosis.* N Engl J Med, 2017. **377**(16): p. 1602.
14. Taylor, J.P., R.H. Brown, Jr., and D.W. Cleveland, *Decoding ALS: from genes to mechanism.* Nature, 2016. **539**(7628): p. 197-206.
15. Kim, G., et al., *ALS Genetics: Gains, Losses, and Implications for Future Therapies.* Neuron, 2020. **108**(5): p. 822-842.
16. Balendra, R. and A.M. Isaacs, *C9orf72-mediated ALS and FTD: multiple pathways to disease.* Nat Rev Neurol, 2018. **14**(9): p. 544-558.
17. Mancuso, R. and X. Navarro, *Amyotrophic lateral sclerosis: Current perspectives from basic research to the clinic.* Prog Neurobiol, 2015. **133**: p. 1-26.
18. Ferraiuolo, L., et al., *Molecular pathways of motor neuron injury in amyotrophic lateral sclerosis.* Nat Rev Neurol, 2011. **7**(11): p. 616-30.
19. Van Harten, A.C.M., H. Phatnani, and S. Przedborski, *Non-cell-autonomous pathogenic mechanisms in amyotrophic lateral sclerosis.* Trends Neurosci, 2021. **44**(8): p. 658-668.
20. Serio, A. and R. Patani, *Concise Review: The Cellular Conspiracy of Amyotrophic Lateral Sclerosis.* Stem Cells, 2018. **36**(3): p. 293-303.
21. Filipi, T., et al., *Glial Cells-The Strategic Targets in Amyotrophic Lateral Sclerosis Treatment.* J Clin Med, 2020. **9**(1).
22. Frey, D., et al., *Early and selective loss of neuromuscular synapse subtypes with low sprouting competence in motoneuron diseases.* J Neurosci, 2000. **20**(7): p. 2534-42.
23. Loeffler, J.P., et al., *The Role of Skeletal Muscle in Amyotrophic Lateral Sclerosis.* Brain Pathol, 2016. **26**(2): p. 227-36.
24. Talbot, K., et al., *Amyotrophic lateral sclerosis: the complex path to precision medicine.* J Neurol, 2018. **265**(10): p. 2454-2462.
25. Couratier, P., et al., *Epidemiology of amyotrophic lateral sclerosis: A review of literature.* Rev Neurol (Paris), 2016. **172**(1): p. 37-45.
26. Wang, M.D., et al., *Identification of risk factors associated with onset and progression of amyotrophic lateral sclerosis using systematic review and meta-analysis.* Neurotoxicology, 2017. **61**: p. 101-130.
27. Manjaly, Z.R., et al., *The sex ratio in amyotrophic lateral sclerosis: A population based study.* Amyotroph Lateral Scler, 2010. **11**(5): p. 439-42.

28. Chio, A., et al., *Phenotypic heterogeneity of amyotrophic lateral sclerosis: a population based study.* J Neurol Neurosurg Psychiatry, 2011. **82**(7): p. 740-6.
29. Talman, P., et al., *Identification and outcomes of clinical phenotypes in amyotrophic lateral sclerosis/motor neuron disease: Australian National Motor Neuron Disease observational cohort.* BMJ Open, 2016. **6**(9): p. e012054.
30. Chio, A., et al., *ALS phenotype is influenced by age, sex, and genetics: A population-based study.* Neurology, 2020. **94**(8): p. e802-e810.
31. Swinnen, B. and W. Robberecht, *The phenotypic variability of amyotrophic lateral sclerosis.* Nat Rev Neurol, 2014. **10**(11): p. 661-70.
32. Kim, W.K., et al., *Study of 962 patients indicates progressive muscular atrophy is a form of ALS.* Neurology, 2009. **73**(20): p. 1686-92.
33. Wijesekera, L.C., et al., *Natural history and clinical features of the flail arm and flail leg ALS variants.* Neurology, 2009. **72**(12): p. 1087-94.
34. Shoesmith, C.L., et al., *Prognosis of amyotrophic lateral sclerosis with respiratory onset.* J Neurol Neurosurg Psychiatry, 2007. **78**(6): p. 629-31.
35. Chio, A., et al., *Cognitive impairment across ALS clinical stages in a population-based cohort.* Neurology, 2019. **93**(10): p. e984-e994.
36. Curtis, A.F., et al., *Sex differences in the prevalence of genetic mutations in FTD and ALS: A meta-analysis.* Neurology, 2017. **89**(15): p. 1633-1642.
37. Esselin, F., et al., *Clinical Phenotype and Inheritance in Patients With C9ORF72 Hexanucleotide Repeat Expansion: Results From a Large French Cohort.* Front Neurosci, 2020. **14**: p. 316.
38. Palmieri, A., et al., *Female gender doubles executive dysfunction risk in ALS: a case-control study in 165 patients.* J Neurol Neurosurg Psychiatry, 2015. **86**(5): p. 574-9.
39. Williams, K.L., et al., *Pathophysiological insights into ALS with C9ORF72 expansions.* J Neurol Neurosurg Psychiatry, 2013. **84**(8): p. 931-5.
40. Trojsi, F., et al., *Comparative Analysis of C9orf72 and Sporadic Disease in a Large Multicenter ALS Population: The Effect of Male Sex on Survival of C9orf72 Positive Patients.* Front Neurosci, 2019. **13**: p. 485.
41. Rooney, J., et al., *C9orf72 expansion differentially affects males with spinal onset amyotrophic lateral sclerosis.* J Neurol Neurosurg Psychiatry, 2017. **88**(4): p. 281.
42. Vasconcelos, K., et al., *Action of hormonal therapy in amyotrophic lateral sclerosis: a systematic review.* Rev Assoc Med Bras (1992), 2020. **66**(11): p. 1589-1594.
43. Rooney, J.P.K., et al., *A case-control study of hormonal exposures as etiologic factors for ALS in women: Euro-MOTOR.* Neurology, 2017. **89**(12): p. 1283-1290.
44. de Jong, S., et al., *Endogenous female reproductive hormones and the risk of amyotrophic lateral sclerosis.* J Neurol, 2013. **260**(2): p. 507-12.
45. Popat, R.A., et al., *Effect of reproductive factors and postmenopausal hormone use on the risk of amyotrophic lateral sclerosis.* Neuroepidemiology, 2006. **27**(3): p. 117-21.
46. Rudnicki, S.A., *Estrogen replacement therapy in women with amyotrophic lateral sclerosis.* J Neurol Sci, 1999. **169**(1-2): p. 126-7.
47. Wise, P.M., *Estrogens and neuroprotection.* Trends Endocrinol Metab, 2002. **13**(6): p. 229-30.
48. Bialek, M., et al., *Neuroprotective role of testosterone in the nervous system.* Pol J Pharmacol, 2004. **56**(5): p. 509-18.
49. Feldman, H.A., et al., *Age trends in the level of serum testosterone and other hormones in middle-aged men: longitudinal results from the Massachusetts male aging study.* J Clin Endocrinol Metab, 2002. **87**(2): p. 589-98.
50. Militello, A., et al., *The serum level of free testosterone is reduced in amyotrophic lateral sclerosis.* J Neurol Sci, 2002. **195**(1): p. 67-70.
51. Sawal, N., et al., *Dihydrotestosterone in Amyotrophic lateral sclerosis-The missing link?* Brain Behav, 2020. **10**(11): p. e01645.
52. Vivekananda, U., et al., *Low index-to-ring finger length ratio in sporadic ALS supports prenatally defined motor neuronal vulnerability.* J Neurol Neurosurg Psychiatry, 2011. **82**(6): p. 635-7.
53. Wicks, P., *Hypothesis: higher prenatal testosterone predisposes ALS patients to improved athletic performance and manual professions.* Amyotroph Lateral Scler, 2012. **13**(3): p. 251-3.
54. Tu, P.H., et al., *Transgenic mice carrying a human mutant superoxide dismutase transgene develop neuronal cytoskeletal pathology resembling human amyotrophic lateral sclerosis lesions.* Proc Natl Acad Sci U S A, 1996. **93**(7): p. 3155-60.

55. Cveticanin, J., et al., *Insight into the Autosomal-Dominant Inheritance Pattern of SOD1-Associated ALS from Native Mass Spectrometry.* J Mol Biol, 2020. **432**(23): p. 5995-6002.
56. Turner, B.J. and K. Talbot, *Transgenics, toxicity and therapeutics in rodent models of mutant SOD1-mediated familial ALS.* Prog Neurobiol, 2008. **85**(1): p. 94-134.
57. Scott, S., et al., *Design, power, and interpretation of studies in the standard murine model of ALS.* Amyotroph Lateral Scler, 2008. **9**(1): p. 4-15.
58. Gurney, M.E., et al., *Motor neuron degeneration in mice that express a human Cu,Zn superoxide dismutase mutation.* Science, 1994. **264**(5166): p. 1772-5.
59. Heiman-Patterson, T.D., et al., *Background and gender effects on survival in the TgN(SOD1-G93A)1Gur mouse model of ALS.* J Neurol Sci, 2005. **236**(1-2): p. 1-7.
60. Pfohl, S.R., M.T. Halicek, and C.S. Mitchell, *Characterization of the Contribution of Genetic Background and Gender to Disease Progression in the SOD1 G93A Mouse Model of Amyotrophic Lateral Sclerosis: A Meta-Analysis.* J Neuromuscul Dis, 2015. **2**(2): p. 137-150.
61. Acevedo-Arozena, A., et al., *A comprehensive assessment of the SOD1G93A low-copy transgenic mouse, which models human amyotrophic lateral sclerosis.* Dis Model Mech, 2011. **4**(5): p. 686-700.
62. Wong, P.C., et al., *An adverse property of a familial ALS-linked SOD1 mutation causes motor neuron disease characterized by vacuolar degeneration of mitochondria.* Neuron, 1995. **14**(6): p. 1105-16.
63. Bruijn, L.I., et al., *ALS-linked SOD1 mutant G85R mediates damage to astrocytes and promotes rapidly progressive disease with SOD1-containing inclusions.* Neuron, 1997. **18**(2): p. 327-38.
64. Liebl, M.P., et al., *Low-frequency magnetic fields do not aggravate disease in mouse models of Alzheimer's disease and amyotrophic lateral sclerosis.* Sci Rep, 2015. **5**: p. 8585.
65. Philips, T. and J.D. Rothstein, *Rodent Models of Amyotrophic Lateral Sclerosis.* Curr Protoc Pharmacol, 2015. **69**: p. 5 67 1-5 67 21.
66. Wegorzewska, I., et al., *TDP-43 mutant transgenic mice develop features of ALS and frontotemporal lobar degeneration.* Proc Natl Acad Sci U S A, 2009. **106**(44): p. 18809-14.
67. Hatzipetros, T., et al., *C57BL/6J congenic Prp-TDP43A315T mice develop progressive neurodegeneration in the myenteric plexus of the colon without exhibiting key features of ALS.* Brain Res, 2014. **1584**: p. 59-72.
68. Herdewyn, S., et al., *Prevention of intestinal obstruction reveals progressive neurodegeneration in mutant TDP-43 (A315T) mice.* Mol Neurodegener, 2014. **9**: p. 24.
69. Arnold, E.S., et al., *ALS-linked TDP-43 mutations produce aberrant RNA splicing and adult-onset motor neuron disease without aggregation or loss of nuclear TDP-43.* Proc Natl Acad Sci U S A, 2013. **110**(8): p. E736-45.
70. Liu, Y., et al., *C9orf72 BAC Mouse Model with Motor Deficits and Neurodegenerative Features of ALS/FTD.* Neuron, 2016. **90**(3): p. 521-34.
71. Mordes, D.A., et al., *Absence of Survival and Motor Deficits in 500 Repeat C9ORF72 BAC Mice.* Neuron, 2020. **108**(4): p. 775-783 e4.
72. Nguyen, L., et al., *Survival and Motor Phenotypes in FVB C9-500 ALS/FTD BAC Transgenic Mice Reproduced by Multiple Labs.* Neuron, 2020. **108**(4): p. 784-796 e3.
73. Watkins, J., et al., *Female sex mitigates motor and behavioural phenotypes in TDP-43(Q331K) knock-in mice.* Sci Rep, 2020. **10**(1): p. 19220.
74. Groeneveld, G.J., et al., *Ovariectomy and 17beta-estradiol modulate disease progression of a mouse model of ALS.* Brain Res, 2004. **1021**(1): p. 128-31.
75. Heitzer, M., et al., *Administration of 17beta-Estradiol Improves Motoneuron Survival and Down-regulates Inflammasome Activation in Male SOD1(G93A) ALS Mice.* Mol Neurobiol, 2017. **54**(10): p. 8429-8443.
76. Yan, L., et al., *Effects of Ovariectomy in an hSOD1-G93A Transgenic Mouse Model of Amyotrophic Lateral Sclerosis (ALS).* Med Sci Monit, 2018. **24**: p. 678-686.
77. Zhao, Z., et al., *Neuroprotective Effects of Genistein in a SOD1-G93A Transgenic Mouse Model of Amyotrophic Lateral Sclerosis.* J Neuroimmune Pharmacol, 2019. **14**(4): p. 688-696.
78. Hayes-Punzo, A., et al., *Gonadectomy and dehydroepiandrosterone (DHEA) do not modulate disease progression in the G93A mutant SOD1 rat model of amyotrophic lateral sclerosis.* Amyotroph Lateral Scler, 2012. **13**(3): p. 311-4.
79. Sheean, R.K., et al., *Effect of thymic stimulation of CD4+ T cell expansion on disease onset and progression in mutant SOD1 mice.* J Neuroinflammation, 2015. **12**: p. 40.
80. Aggarwal, T., et al., *Androgens affect muscle, motor neuron, and survival in a mouse model of SOD1-related amyotrophic lateral sclerosis.* Neurobiol Aging, 2014. **35**(8): p. 1929-38.

81. Kassa, R.M., et al., *Effect of physical exercise and anabolic steroid treatment on spinal motoneurons and surrounding glia of wild-type and ALS mice.* Brain Res, 2017. **1657**: p. 269-278.
82. Yoo, Y.E. and C.P. Ko, *Dihydrotestosterone ameliorates degeneration in muscle, axons and motoneurons and improves motor function in amyotrophic lateral sclerosis model mice.* PLoS One, 2012. **7**(5): p. e37258.
83. Kim, J., et al., *Autophagy activation and neuroprotection by progesterone in the G93A-SOD1 transgenic mouse model of amyotrophic lateral sclerosis.* Neurobiol Dis, 2013. **59**: p. 80-5.
84. Bame, M., et al., *Effect of sex on lifespan, disease progression, and the response to methionine sulfoximine in the SOD1 G93A mouse model for ALS.* Gend Med, 2012. **9**(6): p. 524-35.
85. Weisz, J. and I.L. Ward, *Plasma testosterone and progesterone titers of pregnant rats, their male and female fetuses, and neonatal offspring.* Endocrinology, 1980. **106**(1): p. 306-16.
86. Motelica-Heino, I., et al., *Testosterone levels in plasma and testes of neonatal mice.* J Steroid Biochem, 1988. **31**(3): p. 283-6.
87. van de Beek, C., et al., *Prenatal sex hormones (maternal and amniotic fluid) and gender-related play behavior in 13-month-old Infants.* Arch Sex Behav, 2009. **38**(1): p. 6-15.
88. Walker, D.M. and A.C. Gore, *Transgenerational neuroendocrine disruption of reproduction.* Nat Rev Endocrinol, 2011. **7**(4): p. 197-207.
89. Chen, F., et al., *Direct agonist/antagonist functions of dehydroepiandrosterone.* Endocrinology, 2005. **146**(11): p. 4568-76.
90. Jasuja, R., et al., *Delta-4-androstene-3,17-dione binds androgen receptor, promotes myogenesis in vitro, and increases serum testosterone levels, fat-free mass, and muscle strength in hypogonadal men.* J Clin Endocrinol Metab, 2005. **90**(2): p. 855-63.
91. Laurent, M.R., et al., *Sex hormone-binding globulin regulation of androgen bioactivity in vivo: validation of the free hormone hypothesis.* Sci Rep, 2016. **6**: p. 35539.
92. Janne, M., et al., *Human sex hormone-binding globulin gene expression in transgenic mice.* Mol Endocrinol, 1998. **12**(1): p. 123-36.
93. Michiel Sedelaar, J.P., S.S. Dalrymple, and J.T. Isaacs, *Of mice and men-warning: intact versus castrated adult male mice as xenograft hosts are equivalent to hypogonadal versus abiraterone treated aging human males, respectively.* Prostate, 2013. **73**(12): p. 1316-25.
94. van Weerden, W.M., et al., *Adrenal glands of mouse and rat do not synthesize androgens.* Life Sci, 1992. **50**(12): p. 857-61.
95. Mostaghel, E.A., et al., *Contribution of Adrenal Glands to Intratumor Androgens and Growth of Castration-Resistant Prostate Cancer.* Clin Cancer Res, 2019. **25**(1): p. 426-439.
96. Jin, Y. and T.M. Penning, *Steroid 5alpha-reductases and 3alpha-hydroxysteroid dehydrogenases: key enzymes in androgen metabolism.* Best Pract Res Clin Endocrinol Metab, 2001. **15**(1): p. 79-94.
97. Pozzi, P., et al., *Androgen 5-alpha-reductase type 2 is highly expressed and active in rat spinal cord motor neurones.* J Neuroendocrinol, 2003. **15**(9): p. 882-7.
98. Fukami, M., et al., *Backdoor pathway for dihydrotestosterone biosynthesis: implications for normal and abnormal human sex development.* Dev Dyn, 2013. **242**(4): p. 320-9.
99. Chen, F., et al., *Partial agonist/antagonist properties of androstenedione and 4-androsten-3beta,17beta-diol.* J Steroid Biochem Mol Biol, 2004. **91**(4-5): p. 247-57.
100. Kuhn, C.M., *Anabolic steroids.* Recent Prog Horm Res, 2002. **57**: p. 411-34.
101. Chamberlain, N.L., D.C. Whitacre, and R.L. Miesfeld, *Delineation of two distinct type 1 activation functions in the androgen receptor amino-terminal domain.* J Biol Chem, 1996. **271**(43): p. 26772-8.
102. Choong, C.S. and E.M. Wilson, *Trinucleotide repeats in the human androgen receptor: a molecular basis for disease.* J Mol Endocrinol, 1998. **21**(3): p. 235-57.
103. Bevan, C.L., et al., *The AF1 and AF2 domains of the androgen receptor interact with distinct regions of SRC1.* Mol Cell Biol, 1999. **19**(12): p. 8383-92.
104. Veldscholte, J., et al., *Hormone-induced dissociation of the androgen receptor-heat-shock protein complex: use of a new monoclonal antibody to distinguish transformed from nontransformed receptors.* Biochemistry, 1992. **31**(32): p. 7422-30.
105. Nadal, M., et al., *Structure of the homodimeric androgen receptor ligand-binding domain.* Nat Commun, 2017. **8**: p. 14388.
106. Loy, C.J., K.S. Sim, and E.L. Yong, *Filamin-A fragment localizes to the nucleus to regulate androgen receptor and coactivator functions.* Proc Natl Acad Sci U S A, 2003. **100**(8): p. 4562-7.
107. Cutress, M.L., et al., *Structural basis for the nuclear import of the human androgen receptor.* J Cell Sci, 2008. **121**(Pt 7): p. 957-68.

108. Heemers, H.V. and D.J. Tindall, *Androgen receptor (AR) coregulators: a diversity of functions converging on and regulating the AR transcriptional complex.* Endocr Rev, 2007. **28**(7): p. 778-808.
109. Gioeli, D., et al., *Androgen receptor phosphorylation. Regulation and identification of the phosphorylation sites.* J Biol Chem, 2002. **277**(32): p. 29304-14.
110. Blok, L.J., P.E. de Ruiter, and A.O. Brinkmann, *Forskolin-induced dephosphorylation of the androgen receptor impairs ligand binding.* Biochemistry, 1998. **37**(11): p. 3850-7.
111. Rochette-Egly, C., *Nuclear receptors: integration of multiple signalling pathways through phosphorylation.* Cell Signal, 2003. **15**(4): p. 355-66.
112. Lieberherr, M. and B. Grosse, *Androgens increase intracellular calcium concentration and inositol 1,4,5-trisphosphate and diacylglycerol formation via a pertussis toxin-sensitive G-protein.* J Biol Chem, 1994. **269**(10): p. 7217-23.
113. Foradori, C.D., M.J. Weiser, and R.J. Handa, *Non-genomic actions of androgens.* Front Neuroendocrinol, 2008. **29**(2): p. 169-81.
114. Leung, J.K. and M.D. Sadar, *Non-Genomic Actions of the Androgen Receptor in Prostate Cancer.* Front Endocrinol (Lausanne), 2017. **8**: p. 2.
115. Deng, Q., et al., *Non-Genomic Action of Androgens is Mediated by Rapid Phosphorylation and Regulation of Androgen Receptor Trafficking.* Cell Physiol Biochem, 2017. **43**(1): p. 223-236.
116. Castoria, G., F. Auricchio, and A. Migliaccio, *Extranuclear partners of androgen receptor: at the crossroads of proliferation, migration, and neuritogenesis.* FASEB J, 2017. **31**(4): p. 1289-1300.
117. Koryakina, Y., H.Q. Ta, and D. Gioeli, *Androgen receptor phosphorylation: biological context and functional consequences.* Endocr Relat Cancer, 2014. **21**(4): p. T131-45.
118. Bennett, N.C., et al., *Molecular cell biology of androgen receptor signalling.* Int J Biochem Cell Biol, 2010. **42**(6): p. 813-27.
119. Thomas, P., *Membrane Androgen Receptors Unrelated to Nuclear Steroid Receptors.* Endocrinology, 2019. **160**(4): p. 772-781.
120. Di Donato, M., et al., *Cross-talk between androgen receptor/filamin A and TrkA regulates neurite outgrowth in PC12 cells.* Mol Biol Cell, 2015. **26**(15): p. 2858-72.
121. Matsumoto, T., et al., *Androgen receptor functions from reverse genetic models.* J Steroid Biochem Mol Biol, 2003. **85**(2-5): p. 95-9.
122. Gaspar, M.L., et al., *A single base deletion in the Tfm androgen receptor gene creates a short-lived messenger RNA that directs internal translation initiation.* Proc Natl Acad Sci U S A, 1991. **88**(19): p. 8606-10.
123. He, W.W., M.V. Kumar, and D.J. Tindall, *A frame-shift mutation in the androgen receptor gene causes complete androgen insensitivity in the testicular-feminized mouse.* Nucleic Acids Res, 1991. **19**(9): p. 2373-8.
124. De Gendt, K., et al., *A Sertoli cell-selective knockout of the androgen receptor causes spermatogenic arrest in meiosis.* Proc Natl Acad Sci U S A, 2004. **101**(5): p. 1327-32.
125. Kerkhofs, S., et al., *Androgen receptor knockout and knock-in mouse models.* J Mol Endocrinol, 2009. **42**(1): p. 11-7.
126. De Gendt, K. and G. Verhoeven, *Tissue- and cell-specific functions of the androgen receptor revealed through conditional knockout models in mice.* Mol Cell Endocrinol, 2012. **352**(1-2): p. 13-25.
127. Chang, C., et al., *Androgen receptor (AR) physiological roles in male and female reproductive systems: lessons learned from AR-knockout mice lacking AR in selective cells.* Biol Reprod, 2013. **89**(1): p. 21.
128. Chang, C., et al., *Androgen receptor (AR) pathophysiological roles in androgen-related diseases in skin, bone/muscle, metabolic syndrome and neuron/immune systems: lessons learned from mice lacking AR in specific cells.* Nucl Recept Signal, 2013. **11**: p. e001.
129. Rana, K., R.A. Davey, and J.D. Zajac, *Human androgen deficiency: insights gained from androgen receptor knockout mouse models.* Asian J Androl, 2014. **16**(2): p. 169-77.
130. Notini, A.J., et al., *Genomic actions of the androgen receptor are required for normal male sexual differentiation in a mouse model.* J Mol Endocrinol, 2005. **35**(3): p. 547-55.
131. Yu, I.C., et al., *Neuronal androgen receptor regulates insulin sensitivity via suppression of hypothalamic NF-kappaB-mediated PTP1B expression.* Diabetes, 2013. **62**(2): p. 411-23.
132. Tronche, F., et al., *Disruption of the glucocorticoid receptor gene in the nervous system results in reduced anxiety.* Nat Genet, 1999. **23**(1): p. 99-103.
133. Raskin, K., et al., *Conditional inactivation of androgen receptor gene in the nervous system: effects on male behavioral and neuroendocrine responses.* J Neurosci, 2009. **29**(14): p. 4461-70.

134. Juntti, S.A., et al., *The androgen receptor governs the execution, but not programming, of male sexual and territorial behaviors.* Neuron, 2010. **66**(2): p. 260-72.
135. Bielecki, B., et al., *Unexpected central role of the androgen receptor in the spontaneous regeneration of myelin.* Proc Natl Acad Sci U S A, 2016. **113**(51): p. 14829-14834.
136. Casanova, E., et al., *A CamKIIalpha iCre BAC allows brain-specific gene inactivation.* Genesis, 2001. **31**(1): p. 37-42.
137. Davey, R.A., et al., *Androgen Action via the Androgen Receptor in Neurons Within the Brain Positively Regulates Muscle Mass in Male Mice.* Endocrinology, 2017. **158**(10): p. 3684-3695.
138. Clarke, M.V., et al., *The androgen receptor in the hypothalamus positively regulates hind-limb muscle mass and voluntary physical activity in adult male mice.* J Steroid Biochem Mol Biol, 2019. **189**: p. 187-194.
139. Chen, C.V., et al., *Down, But Not Out: Partial Elimination of Androgen Receptors in the Male Mouse Brain Does Not Affect Androgenic Regulation of Anxiety or HPA Activity.* Endocrinology, 2016. **157**(2): p. 764-73.
140. Karlsson, S.A., et al., *Neural Androgen Receptors Modulate Gene Expression and Social Recognition But Not Social Investigation.* Front Behav Neurosci, 2016. **10**: p. 41.
141. Picot, M., et al., *Neural Androgen Receptor Deletion Impairs the Temporal Processing of Objects and Hippocampal CA1-Dependent Mechanisms.* PLoS One, 2016. **11**(2): p. e0148328.
142. Katsuno, M., et al., *Testosterone reduction prevents phenotypic expression in a transgenic mouse model of spinal and bulbar muscular atrophy.* Neuron, 2002. **35**(5): p. 843-54.
143. Yu, Z., et al., *Androgen-dependent pathology demonstrates myopathic contribution to the Kennedy disease phenotype in a mouse knock-in model.* J Clin Invest, 2006. **116**(10): p. 2663-72.
144. Ryan, C.P. and B.J. Crespi, *Androgen receptor polyglutamine repeat number: models of selection and disease susceptibility.* Evol Appl, 2013. **6**(2): p. 180-96.
145. Davis-Dao, C.A., et al., *Male infertility and variation in CAG repeat length in the androgen receptor gene: a meta-analysis.* J Clin Endocrinol Metab, 2007. **92**(11): p. 4319-26.
146. Hao, Y., et al., *Association between androgen receptor gene CAG repeat polymorphism and breast cancer risk: a meta-analysis.* Breast Cancer Res Treat, 2010. **124**(3): p. 815-20.
147. Giovannucci, E., et al., *The CAG repeat within the androgen receptor gene and benign prostatic hyperplasia.* Urology, 1999. **53**(1): p. 121-5.
148. Ellis, J.A., M. Stebbing, and S.B. Harrap, *Polymorphism of the androgen receptor gene is associated with male pattern baldness.* J Invest Dermatol, 2001. **116**(3): p. 452-5.
149. Lehmann, D.J., et al., *Association of the androgen receptor CAG repeat polymorphism with Alzheimer's disease in men.* Neurosci Lett, 2003. **340**(2): p. 87-90.
150. Gardiner, S.L., et al., *Repeat length variations in ATXN1 and AR modify disease expression in Alzheimer's disease.* Neurobiol Aging, 2019. **73**: p. 230 e9-230 e17.
151. Elden, A.C., et al., *Ataxin-2 intermediate-length polyglutamine expansions are associated with increased risk for ALS.* Nature, 2010. **466**(7310): p. 1069-75.
152. Tazelaar, G.H.P., et al., *ATXN1 repeat expansions confer risk for amyotrophic lateral sclerosis and contribute to TDP-43 mislocalization.* Brain Commun, 2020. **2**(2): p. fcaa064.
153. Seidel, K., et al., *Brain pathology of spinocerebellar ataxias.* Acta Neuropathol, 2012. **124**(1): p. 1-21.
154. Dewan, R., et al., *Pathogenic Huntingtin Repeat Expansions in Patients with Frontotemporal Dementia and Amyotrophic Lateral Sclerosis.* Neuron, 2021. **109**(3): p. 448-460 e4.
155. Garofalo, O., et al., *Androgen receptor gene polymorphisms in amyotrophic lateral sclerosis.* Neuromuscul Disord, 1993. **3**(3): p. 195-9.
156. Kennedy, W.R., M. Alter, and J.H. Sung, *Progressive proximal spinal and bulbar muscular atrophy of late onset. A sex-linked recessive trait.* Neurology, 1968. **18**(7): p. 671-80.
157. Schmidt, B.J., et al., *Expression of X-linked bulbospinal muscular atrophy (Kennedy disease) in two homozygous women.* Neurology, 2002. **59**(5): p. 770-2.
158. Li, M., et al., *Soluble androgen receptor oligomers underlie pathology in a mouse model of spinobulbar muscular atrophy.* J Biol Chem, 2007. **282**(5): p. 3157-64.
159. Lieberman, A.P., et al., *Altered transcriptional regulation in cells expressing the expanded polyglutamine androgen receptor.* Hum Mol Genet, 2002. **11**(17): p. 1967-76.
160. Thomas, P.S., Jr., et al., *Loss of endogenous androgen receptor protein accelerates motor neuron degeneration and accentuates androgen insensitivity in a mouse model of X-linked spinal and bulbar muscular atrophy.* Hum Mol Genet, 2006. **15**(14): p. 2225-38.

161. Adachi, H., et al., *Widespread nuclear and cytoplasmic accumulation of mutant androgen receptor in SBMA patients.* Brain, 2005. **128**(Pt 3): p. 659-70.
162. Taylor, J.P., et al., *Aggresomes protect cells by enhancing the degradation of toxic polyglutamine-containing protein.* Hum Mol Genet, 2003. **12**(7): p. 749-57.
163. Montie, H.L., et al., *Cytoplasmic retention of polyglutamine-expanded androgen receptor ameliorates disease via autophagy in a mouse model of spinal and bulbar muscular atrophy.* Hum Mol Genet, 2009. **18**(11): p. 1937-50.
164. Simeoni, S., et al., *Motoneuronal cell death is not correlated with aggregate formation of androgen receptors containing an elongated polyglutamine tract.* Hum Mol Genet, 2000. **9**(1): p. 133-44.
165. Hauser, K.F. and C.D. Toran-Allerand, *Androgen increases the number of cells in fetal mouse spinal cord cultures: implications for motoneuron survival.* Brain Res, 1989. **485**(1): p. 157-64.
166. Hammond, J., et al., *Testosterone-mediated neuroprotection through the androgen receptor in human primary neurons.* J Neurochem, 2001. **77**(5): p. 1319-26.
167. Pike, C.J., *Testosterone attenuates beta-amyloid toxicity in cultured hippocampal neurons.* Brain Res, 2001. **919**(1): p. 160-5.
168. Ahlbom, E., G.S. Prins, and S. Ceccatelli, *Testosterone protects cerebellar granule cells from oxidative stress-induced cell death through a receptor mediated mechanism.* Brain Res, 2001. **892**(2): p. 255-62.
169. Brooks, B.P., et al., *A cell culture model for androgen effects in motor neurons.* J Neurochem, 1998. **70**(3): p. 1054-60.
170. Marron, T.U., et al., *Androgen-induced neurite outgrowth is mediated by neuritin in motor neurones.* J Neurochem, 2005. **92**(1): p. 10-20.
171. Zhou, S. and J. Zhou, *Neuritin, a neurotrophic factor in nervous system physiology.* Curr Med Chem, 2014. **21**(10): p. 1212-9.
172. Butler, R., P.N. Leigh, and J.M. Gallo, *Androgen-induced up-regulation of tubulin isoforms in neuroblastoma cells.* J Neurochem, 2001. **78**(4): p. 854-61.
173. Duong, P., et al., *Neuroprotective and neurotoxic outcomes of androgens and estrogens in an oxidative stress environment.* Biol Sex Differ, 2020. **11**(1): p. 12.
174. Dadon-Nachum, M., E. Melamed, and D. Offen, *The "dying-back" phenomenon of motor neurons in ALS.* J Mol Neurosci, 2011. **43**(3): p. 470-7.
175. Shaw, P.J., *Molecular and cellular pathways of neurodegeneration in motor neurone disease.* J Neurol Neurosurg Psychiatry, 2005. **76**(8): p. 1046-57.
176. Fischer, L.R., et al., *Amyotrophic lateral sclerosis is a distal axonopathy: evidence in mice and man.* Exp Neurol, 2004. **185**(2): p. 232-40.
177. Hegedus, J., C.T. Putman, and T. Gordon, *Time course of preferential motor unit loss in the SOD1 G93A mouse model of amyotrophic lateral sclerosis.* Neurobiol Dis, 2007. **28**(2): p. 154-64.
178. Yu, W.H. and R. Srinivasan, *Effect of testosterone and 5 alpha-dihydrotestosterone on regeneration of the hypoglossal nerve in rats.* Exp Neurol, 1981. **71**(2): p. 431-5.
179. Yu, W.H., *Effect of testosterone on the regeneration of the hypoglossal nerve in rats.* Exp Neurol, 1982. **77**(1): p. 129-41.
180. Yu, W.H. and M.C. Yu, *Acceleration of the regeneration of the crushed hypoglossal nerve by testosterone.* Exp Neurol, 1983. **80**(2): p. 349-60.
181. Kujawa, K.A., N.B. Kinderman, and K.J. Jones, *Testosterone-induced acceleration of recovery from facial paralysis following crush axotomy of the facial nerve in male hamsters.* Exp Neurol, 1989. **105**(1): p. 80-5.
182. Kujawa, K.A., L. Tanzer, and K.J. Jones, *Inhibition of the accelerative effects of testosterone on hamster facial nerve regeneration by the antiandrogen flutamide.* Exp Neurol, 1995. **133**(2): p. 138-43.
183. Jones, K.J., *Recovery from facial paralysis following crush injury of the facial nerve in hamsters: differential effects of gender and androgen exposure.* Exp Neurol, 1993. **121**(1): p. 133-8.
184. Tanzer, L. and K.J. Jones, *Neurotherapeutic action of testosterone on hamster facial nerve regeneration: temporal window of effects.* Horm Behav, 2004. **45**(5): p. 339-44.
185. Kujawa, K.A., J.M. Jacob, and K.J. Jones, *Testosterone regulation of the regenerative properties of injured rat sciatic motor neurons.* J Neurosci Res, 1993. **35**(3): p. 268-73.
186. Brown, T.J., T. Khan, and K.J. Jones, *Androgen induced acceleration of functional recovery after rat sciatic nerve injury.* Restor Neurol Neurosci, 1999. **15**(4): p. 289-295.
187. O'Hanlon, G.M. and M.B. Lowrie, *Nerve injury in adult rats causes abnormalities in the motoneuron dendritic field that differ from those seen following neonatal nerve injury.* Exp Brain Res, 1995. **103**(2): p. 243-50.

188. Tseng, G.F. and M.E. Hu, *Axotomy induces retraction of the dendritic arbor of adult rat rubrospinal neurons.* Acta Anat (Basel), 1996. **155**(3): p. 184-93.
189. Sengelaub, D.R. and N.G. Forger, *The spinal nucleus of the bulbocavernosus: firsts in androgen-dependent neural sex differences.* Horm Behav, 2008. **53**(5): p. 596-612.
190. Smith, M.R., et al., *Ontogeny of androgen receptor expression in spinal nucleus of the bulbocavernosus motoneurons and their target muscles in male mice.* Neurosci Lett, 2012. **513**(2): p. 119-23.
191. Jordan, C.L., et al., *Ontogeny of androgen receptor immunoreactivity in lumbar motoneurons and in the sexually dimorphic levator ani muscle of male rats.* J Comp Neurol, 1997. **379**(1): p. 88-98.
192. Chambon, C., et al., *Myocytic androgen receptor controls the strength but not the mass of limb muscles.* Proc Natl Acad Sci U S A, 2010. **107**(32): p. 14327-32.
193. Yang, L.Y. and A.P. Arnold, *Interaction of BDNF and testosterone in the regulation of adult perineal motoneurons.* J Neurobiol, 2000. **44**(3): p. 308-19.
194. al-Shamma, H.A. and A.P. Arnold, *Importance of target innervation in recovery from axotomy-induced loss of androgen receptor in rat perineal motoneurons.* J Neurobiol, 1995. **28**(3): p. 341-53.
195. Breedlove, S.M. and A.P. Arnold, *Sexually dimorphic motor nucleus in the rat lumbar spinal cord: response to adult hormone manipulation, absence in androgen-insensitive rats.* Brain Res, 1981. **225**(2): p. 297-307.
196. Kurz, E.M., D.R. Sengelaub, and A.P. Arnold, *Androgens regulate the dendritic length of mammalian motoneurons in adulthood.* Science, 1986. **232**(4748): p. 395-8.
197. Leedy, M.G., M.S. Beattie, and J.C. Bresnahan, *Testosterone-induced plasticity of synaptic inputs to adult mammalian motoneurons.* Brain Res, 1987. **424**(2): p. 386-90.
198. Matsumoto, A., et al., *Androgenic regulation of gap junctions between motoneurons in the rat spinal cord.* J Neurosci, 1988. **8**(11): p. 4177-83.
199. Matsumoto, A., Y. Arai, and S. Hyodo, *Androgenic regulation of expression of beta-tubulin messenger ribonucleic acid in motoneurons of the spinal nucleus of the bulbocavernosus.* J Neuroendocrinol, 1993. **5**(4): p. 357-63.
200. Matsumoto, A., et al., *Effect of androgen on the expression of gap junction and beta-actin mRNAs in adult rat motoneurons.* Neurosci Res, 1992. **14**(2): p. 133-44.
201. Fargo, K.N. and D.R. Sengelaub, *Exogenous testosterone prevents motoneuron atrophy induced by contralateral motoneuron depletion.* J Neurobiol, 2004. **60**(3): p. 348-59.
202. Fargo, K.N. and D.R. Sengelaub, *Androgenic, but not estrogenic, protection of motoneurons from somal and dendritic atrophy induced by the death of neighboring motoneurons.* Dev Neurobiol, 2007. **67**(8): p. 1094-106.
203. Little, C.M., K.D. Coons, and D.R. Sengelaub, *Neuroprotective effects of testosterone on the morphology and function of somatic motoneurons following the death of neighboring motoneurons.* J Comp Neurol, 2009. **512**(3): p. 359-72.
204. Wilson, R.E., K.D. Coons, and D.R. Sengelaub, *Neuroprotective effects of testosterone on dendritic morphology following partial motoneuron depletion: efficacy in female rats.* Neurosci Lett, 2009. **465**(2): p. 123-7.
205. Cai, Y., et al., *Neuroprotective effects of testosterone metabolites and dependency on receptor action on the morphology of somatic motoneurons following the death of neighboring motoneurons.* Dev Neurobiol, 2017. **77**(6): p. 691-707.
206. Sengelaub, D.R. and X.M. Xu, *Protective effects of gonadal hormones on spinal motoneurons following spinal cord injury.* Neural Regen Res, 2018. **13**(6): p. 971-976.
207. Huguenard, A.L., et al., *Overexpression of androgen receptors in target musculature confers androgen sensitivity to motoneuron dendrites.* Endocrinology, 2011. **152**(2): p. 639-50.
208. Rand, M.N. and S.M. Breedlove, *Androgen alters the dendritic arbors of SNB motoneurons by acting upon their target muscles.* J Neurosci, 1995. **15**(6): p. 4408-16.
209. Henderson, C.E., et al., *GDNF: a potent survival factor for motoneurons present in peripheral nerve and muscle.* Science, 1994. **266**(5187): p. 1062-4.
210. Zhao, Z., et al., *Overexpression of glial cell line-derived neurotrophic factor in the CNS rescues motoneurons from programmed cell death and promotes their long-term survival following axotomy.* Exp Neurol, 2004. **190**(2): p. 356-72.
211. Yan, Q., J. Elliott, and W.D. Snider, *Brain-derived neurotrophic factor rescues spinal motor neurons from axotomy-induced cell death.* Nature, 1992. **360**(6406): p. 753-5.
212. Koliatsos, V.E., et al., *Evidence that brain-derived neurotrophic factor is a trophic factor for motor neurons in vivo.* Neuron, 1993. **10**(3): p. 359-67.

213. Tan, S.A., et al., *Rescue of motoneurons from axotomy-induced cell death by polymer encapsulated cells genetically engineered to release CNTF.* Cell Transplant, 1996. **5**(5): p. 577-87.
214. Gatzinsky, K.P., et al., *Early onset of degenerative changes at nodes of Ranvier in alpha-motor axons of Cntf null (-/-) mutant mice.* Glia, 2003. **42**(4): p. 340-9.
215. Dobrowolny, G., et al., *Muscle expression of a local Igf-1 isoform protects motor neurons in an ALS mouse model.* J Cell Biol, 2005. **168**(2): p. 193-9.
216. Kaspar, B.K., et al., *Retrograde viral delivery of IGF-1 prolongs survival in a mouse ALS model.* Science, 2003. **301**(5634): p. 839-42.
217. Campenot, R.B. and B.L. MacInnis, *Retrograde transport of neurotrophins: fact and function.* J Neurobiol, 2004. **58**(2): p. 217-29.
218. DiStefano, P.S., et al., *The neurotrophins BDNF, NT-3, and NGF display distinct patterns of retrograde axonal transport in peripheral and central neurons.* Neuron, 1992. **8**(5): p. 983-93.
219. Henderson, C.E., et al., *Neurotrophins promote motor neuron survival and are present in embryonic limb bud.* Nature, 1993. **363**(6426): p. 266-70.
220. Xu, J., et al., *Blockade of endogenous neurotrophic factors prevents the androgenic rescue of rat spinal motoneurons.* J Neurosci, 2001. **21**(12): p. 4366-72.
221. Sopher, B.L., et al., *Androgen receptor YAC transgenic mice recapitulate SBMA motor neuronopathy and implicate VEGF164 in the motor neuron degeneration.* Neuron, 2004. **41**(5): p. 687-99.
222. Stifani, N., *Motor neurons and the generation of spinal motor neuron diversity.* Front Cell Neurosci, 2014. **8**: p. 293.
223. Fitzpatrick, D., *Lower Motor Neuron Circuits and Motor Control: Overview.*, in *Neuroscience. 2nd edition.*, A.G. Purves D, Fitzpatrick D, et al., Editor. 2001, Sinauer Associates: Sunderland (MA).
224. Lemon, R.N., *Descending pathways in motor control.* Annu Rev Neurosci, 2008. **31**: p. 195-218.
225. Muroishi, Y., et al., *Immunohistochemical and in situ hybridization studies of choline acetyltransferase in large motor neurons of the human spinal cord.* Histol Histopathol, 2000. **15**(3): p. 689-96.
226. Shepherd, G. and R. Burke, *Spinal cord: Ventral horn*. The Synaptic Organization of the Brain, ed. G. Shepherd. 2004, New York: Oxford University Press.
227. Lalancette-Hebert, M., et al., *Gamma motor neurons survive and exacerbate alpha motor neuron degeneration in ALS.* Proc Natl Acad Sci U S A, 2016. **113**(51): p. E8316-E8325.
228. Mohajeri, M.H., D.A. Figlewicz, and M.C. Bohn, *Selective loss of alpha motoneurons innervating the medial gastrocnemius muscle in a mouse model of amyotrophic lateral sclerosis.* Exp Neurol, 1998. **150**(2): p. 329-36.
229. Saxena, S., E. Cabuy, and P. Caroni, *A role for motoneuron subtype-selective ER stress in disease manifestations of FALS mice.* Nat Neurosci, 2009. **12**(5): p. 627-36.
230. Kanning, K.C., A. Kaplan, and C.E. Henderson, *Motor neuron diversity in development and disease.* Annu Rev Neurosci, 2010. **33**: p. 409-40.
231. Hegedus, J., et al., *Preferential motor unit loss in the SOD1 G93A transgenic mouse model of amyotrophic lateral sclerosis.* J Physiol, 2008. **586**(14): p. 3337-51.
232. Atkin, J.D., et al., *Properties of slow- and fast-twitch muscle fibres in a mouse model of amyotrophic lateral sclerosis.* Neuromuscul Disord, 2005. **15**(5): p. 377-88.
233. Colon, A., et al., *Functional analysis of human intrafusal fiber innervation by human gamma-motoneurons.* Sci Rep, 2017. **7**(1): p. 17202.
234. Al-Chalabi, A., et al., *Analysis of amyotrophic lateral sclerosis as a multistep process: a population-based modelling study.* Lancet Neurol, 2014. **13**(11): p. 1108-1113.
235. Chen, J.J., *Overview of current and emerging therapies for amytrophic lateral sclerosis.* Am J Manag Care, 2020. **26**(9 Suppl): p. S191-s197.
236. Villa, A., et al., *Estrogens, Neuroinflammation, and Neurodegeneration.* Endocr Rev, 2016. **37**(4): p. 372-402.
237. Ranson, R.N., et al., *Nuclear expression of PG-21, SRC-1, and pCREB in regions of the lumbosacral spinal cord involved in pelvic innervation in young adult and aged rats.* Anat Cell Biol, 2012. **45**(4): p. 241-58.
238. Zhou, Z.X., et al., *Specificity of ligand-dependent androgen receptor stabilization: receptor domain interactions influence ligand dissociation and receptor stability.* Mol Endocrinol, 1995. **9**(2): p. 208-18.
239. Castelli, M.P., et al., *Regional distribution of 5alpha-reductase type 2 in the adult rat brain: an immunohistochemical analysis.* Psychoneuroendocrinology, 2013. **38**(2): p. 281-93.
240. Seo, Y.K., et al., *Regulation of steroid 5-alpha reductase type 2 (Srd5a2) by sterol regulatory element binding proteins and statin.* Exp Cell Res, 2009. **315**(18): p. 3133-9.

241. Madison, B.B., *Srebp2: A master regulator of sterol and fatty acid synthesis.* J Lipid Res, 2016. **57**(3): p. 333-5.
242. Abdel-Khalik, J., et al., *Defective cholesterol metabolism in amyotrophic lateral sclerosis.* J Lipid Res, 2017. **58**(1): p. 267-278.
243. Cutler, R.G., et al., *Evidence that accumulation of ceramides and cholesterol esters mediates oxidative stress-induced death of motor neurons in amyotrophic lateral sclerosis.* Ann Neurol, 2002. **52**(4): p. 448-57.
244. Dodge, J.C., et al., *Sterol auto-oxidation adversely affects human motor neuron viability and is a neuropathological feature of amyotrophic lateral sclerosis.* Sci Rep, 2021. **11**(1): p. 803.
245. Dodge, J.C., et al., *Neutral Lipid Cacostasis Contributes to Disease Pathogenesis in Amyotrophic Lateral Sclerosis.* J Neurosci, 2020. **40**(47): p. 9137-9147.
246. Taylor, A.E., B. Keevil, and I.T. Huhtaniemi, *Mass spectrometry and immunoassay: how to measure steroid hormones today and tomorrow.* Eur J Endocrinol, 2015. **173**(2): p. D1-12.
247. Wudy, S.A., et al., *The art of measuring steroids: Principles and practice of current hormonal steroid analysis.* J Steroid Biochem Mol Biol, 2018. **179**: p. 88-103.
248. Gargiulo-Monachelli, G.M., et al., *Circulating gonadal and adrenal steroids in amyotrophic lateral sclerosis: possible markers of susceptibility and outcome.* Horm Metab Res, 2014. **46**(6): p. 433-9.
249. Swerdloff, R.S., et al., *Dihydrotestosterone: Biochemistry, Physiology, and Clinical Implications of Elevated Blood Levels.* Endocr Rev, 2017. **38**(3): p. 220-254.
250. Da Cruz, S., et al., *Elevated PGC-1α activity sustains mitochondrial biogenesis and muscle function without extending survival in a mouse model of inherited ALS.* Cell Metab, 2012. **15**(5): p. 778-86.
251. Holzbaur, E.L., et al., *Myostatin inhibition slows muscle atrophy in rodent models of amyotrophic lateral sclerosis.* Neurobiol Dis, 2006. **23**(3): p. 697-707.
252. Bondy, C., et al., *Cellular pattern of type-I insulin-like growth factor receptor gene expression during maturation of the rat brain: comparison with insulin-like growth factors I and II.* Neuroscience, 1992. **46**(4): p. 909-23.
253. Kerkhoff, H., et al., *Insulin-like and fibroblast growth factors in spinal cords, nerve roots and skeletal muscle of human controls and patients with amyotrophic lateral sclerosis.* Acta Neuropathol, 1994. **87**(4): p. 411-21.
254. Chiu, I.M., et al., *T lymphocytes potentiate endogenous neuroprotective inflammation in a mouse model of ALS.* Proc Natl Acad Sci U S A, 2008. **105**(46): p. 17913-8.
255. MacKrell, J.G., et al., *Molecular targets of androgen signaling that characterize skeletal muscle recovery and regeneration.* Nucl Recept Signal, 2015. **13**: p. e005.
256. Musaro, A., et al., *Localized Igf-1 transgene expression sustains hypertrophy and regeneration in senescent skeletal muscle.* Nat Genet, 2001. **27**(2): p. 195-200.
257. Navarro, G., et al., *The role of androgens in metabolism, obesity, and diabetes in males and females.* Obesity (Silver Spring), 2015. **23**(4): p. 713-9.
258. Rossi, J., et al., *Melanocortin-4 receptors expressed by cholinergic neurons regulate energy balance and glucose homeostasis.* Cell Metab, 2011. **13**(2): p. 195-204.
259. Arber, S., et al., *Requirement for the homeobox gene Hb9 in the consolidation of motor neuron identity.* Neuron, 1999. **23**(4): p. 659-74.
260. Zhao, J., et al., *Decreased signalling of EphA4 improves functional performance and motor neuron survival in the SOD1(G93A) ALS mouse model.* Sci Rep, 2018. **8**(1): p. 11393.
261. Beghi, E., et al., *Amyotrophic lateral sclerosis, physical exercise, trauma and sports: results of a population-based pilot case-control study.* Amyotroph Lateral Scler, 2010. **11**(3): p. 289-92.
262. Visser, A.E., et al., *Multicentre, cross-cultural, population-based, case-control study of physical activity as risk factor for amyotrophic lateral sclerosis.* J Neurol Neurosurg Psychiatry, 2018. **89**(8): p. 797-803.
263. Zeng, F., H. Zhao, and J. Liao, *Androgen interacts with exercise through the mTOR pathway to induce skeletal muscle hypertrophy.* Biol Sport, 2017. **34**(4): p. 313-321.
264. Kirkinezos, I.G., et al., *Regular exercise is beneficial to a mouse model of amyotrophic lateral sclerosis.* Ann Neurol, 2003. **53**(6): p. 804-7.
265. Gerber, Y.N., et al., *Unlike physical exercise, modified environment increases the lifespan of SOD1G93A mice however both conditions induce cellular changes.* PLoS One, 2012. **7**(9): p. e45503.
266. Veldink, J.H., et al., *Sexual differences in onset of disease and response to exercise in a transgenic model of ALS.* Neuromuscul Disord, 2003. **13**(9): p. 737-43.
267. Mahoney, D.J., et al., *Effects of high-intensity endurance exercise training in the G93A mouse model of amyotrophic lateral sclerosis.* Muscle Nerve, 2004. **29**(5): p. 656-62.

268. Garbugino, L., et al., *Prolonged Voluntary Running Negatively Affects Survival and Disease Prognosis of Male SOD1G93A Low-Copy Transgenic Mice.* Front Behav Neurosci, 2018. **12**: p. 275.
269. Vecchio, L.M., et al., *The Neuroprotective Effects of Exercise: Maintaining a Healthy Brain Throughout Aging.* Brain Plast, 2018. **4**(1): p. 17-52.
270. Spiegelman, B.M., *The Neuroprotective Effects of Exercise: Maintaining a Healthy Brain Throughout Aging*, ed. B.M. Spiegelman. 2017, Cham (CH): Springer.
271. Willoughby, D.S. and L. Taylor, *Effects of sequential bouts of resistance exercise on androgen receptor expression.* Med Sci Sports Exerc, 2004. **36**(9): p. 1499-506.
272. Bamman, M.M., et al., *Mechanical load increases muscle IGF-I and androgen receptor mRNA concentrations in humans.* Am J Physiol Endocrinol Metab, 2001. **280**(3): p. E383-90.
273. Yin, L., et al., *Crucial role of androgen receptor in resistance and endurance trainings-induced muscle hypertrophy through IGF-1/IGF-1R- PI3K/Akt- mTOR pathway.* Nutr Metab (Lond), 2020. **17**: p. 26.
274. Deschenes, M.R., et al., *Endurance and resistance exercise induce muscle fiber type specific responses in androgen binding capacity.* J Steroid Biochem Mol Biol, 1994. **50**(3-4): p. 175-9.
275. Inoue, K., et al., *Rapid increase in the number of androgen receptors following electrical stimulation of the rat muscle.* Eur J Appl Physiol Occup Physiol, 1993. **66**(2): p. 134-40.
276. Howard, E.E., et al., *Testosterone supplementation upregulates androgen receptor expression and translational capacity during severe energy deficit.* Am J Physiol Endocrinol Metab, 2020. **319**(4): p. E678-E688.
277. Scaricamazza, S., et al., *Skeletal-Muscle Metabolic Reprogramming in ALS-SOD1(G93A) Mice Predates Disease Onset and Is A Promising Therapeutic Target.* iScience, 2020. **23**(5): p. 101087.
278. Okamoto, M., et al., *Mild exercise increases dihydrotestosterone in hippocampus providing evidence for androgenic mediation of neurogenesis.* Proc Natl Acad Sci U S A, 2012. **109**(32): p. 13100-5.
279. Neeper, S.A., et al., *Physical activity increases mRNA for brain-derived neurotrophic factor and nerve growth factor in rat brain.* Brain Res, 1996. **726**(1-2): p. 49-56.
280. Chae, C.H. and H.T. Kim, *Forced, moderate-intensity treadmill exercise suppresses apoptosis by increasing the level of NGF and stimulating phosphatidylinositol 3-kinase signaling in the hippocampus of induced aging rats.* Neurochem Int, 2009. **55**(4): p. 208-13.
281. Park, S.J., M.S. Yong, and S.S. Na, *Effect of exercise on the expression of nerve growth factor in the spinal cord of rats with induced osteoarthritis.* J Phys Ther Sci, 2015. **27**(8): p. 2551-4.
282. Carro, E., et al., *Circulating insulin-like growth factor I mediates the protective effects of physical exercise against brain insults of different etiology and anatomy.* J Neurosci, 2001. **21**(15): p. 5678-84.
283. Ottem, E.N., et al., *Androgen-dependent regulation of brain-derived neurotrophic factor and tyrosine kinase B in the sexually dimorphic spinal nucleus of the bulbocavernosus.* Endocrinology, 2007. **148**(8): p. 3655-65.
284. Verhovshek, T., et al., *Androgen regulates brain-derived neurotrophic factor in spinal motoneurons and their target musculature.* Endocrinology, 2010. **151**(1): p. 253-61.
285. Osborne, M.C., T. Verhovshek, and D.R. Sengelaub, *Androgen regulates trkB immunolabeling in spinal motoneurons.* J Neurosci Res, 2007. **85**(2): p. 303-9.
286. Verhovshek, T., L.M. Rudolph, and D.R. Sengelaub, *Brain-derived neurotrophic factor and androgen interactions in spinal neuromuscular systems.* Neuroscience, 2013. **239**: p. 103-14.
287. Wu, Y., et al., *Identification of androgen response elements in the insulin-like growth factor I upstream promoter.* Endocrinology, 2007. **148**(6): p. 2984-93.
288. Verras, M. and Z. Sun, *Beta-catenin is involved in insulin-like growth factor 1-mediated transactivation of the androgen receptor.* Mol Endocrinol, 2005. **19**(2): p. 391-8.
289. Fan, W., et al., *Insulin-like growth factor 1/insulin signaling activates androgen signaling through direct interactions of Foxo1 with androgen receptor.* J Biol Chem, 2007. **282**(10): p. 7329-38.
290. Palazzolo, I., et al., *Akt blocks ligand binding and protects against expanded polyglutamine androgen receptor toxicity.* Hum Mol Genet, 2007. **16**(13): p. 1593-603.
291. Fargo, K.N., et al., *Androgen regulation of axon growth and neurite extension in motoneurons.* Horm Behav, 2008. **53**(5): p. 716-28.
292. de Boer, E.M.J., et al., *TDP-43 proteinopathies: a new wave of neurodegenerative diseases.* J Neurol Neurosurg Psychiatry, 2020.
293. Butti, Z. and S.A. Patten, *RNA Dysregulation in Amyotrophic Lateral Sclerosis.* Front Genet, 2018. **9**: p. 712.
294. Haile, S., et al., *FUS/TLS is a co-activator of androgen receptor in prostate cancer cells.* PLoS One, 2011. **6**(9): p. e24197.

295. Fondell, E., et al., *Early-onset alopecia and amyotrophic lateral sclerosis: a cohort study.* Am J Epidemiol, 2013. **178**(7): p. 1146-9.
296. Bingham, P.M., et al., *Stability of an expanded trinucleotide repeat in the androgen receptor gene in transgenic mice.* Nat Genet, 1995. **9**(2): p. 191-6.
297. Renier, K.J., et al., *Antiandrogen flutamide protects male mice from androgen-dependent toxicity in three models of spinal bulbar muscular atrophy.* Endocrinology, 2014. **155**(7): p. 2624-34.
298. Furr, B.J. and H. Tucker, *The preclinical development of bicalutamide: pharmacodynamics and mechanism of action.* Urology, 1996. **47**(1A Suppl): p. 13-25; discussion 29-32.
299. Logroscino, G., et al., *Amyotrophic Lateral Sclerosis: An Aging-Related Disease.* Current Geriatrics Reports, 2015. **4**(2): p. 142-153.
300. Park, H.J., S.T. Ahn, and D.G. Moon, *Evolution of Guidelines for Testosterone Replacement Therapy.* J Clin Med, 2019. **8**(3).
301. Veenman, L., *Raloxifene as Treatment for Various Types of Brain Injuries and Neurodegenerative Diseases: A Good Start.* Int J Mol Sci, 2020. **21**(20).
302. Dalton, J.T., *The long and winding road for selective androgen receptor modulators.* Br J Clin Pharmacol, 2017. **83**(10): p. 2131-2133.